uOttawa

L'Université canadienne
Canada's university

FACULTÉ DES ÉTUDES SUPÉRIEURES ET POSTOCTORALES

uOttawa

L'Université canadienne
Canada's university

FACULTY OF GRADUATE AND POSDOCTORAL STUDIES

Matthew Kotyk
AUTEUR DE LA THÈSE / AUTHOR OF THESIS

M.Sc. (Chemistry)
GRADE / DEGREE

Department of Chemistry
FACULTÉ, ÉCOLE, DÉPARTEMENT / FACULTY, SCHOOL, DEPARTMENT

Experimental and Theoretical Investigation of Ligand Effects in Ruthenium- Catalyzed Olefin Metathesis

TITRE DE LA THÈSE / TITLE OF THESIS

Deryn Fogg
DIRECTEUR (DIRECTRICE) DE LA THÈSE / THESIS SUPERVISOR

CO-DIRECTEUR (CO-DIRECTRICE) DE LA THÈSE / THESIS CO-SUPERVISOR

Tom Baker

Sean Barry

Gary W. Slater
Le Doyen de la Faculté des études supérieures et postdoctorales / Dean of the Faculty of Graduate and Postdoctoral Studies

Experimental and Theoretical Investigation of Ligand Effects in Ruthenium-Catalyzed Olefin Metathesis

By

Matthew W. Kotyk

Thesis submitted to the
Faculty of Graduate and Postdoctoral Studies
University of Ottawa
in partial fulfillment of the requirements for the degree of

Master of Science

Centre for Catalysis Research and Innovation
Department of Chemistry
Ottawa-Carleton Chemistry Institute
Faculty of Science
University of Ottawa

Your file Votre référence
ISBN: 978-0-494-69077-2
Our file Notre référence
ISBN: 978-0-494-69077-2

Table of Contents

Abstract

Olefin metathesis, a powerful means of assembling carbon frameworks, was recognized with the 2005 Nobel Prize in Chemistry. Metathesis catalyst $RuCl(OC_6Br_5)(IMes)(py)(=CHPh)$ (**C**) exhibits outstanding performance in macrocyclization and enyne metathesis. This thesis established the trans-anionic geometry of **C**, and undertook a computational study of its cycloaddition behaviour relative to models $RuCl_2L(PMe_3)(=CH_2)$ (**A**: L = PMe_3, **B**: IMe). Both **A** and **B** undergo loss of a stabilizing Cl-Ru π-donation during cycloaddition, but this is almost completely compensated for in **B** by enhanced Cl-Ru electrostatic attraction (a consequence of the poor charge-donor capacity of the NHC ligand, which results in a more electropositive Ru center). This poor donor capacity is also important in **C**, as the NHC ligand is unable to offset the electron-withdrawing effect of the aryloxide. Instead, stronger ethylene binding results. This flattens the energy profile for cycloaddition, accounting for the very high reactivity of **C** once initiation has commenced.

Table of Compound Numbers

#	Compound	#	Compound	#	Compound
1	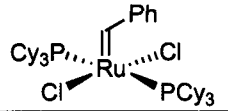	**2** NHC = **a**: IMes **b**: H_2IMes	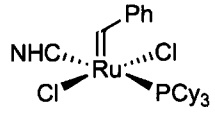	**3** NHC = **a**: IMes **b**: H_2IMes	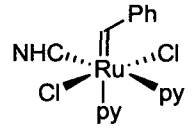
4 **a**: X = *o*-$O_2C_6H_4$ **b**: X_2 = OC_6F_5	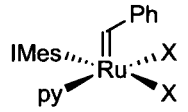	**5** = *trans*-**5a**	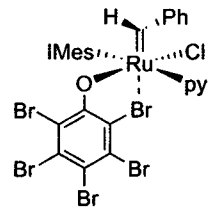	*cis*-**5b**	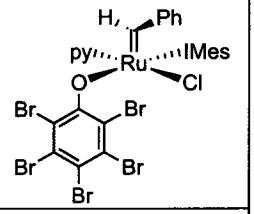
cis-**5c**	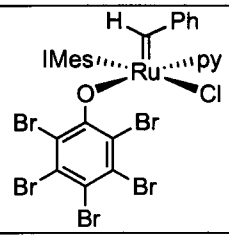	**6**	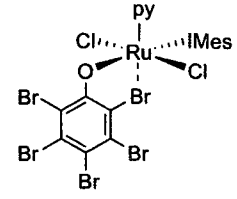	**7(I)**	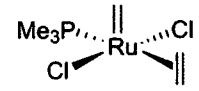
8(I)	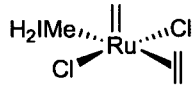	**9(I)**	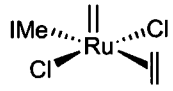	**10(I)**	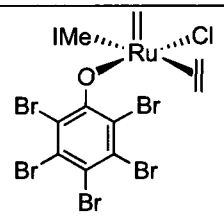
I		**II**	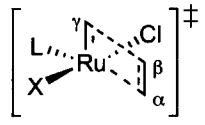	**III**	
11	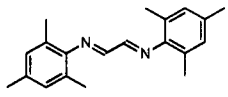	**12**	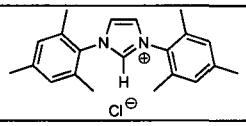	**13**	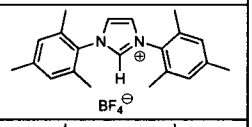
14	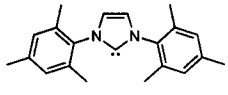	**15**	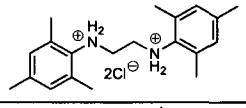	**16**	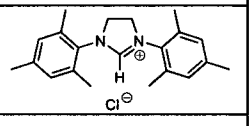
17	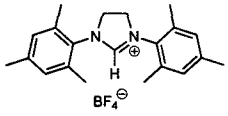	**18**	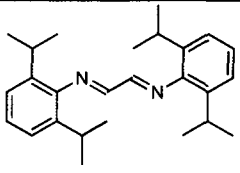	**19**	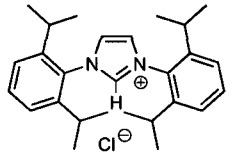

20	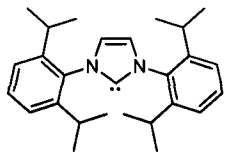	**21**	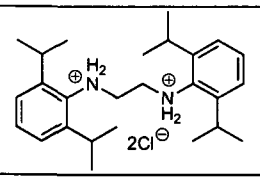	**22**	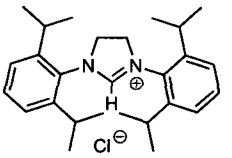
23	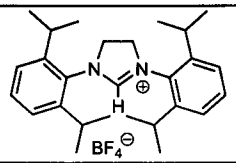	**24**	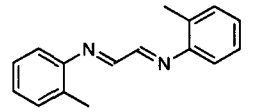	**25**	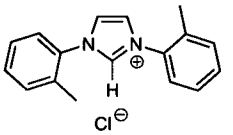
26	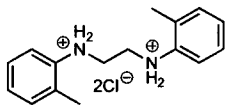	**27**	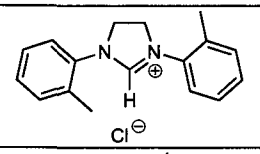	**28**	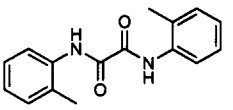
29	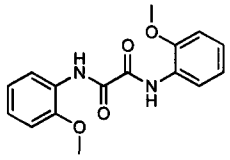	**30**	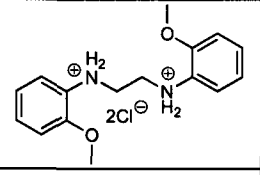	**31**	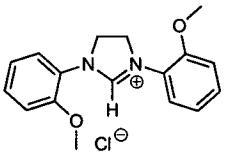
32	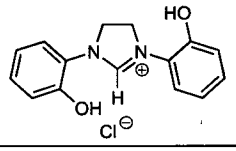	**33** NHC = **a**: IMes **b**: H_2IMes	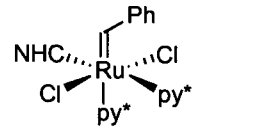	**34**	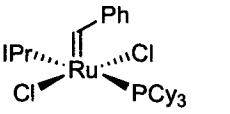
35	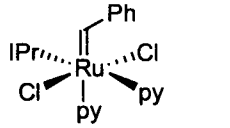	**36**	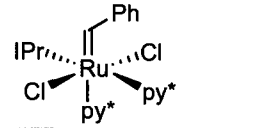	**37**	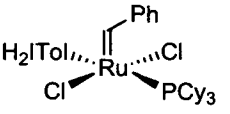
38	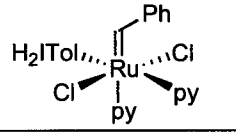				

List of Figures

other hydrogens are not shown. Important bond lengths and angles: Ru-Br1 2.5064(10) Å, Ru-Cl1 2.3409(16) Å, Ru-Cl2 2.3597(16) Å, Ru-O 2.021(4) Å, Ru-N3 2.080(5) Å, Ru-C1 2.116(6) Å, Br1-Ru-O 82.59(12)°, Br1-Ru-C1 98.54(17)°, Cl1-Ru-Cl2 174.65(6)°, N3-Ru-C1 98.7(2)°.

Figure 8. Experimental and TD-DFT-calculated visible absorption spectra, calculated at the B3LYP/DZVP level of theory, for: (a) **3a**; (b) **5**. Experimental traces in black, calculated traces for trans-anionic species in red; for cis isomers, in blue.

Figure 9. Frontier molecular orbitals of *trans*-**5a**, in order of decreasing energy. (a) LUMO+2. (b) LUMO. (c) HOMO. (d) HOMO-1. Spheres are coloured to signify the atoms in keeping with convention: grey for carbon, blue for nitrogen, green for chlorine, red for oxygen, darker red for bromine.

Chapter 4

Figure 1. Model systems studied. The Ru···Br interaction present in perbromoaryloxide catalyst **5** (see Chapter 3) is lost following replacement of pyridine by ethylene.

Figure 2. Gibbs free energy profiles for cycloaddition, normalized to the sum of the free energies for the py-bound precatalysts and ethylene. a) Effect of varying the L-donor in the Grubbs catalysts. b) Effect of replacing one chloride ligand with pentabromoaryloxide. Solid lines indicate gas-phase values; dashed lines, values in CH_2Cl_2.

Figure 3. Effect of L-ligand truncation in **10**: Gibbs free energy profile for cycloaddition, normalized to the free energy of py-bound precatalysts and C_2H_4. Solid lines indicate gas-phase values; dashed lines indicate values in CH_2Cl_2.

Figure 4. Fragment orbitals of $RuL(=CH_2)(C_2H_4)$ in **7(I)** and **7(II)** responsible for binding with the two chloride ligands (σ: LUFO; π: LUFO+1; δ: LUFO+2), showing contribution of Ru and C_γ (methylidene carbon), and the change in population (ΔP) of the fragment orbitals that results from turning on the Ru-Cl_2 interactions. Isosurface contour value for orbitals is 0.04 a.u.

Figure 5. (a) Principal orbital interactions involved in [Ru]-C_2H_4 bonding in **9(II)**, showing the Ru and C_γ character in the Ru=CH_2 LUFO. (b) EDA-derived fragment orbital interaction diagram for **9(II)**, showing changes in orbital populations associated with turning on the interaction between the ethylene and Ru=CH_2 fragments. Changes of <5% omitted.

List of Tables

List of Schemes

Chapter 1

Chapter 3

Chapter 4

Chapter 5

List of Abbreviations

δ	Chemical shift; ppm
κ	Descriptor for hapticity in σ-bonding ligands
$\omega_{1/2}$	Peak width at half height, in Hz
a.u.	Atomic units
ADMET	Acyclic diene metathesis
B	Mayer bond order
BSSE	Basis set superposition error
C	Celsius, in °
cat.	Catalyst
CM	Cross metathesis
COSY	Correlation spectroscopy
CT	Charge transfer, in %
Cy	Cyclohexyl
DFT	Density functional theory
$\Delta E^{\ddagger}$	Electronic energy, in kcal mol^{-1}
E	Orbital energy, in eV
E_{elstat}	Electrostatic interaction energy, in kcal mol^{-1}
E_{int}	Instantaneous fragment interaction energy, in kcal mol^{-1}
E_{orb}	Orbital interaction and polarization energy, in kcal mol^{-1}
E_{Pauli}	Pauli repulsion energy, in kcal mol^{-1}
E_{prep}	Electronic fragment preparation energy, in kcal mol^{-1}
E_{steric}	Steric interaction energy, in kcal mol^{-1}
ECDA	Extended charge decomposition analysis
EDA	Energy decomposition analysis
Et	Ethyl
Et_2O	Diethyl ether
equiv	Equivalents
EXSY	Exchange spectroscopy
FO	Fragment orbital

H_2IAnisole	*N,N'*-bis-(2-methoxyphenyl)imidazolin-2-ylidene
H_2IMe	*N,N'*-dimethylimidazolin-2-ylidene
H_2IMes	*N,N'*-bis-(2,4,6-trimethylphenyl)imidazolin-2-ylidene
H_2IPhenol	*N,N'*-bis-(2-hydroxyphenyl)imidazolin-2-ylidene
H_2IPr	*N,N'*-bis-(2,6-diisopropylphenyl)imidazolin-2-ylidene
H_2ITol	*N,N'*-bis-(2-methylphenyl)imidazolin-2-ylidene
HMBC	Heteronuclear multiple bond correlation
HMQC	Heteronuclear multiple quantum coherence
HOESY	Heteronuclear Overhauser effect spectroscopy
HOFO	Highest occupied fragment orbital
HOMO	Highest occupied molecular orbital
Hz	Hertz (1 Hz = 1 s^{-1})
IMe	*N,N'*-dimethylimidazol-2-ylidene
IMes	*N,N'*-bis-(2,4,6-trimethylphenyl)imidazol-2-ylidene
^{i}Pr	Isopropyl
IPr	*N,N'*-bis-(2,6-diisopropylphenyl)imidazol-2-ylidene
ITol	*N,N'*-bis-(2-methylphenyl)imidazol-2-ylidene
IRC	Intrinsic reaction coordinate
KHMDS	Potassium hexamethyldisilazane
L	Neutral donor ligand
LUFO	Lowest unoccupied fragment orbital
LUMO	Lowest unoccupied molecular orbital
M	Metal
Me	Methyl
Mes	Mesityl, 2,4,6-trimethylphenyl
MO	Molecular orbital
MPA	Mulliken population analysis
NPA	Natural population analysis
NHC	*N*-heterocyclic carbene
NMR	Nuclear magnetic resonance

NOE	Nuclear Overhauser effect
NOESY	Nuclear Overhauser effect spectroscopy
O	Occupied
ΔP	Orbital population change, in %
PCM	Polarizable continuum model
Ph	Phenyl
ppm	Parts per million (μg/g)
py	Pyridine
py*	3-bromopyridine
q	Charge
RCM	Ring closing metathesis
ROM-CM	Ring-opening metathesis-cross metathesis
ROMP	Ring-opening metathesis polymerization
SCF	Self consistent field
SHOP	Shell higher olefin process
τ	Time
T_1	Spin-lattice relaxation time constant
tbp	Trigonal bipyramidal
TD-DFT	Time-dependent density function theory
THF	Tetrahydrofuran
UAHF	United atom topological model
U	Unoccupied
UV	Ultra violet
UV-Vis	Ultra violet - visible
VT-NMR	Variable temperature nuclear magnetic resonance
wt	Weight, in %
X	Anionic donor ligand
XRD	X-ray diffraction
ZPE	Zero point energy

Acknowledgements

I would first and foremost like to thank my parents for their endless support. To my supervisor, Prof. Deryn Fogg, thank you for your guidance and for the opportunity to grow and succeed. Prof. Serge Gorelsky, thank you for all the time and effort spent performing the DFT calculations as well as for your friendship, insight and patience. Thank you Maureen for your companionship and for always being there. Thank you Debbie (and Vivek) for your friendship and advice. Thank you Jo and Seb for showing me the way in the lab. Thanks to all my other labmates: Adrien, Anne, Jon, Justin, Kevin, Nick, Rosa, and Titel for many interesting (and sometimes educational) conversations and for always making the lab fun. Thank you Prof. Cathleen Crudden for your mentorship and for first getting me interested in research. Dr. Glenn Facey is thanked for help with NMR experiments. Mathieu Frenette and Prof. Juan (Tito) Scaiano are thanked for spectrophotometer advice and access. Crystallographer Dr. Bob McDonald is thanked for handling the XRD crystal structure. This thesis was supported by scholarship funding from NSERC and the University of Ottawa. Thanks to all the above for a good time!

1 Introduction

The ability to synthesize complex organic molecules is crucial to advances in the fields of medicine, biology and materials science.[1-3] Despite their enormous progress over the last hundred years, however, classical methods in synthetic organic chemistry are severely restricted in their ability to generate complex molecules,[4] particularly within the context of increasing energy, economic and environmental constraints.[5-7] Catalytic methodologies offer key solutions in this regard, allowing chemical transformations to be performed with high selectivity while reducing energy costs by lowering the barrier to reaction.[8-11] Among such methodologies, transition-metal catalyzed metathesis of olefins is of keen interest for the access it offers to a broad range of chemical transformations.[12,13]

1.1 Olefin Metathesis

Alkene and alkyne metathesis reactions consist of the metal-catalyzed reorganization of the carbon skeleton, enabled by exchange of the unsaturated carbon centres.[13,14] Without a catalyst, the thermal [2+2] cycloaddition of two alkenes is symmetry-forbidden.[15] The metathesis reaction was first discovered in 1955 by Anderson and Merckling, who were working with an ill-defined $TiCl_4$/EtMgBr catalyst mixture.[16,17] Soon after, other catalyst systems were developed, including metal alkylidenes generated *in situ* from a transition-metal salt ($RuCl_3$ among them),[18,19] typically in conjunction with an alkylating agent.[20-25] The reactivity of these catalyst concoctions was explored with both simple substrates (propene, for example, was found to produce ethylene and 2-butene)[26] and more complex substrates (in particular, C_{11}-C_{14} olefins were produced from shorter and longer chains in the Shell higher olefin process [SHOP], still the major industrial application of olefin metathesis).[27] The reaction mechanism remained a subject of debate for 15 years, but a major breakthrough was achieved with Chauvin's 1970 proposal that the key step involved [2+2] cycloaddition of a metal alkylidene with an alkene to form a metallacyclobutane species, which upon retro-addition formed a new alkene (Scheme 1).[28] This mechanism was later confirmed by labelling studies.[29,30]

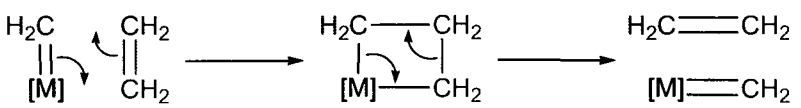

Scheme 1. The Chauvin mechanism for olefin metathesis, as mediated by a metal alkylidene catalyst.

Of the many different metathesis reactions shown in Scheme 2, alkene (or olefin) metathesis has been the most widely used, with many different modes of carbon-carbon bond reorganization possible. Conceptually simplest is cross-metathesis (CM) which exchanges the R-groups of acyclic alkenes. Acyclic diene metathesis (ADMET), which involves sequential, intermolecular CM events, converts acyclic dienes to oligomers, albeit with no control over chain lengths.[31] The alternative, intramolecular reaction cyclizes the diene, in a process termed ring-closing metathesis (RCM).[21,22] Ring-opening metathesis polymerization (ROMP) of cycloolefins has led to key advances in materials design, as the process can be used to generate well-defined polymers from simple cycloolefins or highly-functionalized monomers.[32] ROMP and CM can be combined in ring-opening metathesis-cross metathesis (ROM-CM) where cycloolefins and free olefins are combined to afford the opened and "crossed" acyclic dienes.[17,33] Furthermore, an alkene and alkyne can be converted into a 1,3-diene via enyne metathesis,[34,35] and two alkynes into two new alkynes via alkyne metathesis:[36,37] again, both intramolecular (ring-closing) and intermolecular variants exist. As these are reversible reactions, product distributions are thermodynamically controlled.[38] For example, ROMP and ROM-CM are driven by the release of ring strain in the cyclic olefin, while CM, ADMET and RCM are frequently driven by the volatilization of ethylene, where terminal alkenes are employed. (It should be noted, however, that the latter driving force is unselective, serving to promote both ADMET and RCM: this, in conjunction with the kinetic bias of Ru-NHC systems toward oligomerization, represents a challenge in RCM synthesis of medium and large rings. The enhanced translational entropy attainable in dilute solution has been identified as a key parameter in shifting the ring-chain equilibrium in favour of the desired RCM targets).[38,39] In contrast, the atom-economic enyne metathesis is driven by enthalpy (the stability of the conjugated diene system produced) with no release of volatile by-products. Alkyne metathesis is a direct analogue of the alkene metathesis reaction.

References page 10

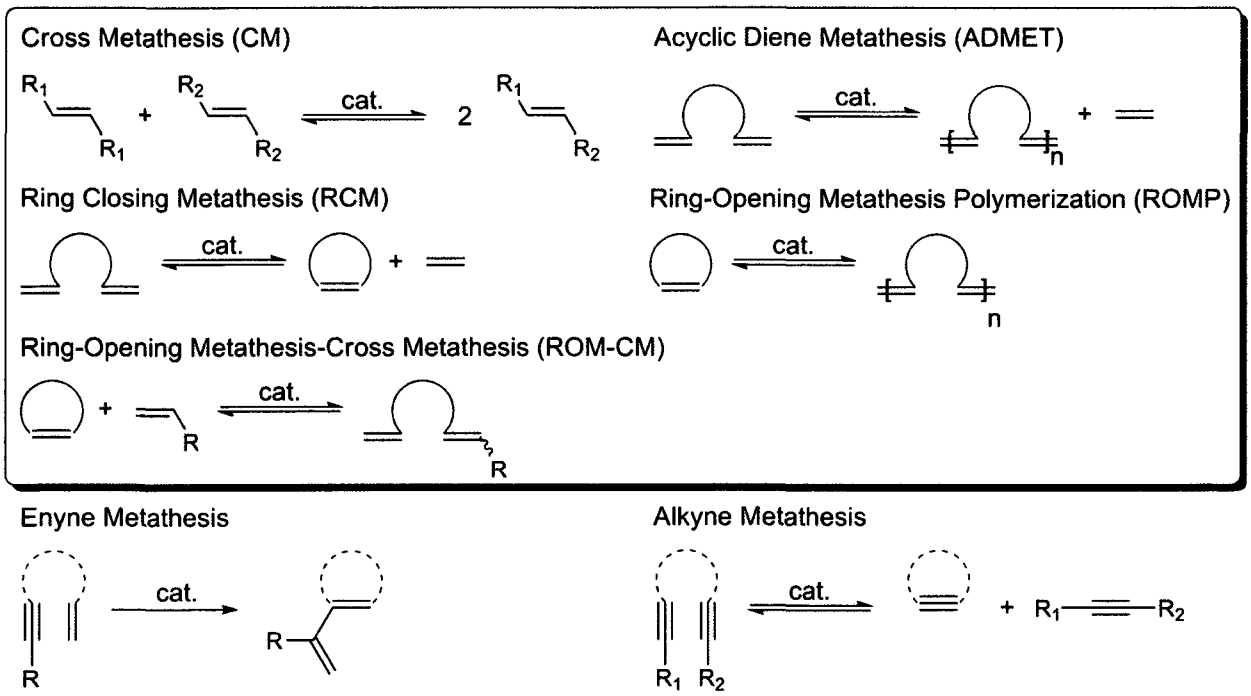

Scheme 2. Types of metathesis reactions. Olefin metathesis reactions are highlighted.

Applications of olefin metathesis explored using the early catalyst systems include the formation of α-olefins,[14,40] macrolactones for perfumery applications,[22] and the industrial ROMP polymers of cyclooctene (Vestenamer), norbornene (Norsorex), dicyclopentadiene (Metton, Telene, Pentam), and tetracyclododecene, which is hydrogenated to form the polymer Zeonex.[40] Nonetheless, selective reactions with more complex substrates required the development of structurally well-defined, highly active catalysts.

Well-defined, single-component metathesis catalysts have long been considered those species containing a metal-alkylidene bond (though it may be noted that in Ti complexes, the resting state can be the titanacyclobutane). Low oxidation state complexes containing a Fischer carbene ([M]=CHOR)[41,42] are less reactive than the high oxidation state Schrock carbenes ([M]=CHR).[43,44] A concentrated research effort by the Schrock group led to the development of well-defined and highly active Mo and W catalysts.[12] A crucial innovation was the development of the ligand set which inhibited bimolecular decomposition pathways, and enabled tuning of catalyst steric and electronic properties. Modulation of substituents on the alkoxide or aryloxide ligands (Figure 1), and, to a lesser extent, the imido ligand, permitted a high degree of control over both reactivity and selectivity. The molybdenum catalysts have been most widely used, as

the voracious reactivity of the tungsten systems is associated with extreme sensitivity to air and water. Despite their high sensitivity to aldehyde or alcohol functionalities, the Mo systems tolerate ketone, ether, and ester groups well, and have been much used in RCM reactions to form oxygen[45] and nitrogen[46] heterocycles. The ease of tuning of the aryloxide sites has been exploited in the synthesis of a large family of chiral catalysts containing binaphtholate- or biphenolate-derived ligands, one example of which is shown. These have been used in the production of isotactic[47] ROMP polymers, and synthesis of chiral organic compounds via asymmetric RCM[12] and asymmetric ROM-CM reactions.[48]

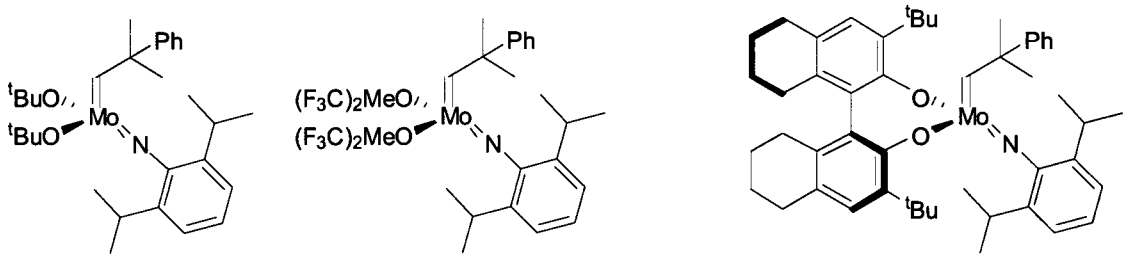

Figure 1. Representative examples of Schrock's Mo metathesis catalysts.

Despite the high metathesis activity and remarkable regioselectivity and stereoselectivity of the well-defined Group 6 catalysts, their use is limited by their thermal sensitivity, and the high oxophilicity of the metal centres, which renders them extremely sensitive to trace oxygen and water. The tremendous growth in the use of metathesis reactions is due in large part to the development of less active, but more easily handled, and commercially available, ruthenium catalysts.[49] The well-defined catalysts developed by the Grubbs group, $Ru(=CHR)Cl_2LL'$ (**1-2**),[50-52] are more thermally stable and less oxophilic than the Group 6 catalysts, and can be used in much less stringently controlled reaction conditions. It may be noted, however, that their "preferential reactivity" toward olefins over other functional groups is frequently overstated: as the reactivity of the olefin is diminished by steric or electronic factors, the susceptibility of the Ru catalysts to unwanted side-reactions increases. As well, these Ru(II) species are oxygen-sensitive, particularly in solution, and most especially following loss of one neutral ligand to generate the coordinatively unsaturated species required for coordination of olefin. Finally, the methylidene species generated on reaction with any terminal olefin is both less metathesis-active,

References page 10

and less stable, than its benzylidene precursor: this species thus represents a key vector for catalyst decomposition.[53]

The latter issues can be more clearly shown by considering the mechanism by which the Grubbs-class catalysts react (Scheme 3). Metathesis via **1-2** is initiated by the loss of a neutral PCy_3 ligand, creating an empty coordination site for the incoming alkene substrate. Upon coordination, the alkene then undergoes a Chauvin [2+2] cycloaddition with the cis-disposed Ru=CHR moiety to form the ruthenacyclobutane intermediate.[54] A new alkene is obtained by retro-addition and dissociation, which reforms the active catalyst.

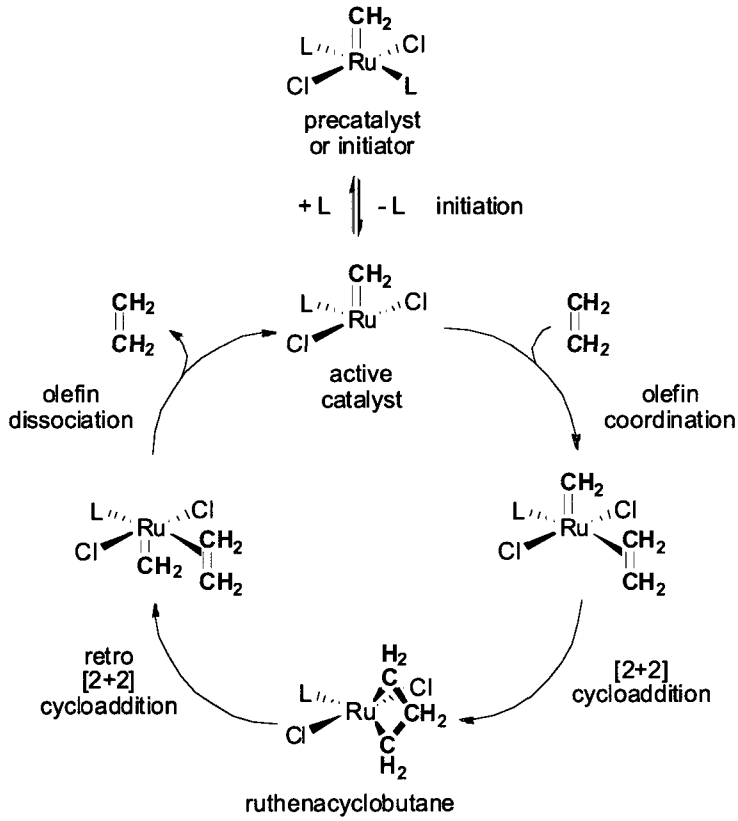

Scheme 3. Catalytic cycle for olefin metathesis mediated by Grubbs-class complexes.

In a groundbreaking discovery that represented the first major step in overcoming the low reactivity of the Ru systems, relative to the Group 6 catalysts, the activity of the first-generation Grubbs catalyst **1** was enhanced by replacement of a PCy_3 group with an *N*-heterocyclic carbene (NHC). Complexes of type **2**, widely known as second-generation Grubbs catalysts, were almost simultaneously reported by the Grubbs[51,52] and Nolan[55] groups; the Herrmann[56,57] group reported on $Ru(=CHPh)Cl_2(NHC)_2$ species at the same time. The most intensively studied derivatives

contain an IMes[51] or H_2IMes[52] ligand (**2a** or **2b** respectively; Figure 2). Depending on the substrate or reaction, either may be superior,[51,52,58,59] but the commercial availability of the H_2IMes complex has made it the default choice among the second-generation Ru catalysts now widely used by organic chemists. While such NHC precatalysts initiate much more slowly than the first-generation catalyst **1**, their faster reaction with olefin substrates greatly amplifies their reactivity.[60,61] Other popular commercially available precatalysts are the styrenyl ether[62-64] and indenylidene[65] derivatives of **2**.

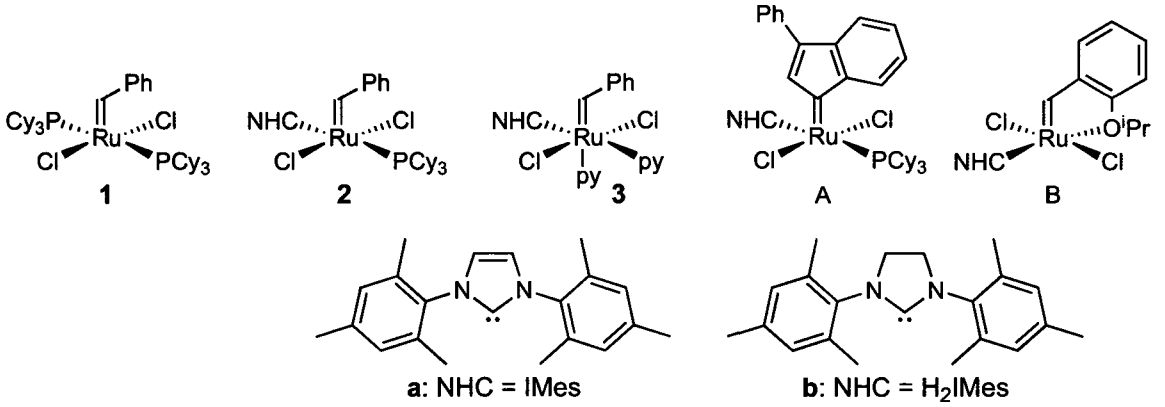

Figure 2. Grubbs catalysts of the first (**1**), second (**2**), and third (**3**) generations and indenylidene (A) and styrenyl ether (B) derivatives of **2**.

The ready accessibility of **1** and **2** has allowed synthetic organic chemists to utilize olefin metathesis as a powerful tool in the formation of carbon-carbon bonds. In particular, the RCM reaction has had a significant impact in the construction of synthetically valuable building blocks such as heterocyclic rings containing phosphorus,[66] sulfur,[66] oxygen,[67] or nitrogen,[67,68] including aromatic heterocycles;[69] spirocyclic,[70,71] cyclophane,[70] and polycyclic compounds;[70,71] and compounds of biological and medicinal relevance such as peptidomimetics,[72,73] carbohydrate derivatives,[73-76] alkaloids,[73,77-81] bioactive cyclic molecules,[82,83] and polycyclic ethers,[84] including macrocyclic aza-crown ethers[85] and topologically unusual molecules[86,87] as well as "molecular machines".[88,89] Arguably the most important application of olefin metathesis has been in the field of total synthesis, with RCM reactions often playing a crucial role in the synthetic campaigns.[13,90,91] Examples include ciguatoxin CTX3C,[92,93] still a record-holder as one of the largest molecules assembled by total synthesis, which employs six different RCM steps (Figure 3), as well as the coleophomones,[94,95] of interest as antifungal agents and heart chymase

inhibitors, anti-cancer agents such as (–)-mucocin,[96] the epothilones,[13,97] amphidinolides[98-101] and ingenol[96] (the latter also of interest for its anti-HIV activity).

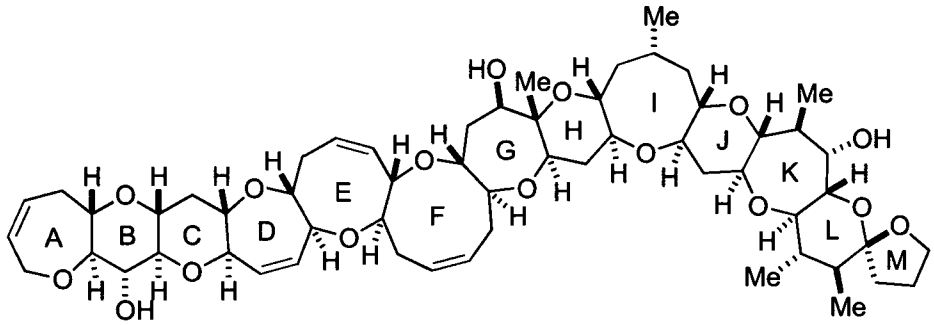

Figure 3. Ciguatoxin CTX3C. Bonds constructed by RCM are highlighted in red.

The impact of olefin metathesis was recognized with the 2005 Nobel Prize in chemistry, awarded to Chauvin, Schrock and Grubbs "for the development of the metathesis method in organic synthesis."[102] However, despite the extraordinary success of the Grubbs catalysts **1** and **2**, in particular, limitations remain the short catalyst lifetimes (hence low total turnover numbers) and limited control over selectivity. Reduced catalyst loadings and increased catalyst productivity will be important to facilitate industrial uptake.[103-105] Despite this, the major focus of research has been on increasing catalyst activity (for the most part through faster or more complete initiation). Increases in activity have increased substrate scope to enable, for example, the RCM formation of tetrasubstituted olefins;[106] advances in stereoselectivity in asymmetric metathesis has also been a major focus of late.[107,108] Increased initiation has been achieved by replacing the PCy_3 ligand in **2** with more labile ligands such pyridine (**3**),[109] PPh_3,[109] or a styrenyl ether[62-64] activated by electronic[110-112] or steric[113,114] destabilization of the chelate ring. The extreme case is Pier's "pre-initiated", four-coordinate phosphonium alkylidene.[115] Nonetheless, all the derivatives of **2** converge on the same the dichloride active species following one turnover (Scheme 3). This leads to common selectivity and decomposition routes, an example of the latter being bimolecular coupling, as pointed out by our group in model studies,[116,117] to form a triply chloride bridged diruthenium species.[117]

The potential to avoid chloride-mediated decomposition pathways, and to modulate catalyst lifetime, tunability and selectivity, motivated our group to explore alternative, "pseudo-halide" anionic ligands. Related studies have also been reported by others,[118-120] though this area remains under-explored relative to the modification of neutral donor ligands in the Grubbs-class

systems. A particular focus in the Fogg studies has been the potential of electron-deficient aryloxide ligands, chosen in preference to electron-rich aryloxides in consequence of studies indicating that the latter can readily isomerize to piano-stool complexes.[121,122] Key examples of the aryloxide catalysts are **4**[123,124] and **5**,[39] which give rise to active species that differ from the ubiquitous $RuCl_2(NHC)(=CH_2)$ structural motif (Figure 4). The aryloxide catalysts are significant for their high kinetic selectivity towards cyclization vs. oligomerization in the RCM of macrocyclic rings, although the origin of their selectivity is as yet unknown. The dichloride analogues, in comparison, show a profound kinetic bias toward oligomerization, with consequences discussed below. It may be noted that the assembly of the common ring sizes (i.e. 5-6 members) using the Grubbs catalysts is straightforward, only medium and large rings being susceptible to the competing oligomerization pathway.[38] Previously, high dilutions have been used in an effort to favour intramolecular cyclization over intermolecular oligomerization (albeit this increases the requirement for elevated temperatures or prolonged reactions times to compensate for the unfavourable effect of dilution on the reaction kinetics).[125] This reflects, in part, the limited understanding then current of the oligomerization-backbiting reaction: it is noteworthy, moreover, that the kinetic bias of the Grubbs systems toward oligomerization was found even at standard high dilutions (dropwise addition of substrate; <<5 mM).

Beyond the interesting and potentially important kinetic selectivity alluded to above, pentabromophenoxide catalyst **5** stands out for its remarkable efficiency in ethylene-free enyne RCM. Ever since Mori's pioneering 1998 report of the accelerating and yield-enhancing effect of ethylene atmosphere in enyne metathesis,[126] virtually all such synthetic reactions have been carried out under C_2H_4. An undesirable consequence, in terms of catalyst lifetime, is obvious from the short lifetime now known to be characteristic of the $[Ru]=CH_2$ species, to which all of the benzylidene or alkylidene species otherwise present will be converted under these conditions (indeed, this was the motivation behind Diver's development[127] of the so-called "methylene-free olefin metathesis). The basis of the beneficial effect of ethylene, however, remained the subject of debate.[128] Very recent preliminary results from the Fogg lab have now identified, for the first time, the preferential formation of oligomeric species in enyne metathesis via the first-generation Grubbs catalyst under nitrogen.[129] These findings may indicate that the bias of the aryloxide catalysts for cyclization, in preference to oligomerization, may extend to enyne metathesis as well as olefin metathesis.

References page 10

Finally, the capacity to tune catalyst reactivity, steric demand and electronic properties is key to the development of reaction-specific catalysts. It is a truism that no single catalyst is optimal for all substrates: each metathesis reaction, for example, has different requirements for catalyst initiation, activity, selectivity and lifetime.[32,35,38,130-133] Thus, better utilization of the anionic sites in the Ru metathesis catalysts offers opportunities for expansion on catalyst properties and reactivity profiles. The intelligent design of new and improved Ru metathesis catalysts requires a thorough understanding of key current catalysts and the active species derived therefrom; specifically, their behaviour in solution and the influence of electronic structure on reactivity.

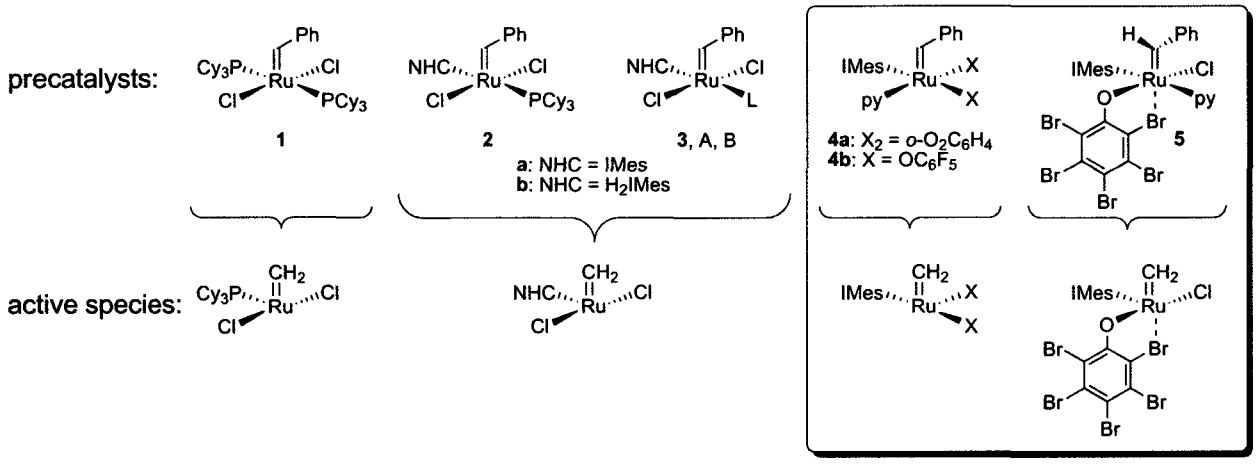

Figure 4. Key Ru precatalysts and the active species derived therefrom.

1.2 Scope of this Thesis

This thesis examines the effects of neutral and anionic ligands in ruthenium metathesis catalysts, with the intention of improving our understanding of how the ligands govern catalyst activity and selectivity. Experimental details are found in Chapter 2; data not appearing in the main text are tabulated in the Appendices. Chapter 3 describes a combined experimental and theoretical structural investigation of the potent bromoaryloxide catalyst **5**, in order to establish its geometry and hence to gain insight into its unusual kinetic selectivity toward RCM, over ADMET products. This study also conferred insight into the rotational behaviour of the Ru-NHC ligand, which has potentially important implications for asymmetric metathesis. Chapter 4 describes a computational investigation of the influence of the neutral and anionic ligands on the key cycloaddition step of metathesis, via examination of the electronic structure of the

intermediates and the energy profile for reaction. Chapter 5 describes the experimental efforts directed at optimizing the synthesis of an NHC library and the corresponding Ru-NHC catalysts. Finally, Chapter 6 offers suggestions for future work, including tandem catalysis.

1.3 References

(1) Nicolaou, K.C. *J. Org. Chem.* **2009**, *74*, 951-972.

(2) Corey, E.J. *Angew. Chem., Int. Ed. Engl.* **1991**, *30*, 455-465.

(3) Nicolaou, K.C.; Vourloumis, D.; Winssinger, N.; Baran, P.S. *Angew. Chem., Int. Ed.* **2000**, *39*, 44-122.

(4) Morrissey, S.R. *Chem. Eng. News* **2006**, *84*, 12-17.

(5) Sheldon, R.A. *Green Chem.* **2005**, *7*, 267-278.

(6) Sheldon, R.A., *Green Chem. and Catalysis*; Wiley-VCH: Chichester, 2007.

(7) Sheldon, R.A. *Green Chem.* **2007**, *9*, 1273-1283.

(8) Parshall, G.W.; Ittel, S.D., *Homogeneous Catalysis, 2nd Edition*; Wiley: New York, 1992; p 342.

(9) Cornils, B.; Herrmann, W.A., *Applied Homogeneous Catalysis with Organometallic Compounds*. Wiley-VCH: Weinheim, 2002.

(10) Cornils, B.; Herrmann, W.A.; Muhler, M.; Wong, C.-H., *Catalysis from A to Z: A Concise Encyclopedia, 3rd Edition*. Wiley-VCH: Weinheim, 2007; p 1544.

(11) Rothenberg, G., *Catalysis*; Wiley-VCH: Weinheim, 2008; p 279.

(12) Schrock, R.R.; Hoveyda, A.H. *Angew. Chem., Int. Ed.* **2003**, *42*, 4592-4633.

(13) Nicolaou, K.C.; Bulger, P.G.; Sarlah, D. *Angew. Chem., Int. Ed.* **2005**, *44*, 4490-4527.

(14) Grubbs, R.H., *Handbook of Metathesis*. Wiley-VCH: Weinheim, 2003.

(15) Carey, F.A.; Sundberg, R.J., *Advanced Organic Chemistry Part A: Structure and Mechanisms, 5th Edition*; Springer: New York, 2007; p 1267.

(16) Anderson, A.W.; Merckling, N.G. *Polymeric bicyclo[2.2.1]hept-2-ene*. U.S. Patent No. 2721189, 1955.

(17) Ivin, K.J.; Mol, J.C., *Olefin Metathesis and Metathesis Polymerization*; Academic Press: New York, 1997.

(18) Michelotti, F.W.; Keaveney, W.P. *J. Polym. Sci., Part A* **1965**, *3*, 895-905.

(19) Rinehart, R.E.; Smith, H.P. *J. Polym. Sci., Part B: Polym. Lett.* **1965**, *3*, 1049-1052.

(20) Calderon, N.; Chen, H.Y.; Scott, K.W. *Tetrahedron Lett.* **1967**, 3327-3329.

(21) Villemin, D. *Tetrahedron Lett.* **1980**, *21*, 1715-1718.

(22) Tsuji, J.; Hashiguchi, S. *Tetrahedron Lett.* **1980**, *21*, 2955-2958.

(23) Tsuji, J.; Hashiguchi, S. *J. Organomet. Chem.* **1981**, *218*, 69-80.

(24) Natta, G.; Dall'Asta, G.; Mazzanti, G. *Angew. Chem., Int. Ed.* **1964**, *3*, 765-772.

(25) Bosma, R.H.A.; Van den Aardweg, F.; Mol, J.C. *J. Chem. Soc., Chem. Commun.* **1981**, 1132-1133.

(26) Freitas, E.R.; Gum, C.R. *Chem. Eng. Prog.* **1979**, *75*, 73-76.

(27) Banks, R.L.; Bailey, G.C. *Ind. Eng. Chem. Prod. Res. Dev.* **1964**, *3*, 170-173.

(28) Hérisson, J.L.; Chauvin, Y. *Makromol. Chem.* **1971**, *141*, 161-176.

(29) Katz, T.J.; Rothchild, R. *J. Am. Chem. Soc.* **1976**, *98*, 2519-2526.

(30) Grubbs, R.H.; Carr, D.D.; Hoppin, C.; Burk, P.L. *J. Am. Chem. Soc.* **1976**, *98*, 3478-3483.

(31) Wagener, K.B.; Boncella, J.M.; Nel, J.G. *Macromolecules* **1991**, *24*, 2649-2657.

(32) Buchmeiser, M.R. *Chem. Rev.* **2000**, *100*, 1565-1604.

(33) Bespalova, N.B.; Bovina, M.A.; Sergeeva, M.B.; Oppengeim, V.D.; Zaikin, V.G. *J. Mol. Catal.* **1994**, *90*, 21-28.

(34) Han, C.C.; Katz, T.J. *Organometallics* **1985**, *4*, 2186-2195.

(35) Diver, S.T.; Giessert, A.J. *Chem. Rev.* **2004**, *104*, 1317-1382.

(36) Bunz, U.H.F.; Kloppenburg, L. *Angew. Chem., Int. Ed.* **1999**, *38*, 478-481.

(37) Fürstner, A.; Davies, P.W. *Chem. Commun.* **2005**, 2307-2320.

(38) Monfette, S.; Fogg, D.E. *Chem. Rev.* **2009**, *253*, ASAP article.

(39) Conrad, J.C.; Parnas, H.H.; Snelgrove, J.L.; Fogg, D.E. *J. Am. Chem. Soc.* **2005**, *127*, 11882-11883.

(40) Mol, J.C. *J. Mol. Catal. A* **2004**, *213*, 39-45.

(41) Fischer, E.O.; Maasbol, A. *Angew. Chem., Int. Ed.* **1964**, *3*, 580-581.

(42) Cardin, D.J.; Cetinkaya, B.; Lappert, M.F. *Chem. Rev.* **1972**, *72*, 545-574.

(43) Schrock, R.R. *J. Am. Chem. Soc.* **1974**, *96*, 6796-6797.

(44) Schrock, R.R. *Acc. Chem. Res.* **1979**, *12*, 98-104.

(45) Fu, G.C.; Grubbs, R.H. *J. Am. Chem. Soc.* **1992**, *114*, 5426-5427.

(46) Fu, G.C.; Grubbs, R.H. *J. Am. Chem. Soc.* **1992**, *114*, 7324-7325.

(47) McConville, D.H.; Wolf, J.R.; Schrock, R.R. *J. Am. Chem. Soc.* **1993**, *115*, 4413.

(48) La, D.S.; Ford, J.G.; Sattely, E.S.; Bonitatebus, P.J.; Schrock, R.R.; Hoveyda, A.H. *J. Am. Chem. Soc.* **1999**, *121*, 11603-11604.

(49) Trnka, T.M.; Grubbs, R.H. *Acc. Chem. Res.* **2001**, *34*, 18-29.

(50) Schwab, P.; Grubbs, R.H.; Ziller, J.W. *J. Am. Chem. Soc.* **1996**, *118*, 100-110.

(51) Scholl, M.; Trnka, T.M.; Morgan, J.P.; Grubbs, R.H. *Tetrahedron Lett.* **1999**, *40*, 2247-2250.

(52) Scholl, M.; Ding, S.; Lee, C.W.; Grubbs, R.H. *Org. Lett.* **1999**, *1*, 953-956.

(53) Ulman, M.; Grubbs, R.H. *J. Org. Chem.* **1999**, *64*, 7202-7207.

(54) Romero, P.E.; Piers, W.E. *J. Am. Chem. Soc.* **2005**, *127*, 5032-5033.

(55) Huang, J.; Stevens, E.D.; Nolan, S.P.; Petersen, J.L. *J. Am. Chem. Soc.* **1999**, *121*, 2674-2678.

(56) Weskamp, T.; Schattenmann, W.C.; Spiegler, M.; Herrmann, W.A. *Angew. Chem., Int. Ed.* **1998**, *37*, 2490-2493.

(57) Weskamp, T.; Kohl, F.J.; Hieringer, W.; Gleich, D.; Herrmann, W.A. *Angew. Chem., Int. Ed.* **1999**, *38*, 2416-2419.

(58) Bielawski, C.W.; Grubbs, R.H. *Angew. Chem., Int. Ed.* **2000**, *39*, 2903-2906.

(59) Fürstner, A.; Ackermann, L.; Gabor, B.; Goddard, R.; Lehmann, C.W.; Mynott, R.; Stelzer, F.; Thiel, O.R. *Chem. Eur. J.* **2001**, *7*, 3236-3253.

(60) Sanford, M.S.; Ulman, M.; Grubbs, R.H. *J. Am. Chem. Soc.* **2001**, *123*, 749-750.

(61) Sanford, M.S.; Love, J.A.; Grubbs, R.H. *J. Am. Chem. Soc.* **2001**, *123*, 6543-6554.

(62) Kingsbury, J.S.; Harrity, J.P.A.; Bonitatebus, P.J.; Hoveyda, A.H. *J. Am. Chem. Soc.* **1999**, *121*, 791-799.

(63) Garber, S.B.; Kingsbury, J.S.; Gray, B.L.; Hoveyda, A.H. *J. Am. Chem. Soc.* **2000**, *122*, 8168-8179.

(64) Hoveyda, A.H.; Gillingham, D.G.; Van Veldhuizen, J.J.; Kataoka, O.; Garber, S.B.; Kingsbury, J.S.; Harrity, J.P.A. *Org. Biomol. Chem.* **2004**, *2*, 8-23.

(65) Jafarpour, L.; Schanz, H.-J.; Stevens, E.D.; Nolan, S.P. *Organometallics* **1999**, *18*, 5416-5419.

(66) McReynolds, M.D.; Dougherty, J.M.; Hanson, P.R. *Chem. Rev.* **2004**, *104*, 2239-2258.

(67) Deiters, A.; Martin, S.F. *Chem. Rev.* **2004**, *104*, 2199-2238.

(68) Collins, S.K. *J. Organomet. Chem.* **2006**, *691*, 5122-5128.

(69) Donohoe, T.J.; Fishlock, L.P.; Procopiou, P.A. *Chem. Eur. J.* **2008**, *14*, 5716-5726.

(70) Kotha, S.; Lahiri, K. *Synlett* **2007**, 2767-2784.

(71) Schmidt, B.; Hermanns, J. *Curr. Org. Chem.* **2006**, *10*, 1363-1396.

(72) Brik, A. *Adv. Synth. Catal.* **2008**, *350*, 1661-1675.

(73) Martin, W.H.C.; Blechert, S. *Curr. Top. Med. Chem.* **2005**, *5*, 1521-1540.

(74) Plumet, J.; Gomez, A.M.; Lopez, J.C. *Mini-Rev. Org. Chem.* **2007**, *4*, 201-216.

(75) Madsen, R. *Eur. J. Org. Chem.* **2007**, 399-415.

(76) Jorgensen, M.; Hadwiger, P.; Madsen, R.; Stutz, A.E.; Wrodnigg, T.M. *Curr. Org. Chem.* **2000**, *4*, 565-588.

(77) Arisawa, M.; Nishida, A.; Nakagawa, M. *J. Organomet. Chem.* **2006**, *691*, 5109-5121.

(78) Gaich, T.; Mulzer, J. *Curr. Top. Med. Chem.* **2005**, *5*, 1473-1494.

(79) Brenneman, J.B.; Martin, S.F. *Curr. Org. Chem.* **2005**, *9*, 1535-1549.

(80) Felpin, F.-X.; Lebreton, J. *Eur. J. Org. Chem.* **2003**, 3693-3712.

(81) Delgado, A. *Eur. J. Org. Chem.* **2008**, 3893-3906.

(82) Van de Weghe, P.; Eustache, J. *Curr. Top. Med. Chem.* **2005**, *5*, 1495-1519.

(83) Schall, A.; Reiser, O. *Eur. J. Org. Chem.* **2008**, 2353-2364.

(84) Clark, J.S. *Chem. Commun.* **2006**, 3571-3581.

(85) Ibrahim, Y.A. *J. Mol. Catal. A.* **2006**, *254*, 43-52.

(86) Shima, T.; Hampel, F.; Gladysz, J.A. *Angew. Chem., Int. Ed.* **2004**, *43*, 5537-5540.

(87) Sakurai, H.; Daiko, T.; Hirao, T. *Science* **2003**, *301*, 1878-1882.

(88) Collin, J.P.; Dietrich-Buchecker, C.; Hamann, C.; Jouvenot, D.; Kern, J.M.; Mobian, P.; Sauvage, J.P. *Compr. Coord. Chem. II* **2004**, *7*, 303-326.

(89) Champin, B.; Mobian, P.; Sauvage, J.-P. *Chem. Soc. Rev.* **2007**, *36*, 358-366.

(90) Fürstner, A. *Angew. Chem., Int. Ed.* **2000**, *39*, 3012-3043.

(91) Maier, M.E. *Angew. Chem., Int. Ed.* **2000**, *39*, 2073-2077.

(92) Hirama, M.; Oishi, T.; Uehara, H.; Inoue, M.; Maruyama, M.; Oguri, H.; Satake, M. *Science* **2001**, *294*, 1904-1907.

(93) Inoue, M.; Miyazaki, K.; Uehara, H.; Maruyama, M.; Hirama, M. *Proc. Natl. Acad. Sci. USA* **2004**, *101*, 12013-12018.

(94) Nicolaou, K.C.; Montagnon, T.; Vassilikogiannakis, G.; Mathison, C.J.N. *J. Am. Chem. Soc.* **2005**, *127*, 8872-8888.

(95) Nicolaou, K.C.; Vassilikogiannakis, G.; Montagnon, T. *Angew. Chem., Int. Ed.* **2002**, *41*, 3276-3281.

(96) Evans, P.A.; Cui, J.; Gharpure, S.J.; Polosukhin, A.; Zhang, H.-R. *J. Am. Chem. Soc.* **2003**, *125*, 14702-14703.

(97) Watkins, E.B.; Chittiboyina, A.G.; Avery, M.A. *Eur. J. Org. Chem.* **2006**, 4071-4084.

(98) Maleczka, R.E., Jr.; Terrell, L.R.; Geng, F.; Ward, J.S., III. *Org. Lett.* **2002**, *4*, 2841-2844.

(99) Aissa, C.; Riveiros, R.; Ragot, J.; Fürstner, A. *J. Am. Chem. Soc.* **2003**, *125*, 15512-15520.

(100) Fürstner, A.; Bouchez, L.C.; Funel, J.-A.; Liepins, V.; Poree, F.-H.; Gilmour, R.; Beaufils, F.; Laurich, D.; Tamiya, M. *Angew. Chem., Int. Ed.* **2007**, *46*, 9265-9270.

(101) Fürstner, A.; Bouchez, L.C.; Morency, L.; Funel, J.-A.; Liepins, V.; Poree, F.-H.; Gilmour, R.; Laurich, D.; Beaufils, F.; Tamiya, M. *Chem. Eur. J.* **2009**, *15*, 3983-4010.

(102) (a) Chauvin, Y. *Angew. Chem., Int. Ed.* **2006**, **20***45*, 3740-3747. (b) Schrock, R. R. *Angew. Chem., Int. Ed.* **2006**, **20***45*, 3748-3759. (c) Grubbs, R. H. *Angew. Chem., Int. Ed.* **2006**, **20***45*, 3760-3765.

(103) Farina, V.; Zeng, X.; Wei, X.; Xu, Y.; Zhang, L.; Haddad, N.; Yee, N.K.; Senanayake, C.H. *Catal. Today* **2009**, *140*, 74-83.

(104) Shu, C.; Zeng, X.; Hao, M.-H.; Wei, X.; Yee, N.K.; Busacca, C.A.; Han, Z.; Farina, V.; Senanayake, C.H. *Org. Lett.* **2008**, *10*, 1303-1306.

(105) Yee, N.K.; Farina, V.; Houpis, I.N.; Haddad, N.; Frutos, R.P.; Gallou, F.; Wang, X.-J.; Wei, X.; Simpson, R.D.; Feng, X.; Fuchs, V.; Xu, Y.; Tan, J.; Zhang, L.; Xu, J.; Smith-Keenan, L.L.; Vitous, J.; Ridges, M.D.; Spinelli, E.M.; Johnson, M.; Donsbach, K.; Nicola, T.; Brenner, M.; Winter, E.; Kreye, P.; Samstag, W. *J. Org. Chem.* **2006**, *71*, 7133-7145.

(106) Stewart, I.C.; Ung, T.; Pletnev, A.A.; Berlin, J.M.; Grubbs, R.H.; Schrodi, Y. *Org. Lett.* **2007**, *9*, 1589-1592.

(107) Berlin, J.M.; Goldberg, S.D.; Grubbs, R.H. *Angew. Chem., Int. Ed.* **2006**, *45*, 7591-7595.

(108) Funk, T.W.; Berlin, J.M.; Grubbs, R.H. *J. Am. Chem. Soc.* **2006**, *128*, 1840-1846.

(109) Sanford, M.S.; Love, J.A.; Grubbs, R.H. *Organometallics* **2001**, *20*, 5314-5318.

(110) Grela, K.; Harutyunyan, S.; Michrowska, A. *Angew. Chem., Int. Ed.* **2002**, *41*, 4038-4040.

(111) Michrowska, A.; Bujok, R.; Harutyunyan, S.; Sashuk, V.; Dolgonos, G.; Grela, K. *J. Am. Chem. Soc.* **2004**, *126*, 9318-9325.

(112) Barbasiewicz, M.; Szadkowska, A.; Makal, A.; Jarzembska, K.; Wozniak, K.; Grela, K. *Chem. Eur. J.* **2008**, *14*, 9330-9337.

(113) Wakamatsu, H.; Blechert, S. *Angew. Chem., Int. Ed.* **2002**, *41*, 794-796.

(114) Wakamatsu, H.; Blechert, S. *Angew. Chem., Int. Ed.* **2002**, *41*, 2403-2405.

(115) Romero, P.E.; Piers, W.E.; McDonald, R. *Angew. Chem., Int. Ed.* **2004**, *43*, 6161-6165.

(116) Amoroso, D.; Snelgrove, J.L.; Conrad, J.C.; Drouin, S.D.; Yap, G.P.A.; Fogg, D.E. *Adv. Synth. Catal.* **2002**, *344*, 757-763.

(117) Amoroso, D.; Yap, G.P.A.; Fogg, D.E. *Organometallics* **2002**, *21*, 3335-3343.

(118) Denk, K.; Fridgen, J.; Herrmann, W.A. *Adv. Synth. Catal.* **2002**, *344*, 666-670.

(119) Gawin, R.; Makal, A.; Wozniak, K.; Mauduit, M.; Grela, K. *Angew. Chem., Int. Ed.* **2007**, *46*, 7206-7209.

(120) Jordaan, M.; Vosloo, H.C.M. *Adv. Synth. Catal.* **2007**, *349*, 184-192.

(121) Snelgrove, J.L.; Conrad, J.C.; Yap, G.P.A.; Fogg, D.E. *Inorg. Chim. Acta* **2003**, *345*, 268-278.

(122) Snelgrove, J.L.; Conrad, J.C.; Moriarty, M.M.; Yap, G.P.A.; Fogg, D.E. *Organometallics* **2005**, *24*, 103-109.

(123) Conrad, J.C.; Amoroso, D.; Czechura, P.; Yap, G.P.A.; Fogg, D.E. *Organometallics* **2003**, *22*, 3634-3636.

(124) Monfette, S.; Fogg, D.E. *Organometallics* **2006**, *25*, 1940-1944.

(125) Yamamoto, K.; Biswas, K.; Gaul, C.; Danishefsky, S.J. *Tetrahedron Lett.* **2003**, *44*, 3297-3299.

(126) Mori, M.; Sakakibara, N.; Kinoshita, A. *J. Org. Chem.* **1998**, *63*, 6082-6083.

(127) Diver, S.T. *Abstracts, 32nd Northeast Regional Meeting of the American Chemical Society, Rochester, NY, United States, October 31-November 3 FIELD Full Journal Title:Abstracts, 32nd Northeast Regional Meeting of the American Chemical Society, Rochester, NY, United States, October 31-November 3* **2004**, GEN-042.

(128) Lloyd-Jones, G.C.; Margue, R.G.; de Vries, J.G. *Angew. Chem., Int. Ed.* **2005**, *44*, 7442-7447.

(129) Grotevendt, A.G.; Fogg, D.E., unpublished work.

(130) Fürstner, A.; Nagano, T.; Müller, C.; Seidel, G.; Müller, O. *Chem. Eur. J.* **2007**, *13*, 1452-1462.

(131) Camm, K.D.; Castro, N.M.; Liu, Y.; Czechura, P.; Snelgrove, J.L.; Fogg, D.E. *J. Am. Chem. Soc.* **2007**, *129*, 4168-4169.

(132) Grela, K. *Angew. Chem., Int. Ed.* **2008**, *47*, 5504-5507.

(133) Bieniek, M.; Michrowska, A.; Usanov, D.L.; Grela, K. *Chem. Eur. J.* **2008**, *14*, 806-818.

2 Experimental Methods

2.1 General Procedures

2.1.1 Reaction Conditions

Synthetic experiments were carried out at room temperature (22 °C), unless otherwise specified, using standard drybox or Schlenk line techniques under an atmosphere of N_2. Reactions carried out in air are indicated in the individual experimental procedures, except where these are referred back to a previously-described standard procedue. All reactions were stirred with Teflon-coated magnetic stir-bars in glassware dried at 125 °C in an oven and cooled under vacuum.

2.1.2 Solvents

Dry, oxygen-free benzene (HPLC grade), hexanes (HPLC grade), toluene (reagent grade), dichloromethane (CH_2Cl_2, HPLC grade), tetrahydrofuran (THF, unstabilized, HPLC grade), and diethyl ether (Et_2O, reagent grade) were obtained using a Glass Contour solvent purification system, and stored over Linde 4 Å molecular sieves. Other solvents were purified and degassed by distillation.[1] Pyridine and 3-bromopyridine were distilled from CaH_2. All deuterated solvents were purchased from Aldrich. For NMR analysis of organic molecules, deuterated solvents were used without further purification. For organometallic complexes, $CDCl_3$ was refluxed over and distilled from CaH_2, degassed by a minimum of three freeze-pump-thaw cycles and stored over activated sieves (Linde 4 Å); ampoules of C_6D_6 were opened in the drybox and used as received. *Note:* To obtain clean ^1H NMR spectra for samples made up in the glovebox, it was essential to purge residual solvents from the atmosphere prior to opening vessels containing deuterated solvents.

2.1.3 Reagents.

All commercial reagents were purchased from Aldrich with the exception of triethylorthoformate ($HC(OEt)_3$), oxalyl chloride and 3-bromopyridine, which were purchased from Acros. Compound **1**[2] was kindly provided by Mr. Justin Lummiss of this research group. Compounds **11**[3] and **4a**[4] were kindly provided by M. Sebastien Monfette of this research group.

References page 39

2.1.4 NMR Spectroscopy

Routine ^{1}H (300, 400, or 500 MHz), $^{31}P\{^{1}H\}$ (121 MHz), $^{11}B\{^{1}H\}$ (128 MHz), $^{13}C\{^{1}H\}$ NMR (75, 100, or 125 MHz), and 2D-correlation spectra (^{1}H-^{13}C HMQC, ^{1}H-^{13}C HMBC, ^{1}H-^{1}H COSY, NOESY-EXSY) were recorded on Bruker Avance-300 ($^{1}H/^{13}C/^{31}P/^{19}F/^{2}H$ QNP probe with Z gradient), Avance-400 (broadband probe with Z gradient) and Avance-500 (inverse broadband probe with Z gradient) spectrometers at 25 °C. For organometallic complexes and reactions, sample solutions were prepared in the drybox using screw-thread NMR tubes with PTFE/silicon septum caps. Spectral widths used for the acquisition of NMR spectra, in δ (ppm): ^{1}H: +25 to -35; $^{31}P\{^{1}H\}$: +150 to -150; $^{11}B\{^{1}H\}$: +110 to -80; $^{13}C\{^{1}H\}$: +350 to 0. ^{1}H and ^{13}C NMR spectra were referenced to residual solvent peaks and recorded on the 300 MHz instrument unless stated otherwise. Coupling constants are given as absolute values in Hz. ^{31}P NMR spectra were referenced to external 85% H_3PO_4 at δ 0.0 ppm, by adding a flame-sealed capillary of H_3PO_4 to the NMR samples.

2.1.5 Other Instrumentation

Electronic absorption spectra were recorded using a Varian Cary-50 spectrophotometer by kind permission of Prof. Juan (Tito) Scaiano. The wavelength range used for acquisition of UV-Vis spectra was 450 to 1000 nm. The detector was zeroed, then calibrated for 100% transmittance with an acquisition of a spectrum using an empty cuvette, followed by calibration for 0% transmittance with the beam blocked. No baseline correction was used; a flat baseline was verified from the spectrum obtained using an empty cuvette. Absorption spectra for the solvent and sample solutions were acquired at room temperature at a scan rate of 600 nm min^{-1}. Corrected absorption spectra were calculated by subtracting solvent spectra from sample spectra. Molar extinction coefficients (ε, $cm^{-1}M^{-1}$) were calculated by dividing the corrected absorption by the sample concentration and plotting as a function of energy. Samples and blank controls were prepared under N_2 in the drybox by filling a septum-capped quartz or screw-top optical glass UV-Vis cell (Hellma) with ca. 2 mL of solvent or a catalyst solution of known concentration. The latter were sealed prior to removal from the drybox.

X-ray diffraction (XRD) analysis of single crystals was performed by Dr. Robert McDonald (University of Alberta) on a Bruker D8 diffractometer using the Bruker-supplied APEX II CCD program suite for diffractometer operation, data collection, data reduction and

absorption correction. Data were collected using graphite-monochromated Mo K_α (λ = 0.71073 Å) radiation at -100 °C.

2.1.6 Computational Details

All DFT calculations were performed by Prof. Serge Gorelsky using the Gaussian 03 package.[5] Stationary points on the potential energy surface were obtained using the B3LYP hybrid density functional method.[6,7] For calculations in Chapter 3, geometry optimizations were performed using the DZVP basis set[8] for all atoms. Absorption spectra were calculated from time-dependent DFT (TD-DFT) simulations at the B3LYP/DZVP level. Calculated excitation energies and oscillator strengths were converted into absorption spectra using the pseudo-Voigt functions (50% Gaussian and 50% Lorentzian) and the 4000 cm^{-1} half-bandwidths. For calculations in Chapter 4, geometry optimizations of the Ru-IMes complexes were performed using the DZVP basis set[8] for all atoms. Subsequent single-point calculations were performed using the DZVP basis for the Ru atom and the TZVP basis set[9] for the other atoms. For the other Ru complexes, geometry optimizations were performed using the DZVP basis for the transition metal atom and the TZVP basis set for the other atoms. Such a combination proved necessary to reduce the effects of basis set superposition errors (BSSE) in geometry and thermochemistry, and to provide a balanced description of ionic and covalent contributions to chemical bonding. Tight SCF convergence criteria were used for all calculations. The converged wave functions were tested to confirm that they correspond to the ground-state surface. The second-order derivative of the energy with respect to nuclear positions was evaluated to determine the nature of the stationary points. Intrinsic reaction coordinate (IRC)[10,11] calculations were used to confirm the reaction pathways through the transition states for all reactants. Vibrational zero point energies (ZPE) and thermal corrections were included in the calculation of free energies at 25 °C and 1 atm. BSSE effects were evaluated using the Boys-Bernardi counterpoise method.[12] As the corrections are less than 1.5 kcal/mol, they were not applied to the reported thermochemical parameters.

Solvation energies of Ru species in dichloromethane were calculated using the PCM model with the united atom topological model (UAHF). All calculations for the analysis of the electronic structure were performed using the DZVP basis for the transition-metal atom and the TZVP basis set for the other atoms. Electronic fragment preparation energies were calculated

References page 39

relative to the initiated 14-electron active species plus free ethylene. Atomic charges were calculated by natural population analysis (NPA)[13] as implemented in Gaussian 03. The AOMix program was used for extended charge and energy decomposition analysis (ECDA[14] and EDA[15]), analysis of MOs in terms of FO contributions, construction of the FO interaction diagram, Mayer 2- and 3-center bond orders[16,17] and assessment of MO compositions in terms of atomic contributions.[18]

2.2 Synthesis of NHC Ligands

2.2.1 Synthesis of *N,N'*-bis(mesityl)imidazolium chloride (IMes•HCl), **12**

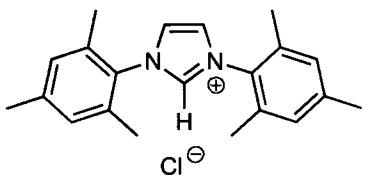

Reaction carried out in air. The known compound **12** was prepared by the patented* variation of the literature method,[3] involving modification of the carbene-carbon reagent and reaction time. A pre-stirred (15 min) white suspension of paraformaldehyde (1.3 equiv, 13.6 g, 0.454 mol) in HCl (2.0 equiv, 167 mL of a 4M solution in dioxane, 0.699 mol) was slowly added to a yellow solution of *N,N'*-bis(mesityl)ethylenediimine (**11**, 102.2 g, 0.349 mol) in 600 mL THF at 0 °C. The solution turned red-brown immediately. Stirring was continued for 10 h at room temperature, after which the precipitate was filtered off, washed with THF (5 × 50 mL) until the filtrate was clear, then dried under vacuum for 12 h to yield a pale beige powder. Yield 67.0 g (56%). NMR data agree with the values reported.[3] ^{1}H NMR ($CDCl_3$, δ): 10.19 (t, $^4J_{HH}$ = 1.5 Hz, 1H, NC(*H*Cl)N), 7.63 (d, $^4J_{HH}$ = 1.5 Hz, 2H, NC*H*), 7.02 (s, 4H, Mes C*H*), 2.33 (s, 6H, Mes Me_p), 2.16 (s, 12H, Mes Me_o).

2.2.2 Synthesis of *N,N'*-bis(mesityl)imidazolium tetrafluoroborate (IMes•HBF_4), **13**

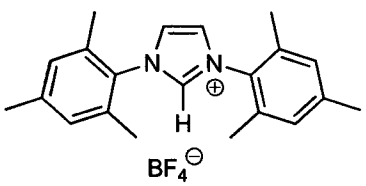

Reaction carried out in air. The known compound **13**[19] was prepared by stirring a solution of *N,N'*-bis(mesityl)imidazolium chloride (IMes•HCl, **12**, 10.2 g, 0.030 mol) in 300 mL H_2O for 30 min and filtering. Addition of HBF_4 (1.3 equiv, 5.1 mL of a 48% wt solution in H_2O, 0.039 mol) to the filtrate caused a suspension to form. This was stirred for 10 min, after which the white precipitate was filtered off and washed with H_2O (3 × 10 mL). The solid was reprecipitated from a minimum of CH_2Cl_2-hexanes (30 mL + 100 mL), filtered off and

dried under vacuum for 12 h to yield a white powder. Yield 7.9 g (67%). NMR data agree with the values reported.[19] ^{1}H NMR ($CDCl_3$, 400 MHz, δ): 8.83 (t, $^4J_{HH}$ = 1.5 Hz, 1H, NC(*H*BF_4)N), 7.55 (d, $^4J_{HH}$ = 1.5 Hz, 2H, NC*H*), 7.01 (s, 4H, Mes C*H*), 2.33 (s, 6H, Mes Me_p), 2.09 (s, 12H, Mes Me_o).

2.2.3 Synthesis of *N,N'*-bis-(mesityl)imidazol-2-ylidene (IMes), **14**

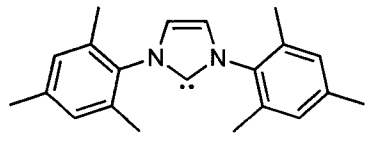

The known compound **14** was prepared by a modification of the literature method,[20] involving variation of the base(s) and the NHC salt (for comparison to the reported method, see Chapter 5). Solid NaH (2.0 equiv, 1.6 g, 0.067 mol) followed by solid KO^{t}Bu (0.03 equiv, 100 mg, 0.891 mmol) were added to a white suspension of *N,N'*-bis(mesityl)imidazolium tetrafluoroborate (IMes•HBF_4, **13**, 13.1 g, 0.033 mol) in dry THF (250 mL). The resulting solution was stirred for 8 h, then reduced to dryness under vacuum. The residue was dissolved in a minimum of 100 mL benzene, filtered through Celite, and reduced to dryness under vacuum. The residue was taken up in hexanes (75 mL). The precipitate was filtered off, washed with hexanes (3 × 10 mL), then dried for 12 h to yield a light beige powder. Yield 6.8 g (67%). NMR data agree with the values reported.[21] ^{1}H NMR (C_6D_6, δ): 6.81 (s, 4H, Mes C*H*), 6.48 (s, 2H, NC*H*), 2.16 (s, 18H, Mes Me).

2.2.4 Attempted Synthesis of *N,N'*-bis(mesityl)ethylenediamine dihydrochloride, **15**

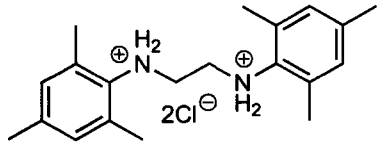

Reaction carried out in air. Preparation of **11** was attempted by a variation of the literature method,[3] involving increased equivalents of $NaBH_4$ and extended reaction time at elevated temperature. To a yellow solution of *N,N'*-bis(mesityl)ethylenediimine (**11**, 112 mg, 0.384 mmol) in dry THF (15 mL) at 0 °C was added solid $NaBH_4$ (10.0 equiv, 152 mg, 3.837 mmol). The solution was stirred for 12 h at 70 °C, then cooled to room temperature and diluted with water (5 mL). The solution was then reduced to a minimum volume under vacuum, and extracted with CH_2Cl_2 (3 × 10 mL). The combined CH_2Cl_2 layers were dried with Na_2SO_4 and reduced to dryness under vacuum. The residue was redissolved in a minimum of Et_2O (10 mL), to which was added HCl (3.0 equiv, 0.3 mL of a 4M solution in dioxane, 1.151 mmol). No precipitate was observed. The solution was reduced to dryness. ^{1}H NMR analysis indicated no reaction.

References page 39

2.2.5 Synthesis of *N,N'*-bis(mesityl)ethylenediamine dihydrochloride, **15**

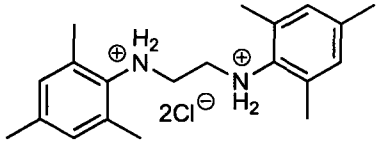

Reaction carried out in air. The known compound **15** was prepared by a variation of the literature method,[3] involving modification of the reducing agent. A yellow solution of *N,N'*-bis(mesityl)ethylenediimine (**11**, 20.3 g, 0.069 mol) in 500 mL dry THF was chilled to 0 °C. To it was added solid $LiAlH_4$ (3.0 equiv, 7.9 g, 0.208 mol) in ca. 0.5 g portions, every 5 min. The mixture was stirred for 12 h while allowing to warm to room temperature, then cooled to 0 °C. Methanol was added dropwise until bubbling ceased, followed by dropwise addition of water until bubbling ceased. The resulting slurry was filtered through Celite and washed with Et_2O (3 × 30 mL). The filtrate was reduced to a minimum volume under vacuum, diluted with CH_2Cl_2 (100 mL), separated, and re-extracted with CH_2Cl_2 (3 × 30 mL). The combined CH_2Cl_2 layers were dried with Na_2SO_4 and reduced to dryness under vacuum. The residue was redissolved in a minimum of Et_2O (100 mL), to which was added HCl (4M solution in dioxane, 3.0 equiv, 52 mL, 0.208 mol). The precipitate was filtered off, washed with Et_2O (3 × 20 mL) and dried under vacuum for 12 h to yield a light beige powder. Yield 22.1 g (86%). NMR data agree with the values reported.[3] ^{1}H NMR (D_2O, δ): 7.04 (s, 4H, Mes C*H*), 3.75 (s, 4H, NCH_2), 2.28 (s, 6H, Mes Me_p), 2.24 (s, 12H, Mes Me_o).

2.2.6 Synthesis of *N,N'*-bis(mesityl)imidazolinium chloride (H_2IMes•HCl), **16**

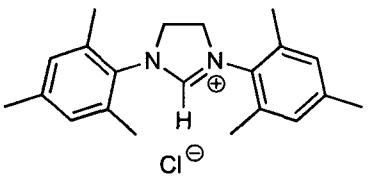

Reaction carried out in air. The known compound **16** was prepared by the patented* variation of the literature method,[3] involving modification of the workup procedure to remove excess triethylorthoformate. A suspension of *N,N'*-bis(mesityl)ethylenediamine dihydrochloride (**15**, 6.5 g, 0.018 mol) in triethylorthoformate ($HC(OEt)_3$, 30 mL, 0.180 mol) was heated at 120 °C for 3 h in a microdistillation apparatus. The triethylorthoformate was then distilled off and collected for re-use (purity confirmed by GC). The remaining suspension, of ca. 10 mL volume, was cooled to room temperature and diluted with 30 mL hexanes. The resulting precipitate was filtered off, washed with hexanes (2 × 10

* Note added in revisions: see Nolan, S.P. "Synthesis of 1,3 disubstituted imidazolium salts", US Patent 7,109,348, 2006.

References page 39

mL), then Et_2O (2 × 10 mL), and dried under vacuum for 12 h to yield a white powder. Yield 5.4 g (90%). NMR data agree with the values reported.[3] ^1H NMR ($CDCl_3$, δ): 9.36 (s, 1H, NC(*H*Cl)N), 6.93 (s, 4H, Mes C*H*), 4.57 (s, 4H, NCH_2), 2.37 (s, 12H, Mes Me_o), 2.27 (s, 6H, Mes Me_p).

2.2.7 Synthesis of *N,N'*-bis(mesityl)imidazolinium tetrafluoroborate (H_2IMes•HBF_4), **17**

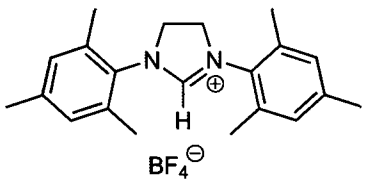

Reaction carried out in air. Synthesis of known **17** was carried out as described for **13**. *N,N'*-bis(mesityl) imidazolinium chloride (H_2IMes•HCl, **16**, 5.4 g, 0.016 mol), HBF_4 (1.3 equiv, 2.7 mL of a 48% wt solution in H_2O, 0.021 mol). The solid was reprecipitated from a minimum volume of CH_2Cl_2-hexanes (10 mL + 30 mL), filtered off, and dried under vacuum for 12 h to yield a white powder. Yield 5.0 g (80%). ^1H NMR ($CDCl_3$, δ): 7.89 (s, 1H, NC(*H*BF_4)N), 6.99 (s, 4H, Mes C*H*), 4.54 (s, 4H, NCH_2), 2.36 (s, 12H, Mes Me_o), 2.31 (s, 6H, Mes Me_p).

2.2.8 Synthesis of *N,N'*-bis(2,6-diisopropylphenyl)ethylenediimine, **18**

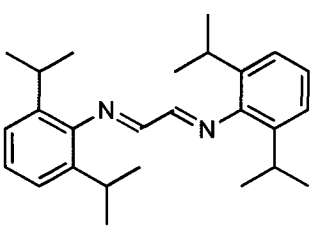

Reaction carried out in air. The known compound **18** was prepared by variation of the literature methods,[3,22] involving the use of methanol* (1 L) as the reaction solvent with 2,6-diisopropylaniline (2.05 equiv, 105.4 g, 0.594 mol), glyoxal (33.3 mL of a 40% wt solution in water, 0.290 mol), formic acid (0.07 equiv, 0.75 mL, 0.020 mol). Yield 85.3 g (76%). NMR data agree with the values reported.[3,22] ^1H NMR ($CDCl_3$, δ): 8.11 (s, 2H, NC*H*), 7.21-7.15 (m, 6H, Ar C*H*), 2.94 (sept, $^3J_{HH}$ = 6.9 Hz, 4H, Ar C*H*$(CH_3)_2$), 1.21 (d, $^3J_{HH}$ = 6.9 Hz, 24H, Ar CH$(CH_3)_2$).

2.2.9 Synthesis of *N,N'*-bis(2,6-diisopropylphenyl)imidazolium chloride (IPr•HCl), **19**

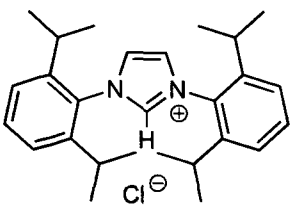

Reaction carried out in air. Synthesis of known **19** was carried out as described for **12**. Paraformaldehyde (1.4 equiv, 2.4 g, 0.079 mol), 4M HCl in dioxane (2.0 equiv, 28 mL, 0.113 mol), *N,N'*-bis(2,6-diisopropylphenyl)ethylenediimine (**18**, 21.2 g, 0.056 mol). The beige solid was reprecipitated from a minimum volume of CH_2Cl_2-hexanes (30 mL + 100 mL), filtered

off, and dried under vacuum for 12 h to yield a white powder. Yield 15.5 g (65%). NMR data agree with the values reported.[22] ^{1}H NMR ($CDCl_3$, δ): 10.06 (s, 1H, NC(*H*Cl)N), 8.15 (s, 2H, NC*H*), 7.57 (t, $^3J_{HH}$ = 7.8 Hz, 2H, Ar CH_p), 7.34 (d, $^3J_{HH}$ = 7.8 Hz, 4H, Ar CH_m), 2.44 (sept, $^3J_{HH}$ = 6.8 Hz, 4H, Ar C*H*$(CH_3)_2$), 1.28 (d, $^3J_{HH}$ = 6.8 Hz, 12H, Ar CH(C$H_3)_2$), 1.24 (d, $^3J_{HH}$ = 6.8 Hz, 12H, Ar CH(C$H_3)_2$).

2.2.10 Synthesis of *N,N'*-bis-(2,6-diisopropylphenyl)imidazol-2-ylidene (IPr), **20**

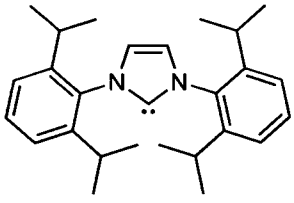

To a white suspension of *N,N'*-bis(2,6-diisopropylphenyl)imidazolium chloride (IPr•HCl, **19**, 1.6 g, 3.657 mmol) in 25 mL dry THF was added solid NaH (2.0 equiv, 175 mg, 7.275 mmol), followed by solid KO^{t}Bu (0.1 equiv, 50 mg, 0.446 mmol). The resulting solution was stirred for 2 h, then filtered through Celite and reduced to dryness under vacuum. To the residue was added 25 mL hexanes. The precipitate was filtered off, washed with hexanes (3 × 5 mL) and dried for 12 h to yield a light beige powder. Yield 1.0 g (71%). NMR data agree with the values reported.[22] ^{1}H NMR (C_6D_6, δ): (mk-01-42) 7.26 (m, 2H, Ar CH_p), 7.13 (m, 4H, Ar CH_m), 6.58 (s, 2H, NC*H*), 2.93 (sept, $^3J_{HH}$ = 6.9 Hz, 4H, Ar C*H*$(CH_3)_2$), 1.25 (d, $^3J_{HH}$ = 6.9 Hz, 12H, Ar CH(C$H_3)_2$), 1.15 (d, $^3J_{HH}$ = 6.9 Hz, 12H, Ar CH(C$H_3)_2$).

2.2.11 Synthesis of *N,N'*-bis(2,6-diisopropylphenyl)ethylenediamine dihydrochloride, **21**

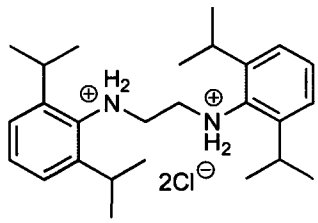

Reaction carried out in air. Synthesis of known **21** was carried out as described for **15**. $LiAlH_4$ (3.0 equiv, 4.9 g, 0.130 mol), *N,N'*-bis(2,6-diisopropylphenyl)ethylenediimine (**18**, 16.3 g, 0.043 mol), HCl (3.0 equiv, 21 mL of a 4M solution in dioxane, 0.130 mol). Yield 16.7 g (85%). NMR data agree with the values reported.[3] ^{1}H NMR (D_2O, δ): 7.57-7.37 (m, 6H, Ar C*H*), 3.75 (s, 4H, NCH_2), 3.07 (m, 4H, Ar C*H*$(CH_3)_2$), 1.30 (d, $^3J_{HH}$ = 6.7 Hz, 12H, Ar CH(C$H_3)_2$), 1.14 (d, $^3J_{HH}$ = 6.7 Hz, 12H, Ar CH(C$H_3)_2$).

2.2.12 Synthesis of *N,N'*-bis(2,6-diisopropylphenyl)imidazolinium chloride (H_2IPr•HCl), **22**

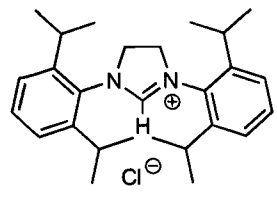

Synthesis of known **22** was carried out as described for **16**, using *N,N'*-bis(2,6-diisopropylphenyl)ethylenediamine dihydrochloride (**21**, 3.4 g, 0.008 mol) and triethylorthoformate ($HC(OEt)_3$, 30 mL, 0.180 mol).

Yield 2.4 g (75%). NMR data agree with the values reported.[3] ^{1}H NMR ($CDCl_3$, δ): 8.32 (s, 1H, NC(*H*Cl)N), 7.47 (t, $^3J_{HH}$ = 7.6 Hz, 2H, Ar C*H*$_p$), 7.27 (d, $^3J_{HH}$ = 7.6 Hz, 4H, Ar C*H*$_m$), 4.86 (s, 4H, NC*H*$_2$), 3.01 (sept, $^3J_{HH}$ = 6.7 Hz, 4H, Ar C*H*(CH$_3$)$_2$), 1.39 (d, $^3J_{HH}$ = 6.7 Hz, 12H, Ar CH(C*H*$_3$)$_2$), 1.25 (d, $^3J_{HH}$ = 6.7 Hz, 12H, Ar CH(C*H*$_3$)$_2$).

2.2.13 Synthesis of *N,N'*-bis(2,6-diisopropylphenyl)imidazolinium tetrafluoroborate (H_2IPr•HBF$_4$), **23**

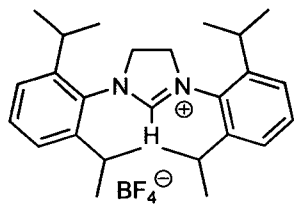

Reaction carried out in air. A solution of *N,N'*-bis(2,6-diisopropylphenyl)imidazolinium chloride (H_2IPr•HCl, **22**, 1.2 g, 2.778 mmol) in 75 mL H_2O was stirred for 30 min and filtered. To the filtrate was added HBF_4 (1.3 equiv, 0.5 mL of a 48% wt solution in H_2O, 3.612 mmol) dropwise, which caused the formation of a precipitate. The white suspension was stirred for 10 min, following which the white precipitate was filtered off, washed with H_2O (3 × 5 mL) and dried under vacuum for 12 h. Yield 1.2 g (92%). ^{1}H NMR ($CDCl_3$, δ): 7.67 (s, 1H, NC(*H*BF$_4$)N), 7.50 (t, $^3J_{HH}$ = 7.8 Hz, 2H, Ar C*H*$_p$), 7.30 (d, $^3J_{HH}$ = 7.8 Hz, 4H, Ar C*H*$_m$), 4.72 (s, 4H, NC*H*$_2$), 3.04 (sept, $^3J_{HH}$ = 6.8 Hz, 4H, Ar C*H*(CH$_3$)$_2$), 1.42 (d, $^3J_{HH}$ = 6.8 Hz, 12H, Ar CH(C*H*$_3$)$_2$), 1.25 (d, $^3J_{HH}$ = 6.8 Hz, 12H, Ar CH(C*H*$_3$)$_2$).

2.2.14 Synthesis of *N,N'*-bis(2-methylphenyl)ethylenediimine, **24**

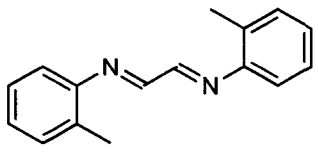

Reaction carried out in air. The known compound **24** was prepared by a variation of the literature method,[23] without additional solvent. To 2-methylaniline (2.0 equiv, 10.2 g, 0.095 mol) was added aqueous glyoxal (5.4 mL of a 40% wt solution in water, 0.047 mol). The solution was stirred for 10 min, over which time the solution solidified. CH_2Cl_2 (20 mL) was added to dissolve the solid, and the aqueous and organic layers were separated. The CH_2Cl_2 layer was dried with Na_2SO_4. Addition of hexanes (50 mL) caused precipitation of a yellow solid, which was filtered off, washed with hexanes (3 × 15 mL), and dried under vacuum for 12 h. Yield 6.7 g (60%). NMR data agree with the values reported.[23] ^{1}H NMR ($CDCl_3$, δ): 8.32 (s, 2H, NC*H*), 7.30-7.17 (m, 6H, Ar C*H*), 7.05 (t, $^3J_{HH}$ = 7.4 Hz, 2H, Ar C*H*), 2.41 (s, 6H, Ar Me). Use of benzene or CH_2Cl_2 as reaction solvents resulted in lower isolated yields.

References page 39

2.2.15 Attempted Synthesis of *N,N'*-bis(2-methylphenyl)imidazolium chloride (ITol•HCl), **25**

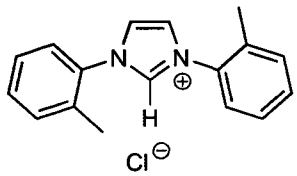

Synthesis of **25** was carried out as described for **12** with longer (4 days) reaction, by addition of paraformaldehyde (1.4 equiv, 183 mg, 6.087 mmol), to *N,N'*-bis(2-methylphenyl)ethylenediimine (**24**, 997 mg, 4.219 mmol) and 4M HCl in dioxane (2.0 equiv, 2.1 mL, 8.439 mmol). Yield 107 mg (9%). ^{1}H NMR ($CDCl_3$, δ): 10.62 (s, 1H, NC(*H*Cl)N), 7.79 (d, $^3J_{HH}$ = 7.8 Hz, 2H, Ar C*H*), 7.67 (s, 2H, NC*H*), 7.47-7.30 (m, 6H, Ar C*H*), 2.36 (s, 6H, Ar Me).

2.2.16 Synthesis of *N,N'*-bis(2-methylphenyl)ethylenediamine dihydrochloride, **26**

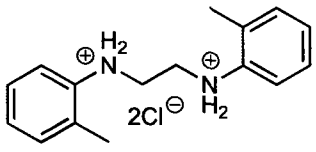

Synthesis of known **26** was carried out as described for **15**, by reaction of $LiAlH_4$ (3.0 equiv, 2.4 g, 0.063 mol), *N,N'*-bis(2-methylphenyl)ethylenediimine (**24**, 4.9 g, 0.021 mol), HCl (3.0 equiv, 16 mL of a 4M solution in dioxane, 0.063 mol). Yield 5.8 g (89%). ^{1}H NMR (D_2O, δ): 7.28 (t, $^3J_{HH}$ = 7.8 Hz, 4H, Ar C*H*), 7.18 (td, $^3J_{HH}$ = 7.4 Hz, $^4J_{HH}$ = 1.3 Hz, 2H, Ar C*H*), 7.09 (d, $^3J_{HH}$ = 7.9 Hz, 2H, Ar C*H*), 3.67 (s, 4H, NCH_2), 2.25 (s, 6H, Ar Me).

2.2.17 Synthesis of *N,N'*-bis(2-methylphenyl)imidazolinium chloride (H_2ITol•HCl), **27**

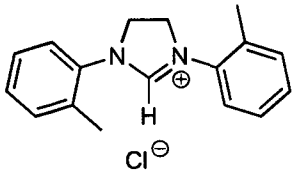

Synthesis of known[24] **27** was carried out as described for **16**, by reaction of *N,N'*-bis(2-methylphenyl)ethylenediamine dihydrochloride (**26**, 4.2 g, 0.014 mol) and triethylorthoformate ($HC(OEt)_3$, 30 mL, 0.180 mol). Yield 3.8 g (95%). NMR data agree with the values reported.[24] ^{1}H NMR ($CDCl_3$, δ): 8.74 (s, 1H, NC(*H*Cl)N), 7.85 (d, $^3J_{HH}$ = 7.4 Hz, 2H, Ar C*H*), 7.33-7.20 (m, 6H, Ar C*H*), 4.67 (s, 4H, NCH_2), 2.44 (s, 6H, Ar Me).

2.2.18 Synthesis of *N,N'*-bis(2-methylphenyl)oxalamide, **28**

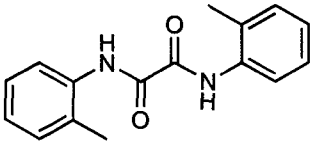

Reaction carried out in air. The known compound **28** was prepared according to the literature procedure.[24] Yield 8.3 g (92%). ^{1}H NMR ($CDCl_3$, δ): 9.38 (s, 2H, N*H*), 8.09 (d, $^3J_{HH}$ = 8.0 Hz, 2H, Ar C*H*), 7.32-7.23 (m, 4H, Ar C*H*), 7.17 (td, $^3J_{HH}$ = 7.4 Hz, $^4J_{HH}$ = 1.1 Hz, 2H, Ar C*H*), 2.39 (s, 6H, Ar Me).

2.2.19 Synthesis of *N,N'*-bis(2-methylphenyl)ethylenediamine dihydrochloride, **26**

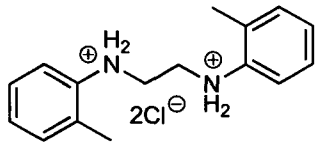

Synthesis of known **26** was carried out as described for **15**. $LiAlH_4$ (4.0 equiv, 4.7 g, 0.124 mol), *N,N'*-bis(2-methylphenyl)oxalamide (**28**, 8.3 g, 0.031 mol), HCl (3.0 equiv, 25 mL of a 4M solution in dioxane, 0.099 mol). Yield 6.1 g (63%). ^{1}H NMR (D_2O, δ): 7.28 (t, $^3J_{HH}$ = 7.8 Hz, 4H, Ar C*H*), 7.18 (td, $^3J_{HH}$ = 7.4 Hz, $^4J_{HH}$ = 1.3 Hz, 2H, Ar C*H*), 7.09 (d, $^3J_{HH}$ = 7.9 Hz, 2H, Ar C*H*), 3.67 (s, 4H, NCH_2), 2.25 (s, 6H, Ar Me).

2.2.20 Synthesis of *N,N'*-bis(2-methoxyphenyl)oxalamide, **29**

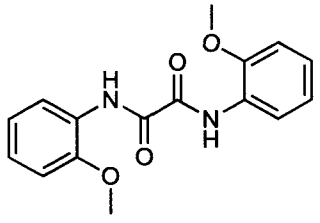

Synthesis of known[25] **29** was carried out as for **28**, by reaction of 2-methoxyaniline (2.1 equiv, 6.1 g, 0.050 mol), NEt_3 (2.1 equiv, 7.0 mL, 0.050 mol), oxalyl chloride (2.0 mL, 0.024 mol). The precipitate was washed with methanol (3 × 20 mL) then Et_2O (2 × 10 mL) and dried under vacuum for 12 h to yield a white powder. Yield 6.7 g (94%). NMR data agree with the values reported.[25] ^{1}H NMR ($CDCl_3$, δ): 9.97 (s, 2H, N*H*), 8.41 (dd, $^3J_{HH}$ = 8.0 Hz, $^4J_{HH}$ = 1.3 Hz, 2H, Ar *H*), 7.15 (td, $^3J_{HH}$ = 7.8 Hz, $^4J_{HH}$ = 1.4 Hz, 2H, Ar *H*), 7.01 (t, J_{HH} = 7.5 Hz, 2H, Ar *H*), 6.94 (d, J_{HH} = 8.1 Hz, 2H, Ar *H*), 3.94 (s, 6H, OMe).

2.2.21 Synthesis of *N,N'*-bis(2-methoxyphenyl)ethylenediamine dihydrochloride, **30**

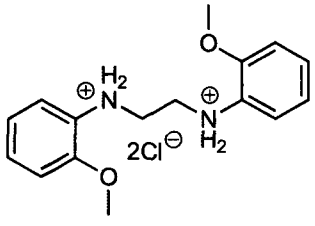

Synthesis of known **30** was carried out as described for **15**, using $LiAlH_4$ (3.0 equiv, 2.6 g, 0.067 mol), *N,N'*-bis(2-methoxyphenyl)oxalamide (**29**, 6.7 g, 0.022 mol) and HCl (3.0 equiv, 17 mL of a 4M solution in dioxane, 0.067 mol). Yield 7.1 g (92%). NMR data agree with the values reported.[25] ^{1}H NMR (D_2O, δ): 7.31 (td, $^3J_{HH}$ = 7.8 Hz, $^4J_{HH}$ = 1.6 Hz, 2H, Ar *H*), 7.15 (dd, $^3J_{HH}$ = 8.0 Hz, $^4J_{HH}$ = 1.6 Hz, 2H, Ar *H*), 7.11 (dd, $^3J_{HH}$ = 8.3 Hz, $^4J_{HH}$ = 1.0 Hz, 2H, Ar *H*), 7.03 (td, $^3J_{HH}$ = 7.8 Hz, $^4J_{HH}$ = 1.2 Hz, 2H, Ar *H*), 3.84 (s, 6H, OMe), 3.66 (s, 4H, NCH_2).

References page 39

2.2.22 Synthesis of *N,N'*-bis(2-methoxyphenyl)imidazolinium chloride (H_2IAnisole•HCl), **31**

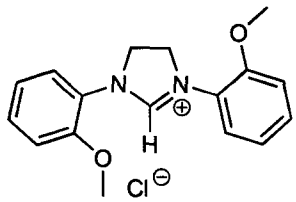

Synthesis of known **31** was carried out as described for **16**. *N,N'*-bis(2-methoxyphenyl)ethylenediamine dihydrochloride (**30**, 7.1 g, 0.021 mol), $HC(OEt)_3$ (125 mL, 0.742 mol). Yield 6.1 g (94%). NMR data agree with the values reported.[25] ^{1}H NMR (DMSO-d_6, 500 MHz, δ): 9.51 (s, 1H, NC(*H*Cl)N), 7.53 (dd, $^3J_{HH}$ = 7.9 Hz, $^4J_{HH}$ = 1.6 Hz, 2H, Ar *H*), 7.43 (td, $^3J_{HH}$ = 7.9 Hz, $^4J_{HH}$ = 1.6 Hz, 2H, Ar *H*), 7.30 (dd, $^3J_{HH}$ = 8.4 Hz, $^4J_{HH}$ = 1.2 Hz, 2H, Ar *H*), 7.12 (td, $^3J_{HH}$ = 7.7 Hz, $^4J_{HH}$ = 1.3 Hz, 2H, Ar *H*), 4.56 (s, 4H, NCH_2), 3.94 (s, 6H, OMe).

2.2.23 Attempted Synthesis of *N,N'*-bis(2-hydroxyphenyl)imidazolinium chloride (H_2IPhenol•HCl), **32**

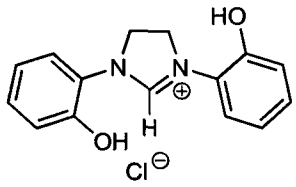

Reaction carried out in air. A solution of *N,N'*-bis(2-methoxyphenyl)imidazolinium chloride (H_2IAnisole•HCl, **31**, 190 mg, 0.596 mmol) in HBr (5.1 mL of a 48% wt solution in water, 0.045 mol) was heated at 100 °C for 12 h, then cooled to 0 °C. The precipitate was filtered off, washed with distilled water (3 × 10 mL) and dried under vacuum for 12 h. ^{1}H NMR analysis indicated no reaction.

2.2.24 Synthesis of *N,N'*-bis(2-hydroxyphenyl)imidazolinium chloride (H_2IPhenol•HCl), **32**

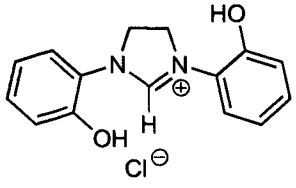

To a solution of *N,N'*-bis(2-methoxyphenyl)imidazolinium chloride (H_2IAnisole•HCl, **31**, 1.062 g, 3.330 mmol) in dry CH_2Cl_2 (15 mL) at 0 °C was added BBr_3 (3.0 equiv, 10.0 mL of a 1M solution in CH_2Cl_2, 10.0 mmol) at 0 °C. The solution was stirred for 2 h at 0 °C, then allowed to warm to room temperature and stirred for an additional 4 h, then reduced to dryness under vacuum. To the residue was added 15 mL brine and 5 mL distilled water. The solution was stirred for 2 h at 70 °C, then allowed to cool to room temperature. The brown precipitate was filtered off, washed with distilled water (2 × 10 mL), then acetone (3 × 10 mL) and dried under vacuum for 12 h to yield a beige powder. Yield 803 mg (83%). ^{1}H NMR (DMSO-d_6, 400 MHz, δ): 11.12 (br s, 2H, Ar O*H*; exchanges with D_2O), 9.72 (s, 1H, NC(*H*Cl)N; *H*; exchanges with D_2O), 7.39 (dd, $^3J_{HH}$ = 8.0 Hz, $^4J_{HH}$ = 1.5 Hz, 2H, Ar H_6), 7.23 (td, $^3J_{HH}$ = 7.7 Hz, $^4J_{HH}$ = 1.6 Hz, 2H, Ar H_4), 7.16 (dd, $^3J_{HH}$ = 8.2 Hz, $^4J_{HH}$ = 1.5 Hz, 2H, Ar H_3), 6.95 (td, $^3J_{HH}$ = 7.5 Hz, $^4J_{HH}$ =

1.5 Hz, 2H, Ar H_5), 4.54 (s, 4H, NCH_2). $^{13}C\{^1H\}$ NMR (DMSO-d_6, 100 MHz, δ): 156.1 (Ar C_1), 150.0 (N*C*(HCl)N), 128.6 (Ar C_4), 123.6 (Ar C_2), 122.7 (Ar C_6), 119.7 (Ar C_5), 117.0 (Ar C_3), 49.4 (NCH_2). $^{11}B\{^1H\}$ NMR (DMSO-d_6, δ): No signals other than that for the borosilicate glass (confirmed by running a control spectrum of DMSO-d_6).

2.3 Synthesis of $RuCl_2(L)(L')(=CHPh)$ Complexes

Note: In complexes containing two pyridine or 3-bromopyridine ligands, exchange of the pyridine ligands is observed on the NMR timescale (EXSY) and is sufficiently slow that independent NOESY correlations can be observed between Ru=C*H*Ph and H_o of the pyridine ligand cis to the alkylidene (py_c), and between the IMes Me_o or IPr $CH(CH_3)_2$ and H_o of the pyridine ligand trans to the alkylidene group (py_t).

2.3.1 Synthesis of $RuCl_2(IMes)(PCy_3)(=CHPh)$, **2a**

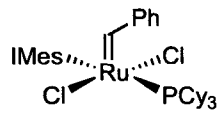

The known compound **2a** was prepared by the literature methods, [28-30] but in benzene solvent. A solution of IMes (**14**, 1.05 equiv, 5.4 g, 0.018 mol) in 50 mL benzene was added to a dark purple solution of $RuCl_2(PCy_3)_2(=CHPh)$ (**1**, 13.9 g, 0.017 mol) in 200 mL benzene. The solution was stirred for 1.5 h, then reduced to dryness under vacuum. To the residue was added 100 mL hexanes to give a slurry which was cooled in acetone-dry ice for 15 min, then filtered off. This purification procedure was then repeated. The pink powder was dried under vacuum for 16 h. Yield 12.3 g (86%). NMR data agree with the values reported.[28-30] ^1H NMR ($CDCl_3$, 500 MHz, δ): 19.43 (s, 1H, Ru=C*H*Ph), 8.95 (br s, 1H, Ph H_o), 7.39 (t, $^3J_{HH}$ = 7.3 Hz, 1H, Ph H_p), 7.12 (t, $^3J_{HH}$ = 7.3 Hz, 2H, Ph H_m), 7.05 (s, 2H, Mes C*H*), 7.04 (s, 1H, Ph H_o), 6.97 (s, 2H, NC*H*), 6.76 (br s, 1H, Mes C*H*), 5.92 (br s, 1H, Mes C*H*), 2.46 (br s, 6H, Mes Me_o), 2.35 (s, 6H, Mes Me_p), 2.23 (m, 3H, PCy_3 PC*H*), 2.17 (s, 3H, Mes Me_o), 1.96 (s, 3H, Mes Me_o), 1.62-0.85 (m, 30H, PCy_3 CH_2). $^{31}P\{^1H\}$ NMR ($CDCl_3$, δ): 32.4 ppm.

2.3.2 Synthesis of $RuCl_2(H_2IMes)(PCy_3)(=CHPh)$, **2b**

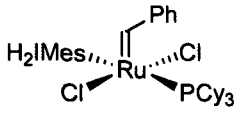

The known compound **2b** was prepared by the literature methods, [28,31] but at lower reaction and workup tempertures.

(a) To a slurry of H_2IMes•HBF_4 (**17**, 1.2 equiv, 1.1 g, 2.8 mmol) in 20 mL THF was added solid NaH (1.1 equiv, 61 mg, 2.5 mmol), followed by solid KO^{t}Bu (0.1 equiv, 26 mg, 0.2 mmol). The mixture was stirred for 1 h to afford a colourless solution containing minor amounts of a precipitate (presumed to be MBF_4; M = Na, K). This was added to a dark purple solution of $RuCl_2(PCy_3)_2$(=CHPh) (**1**, 1.9 g, 2.3 mmol) in 25 mL benzene. The mixture was stirred for 1 h at 60 °C to yield a red-brown solution, which was filtered through Celite. The filtrate was reduced to dryness under vacuum, and the residue was taken up in 20 mL hexanes with vigorous stirring. The resulting slurry was cooled to -94 °C in an acetone-liquid nitrogen bath for 10 min, filtered off, and repeated. The pink powder was dried under vacuum for 16 h. Yield 1.7 g (87%). NMR data agree with the values reported.[28,31] ^{1}H NMR ($CDCl_3$, δ): 19.14 (s, 1H, Ru=C*H*Ph), 8.99 (br s, 1H, Ph H_o), 7.35 (t, $^3J_{HH}$ = 7.2, 1H, Ph H_p), 7.10 (br t, 2H, Ph H_m), 7.02 (s, 2H, Mes C*H*), 6.94 (s, 1H, Ph H_o), 6.74 (br s, 1H, Mes C*H*), 5.82 (br s, 1H, Mes C*H*), 3.98 (s, 4H, NCH_2), 2.86-0.68 (m, 51H, Mes Me, PCy_3). ^{31}P{^{1}H} NMR (C_6D_6, δ): 30.3 ppm.

(b) Larger-scale synthesis of **2b**. The reaction was carried out as above, using 5 g of **1** (2.3 mmol) in 75 mL benzene. Other amounts: 2.9 g **17** (1.2 equiv, 7.3 mmol) in 20 mL THF; 146 mg KO^{t}Bu (0.2 equiv, 1.3 mmol), and 147 mg NaH (1.0 equiv, 6.1 mmol). The reaction time at 60 °C was extended to 2.5 h. Yield 4.2 g (80%).

2.3.3 Synthesis of $RuCl_2$(IMes)$(py)_2$(=CHPh), **3a**

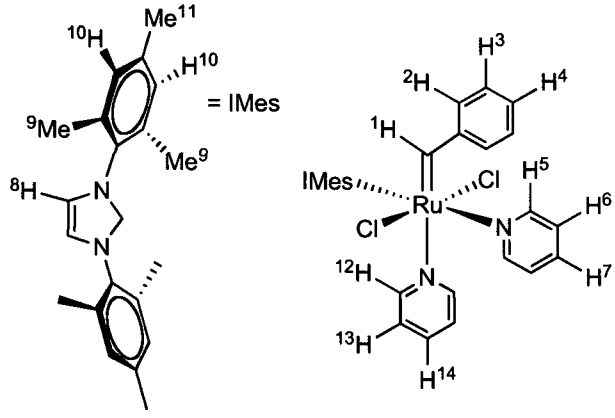

The known compound **3a** was prepared according to the literature procedure,[32] by addition of pyridine (py, 20 equiv, 2.0 mL, 24.7 mmol) to $RuCl_2$(IMes)(PCy_3)(=CHPh) (**2a**, 1.056 g, 1.247 mmol). The precipitate was washed with hexanes (3 × 10 mL), then dried under vacuum for 12 h to yield a dark green powder. Yield 769 mg (85%). NMR data agree with the values reported.[32] ^{1}H NMR (C_6D_6, δ): 19.97 (s, 1H, Ru=C*H*Ph; H^1), 9.11 (d, $^3J_{HH}$; 4.6 Hz, 2H, py_t H_o; H^{12}), 8.54 (d, $^3J_{HH}$ = 5.1 Hz, 2H, py_c H_o; H^5), 8.21 (d, $^3J_{HH}$ = 7.6 Hz, 2H, Ph H_o; H^2), 7.21 (t, $^3J_{HH}$ = 7.3 Hz, 1H, Ph H_p; H^4), 6.95 (t, $^3J_{HH}$ = 7.8 Hz, 2H, Ph H_m; H^3), 6.83 (t, $^3J_{HH}$ =

7.5 Hz, 1H, py$_t$ H_p; H^{14}), 6.59 (s, 4H, Mes C*H*; H^{10}), 6.50 (t, $^3J_{HH}$ = 6.5 Hz, 2H, py$_t$ H_m; H^{13}), 6.32 (t, $^3J_{HH}$ = 7.5 Hz, 1H, py$_c$ H_p; H^7), 6.30 (s, 2H, NC*H*; H^8), 6.03 (t, $^3J_{HH}$ = 6.6 Hz, 2H, py$_c$ H_m; H^6), 2.51 (br s, 12H, Mes Me$_o$; H^9), 2.04 (s, 6H, Mes Me$_p$; H^{11}). ^{1}H NMR ($CDCl_3$, 500 MHz, δ) 19.45 (s, 1H, Ru=C*H*Ph), 8.73 (d, $^3J_{HH}$ = 4.3 Hz, 2H, py$_t$ H_o), 7.99 (d, $^3J_{HH}$ = 5.2 Hz, 2H, py$_c$ H_o), 7.73 (d, $^3J_{HH}$ = 7.8 Hz, 2H, Ph H_o), 7.59 (t, $^3J_{HH}$ = 7.5 Hz, 1H, py$_t$ H_p), 7.45 (t, $^3J_{HH}$ = 7.3 Hz, 1H, Ph H_p), 7.32 (t, $^3J_{HH}$ = 7.5 Hz, 1H, py$_c$ H_p), 7.16 (t, $^3J_{HH}$ = 6.4 Hz, 2H, py$_t$ H_m), 7.04 (m, 4H, Mes C*H*, NC*H*), 6.80 (m, 6H, py$_c$ H_m, Ph H_m, Mes C*H*), 2.35-2.20 (m, 18H, Mes Me). ^{31}P{^{1}H} NMR ($CDCl_3$, δ): no signals. ^{1}H NMR assignments confirmed by ^{1}H-^{1}H COSY, ^{1}H-^{13}C HMBC, NOESY-EXSY (see Appendix A). Electronic spectroscopy: $RuCl_2(IMes)(py)_2(=CHPh)$ (**3b**, 11.0 mg, 0.0152 mmol) was dissolved in 5.0 mL of benzene (3.03 mM), λ_{max} = 13,600 cm^{-1} (735 nm); ε = 221 cm^{-1}M^{-1}.

2.3.4 Synthesis of $RuCl_2(H_2IMes)(py)_2(=CHPh)$, **3b**

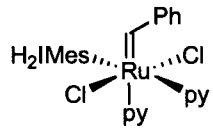

Synthesis of known **3b** was carried out by the reported method[33] by addition of pyridine (py, 15 equiv, 0.75 mL, 9.3 mmol) to $RuCl_2(H_2IMes)(PCy_3)(=CHPh)$ (**2b**, 500 mg, 0.589 mmol) as described for **3a** above. Yield 375 mg (88%). NMR data agree with the values reported.[33] ^{1}H NMR ($CDCl_3$, δ): 19.18 (s, 1H, Ru=C*H*Ph), 8.64 (d, $^3J_{HH}$ = 4.1 Hz, 2H, py$_t$ H_o), 7.83 (d, $^3J_{HH}$ = 5.0 Hz, 2H, py$_c$ H_o), 7.68 (br s, 1H, py$_t$ H_p), 7.64 (d, $^3J_{HH}$ = 7.6 Hz, 2H, Ph H_o), 7.50-7.41 (m, 3H, py$_c$ H_p, Ph H_p), 7.25 (m, 2H, py$_t$ H_m), 7.07 (t, $^3J_{HH}$ = 7.6 Hz, 2H, Ph H_m), 7.02 (br, 2H, Mes C*H*), 6.95 (t, $^3J_{HH}$ = 6.7 Hz, 2H, py$_c$ H_m), 6.75 (br, 2H, Mes C*H*), 4.16 (br s, 2H, NCH_2), 4.06 (br s, 2H, NCH_2), 2.64 (br s, 6H, Mes Me), 2.39-2.17 (m, 12H, Mes Me). ^{31}P{^{1}H} NMR ($CDCl_3$, δ): null signal.

2.3.5 Synthesis of $RuCl_2(IMes)(py^*)_2(=CHPh)$, **33a**

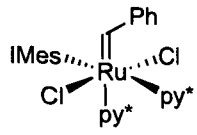

While **33a** is a known compound,† its synthesis and NMR data have not been reported. It was prepared by the method reported for its H_2IMes analogue[33] **33b**, by addition of 3-bromopyridine (py*, 10 equiv, 2.5 mL, 25.9 mmol) to $RuCl_2(IMes)(PCy_3)(=CHPh)$ (**2a**, 2.2 g, 2.6 mmol). The precipitate was washed with hexanes (3 × 10 mL), then dried under vacuum for 12 h to yield a light green powder. Yield 2.0 g (89%). ^{1}H

† Conrad, J.C.; Snelgrove, J.L.; Eelman, M.D.; Hall, S.; Fogg, D.E. *J. Mol. Catal. A* **2006**, *254*, 105-110.

NMR (C_6D_6, δ): 19.78 (s, 1H, Ru=C*H*Ph), 9.19 (s, 1H, py_t H_2), 9.00 (s, 1H, py_c H_2), 8.84 (d, $^3J_{HH}$ = 3.9 Hz, 1H, py_t H_6), 8.29 (d, $^3J_{HH}$ = 4.1 Hz, 1H, py_c H_6), 8.14 (d, $^3J_{HH}$ = 7.4 Hz, 2H, Ph H_o), 7.18 (br t, 1H, Ph H_p), 6.98 (d, $^3J_{HH}$ = 8.2 Hz, 1H, py_t H_4), 6.92 (t, $^3J_{HH}$ = 6.8 Hz, 2H, Ph H_m), 6.59 (s, 4H, Mes C*H*), 6.42 (d, $^3J_{HH}$ = 7.7 Hz, 1H, py_c H_4), 6.26 (s, 2H, NC*H*), 6.14 (t, $^3J_{HH}$ = 6.3 Hz, 1H, py_t H_5), 5.59 (t, $^3J_{HH}$ = 6.0 Hz, 1H, py_c H_5), 2.47 (br s, 12H, Mes Me_o), 2.05 (s, 6H, Mes Me_p). ^{1}H NMR ($CDCl_3$, 500 MHz, δ): 19.34 (s, 1H, Ru=C*H*Ph), 8.85 (s, 1H, py_t H_2), 8.72 (d, $^3J_{HH}$ = 4.2 Hz, 1H, py_c H_2), 8.16 (s, 1H, py_t H_6), 7.93 (d, $^3J_{HH}$ = 5.1 Hz, 1H, py_c H_6), 7.74 (m, 3H, py_t H_4, Ph H_o), 7.46 (m, 2H, py_c H_4, Ph H_p), 7.09-7.03 (m, 5H, py_t H_5, Ph H_m, Mes C*H*), 6.82 (br s, 4H, Mes C*H*, NC*H*), 6.69 (t, $^3J_{HH}$ = 6.7 Hz, 1H, py_c H_5), 2.37-2.15 (m, 18H, Mes Me).

2.3.6 Synthesis of $RuCl_2(H_2IMes)(py^*)_2(=CHPh)$, **33b**

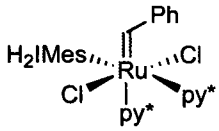

Synthesis of known **33b** was carried out by the reported method[34] (as also described for **3a** above) by addition of 3-bromopyridine (py*, 20 equiv, 1.0 mL, 10.4 mmol) to $RuCl_2(H_2IMes)(PCy_3)(=CHPh)$ (**2b**, 489 mg, 0.576 mmol). The precipitate was washed with hexanes (3 × 5 mL) and pentane (3 × 5 mL), then dried under vacuum for 12 h to yield a dark green powder. Yield 484 mg (95%). NMR data agree with the values reported.[34] ^{1}H NMR ($CDCl_3$, δ): 19.10 (s, 1H, Ru=C*H*Ph), 8.72 (s, 1H, py_t H_2), 8.57 (s, 1H, py_c H_2), 7.97 (s, 1H, py_t H_6), 7.79 (s, 1H, py_c H_6), 7.73 (s, 1H, py_t H_4), 7.64 (d, $^3J_{HH}$ = 7.5 Hz, 2H, Ph H_o), 7.58 (s, 1H, py_c H_4), 7.49 (t, $^3J_{HH}$ = 7.3 Hz, 1H, Ph H_p), 7.18 (br s, 1H, py_t H_5), 7.09 (t, $^3J_{HH}$ = 7.7 Hz, 2H, Ph H_m), 7.03 (br s, 2H, Mes C*H*), 6.81 (br s, 1H, py_c H_5), 6.75 (br s, 2H, Mes C*H*), 4.16 (br s, 2H, NCH_2), 4.07 (br s, 2H, NCH_2), 2.63 (br s, 6H, Mes Me), 2.42-2.16 (m, 12H, Mes Me). ^{31}P{^{1}H} NMR ($CDCl_3$, δ): no signals.

2.3.7 Synthesis of $RuCl_2(IPr)(PCy_3)(=CHPh$, **34**

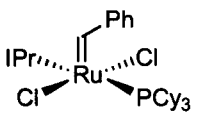

The known compound **34** was prepared by a minor variation on the literature methods,[22,30] involving the use of lower temperatures, and different solvents for reaction and workup.

(a) In situ. A solution of IPr (**20**, 1.05 equiv, 10 mg, 0.024 mol) in 0.4 mL C_6D_6 was transferred from a 1-dram vial to a 1-dram vial charged with solid $RuCl_2(PCy_3)_2(=CHPh)$ (**1**, 19 mg, 0.023 mmol) and equipped with a stirbar. Residues of IPr were transferred to the reaction by rinsing the IPr vessel with C_6D_6 (2 × 0.4 mL).The solution was stirred for 2.5 h at room temperature,

following which ^{1}H NMR analysis showed 93% conversion to the product, **34**. The NMR sample was heated in 10° intervals to 60 °C, allowing to equilibrate for 5 minutes at each interval, and then measuring the 1H NMR spectrum. Complete reaction was evident after the equilibration period at 60 °C. ^{1}H NMR (C_6D_6, δ): 20.62 (s, 1H, Ru=C*H*Ph, **1**), 20.05 (s, 1H, Ru=C*H*Ph, **34**).

(b) Small preparative scale. To a solution of $RuCl_2(PCy_3)_2$(=CHPh) (**1**, 927 mg, 1.127 mmol) in benzene (10 mL) was added a solution of IPr (**20**, 1.05 equiv, 455 mg, 1.172 mmol) in benzene (10 mL). The solution was stirred for 3 h at 45 °C, then reduced to dryness under vacuum. The residue was taken up in 15 mL hexanes with vigorous stirring, after which the slurry cooled to -94 °C in an acetone-liquid nitrogen bath for 10 min and filtered off. The purification process was repeated and the pink powder dried under vacuum for 12 h. Yield 755 mg (72%). NMR data agree with the values reported.[22,30] ^{1}H NMR ($CDCl_3$, δ): 20.05 (s, 1H, Ru=C*H*Ph), 8.35 (br s, 2H, Ph H_o), 7.31 (s, 4H, Ar H_m), 7.22 (t, $^3J_{HH}$ = 7.2 Hz, 1H, Ph H_p), 7.04 (t, $^3J_{HH}$ = 7.5 Hz, 2H, Ar H_p), 6.77 (s, 2H, NC*H*), 6.70 (s, 1H, Ph H_m), 6.66 (s, 1H, Ph H_m), 3.89 (quintet, $^3J_{HH}$ = 6.5 Hz, 2H, Ar C*H*$(CH_3)_2$), 3.44 (quintet, $^3J_{HH}$ = 6.5 Hz, 2H, Ar C*H*$(CH_3)_2$), 2.42 (m, 3H, PCy_3 PC*H*), 1.73-0.97 (m, 54H, PCy_3 CH_2, Ar CH(CH_3)$_2$). ^{31}P{^{1}H} NMR (C_6D_6, δ): 30.9 ppm.

(c) Larger-scale synthesis. The reaction was carried out as in (b) using 3.5 g of **1** (4.2 mmol) in 50 mL benzene, to which was added solution of IPr (**20**, 1.05 equiv, 1.7 g, 4.4 mmol) in 10 mL benzene. To the residue was added hexanes (20 mL), the stirring slurry was then cooled to -94 °C in an acetone-liquid nitrogen bath for 10 min, filtered and repeated. The brown powder was dried under vacuum for 12 h. Yield 2.6 g (65%).

2.3.8 Synthesis of $RuCl_2(IPr)(py)_2$(=CHPh), **35**

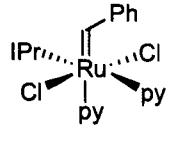

Synthesis of compound **35** was carried out as described for **3a**. Pyridine (py, 15 equiv, 1.5 mL, 18.6 mmol), $RuCl_2(IPr)(PCy_3)$(=CHPh) (**34**, 1.1 g, 1.2 mmol). The precipitate was washed with hexanes (3 × 5 mL) and pentane (3 × 5 mL), then dried under vacuum for 12 h to yield a dark green powder. Yield 911 mg (93%). ^{1}H NMR (C_6D_6, δ): 19.75 (s, 1H, Ru=C*H*Ph), 8.63 (d, $^3J_{HH}$ = 4.1 Hz, 2H, py_t H_o), 8.37 (d, $^3J_{HH}$ = 5.1 Hz, 2H, py_c H_o), 7.89 (d, $^3J_{HH}$ = 7.6 Hz, 2H, Ph H_o), 7.30 (t, $^3J_{HH}$ = 7.5 Hz, 2H, Ar H_p), 7.20 (br d, $^3J_{HH}$ = 8.7 Hz, 4H, Ar H_m), 7.17 (br t, 1H, Ph H_p), 6.93 (t, $^3J_{HH}$ = 7.6 Hz, 1H, py_t H_p), 6.88 (t, $^3J_{HH}$ = 7.6 Hz,

2H, Ph H_m), 6.75 (br s, 2H, NC*H*), 6.60 (t, $^3J_{HH}$ = 6.2 Hz, 2H, py$_t$ H_m), 6.39 (t, $^3J_{HH}$ = 7.4 Hz, 1H, py$_c$ H_p), 6.07 (t, $^3J_{HH}$ = 6.6 Hz, 2H, py$_c$ H_m), 3.63 (br s, 4H, Ar C*H*(CH$_3$)$_2$), 1.47 (br s, 12 H, Ar CH(C*H*$_3$)$_2$-Ru), 1.11 (d, $^3J_{HH}$ = 6.8 Hz, 12 H, Ar CH(C*H*$_3$)$_2$-NCH). ^{13}C{^{1}H} NMR (C$_6$D$_6$, 75 MHz, δ): 312.6 (Ru=*C*HPh), 187.3 (N*C*N), 153.3 (py$_c$ C_o), 152.7 (Ph C_i), 150.6 (py$_t$ C_o), 148.0 (Ar C_o), 137.4 (Ar C_i), 135.7 (py$_c$ C_p), 135.1 (py$_t$ C_p), 130.5 (Ar C_p), 130.2 (Ph C_m), 129.7 (Ar C_m), 128.6 (Ph C_p), 128.4 (Ph C_o), 126.1 (N*C*H), 124.4 (Ar C_m), 123.3 (py$_t$ C_m), 123.1 (py$_c$ C_m), 28.9 (Ar *C*H(CH$_3$)$_2$), 26.7 (Ar CH(*C*H$_3$)$_2$-NCH), 23.3 (Ar CH(*C*H$_3$)$_2$-Ru). ^{1}H and ^{13}C{^{1}H} NMR assignments confirmed by ^{1}H-^{1}H COSY, ^{1}H-^{13}C HMQC, ^{1}H-^{13}C HMBC, NOESY-EXSY (see Appendix A). Note: The IPr isopropyl methyls are inequivalent: one methyl of each pair is oriented toward the NHC backbone, with the protons of which it correlates by NOESY-NMR; the other points toward the Ru center and shows NOESY correlations with the py$_t$ H_o and Ph H_o signals.

2.3.9 Synthesis of $RuCl_2(IPr)(py^*)_2(=CHPh)$, **36**

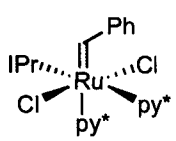

Neat 3-bromopyridine (py*, 15 equiv, 0.75 mL, 7.785 mmol) was added to $RuCl_2(IPr)(PCy_3)(=CHPh)$ (**34**, 409 mg, 0.439 mmol) and the solution was stirred for 5 min. Pentane (15 mL) was then added, and the solution was concentrated under vacuum until a green precipitate appeared. The solid was filtered off, washed with pentane (3 × 10 mL), then dried under vacuum for 12 h to yield a light green powder. Yield 335 mg (79%). ^{1}H NMR (C$_6$D$_6$, 500 MHz, δ): 19.73 (s, 1H, Ru=C*H*Ph), 8.88 (br s, 1H, py$_t$ H_2), 8.83 (br s, 1H, py$_c$ H_2), 8.49 (br s, 1H, py$_t$ H_6), 8.18 (br s, 1H, py$_c$ H_6), 7.92 (d, $^3J_{HH}$ = 7.6 Hz, 2H, Ph H_o), 7.20 (t, $^3J_{HH}$ = 7.6 Hz, 2H, Ar H_p), 7.15 (br s, 1H, Ph H_p), 7.12 (t, $^3J_{HH}$ = Hz, 4H, Ar H_m), 6.99 (br d, $^3J_{HH}$ = 6.9 Hz, 1H, py$_t$ H_4), 6.86 (t, $^3J_{HH}$ = 7.7 Hz, 2H, Ph H_m), 6.70 (br s, 2H, NC*H*), 6.48 (br s, 1H, py$_c$ H_4), 6.15 (b s, 1H, py$_t$ H_5), 5.63 (br s, 1H, py$_c$ H_5), 3.64 (br s, 4H, IPr C*H*(CH$_3$)$_2$), 1.49 (br s, 12 H, IPr CH(C*H*$_3$)$_2$-Ru), 1.10 (d, $^3J_{HH}$ = 6.9 Hz, 12 H, IPr CH(C*H*$_3$)$_2$-NCH). ^{13}C{^{1}H} NMR (C$_6$D$_6$, 125 MHz, δ): 315.3 (Ru=*C*HPh), 185.1 (N*C*N), 153.7 (py$_c$ C_2), 152.8 (Ph C_i), 151.6 (py$_t$ C_2), 151.5 (py$_c$ C_6), 148.6 (py$_t$ C_6), 147.8 (Ar C_o), 138.3 (py$_c$ C_4), 138.0 (py$_t$ C_4), 137.7 (Ar C_i), 130.5 (Ar C_p), 130.1 (Ph C_o), 129.9 (Ph C_p), 128.4 (Ph C_m), 126.3 (N*C*H), 124.2 (Ar C_m, py$_t$ C_5), 123.8 (py$_c$ C_5), 120.6 (py$_c$ C_3), 119.1 (py$_t$ C_3), 28.8 (IPr *C*H(CH$_3$)$_2$), 26.6 (IPr CH(*C*H$_3$)$_2$-NCH), 23.2 (IPr CH(*C*H$_3$)$_2$-Ru). ^{1}H and ^{13}C{^{1}H} NMR assignments confirmed by ^{1}H-^{1}H COSY, ^{1}H-^{13}C HMQC, ^{1}H-^{13}C HMBC, NOESY-EXSY (see Appendix A). Note: The IPr isopropyl

methyls are inequivalent in the plane of the aromatic ring with one methyl of the pair (Ar CH(CH_3)$_2$-NCH) oriented towards the NHC backbone and showing a NOESY correlation with the NC*H* backbone signal, the other methyl of the pair (Ar CH(CH_3)$_2$-Ru) is oriented towards the Ru center and shows NOESY correlations with the py$_t$ H_6 and Ph H_o signals.

2.3.10 In situ Synthesis of $RuCl_2(H_2ITol)(PCy_3)$(=CHPh), **37**

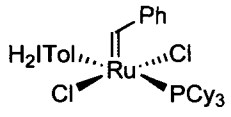

The known compound **37** was prepared by variation of the literature method,[24] involving the use of additional equivalents of NHC, different reaction solvents, and purification methods. To a slurry of H_2ITol•HCl (**27**, 1.1 equiv, 96 mg, 0.334 mmol) in THF (3 mL) was added solid potassium hexamethyldisilazane (KHMDS, 1.1 equiv, 146 mg, 1.3 mmol), the solution turned clear instantly. The solution was stirred for 30 min, a yellow precipitate formed, the solution was added to a dark purple solution of $RuCl_2(PCy_3)_2$(=CHPh) (**1**, 250 mg, 0.304 mmol) in benzene (10 mL). The suspension was stirred for 1 h at room temperature, $^{31}P\{^1H\}$ NMR analysis indicated no conversion. Additional equivalents of H_2ITol were deprotonated similarly to above, but with only 5 min of stirring before the addition to **1**. The reaction was monitored In situ by $^{31}P\{^1H\}$ NMR 1 h after each addition (conversion shown in Chapter 5, Figure 2), followed by addition of H_2ITol [$RuCl_2(PCy_3)_2$(=CHPh) (**1**, 36.8 ppm) → $RuCl_2(H_2ITol)(PCy_3)$(=CHPh) (**37**, 27.4 + 24.7 ppm) + PCy_3 (10.8 ppm)]. At 90% conversion, the red-brown suspension was filtered through Celite and the filtrate was reduced to dryness under vacuum. To the residue was added hexanes (5 mL), the stirring slurry was then cooled to -94 °C in an acetone-liquid nitrogen bath for 10 min, filtered and repeated. The brown powder was dried under vacuum for 12 h. Yield 200 mg (83%). NMR data agree with the values reported.[24] ^1H NMR ($CDCl_3$, δ): 19.07 (s, 1H, Ru=C*H*Ph), 8.28 (d, $^3J_{HH}$ = 6.5 Hz, 1H, Ph H_o), 7.39-7.30 (m, 5H, Ar *H*), 7.15-7.02 (m, 4H, Ar *H*), 6.81-6.71 (m, 1H, Ar *H*), 6.64 (d, $^3J_{HH}$ = 6.5 Hz, 1H, Ar *H*), 6.52-6.32 (m, 1H, Ar *H*), 4.11-3.80 (m, 4H, NCH_2), 2.66-0.77 (m, 39H, PCy_3, Ar Me). $^{31}P\{^1H\}$ NMR ($CDCl_3$, δ): 30.5 and 22.4 ppm.

References page 39

2.3.11 Synthesis of $RuCl_2(H_2ITol)(py)_2(=CHPh)$, **38**

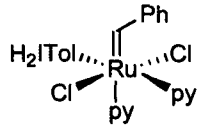

Synthesis of known **38** was carried out as described for **3a**. Pyridine (py, 40 equiv, 0.75 mL, 9.3 mmol), $RuCl_2(H_2ITol)(PCy_3)(=CHPh)$ (**37**, 188 mg, 0.237 mmol). The precipitate was washed with hexanes (3 × 5 mL) and pentane (3 × 5 mL), then dried under vacuum for 12 h to yield a dark green powder. Yield 135 mg (85%). ^1H NMR (C_6D_6, δ): 19.31 (s, 1H, Ru=C*H*Ph), 9.52 (d, $^3J_{HH}$ = 7.4 Hz, 1H, Ar *H*), 8.55 (br s, 2H, Ar *H*), 8.51 (d, $^3J_{HH}$ = 5.1 Hz, 2H, Ar *H*), 7.91 (d, $^3J_{HH}$ = 7.4 Hz, 2H, Ar *H*), 7.51 (br s, 1H, Ar *H*), 7.26 (m, 1H, Ar *H*), 7.22 (m, 1H, Ar H), 7.02-6.86 (m, 7H, Ar *H*), 6.81 (t, $^3J_{HH}$ = 6.6 Hz, 1H, Ar *H*), 6.66 (t, $^3J_{HH}$ = 5.9 Hz, 2H, Ar *H*), 6.53 (t, $^3J_{HH}$ = 7.5 Hz, 1H, Ar *H*), 6.23 (t, $^3J_{HH}$ = 6.7 Hz, 2H, Ar C*H*), 3.61 (m, 1H, NCH_2), 3.50 (m, 1H, NCH_2), 3.34 (m, 1H, NCH_2), 3.22 (m, 1H, NCH_2), 2.51 (s, 3H, Ar Me), 2.32 (br s, 3H, Mes Me). $^{31}P\{^1H\}$ NMR ($CDCl_3$, δ): no signals.

2.4 General Procedures for the Synthesis of Thallium Salts

Note: The toxicity of thallium (particularly in the +1 oxidation state) is well established, and the subject has been reviewed.[35] Care must be taken to prevent introduction into the body by inhalation, by ingestion via contaminated hands or gloves, or through the skin. All thallium reagents and wastes, including contaminated solvents, were handled using double-glove and secondary containment procedures, with separate disposal of all wastes in accordance with government regulations. Thallium ethoxide (TlOEt) is a very dense clear liquid, which was weighed instead of measured out using a syringe. Over time TlOEt degrades forming a black precipitate that is easily decanted off.

To a flask containing TlOEt (3.0 g, 0.012 mol) in 5 mL Et_2O was added HOC_6Br_5 (1.05 equiv, 6.4 g, 0.013 mol) as a slurry in diethyl ether (15 mL). The resulting solution was stirred for 12 h, then precipitated with 20 mL hexanes and filtered. The resulting solid was washed with hexanes (3 x 8 mL), then dried under vacuum for 12 h to yield a cream-coloured powder. Yield 7.3 g (85%).

References page 39

2.5 Synthesis and Characterization of RuXX'(L)(L)(=CHPh) Complexes

2.5.1 Characterization of Ru(*o*-cat)(IMes)(py)(=CHPh), **4a**

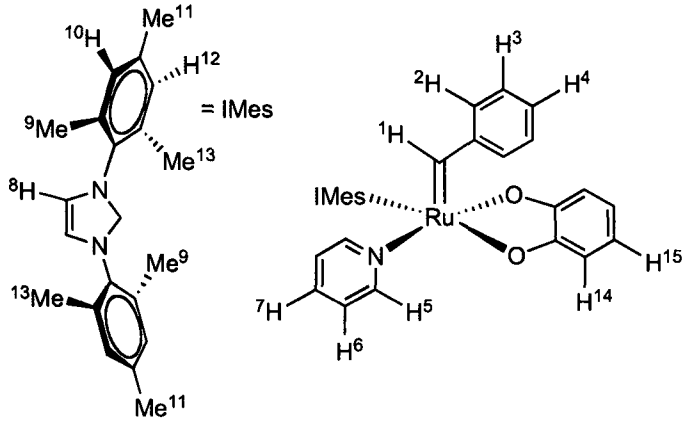

^{1}H NMR ($CDCl_3$, 500 MHz, δ) 16.99 (s, 1H, Ru=C*H*Ph; H^1), 8.36 (d, $^3J_{HH}$ = 6.6 Hz, 2H, py H_o; H^5), 7.45 (t, $^3J_{HH}$ = 7.8 Hz, 1H, py H_p; H^7), 7.28 (d, $^3J_{HH}$ = 7.0 Hz, 2H, Ph H_o; H^2), 7.17 (t, $^3J_{HH}$ = 7.5 Hz, 1H, Ph H_p; H^4), 7.08 (s, 2H, NC*H*; H^8), 6.94 (t, $^3J_{HH}$ = 6.1 Hz, 2H, py H_m; H^6), 6.89 (t, $^3J_{HH}$ = 7.2 Hz, 2H, Ph H_m; H^3), 6.85 (s, 2H, Mes C*H*; H^{10}), 6.71 (t, $^3J_{HH}$ = 7.0 Hz, 2H, cat CH_o; H^{14}), 6.58 (s, 2H, Mes C*H*; H^{12}), 6.49 (t, $^3J_{HH}$ = 7.0 Hz, 1H, cat CH_m; H^{15}), 6.36 (t, $^3J_{HH}$ = 7.0 Hz, 1H, cat CH_m; H^{15}), 2.22 (s, 6H, Mes Me$_p$; H^{11}), 2.16 (s, 6H, Mes Me$_o$; H^9), 1.88 (s, 6H, Mes Me$_o$; H^{13}). ^{1}H NMR assignments confirmed by ^{1}H-^{1}H COSY, ^{1}H-^{13}C HMBC, NOESY-EXSY (see Appendix A).

2.5.2 Synthesis of RuCl(κ^2-*O,Br*-OC_6Br_5)(IMes)(py)(=CHPh), **5**

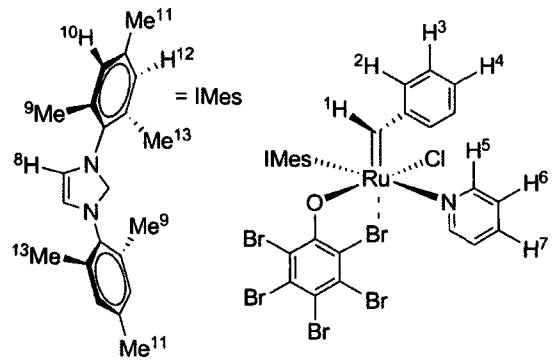

(a) Improved Synthesis of RuCl(κ^2-*O,Br*-OC_6Br_5)(IMes)(py)(=CHPh), **5**. Solid $TlOC_6Br_5$ (1.1 equiv, 485 mg, 0.701 mmol) was added to a solution of $RuCl_2$(IMes)$(py)_2$(=CHPh) (**3a**, 455 mg, 0.627 mmol) in benzene (50 mL). The green solution was stirred overnight (12 h), after which the white precipitate of TlCl was removed by filtration through Celite. The Celite was washed with CH_2Cl_2 (2 × 10 mL) and the combined solutions were reduced to dryness under vacuum. The residue was redissolved in a minimum of CH_2Cl_2 (25 mL), precipitated by reduction of solution volume (to 5 mL) under vacuum and filtered. The resulting solid was washed with pentane (-35 °C, 2 × 5 mL), then dried under vacuum (16 h) to yield a bright green powder. Yield 462 mg (61%). ^{1}H NMR ($CDCl_3$, 500 MHz, δ): 19.31 (s, 1H, Ru=C*H*Ph; H^1), 8.01 (br s, 2H, py H_o; H^5), 7.88 (d, J_{HH} =

7.6 Hz, 2H, Ph H_o; H^2), 7.39 (t, J_{HH} = 7.1 Hz, 1H, Ph H_p; H^4), 7.24 (t, J_{HH} = 7.9 Hz, 1H, py H_p; H^7), 7.04 (t, J_{HH} = 7.4 Hz, 2H, Ph H_m; H^3), 6.97 (s, 2H, NC*H*; H^8), 6.87 (s, 2H, Mes C*H*; H^{10}), 6.73 (t, J_{HH} = 5.7 Hz, 2H, py H_m; H^6), 6.54 (s, 2H, Mes C*H*; H^{12}), 2.31 (s, 6H, Mes Me_o; H^9), 2.23 (s, 6H, Mes Me_p; H^{11}), 1.86 (s, 6H, Mes Me_o; H^{13}). ^{1}H NMR (C_6D_6, 500 MHz, δ): 19.69 (s, 1H, Ru=C*H*Ph; H^1), 8.32 (br s, 2H, py H_o; H^5), 8.08 (br s, 2H, Ph H_o; H^2), 7.12 (br s, 1H, Ph H_p; H^4), 6.89 (t, $^3J_{HH}$ = 7.5 Hz, 2H, Ph H_m; H^3), 6.77 (s, 2H, Mes C*H*; H^{10}), 6.37 (s, 2H, Mes C*H*; H^{12}), 6.19 (t, $^3J_{HH}$ = 7.1 Hz, 1H, py H_p; H^7), 6.15 (s, 2H, NC*H*; H^8), 5.92 (br s, 2H, py H_m; H^6), 2.47 (s, 6H, Mes Me_o; H^9), 2.11 (s, 6H, Mes Me_p; H^{11}), 1.99 (s, 6H, Mes Me_o; H^{13}). ^{1}H NMR assignments were confirmed by ^{1}H-^{1}H COSY, ^{1}H-^{13}C HMBC, and NOESY-EXSY analysis (for spectra, see Appendix A). Electronic spectroscopy: RuCl(κ^2-*O,Br*-OC_6Br_5)(IMes)(py)(=CHPh) (**5**, 21.1 mg, 0.0192 mmol) was dissolved in 10.0 mL of benzene (1.92 mM), λ_{max} = 13,300 cm^{-1} (752 nm); ε = 269 $cm^{-1}M^{-1}$.

Variants on this process (including our earlier procedure[32]) gave less satisfactory results. Washing the Celite with benzene and reprecipitating from benzene-hexanes at -35 °C caused co-formation of small amounts of an unidentified byproduct, characterized by a benzylidene proton singlet at 19.81 (16%; C_6D_6), in addition to that for **5**. Use of THF as a reaction solvent resulted in a lower proportion of **5** (76%), with singlets for by-products being evident at 18.16 ppm (19%) and 18.38 ppm (2%), in addition to a small amount (3%) of the unassigned species at 19.80 ppm. Identification of these species was not pursued.

(b) Time profile for formation of **5**. A solution of 1,3,5-trimethoxybenzene (1.7 mg, 0.010 mmol) (used as internal NMR standard) in 2.0 mL C_6D_6 was added to $RuCl_2$(IMes)$(py)_2$(=CHPh) (**3a**, 30.4 mg, 0.042 mmol). One 1.0 mL aliquot of this solution was transferred to an NMR tube (t_0); the other was added to solid $TlOC_6Br_5$ (1.1 equiv, 16.1 mg, 0.023 mmol) and added to an NMR tube. The reaction was monitored by ^{1}H NMR spectroscopy every 5 min for 15 min, every 15 min for the next hour, then every hour to 7 h at which point the reaction was terminated prior to complete conversion. The benzylidene proton singlets for starting **3a** (19.97 ppm) and desired **5** (19.69 ppm) were integrated at each time interval to generate the conversion plot (Chapter 3, Figure 2). No by-products were observed. A parallel reaction carried out with stirring in a reaction vial in the glovebox proceeded more rapidly, formation of **5** being complete in 3 h.

References page 39

2.6 Chlorination of Ruthenium Benzylidene Complexes by $CDCl_3$

2.6.1 Chlorination of $RuCl_2(H_2IMes)(py)_2(=CHPh)$, **3b**

A solution of $RuCl_2(H_2IMes)(py)_2(=CHPh)$ (**3b**, 7.3 mg, 0.010 mmol) in 0.75 mL $CDCl_3$ in a screw-capped 1 dram vial was monitored by ^1H NMR every ca. 3-4 days for the first 2 weeks followed by 2 week intervals. The solution gradually turned brown. Additional signals appeared in the aromatic and aliphatic regions after 1 week. After 8 weeks, no signals were apparent in the benzylidene region (15-20 ppm).

2.6.2 Formation of $RuCl_2(\kappa^2\text{-}O,Br\text{-}OC_6Br_5)(IMes)(py)$ **6** by Chlorination of **5**

A bright green solution of $RuCl(\kappa^2\text{-}O,Br\text{-}OC_6Br_5)(IMes)(py)(=CHPh)$ (**5**, 10.0 mg, 0.009 mmol) in 0.75 mL $CDCl_3$ in a screw-capped NMR tube was allowed to stand for 2 days at room temperature. After this time the solution was dark green and no signals were apparent in the benzylidene region (15-20 ppm). Dark green crystals were obtained from the solution and analyzed by single crystal X-ray diffraction (XRD). See Appendix B for further XRD details.

2.7 References

(1) Armarego, W.L.F.; Perrin, D.D., *Purification of Common Laboratory Chemicals, 4th Edition*; Butterworth-Heinemann: Oxford, 1997; p 529.

(2) Schwab, P.; Grubbs, R.H.; Ziller, J.W. *J. Am. Chem. Soc.* **1996**, *118*, 100-110.

(3) Arduengo, A.J.; Krafczyk, R.; Schmutzler, R.; Craig, H.A.; Goerlich, J.R.; Marshall, W.J.; Unverzagt, M. *Tetrahedron* **1999**, *55*, 14523-14534.

(4) Monfette, S.; Fogg, D.E. *Organometallics* **2006**, *25*, 1940-1944.

(5) Frisch, M.J.; Trucks, G.W.; Schlegel, H.B.; Scuseria, G.E.; Robb, M.A.; Cheeseman, J.R.; J. A. Montgomery, J.; Vreven, T.; Kudin, K.N.; Burant, J.C.; Millam, J.M.; Iyengar, S.S.; Tomasi, J.; Barone, V.; Mennucci, B.; Cossi, M.; Scalmani, G.; Rega, N.; Petersson, G.A.; Nakatsuji, H.; Hada, M.; Ehara, M.; Toyota, K.; Fukuda, R.; Hasegawa, J.; Ishida, M.; Nakajima, T.; Honda, Y.; Kitao, O.; Nakai, H.; Klene, M.; Li, X.; Knox, J.E.; Hratchian, H.P.; Cross, J.B.; Bakken, V.; Adamo, C.; Jaramillo, J.; Gomperts, R.; Stratmann, R.E.; Yazyev, O.; Austin, A.J.; Cammi, R.; Pomelli, C.; Ochterski, J.W.; Ayala, P.Y.; Morokuma, K.; Voth, G.A.; Salvador, P.; Dannenberg, J.J.; Zakrzewski, V.G.; Dapprich, S.; Daniels, A.D.; Strain, M.C.; Farkas, O.; Malick, D.K.; Rabuck, A.D.; Raghavachari, K.; Foresman, J.B.; Ortiz, J.V.; Cui, Q.; Baboul, A.G.; Clifford, S.;

Cioslowski, J.; Stefanov, B.B.; Liu, G.; Liashenko, A.; Piskorz, P.; Komaromi, I.; Martin, R.L.; Fox, D.J.; Keith, T.; Al-Laham, M.A.; Peng, C.Y.; Nanayakkara, A.; Challacombe, M.; Gill, P.M.W.; Johnson, B.; Chen, W.; Wong, M.W.; Gonzalez, C.; Pople, J.A. *Gaussian 03*, Revision C.02; Gaussian, Inc.: Wallingford, CT, 2003.

(6) Becke, A.D. *J. Chem. Phys.* **1993**, *98*, 5648-5652.

(7) Lee, C.; Yang, W.; Parr, R.G. *Phys. Rev. B* **1988**, *37*, 785-789.

(8) Godbout, N.; Salahub, D.R.; Andzelm, J.; Wimmer, E. *Can. J. Chem.* **1992**, *70*, 560-571.

(9) Schaefer, A.; Huber, C.; Ahlrichs, R. *J. Chem. Phys.* **1994**, *100*, 5829-5835.

(10) Gonzalez, C.; Schlegel, H.B. *J. Chem. Phys.* **1989**, *90*, 2154-2161.

(11) Gonzalez, C.; Schlegel, H.B. *J. Phys. Chem.* **1990**, *94*, 5523-5527.

(12) Boys, S.F.; Bernardi, F. *Molec. Phys.* **1970**, *19*, 553-566.

(13) Reed, A.E.; Weinstock, R.B.; Weinhold, F. *J. Chem. Phys.* **1985**, *83*, 735-746.

(14) Gorelsky, S.I.; Ghosh, S.; Solomon, E.I. *J. Am. Chem. Soc.* **2006**, *128*, 278-290.

(15) Kitaura, K.; Morokuma, K. *Int. J. Quantum Chem.* **1976**, *10*, 325-340.

(16) Mayer, I. *Chem Phys. Lett.* **1983**, *97*, 270-274.

(17) Sannigrahi, A.B.; Kar, T. *Chem Phys. Lett.* **1990**, *173*, 569-572.

(18) Gorelsky, S.I. *AOMix: Program for Molecular Orbital Analysis*, Version 6.42; University of Ottawa: Ottawa, Canada, 2009.

(19) Thomson, J.E.; Campbell, C.D.; Concellon, C.; Duguet, N.; Rix, K.; Slawin, A.M.Z.; Smith, A.D. *J. Org. Chem.* **2008**, *73*, 2784-2791.

(20) Arduengo, A.J.; Harlow, R.L.; Kline, M. *J. Am. Chem. Soc.* **1991**, *113*, 361-363.

(21) Gorodetsky, B.; Ramnial, T.; Branda, N.R.; Clyburne, J.A.C. *Chem. Commun.* **2004**, 1972-1973.

(22) Jafarpour, L.; Stevens, E.D.; Nolan, S.P. *J. Organomet. Chem.* **2000**, *606*, 49-54.

(23) Kliegman, J.M.; Barnes, R.K. *J. Org. Chem.* **1970**, *35*, 3140-3143.

(24) Stewart, I.C.; Ung, T.; Pletnev, A.A.; Berlin, J.M.; Grubbs, R.H.; Schrodi, Y. *Org. Lett.* **2007**, *9*, 1589-1592.

(25) Stylianides, N.; Danopoulos, A.A.; Pugh, D.; Hancock, F.; Zanotti-Gerosa, A. *Organometallics* **2007**, *26*, 5627-5635.

(26) Jafarpour, L.; Nolan, S.P. *Organometallics* **2000**, *19*, 2055-2057.

(27) Jafarpour, L.; Hillier, A.C.; Nolan, S.P. *Organometallics* **2002**, *21*, 442-444.

(28) Scholl, M.; Ding, S.; Lee, C.W.; Grubbs, R.H. *Org. Lett.* **1999**, *1*, 953-956.

(29) Huang, J.; Stevens, E.D.; Nolan, S.P.; Petersen, J.L. *J. Am. Chem. Soc.* **1999**, *121*, 2674-2678.

(30) Fürstner, A.; Ackermann, L.; Gabor, B.; Goddard, R.; Lehmann, C.W.; Mynott, R.; Stelzer, F.; Thiel, O.R. *Chem. Eur. J.* **2001**, *7*, 3236-3253.

(31) Gallagher, M.M.; Rooney, A.D.; Rooney, J.J. *J. Organomet. Chem.* **2008**, *693*, 1252-1260.

(32) Conrad, J.C.; Parnas, H.H.; Snelgrove, J.L.; Fogg, D.E. *J. Am. Chem. Soc.* **2005**, *127*, 11882-11883.

(33) Sanford, M.S.; Love, J.A.; Grubbs, R.H. *Organometallics* **2001**, *20*, 5314-5318.

(34) Love, J.A.; Morgan, J.P.; Trnka, T.M.; Grubbs, R.H. *Angew. Chem., Int. Ed.* **2002**, *41*, 4035-4037.

(35) Galvan-Arzate, S.; Santamaria, A. *Toxicol. Lett.* **1998**, *99*, 1-13.

3 Structural Investigation of a C_1-Symmetric Ru-Aryloxide Catalyst[1]

3.1 Introduction

Previous work in the Fogg group has explored the opportunities presented by modification of the anionic ligands in the Grubbs-class catalysts, as shown in Figure 1. Of particular interest is the capacity of modular aryloxide ligands (within, e.g., bis-aryloxy catalysts **4**[1-3] and mono-aryloxy **5**[4]) to tune catalyst behaviour. These studies offer the potential to expand our understanding of the influence of ligand class and geometry on catalyst activity, initiation, and selectivity. Recent reports have highlighted, for example, the higher initiation efficiency of Grubbs-class catalysts containing trans-disposed chloride ligands,[5] though whether this holds true for non-chloride complexes had not been established at the outset of this study.

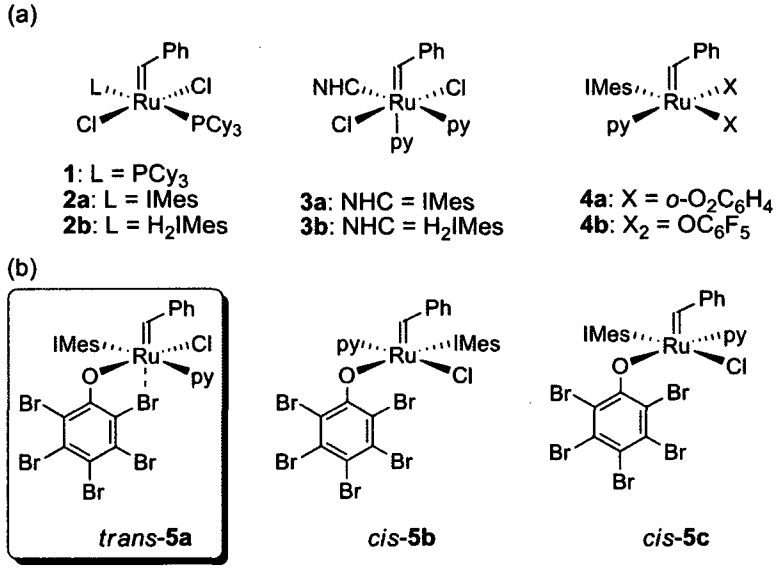

Figure 1. (a) Selected Ru metathesis catalysts containing chloride and/or aryloxide ligands. (b) Possible structures considered for **5**. The Ru···Br dative interaction shown for trans-**5a** emerged from the DFT study (Section 3.4). NHC = N-heterocyclic carbene; IMes = *N,N'*-bis-(2,4,6-trimethylphenyl)imidazol-2-ylidene; py = pyridine.

As pointed out in Chapter 1, the catecholate complex **4a**[1] and bromoaryloxide complex **5**[5] stand out among the Ru-pseudohalide metathesis catalysts for their high productivity (particularly notable given their low initiation efficiency), their avidity in enyne metathesis, and their high kinetic selectivity for cyclization, vs. oligomerization[5,6] in the RCM of large rings. The

[1] The contents of this chapter have been published: "Geometric and Electronic Structure of a C_1-Symmetric Ru-Aryloxide Metathesis Catalyst: An Experimental and Computational Study", M.W. Kotyk, S.I. Gorelsky, J.C. Conrad, C. Carra, D.E. Fogg*, *Organometallics* **2009**, *28*, 5424-5431.

relationship between these properties and ligand geometry is unclear, however, given the absence of unambiguous structural information for **5**. Several geometric isomers are possible (Figure 1b), even without considering isomers in which the benzylidene ligand is situated in the basal plane of the square pyramid (the latter are ruled out on the basis of the strong apical site preference of the alkylidene group).[7,8] A cis-anionic structure was originally favoured[5] on the basis of a preliminary computational analysis using a heavily truncated ligand set, but attempts to grow X-ray-quality crystals that could confirm or refute this suggestion have not yet succeeded.

This chapter describes a detailed experimental and computational investigation which enabled identification of the geometry of this complex as *trans*-**5a**. Support for this conclusion comes from the use of 1D and 2D NMR analysis methods to establish both through-bond and through-space interactions, a density functional theory (DFT) analysis of the full molecular system at the B3LYP level of theory, and comparison of the experimental electronic spectrum with that predicted by time-dependent DFT (TD-DFT). To establish benchmarks for comparison, a parallel spectroscopic and computational analysis of **5** and closely related complexes in which the geometry is unequivocal (that is, the dichloride catalyst **3a**,[5] and the *o*-catecholate catalyst **4a**[1]) was undertaken. The cis-anionic geometry in the latter is enforced by the ligand bite angle; the trans-anionic geometry of **3**, expected on the basis of crystallographic reports on similar complexes,[9] was established by X-ray analysis for the H_2IMes analogue **3b**.[2] As a secondary purpose, prompted by conflicting views of the rotational processes in second- and third-generation Grubbs complexes, the C_1 symmetry of **5** was utilized to confirm by NMR analysis that Ru-C_{NHC} rotation encounters a lower energy barrier than N-C_{Mes} rotation. DFT analysis strongly supports this finding.

3.2 Synthesis of Ru(=CHPh)Cl(κ^2-*O,Br*-OC_6Br_5)(IMes)(py)

Preparation of catalyst **5** according to the procedure we had originally developed,[5] but on larger scale (ca. 450 mg), required an extension of the reaction time to 12 hours (Figure 2). This reaction was consistently found to result in 5-20% of an unknown byproduct characterized by a ^{1}H NMR singlet at 19.81 ppm, accompanying the expected singlet for **5** at 19.69 ppm (C_6D_6). In NMR-scale experiments carried out using 15 mg **3a**, solely the desired product was observed over 7 h, and formation of **5** was only ca. 60% complete. A parallel experiment carried out in a vial with stirring resulted in complete, clean conversion to **5** within 3 h at room temperature: the

References page 60

difference is unsurprising, given the heterogeneous nature of this salt metathesis reaction, which is inhibited by poor mixing.

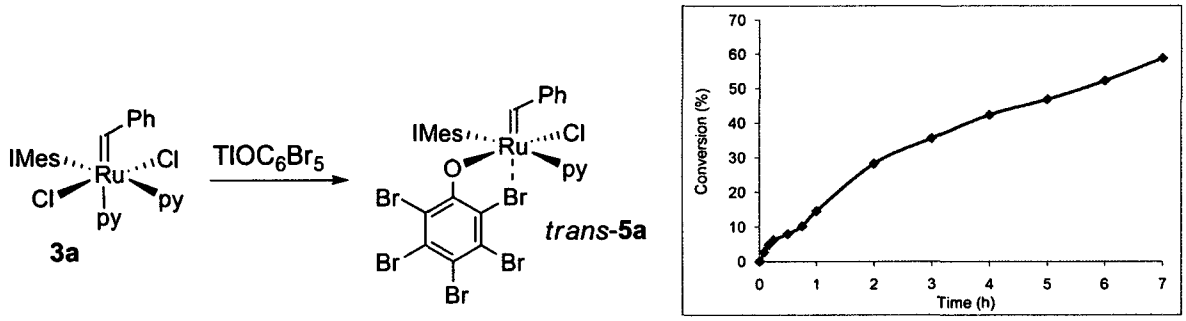

Figure 2. Synthesis of **5** and timescale for its formation; ^{1}H NMR analysis.

The difference between the large-scale and NMR-scale reactions suggests that byproduct formation may be unavoidable on extended reaction time, though we cannot rule out the possible influence of the higher concentration of the NMR-scale reactions. Attempts at purification by reprecipitation from standard solvent mixtures (including hexane and pentane, added to a minimum volume of benzene, THF, or CH_2Cl_2) were hampered by the moderate solubility of **5** in both hexane and pentane, with the net result being an increased proportion of the by-product with successive reprecipitations. The most effective purification method, albeit one that limited isolated yields to ca. 60%, involved simply concentration of CH_2Cl_2 solutions of **5**, followed by filtration. This enabled preparation of clean **5** on synthetic scale, facilitating the detailed analysis of its geometry described in the sections that follow.

3.3 NMR Analysis

3.3.1 NMR Assignments for Ru(=CHPh)X_2(IMes)$(py)_n$ Complexes

Spectra of **4a** and **5** were measured in $CDCl_3$, to maximize solubility. Deuterobenzene was used as solvent for **3a** to simplify the spectrum: multiple broad signals for the mesityl methyl groups, in particular, in $CDCl_3$ at room temperature, suggest partial decoalescence. Cooling to -50 °C did not enable complete resolution. Heating to 50 °C resulted in some sharpening of the signals, but coalescence was incomplete, and decomposition was observed over the timescale of analysis. Furstner and co-workers previously reported[3] lower rotational barriers for **2a** in C_6D_6, relative to CD_2Cl_2. Assignment of the ^{1}H NMR signals for **3a**, **4a** and **5** (designated by ligand, but not by site, in the NMR data reported for **3a** and **5**)[5] was confirmed by

detailed 1D and 2D NMR analysis; for key data, see Table 1. Briefly, the benzylidene and pyridine signals were differentiated on the basis of the isolated spin system characteristic of the latter, vs. coupling of the benzylidene carbon (ca. 300 ppm) to the phenyl H_o, and of the benzylidene proton to C_i (HMBC). Signals for the remaining pyridine and phenyl protons were assigned via ^{1}H-^{1}H COSY analysis, those for the IMes backbone NC*H* protons via their HMBC correlation with the carbene carbon (ca. 190 ppm). The Me_o and Me_p signals were distinguished by the NOESY correlation (vide infra) between the former and the singlets corresponding to the benzylidene and NHC backbone protons. Within all three complexes, a systematic trend emerges for the aromatic proton chemical shifts in which the H_o signals within each of the phenyl and the pyridine groups appear furthest downfield, followed by the corresponding H_p and H_m signals. For **3a**, the pyridine group trans to the alkylidene ligand (py_t, assigned on the basis of NOESY analysis; vide infra) exhibits chemical shifts consistently further downfield than those for the corresponding protons on the pyridine group cis to the alkylidene (py_c).

Table 1. ^{1}H NMR assignments for key proton signals in **3a**, **4a** and **5**.[a]

Cat.	py H_o (2H)	Ph H_o (2H)	IMes Me_o (12H or 2 × 6H)	IMes Me_p (6H)	Mes C*H* (4H or 2 × 2H)	NC*H* (2H)
3a	8.54 (d, 5.1)[b]	8.21 (d, 7.6)	2.51 (br s)	2.04 (s)	6.59 (s)	6.30 (s)
4a	8.36 (d, 6.6)	7.28 (d, 7.0)	2.16 (s), 1.88 (s)	2.22 (s)	6.85 (s), 6.58 (s)	7.08 (s)
5	8.01 (br)	7.88 (d, 7.6)	2.31 (s), 1.86 (s)	2.23 (s)	6.87 (s), 6.54 (s)	6.97 (s)

[a]Values at 298 K, 300 or 500 MHz. Solvent for **3a**: C_6D_6; for **4a**, **5**: $CDCl_3$. Multiplicity and coupling constants ($^3J_{HH}$, in Hz) given in parentheses. Values for H_o of free py in C_6D_6: 8.53; in $CDCl_3$: 8.59 ppm. [b]Values for py_t: 9.11 (d, 4.6); py_t designates the pyridine trans to benzylidene.

3.3.2 Rotational Behaviour

Of interest in the spectrum of **5** is the breadth of the singlet due to H_o of the pyridine ligand ($w_{1/2}$ = 35 Hz at 300 MHz; 70 Hz at 500 MHz), which undergoes little improvement in resolution down to 223 K. Line broadening is attributed to rotation about the Ru-N bond, given the low lability of this ligand established in prior reactivity studies[5,11] and confirmed by DFT calculations. The gas-phase electronic energy (i.e. enthalpic energy, less zero-point energy contribution) for loss of pyridine from *trans*-**5a** is 21.7 kcal mol^{-1}; values for **3a** and **4a**, in comparison are 18.3 and 22.5 kcal mol^{-1} respectively. The relative sharpness of the pyridine H_o signals for **3a** and **4a** is consistent with faster rotation: EXSY-NMR analysis indicates that this is

augmented by chemical exchange for **3a**. The equivalence of corresponding protons on the phenyl ring likewise points toward rapid motion about the C-Ph bond. Back-and-forth swivelling about the metal-alkylidene bond is also a relatively low-energy process, with a calculated free energy barrier of only 8.1 kcal/mol (complete rotation, which would incur greater steric conflicts, would be considerably higher in energy). Finally, rotation about the Ru-C_{NHC} bond in **4** and **5** is indicated by the presence of one IMes backbone NC*H* signal, rather than two, and two sets of mesityl C*H* and Me_o protons, rather than four, despite the C_1-symmetric nature of the complexes. The coupling between the two sp^2 mesityl protons, and between these and all three unique methyl groups, indicates that it is the two mesityl groups that are equivalent, rather than groups on opposite sides of a given mesityl ring (see Figure 3). The inequivalence of the signals within a given mesityl group indicates that N-C_{Mes} rotation is inaccessible at room temperature within these complexes. DFT analysis supports this interpretation: the free energy barriers ($\Delta G_{298K}^{\ddagger}$) for Ru-$C_{NHC}$ rotation calculated for **4a** and **5** are 9.3 and 6.7 kcal mol^{-1}, respectively; for N-C_{Mes} rotation in **4a**, 39.4 kcal mol^{-1}, as compared to a barrier of 16.9 kcal mol^{-1} for free IMes).

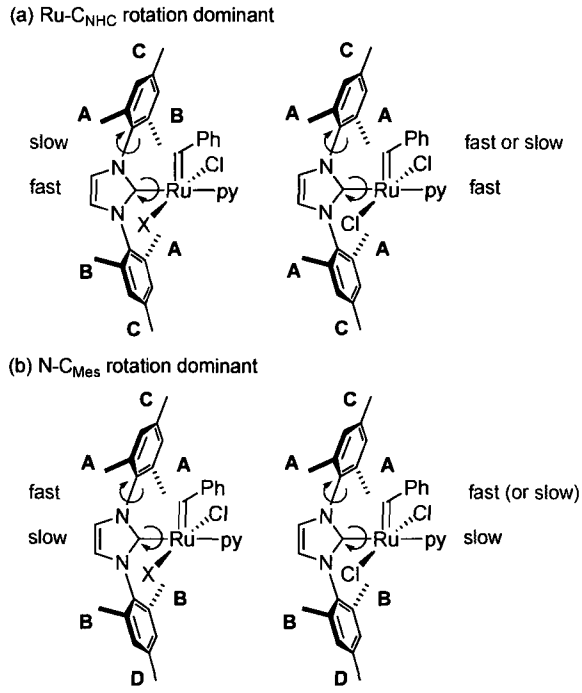

Figure 3. Rotation and resulting symmetry relationships for the mesityl groups in RuClX(IMes)(py)(=CHPh) (X=OC_6Br_5) and $RuCl_2$(IMes)$(py)_n$(=CHPh), where swivelling or rotation of the Ru=C_{CHPh} and Ru-py bonds is rapid on the NMR analysis timescale. For clarity, only methyl groups are labeled, and the redundant sixth ligand is omitted. The trans-anionic

structure is depicted for the aryloxide complex for convenience, but is not material to the symmetry behaviour.

Within the trans-dichloro complexes, the C_s symmetry enabled by rapid swivelling about the Ru-benzylidene bond hampers detection of N-C_{Mes} rotation, irrespective of whether the latter process is fast or slow. The N-C_{Mes} rotational barrier calculated for **3a** is very high, however ($\Delta G_{298K}^{\ddagger}$ = 36.1 kcal mol^{-1}). Consistent with the trend above, Ru-C_{NHC} rotation is considerably lower in energy, at only 14.8 kcal mol^{-1}. The latter process is clearly accessible for **3a** (just as for **4a** and **5a**) at the field strength of 500 MHz employed here, at least in benzene solvent, in which a single Me_o and a single Me_p resonance are found. The barrier was somewhat higher in $CDCl_3$, as noted above, though partial averaging remains apparent at room temperature. In contrast, restricted Ru-C_{NHC} bond rotation (inferred from the inequivalence of the two *N*-substituents) was reported for $RuCl_2(NHC)_2$(=CHPh) complexes (NHC = I^iPr, ICy) by Herrmann and co-workers,[4] while Furstner and co-workers likewise proposed hindered rotation about the Ru-C_{NHC} bond (and one N-C_{Mes} bond) in an NMR analysis study of **2a** in CD_2Cl_2.[3] Inter-ligand steric interactions have long been known to play a key role in determining the barrier to rotation about the metal-carbene bond.[13,14] However, rapid rotation at 500 MHz in C_6D_6 can be inferred from the NMR data supplied in Nolan's original report of **2a**.[5] As well as the solvent, the high field strength (600 MHz) utilized in the Fürstner study should be noted due to the larger energy gap between the two magnetic spin states for each signal which gives rise to a shorter timescale for the detection motion/rotation.

A different perspective is advanced in two recent NMR analysis studies, which suggest a relatively low energy for N-C_{Mes} rotation in **2b**[6] and analogues containing unsymmetrically *p*-substituted *N*-aryl groups.[17] This is clearly not the case for **3a**, **4a**, and **5**. The NMR evidence attests to Ru-C_{NHC} rotation at room temperature for all three complexes, while the absence of N-C_{Mes} rotation in **4a** and **5** is indicated by the inequivalence of the signals within a given mesityl ring, and supported by the computational data (in agreement with reports for other, non-alkylidene complexes).[18-20] By extension, the averaging of the mesityl signals often seen in Ru metathesis catalysts appears more likely to arise from a combination of Ru-C_{NHC} and Ru=$C_{alkylidene}$ rotation: rotation about the N-C_{Mes} bond–already moderately high in energy in the free ligand–is severely restricted following coordination. While a more detailed treatment is

References page 60

beyond the scope of the present work, these issues are of keen interest in the context of asymmetric metathesis mediated by related Ru complexes containing chiral NHC ligands.

3.3.3 NOESY Analysis

NOESY analysis of near-neighbour (<4-5 Å),[7] through-space ligand interactions can enable identification of cis-ligand dispositions.[22,23] The key relationships in the present analysis are those between the H_o and Me_o protons present on the pyridine and mesityl ligands, respectively. Correlations between these signals and those due to the benzylidene phenyl H_o and =C*H* protons are of secondary importance, but remain useful as a control to verify the suitability of the NOESY parameters (NOESY mixing times were set to the average T_1 relaxation times for the signals of interest [=C*H*Ph, Ph H_o and Mes Me_o]; average T_1 values were determined using the standard inversion recovery sequence [180°-τ-90°]).[8] Observed correlations for **3a**, **4a**, and **5** are summarized in Figure 4; the spectrum of **5** is shown in Figure 5. For all three complexes, the expected interactions are observed between the benzylidene (=C*H*, Ph H_o) group, and the ligands cis to it; i.e., both the pyridine (H_o) and IMes (Me_o) groups. Ligand rotation does not impede observation of these correlations at room temperature. For the benchmark trans-anionic complex **3a**, additional correlations involving H_o and H_m relate the mutually cis pyridine ligands, as well as the IMes and py_t ligands (Me_o-H_o). For **4a**, a Me_o-H_o (Mes-py) correlation is observed, this reflecting the cis-disposition of the IMes and the pyridine ligands. For **3a** and **5**, in contrast, no such interaction is present, excluding that due to py_t in **3a**. This is consistent with the trans-disposition of the IMes and the remaining pyridine ligand known to be present in **3a**, and supports identification of **5** as a trans-anionic structure.

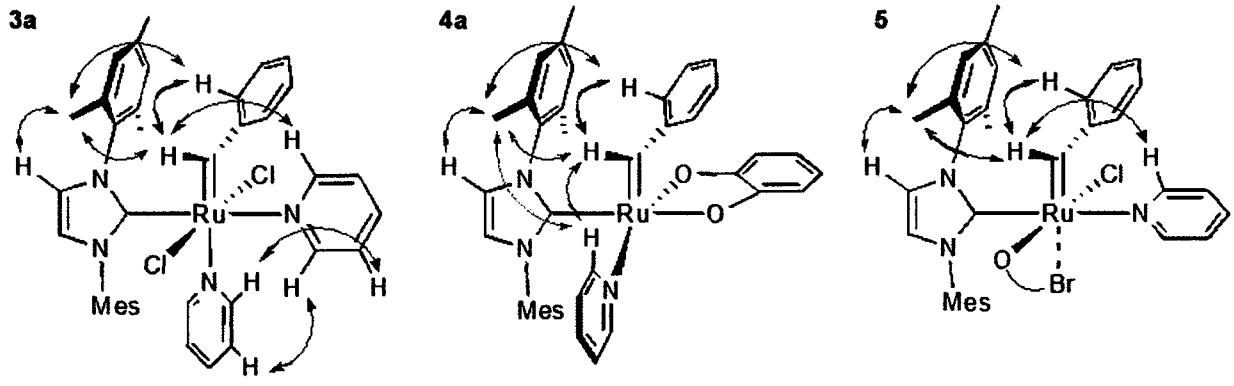

Figure 4. Key NOESY correlations observed for **3a**, **4a**, and **5**. The NOE correlation confirming the cis relationship between the IMes and pyridine ligands in **4a** is highlighted in blue.

Redundant couplings are not depicted. The NOE correlation between the H_o signals for the mutually cis pyridine ligands in **3a** are masked by the stronger EXSY correlation.

Of lesser but noteworthy interest, a through-space correlation is also observed between Me_o groups on opposite rings in **5**. A distance of 2.83 Å is calculated for the DFT-optimized structure *trans*-**5a**, this value dropping to 2.27 Å if rotation is permitted. In the crystal structure of **3b**, the Me_o groups on opposite mesityl rings are as little as 2.75 Å apart, well within the 4-5 Å internuclear distance for direct NOE correlations (distances based on analysis of the crystallographic data for **3b**; CCDC-143577). It is worth noting that ^{1}H-^{13}C HOESY correlations between the mesityl or pyridine protons and the carbons of the pentabromoaryloxide ring could in principle provide positive confirmation of the trans-anionic structure. These experiments are hampered, however, by the very poor signal-to-noise ratios characteristic of these quaternary carbons, each of which bears a quadrupolar nuclide. The relative weakness of the NOE enhancement (ca. 2% of the original signal) is insufficient to compensate for these effects.

References page 60

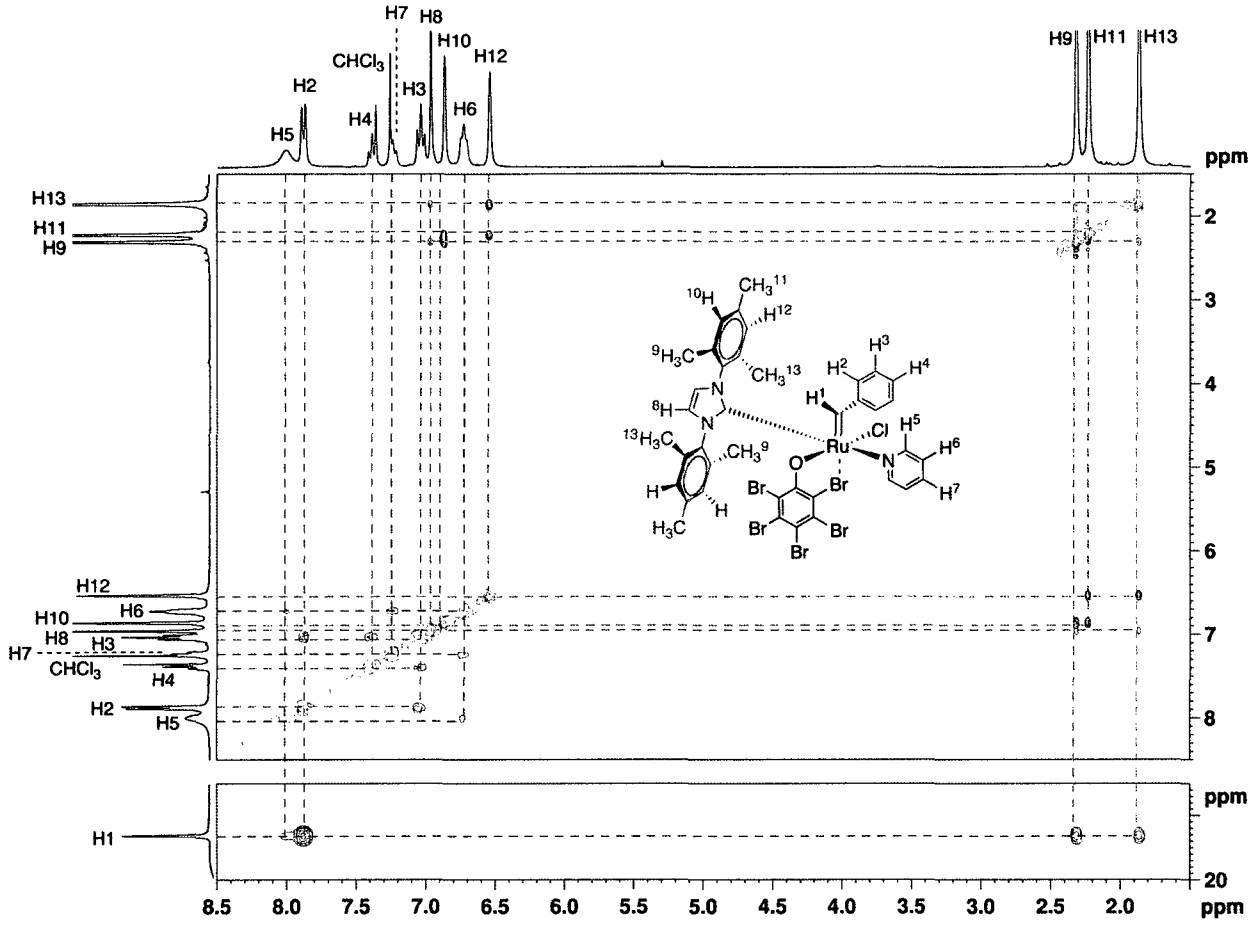

Figure 5. NOESY NMR analysis spectrum for **5** ($CDCl_3$, 300 MHz, 298 K, 900 ms mixing time). Contours in red indicate negative self-correlations; in black, positive (NOE) correlations.

3.4 DFT Analysis of Ru(=CHPh)Cl(κ^2-*O,Br*-OC_6Br_5)(IMes)(py)

While the NOESY evidence is strongly suggestive, independent corroboration of the structure of **5** was sought by computational analysis, using density functional theory at the B3LYP[25,26] / DZVP[9] level of theory. Of the trans-anionic and cis-anionic isomers **5a-c** depicted in Figure 1b, *trans*-**5a** is found to be most stable, by >8 kcal mol^{-1} relative to *cis*-**5b**, and nearly 13 kcal mol^{-1} relative to *cis*-**5c**, in the gas phase, as shown in Table 2, although these figures drop to ca. 5 and 7 kcal mol^{-1} once CH_2Cl_2 solvation is taken into account. The high energy of *cis*-**5c** is due to the enforced electrostatic interaction between the negative charges present on the cis-disposed chloride and pentabromoaryloxide ligands (affecting both the oxygen and the bromine atoms of the latter). Given its high energy relative to the other two geometries considered, *cis*-**5c** was discarded in our subsequent MO analysis.

References page 60

Table 2. Energies (kcal mol^{-1}) calculated for possible isomers of **5**.[a]

Structure	Gas-phase free energy	Free energy in solution (CH_2Cl_2)	Electronic energy
trans-**5a**	0	0	0
cis-**5b**	8.6	4.9	8.5
cis-**5c**	12.8	6.7	11.2

[a]Values are relative to the energy of *trans*-**5a**.

In both *trans*-**5a** and *cis*-**5b**, the benzylidene phenyl ring is oriented above the chloride ligand, and exhibits a π-stacking arrangement with one mesityl ring (a feature commonly observed in the Ru-NHC family of catalysts,[10] and retained in their indenylidene[11] analogues; evidence for such an interaction at low temperature for **2b** was described by Rooney and co-workers[6]). A moderate H-bonding interaction between the benzylidene proton and the aryloxide oxygen (2.50 Å) is found for *trans*-**5a**, which stabilizes the structure by ca. 3 kcal mol^{-1} relative to the corresponding structure in which the benzylidene unit is rotated by 180°. Also present in *trans*-**5a** is a weak Ru···Br dative interaction (2.94 Å) that forms a five-membered κ^2-*O,Br*-OC_6Br_5 chelate ring as depicted in Figure 6. The average Ru···Br distance found in the Cambridge Crystallographic Database, in comparison, is 2.55 Å. Attempts to impose a κ^2-chelating interaction on *cis*-**5b** (or indeed *cis*-**5c**) regenerate the monodentate coordination mode. Alternatively, breaking the Ru···Br interaction in *trans*-**5a** by constraining the Ru-O-C-C_{Ar} dihedral angle to 90°, and re-minimizing, restores the chelated structure. Precedents for this coordination mode are found in other *o*-haloaryloxide complexes, including Ru(κ^2-*O,Br*-2,4,6-$OC_6H_2Br_3$)$(PPh_3)_2$ (Ru-Br = 2.63 Å),[30] $Ru_3(CO)_8(\kappa^2$-*O,Cl*-$OC_6H_4Cl)_2$,[12] CpRu(κ^2-*O,Cl*-OC_6Cl_5),[13] Ru(κ^2-*O,Cl*-$OC_6Cl_5)_2(\kappa^2$-*P,P*-$Ph_2PCH_2CH_2PPr^i_2$)[14] and Ru(κ^2-*S,F*-SC_6F_5)$(SC_6F_5)(PMe_2Ph)_2$.[15]

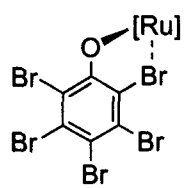

Figure 6. Five-membered κ^2-*O,Br*-OC_6Br_5 chelate ring in *trans*-**5a**.

References page 60

3.5 Chlorination Product

Unsurprisingly, given its higher positive charge at Ru (see Section 4.3), **5** appears more susceptible than **3** to attack by chlorinated solvents. Previous decomposition studies of **1** and **2a** found that alkylidene decomposition is predominantly second order,[16] requiring phosphine dissociation. This implies a greater susceptibility to decomposition with the more labile pyridine ligands in **3a/b**; however, no decomposition studies have examined pyridine precatalysts **3a/b**.[36] In our study, we observed the appearance of new signals in the aromatic and aliphatic regions after 1 week, but remarkably the benzylidene signal remained for 8 weeks. Thus, while **3b** exhibits complete loss of the diamagnetic NMR signals over 2 months in $CDCl_3$ at room temperature, the same is true for **5** over 2 days. At least one of the products formed arises from displacement of the benzylidene ligand (Scheme 1), as indicated by X-ray analysis of crystals that deposit from solution. An ORTEP diagram of the paramagnetic Ru(III) chlorination product $RuCl_2(\kappa^2\text{-}O,Br\text{-}OC_6Br_5)$(IMes)(py) **6** is shown as an inset in Scheme 1. The structure of **6** clearly displays the Ru···Br dative interaction predicted by DFT for **5**, with a length of 2.51 Å being dramatically shorter than that predicted for **5** (2.94 Å).

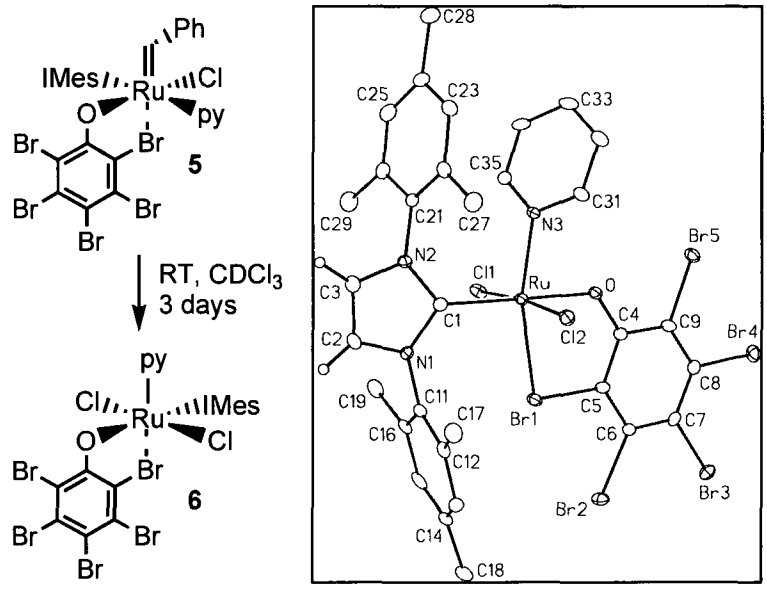

Scheme 1. Chlorination of Ru(=CHPh)Cl(κ^2-*O,Br*-OC_6Br_5)(IMes)(py) (**5**) in $CDCl_3$. Shown in box is an ORTEP diagram depicting perspective view of $RuCl_2(\kappa^2\text{-}O,Br\text{-}OC_6Br_5)$(IMes)(py), **6** with the atom labelling scheme. Non-hydrogen atoms are represented by Gaussian ellipsoids at the 20% probability level. Hydrogen atoms attached to C2 and C3 are shown with arbitrarily small thermal parameters; all other hydrogens are not shown. Important bond lengths and angles: Ru-Br1 2.5064(10) Å, Ru-Cl1 2.3409(16) Å, Ru-Cl2 2.3597(16) Å, Ru-O 2.021(4) Å, Ru-N3 2.080(5) Å, Ru-C1 2.116(6) Å, Br1-Ru-O 82.59(12)°, Br1-Ru-C1 98.54(17)°, Cl1-Ru-Cl2 174.65(6)°, N3-Ru-C1 98.7(2)°.

3.6 Electronic Analysis

Electronic transitions within organometallic complexes are highly dependent on geometric structure. Experimental corroboration of the structural inference emerging from the NMR analysis study was sought by comparing the experimentally measured electronic spectrum of **5** with the spectra predicted for *trans*-**5a** and *cis*-**5b** by TD-DFT analysis. To validate the calculated energies and transition probabilities, a parallel comparison of the experimentally-measured and predicted spectra for the known trans-chloride species **3a** and its hypothetical cis isomer was undertaken. The presence of the Ru···Br interaction in *trans*-**5a** is fortuitous, the bromine ligand serving as a proxy for the pyridine group trans to benzylidene in **3a**. That is, both complexes are octahedral, with a weakly coordinated L-donor ligand trans to the alkylidene unit. The experimental and calculated spectra for **3** and **5** are depicted in Figure 7. The energies and probabilities of the electronic transitions, with band assignments, are given for the trans isomers in Table 3 (for the cis isomers, see Table 5). The corresponding frontier molecular orbital energies and compositions for the trans isomers of **3a** and **5a** are summarized in Table 4, with the corresponding data for the cis isomers in Table 6. A visual representation of the frontier orbitals for *trans*-**5a** appears in Figure 8 below. For *trans*-**3a**, the predicted energy of the principal visible absorption band is 14,600 cm^{-1} (Figure 7), being primarily due to an electronic transition from HOMO–1 to the LUMO level (Table 3). A minor contribution to the band envelope, centered at 13,700 cm^{-1}, arises from the HOMO to LUMO transition. The orthogonal HOMO and HOMO-1 orbitals are both localized on Ru-Cl, and the LUMO on the Ru(4d)=CHPh π^* orbital (Table 4).

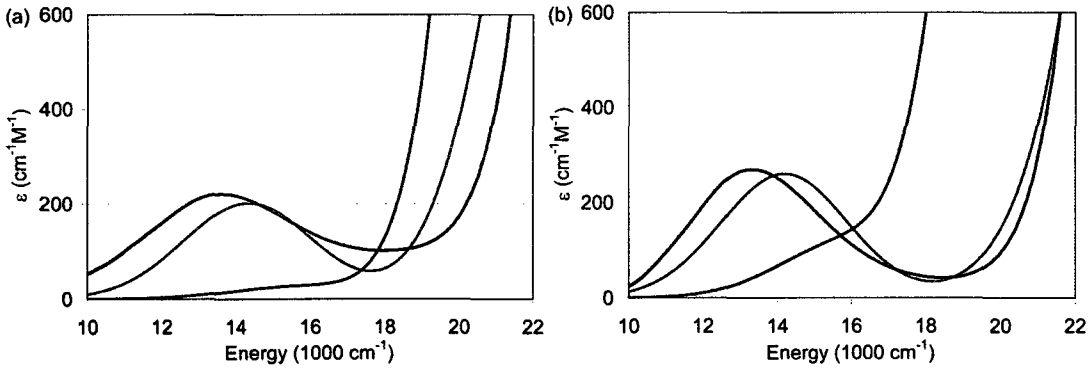

Figure 7. Experimental and TD-DFT-calculated visible absorption spectra, calculated at the B3LYP/DZVP level of theory, for: (a) **3a**; (b) **5**. Experimental traces in black, calculated traces for trans-anionic species in red; for cis isomers, in blue.

The transitions calculated for *trans*-**5a** are very similar. Thus, the predicted energy of the principal visible absorption band is 14,200 cm^{-1} (HOMO–1 to LUMO), with a minor contribution at 13,900 cm^{-1} (HOMO to LUMO); again, the major orbitals involved are Ru-X (HOMO and HOMO-1) and the Ru(4d)=CHPh π^* orbitals (LUMO). For *cis*-**5b**, in contrast, the principal absorption band is expected at considerably higher energy (21,000 cm^{-1}): it arises from transitions from HOMO-2 to the LUMO, and from HOMO to LUMO+1. A shoulder at 15,500 cm^{-1} is due to the HOMO to LUMO excitation. The principal band is not only ca. 7,000 cm^{-1} higher in energy than that for *trans*-**5a**, but nearly an order of magnitude higher in intensity. In the experimentally measured absorption spectrum, the principal visible absorption band appears at 13,300 cm^{-1}, in good agreement with the value calculated for *trans*-**5a**. These data provide further strong support for the trans-anionic structure for **5**. They also suggest that the favoured geometry of these aryloxide complexes–in which both cis- and trans-anionic structures have now been established–will have a powerful influence on the extent of donation into the Ru=CHR antibonding orbital, and hence on catalyst activity.

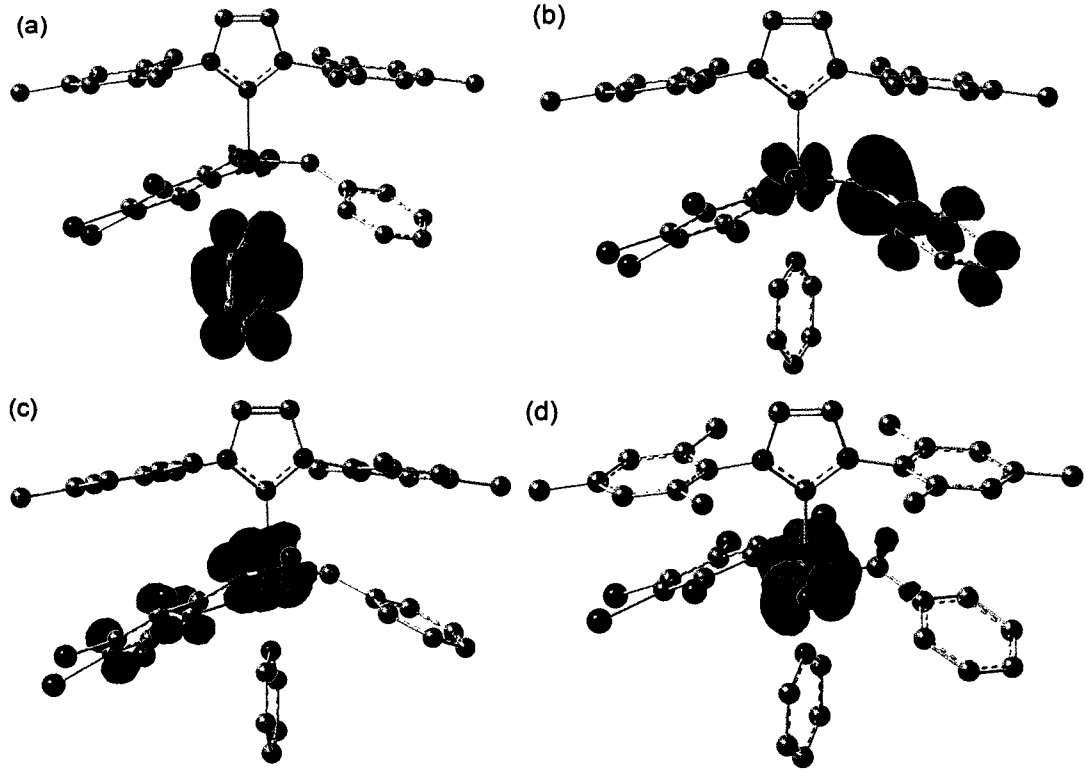

Figure 9. Frontier molecular orbitals of *trans*-**5a**. (a) LUMO+2. (b) LUMO. (c) HOMO. (d) HOMO-1. Spheres are coloured to signify the atoms in keeping with convention: grey for carbon, blue for nitrogen, green for chlorine, red for oxygen, darker red for bromine.

References page 60

The experimental and calculated absorption spectra for both **3a** and **5** exhibit a broad, intense band at ca. 24,000 cm^{-1}, due principally to transitions from HOMO to LUMO+1 (*trans*-**3a**) or HOMO to LUMO+2 (*trans*-**5a**). In both cases, the acceptor orbitals are located primarily on the pyridine ligand. The characteristically lower energy of the LUMO for **3a**, relative to its cis-anionic counterpart, is intriguing. Conservation of this feature in the active, pyridine-free species would account for the higher reactivity reported for closely related trans-dichloride catalysts.[5] The correspondence between the electronic features for **3** and **5**, including the presence of a lower-lying LUMO for *trans*-**5a**, vs. *cis*-**5b**, suggests that a similar correlation between trans-anionic geometry and higher activity can be anticipated for **5**, and indeed that this may be a general feature in this class of complexes.

Table 3. Spin-allowed absorption bands calculated for *trans*-**3a** and *trans*-**5a**.[a]

trans-**3a**			*trans*-**5a**		
Energy (cm^{-1})	f^b	Assignment	Energy (cm^{-1})	f^b	Assignment
13700	0.0011	HOMO→LUMO (82%)	13900	0.0007	HOMO→LUMO (83%)
14600	0.0027	HOMO-1→LUMO (78%)	14200	0.0041	HOMO-1→LUMO (84%)
21700	0.0034	HOMO→LUMO+3 (35%) HOMO→LUMO+5 (23%) HOMO→LUMO+1 (18%)	21000	0.0003	HOMO→LUMO+1 (29%) HOMO→LUMO+6 (21%) HOMO→LUMO+4 (18%)
21900	0.0054	HOMO-1→LUMO+3 (38%) HOMO-1→LUMO+1 (28%) HOMO-1→LUMO+5 (11%)	21900	0.0018	HOMO-1→LUMO+4 (23%) HOMO-1→LUMO+6 (22%) HOMO-2→LUMO (13%)
23700	0.0202	HOMO→LUMO+1 (64%) HOMO→LUMO+9 (12%)	22600	0.0005	HOMO→LUMO+1 (42%)
25000	0.0088	HOMO-1→LUMO+1 (63%)	22800	0.0007	HOMO-2→LUMO (66%) HOMO→LUMO+1 (14%)

References page 60

		HOMO-1→LUMO+3 (14%)			
26200	0.1067	HOMO-2→LUMO (65%)	24000	0.0160	HOMO→LUMO+2 (85%)
			25100	0.0019	HOMO-1→LUMO+2 (71%)
			25900	0.0166	HOMO-1→LUMO+1 (71%)
			26900	0.1782	HOMO-3→LUMO (69%)

[a]Transitions in the visible and near-UV region (10,000–27,500 cm^{-1}), calculated at the B3LYP/DZVP level of theory. Excitation contributions greater than 10% are shown, smaller contributions are omitted. [b]f = oscillator strength.

Table 4. Frontier molecular orbital energies and compositions (%) for *trans*-**3a** and *trans*-**5a**.

	Energy (eV)	Ru	Cl	OC_6Br_5	IMes	=CHPh	py
trans-**3a**							
LUMO+9	-0.02	53	3	–	29	9	6
LUMO+5	-0.39	25	9	–	63	1	1
LUMO+3	-0.63	37	9	–	23	10	20
LUMO+2	-0.76	10	2	–	2	4	82
LUMO+1	-1.36	6	1	–	1	4	88
LUMO	-2.20	21	2	–	2	72	4
HOMO	-5.08	59	30	–	8	1	2
HOMO-1	-5.17	61	29	–	2	7	1
HOMO-2	-6.05	49	15	–	5	29	3
trans-**5a**							
LUMO+6	-0.69	29	5	12	46	7	1
LUMO+4	-0.83	22	3	17	38	5	14
LUMO+2	-1.50	2	0	6	0	1	90
LUMO+1	-1.66	2	0	93	0	1	4
LUMO	-2.43	20	1	1	2	74	2
HOMO	-5.17	42	7	46	4	1	1

HOMO-1	-5.38	65	18	7	4	6	0
HOMO-2	-5.96	26	10	55	6	1	1
HOMO-3	-6.27	43	4	20	7	25	1

Table 5. Spin-allowed absorption bands calculated for *cis*-**3a** and *cis*-**5b**.[a]

cis-**3a**			*cis*-**5b**		
Energy (cm^{-1})	f^b	Assignment	Energy (cm^{-1})	f^b	Assignment
15100	0.0002	HOMO→LUMO (86%)	15600	0.0018	HOMO→LUMO (61%) HOMO-2→LUMO (21%)
16100	0.0003	HOMO-1→LUMO (83%)	16800	0.0003	HOMO-1→LUMO (82%)
21400	0.0052	HOMO→LUMO+1 (63%) HOMO-1→LUMO+1 (27%)	21000	0.0367	HOMO-2→LUMO (62%) HOMO→LUMO (30%)
22800	0.0329	HOMO-1→LUMO+1 (36%) HOMO→LUMO+7 (23%) HOMO→LUMO+1 (15%)	21700	0.0206	HOMO→LUMO+1 (80%)
23000	0.0554	HOMO→LUMO+7 (36%) HOMO-2→LUMO (19%) HOMO-1→LUMO+1 (10%)	23200	0.0087	HOMO-2→LUMO+6 (10%) HOMO→LUMO+6 (10%)
23700	0.0132	HOMO-2→LUMO (38%) HOMO-3→LUMO (30%)	23300	0.0235	HOMO-1→LUMO+1 (60%)
24900	0.0129	HOMO-3→LUMO (19%) HOMO-1→LUMO+7 (16%) HOMO-1→LUMO+1 (11%)	24800	0.0014	HOMO-2→LUMO+1 (45%) HOMO→LUMO+1 (15%)
25400	0.0520	HOMO-3→LUMO (37%) HOMO-2→LUMO (16%)	25400	0.0408	HOMO→LUMO+2 (43%) HOMO-3→LUMO (18%)
26000	0.0018	HOMO→LUMO+4 (22%) HOMO→LUMO+8 (20%) HOMO-2→LUMO+1 (14%)	25500	0.0332	HOMO-3→LUMO (45%) HOMO→LUMO+2 (33%)

		HOMO-1→LUMO+7 (11%)			
26500	0.0048	HOMO-1→LUMO+8 (25%)	25800	0.0317	HOMO-4→LUMO (39%)
		HOMO-1→LUMO+4 (17%)			HOMO-3→LUMO (28%)
		HOMO-2→LUMO+1 (12%)			HOMO-2→LUMO+1 (11%)
26700	0.0030	HOMO→LUMO+2 (85%)	26300	0.0429	HOMO-4→LUMO (35%)
					HOMO-2→LUMO+1 (11%)
27000	0.0136	HOMO-2→LUMO+1 (64%)	26700	0.0176	HOMO→LUMO+5 (11%)
					HOMO-2→LUMO+1 (9%)
			27400	0.0101	HOMO→LUMO+3 (89%)

[a]Transitions in the visible and near-UV region (10,000–27,500 cm^{-1}), calculated at the B3LYP/DZVP level of theory. Excitation contributions greater than 10% are shown, smaller contributions are omitted. [b]f = oscillator strength.

Table 6. Frontier molecular orbital energies and compositions (%) for *cis*-**3a** and *cis*-**5a**.

	Energy (eV)	Ru	Cl	OC_6Br_5	IMes	=CHPh	py
cis-**3a**							
LUMO+8	-0.24	50	5	–	27	16	2
LUMO+7	-0.31	48	13	–	26	3	10
LUMO+4	-0.71	12	1	–	77	5	4
LUMO+2	-1.07	1	0	–	10	2	87
LUMO+1	-1.63	4	1	–	2	2	91
LUMO	-2.03	20	3	–	3	70	4
HOMO	-5.06	56	33	–	8	1	3
HOMO-1	-5.23	63	26	–	3	7	2
HOMO-2	-5.60	21	46	–	3	20	1
HOMO-3	-5.88	5	85	–	3	5	2
cis-**5b**							
LUMO+6	-0.73	20	3	11	64	1	2

LUMO+5	-0.80	20	0	6	66	7	1
LUMO+3	-1.24	0	0	2	2	1	95
LUMO+2	-1.26	2	0	93	2	1	2
LUMO+1	-1.86	5	0	0	1	0	94
LUMO	-2.28	22	0	3	3	71	1
HOMO	-5.24	24	7	62	3	2	1
HOMO-1	-5.56	62	25	2	5	4	2
HOMO-2	-5.63	38	21	30	6	5	1
HOMO-3	-5.97	7	1	84	1	7	0
HOMO-4	-6.03	20	3	58	2	18	0

3.7 Conclusions

On the basis of DFT calculations, electronic absorption spectra, 2D NMR analysis, and X-ray crystallographic analysis of chlorination product **6**, the ground-state structure of the perbromoaryloxide catalyst **5** is identified as containing trans-anionic ligands with additional ligation of an ortho-bromine group resulting in a six-coordinate complex containing a κ^2-*O,Br*-chelated aryloxide ligand. Catalysts of known trans- or cis-anionic geometry (the third-generation Grubbs catalyst **3a** and the *o*-catecholate catalyst **4a**, respectively), provided a basis for comparison. Of interest, the symmetry deduced from coupling relationships within the C_1-symmetric complexes **4a** and **5** indicate that rotation about the Ru-C_{NHC} bond is more favourable than N-C_{Mes} rotation. Evidence for the trans-anionic structure for **3a** and **5** includes the absence of a NOESY NMR analysis correlation between the IMes and pyridine signals (a feature observed in cis-anionic **4a**), and the greater stability calculated by DFT methods for *trans*-**5a**, relative to its cis isomers. As well, TD-DFT analysis predicts electronic absorption maxima consisting of a Ru 4d-CHPh π^* orbital transition for both *trans*-**3a** and *trans*-**5a** species. Both the energy and the intensity of these bands match well with those experimentally observed for **3a** and **5**. These features of the principal visible absorption band are closely conserved for **3a** and **5**, and may thus constitute a spectroscopic signature for the trans-anionic geometry. These data point toward the trans-anionic structure of **5** as a contributor to its dramatically higher activity relative to **4b** and (albeit to a lesser extent) **4a**.

References page 60

3.8 References

(1) Conrad, J.C.; Amoroso, D.; Czechura, P.; Yap, G.P.A.; Fogg, D.E. *Organometallics* **2003**, *22*, 3634-3636.

(2) Monfette, S.; Fogg, D.E. *Organometallics* **2006**, *25*, 1940-1944.

(3) Monfette, S.; Camm, K.D.; Gorelsky, S.I.; Fogg, D.E. *Organometallics* **2009**, *28*, 944-946.

(4) Conrad, J.C.; Parnas, H.H.; Snelgrove, J.L.; Fogg, D.E. *J. Am. Chem. Soc.* **2005**, *127*, 11882-11883.

(5) Several ruthenium metathesis catalysts containing cis-Cl_2 ligands have been shown to initiate more slowly than their trans-Cl_2 isomers. See: (a) Barbasiewicz, M.; Szadkowska, A.; Bujok, R.; Grela, K. *Organometallics* **2006**, *25*, 3599-3604. (b) Ung, T.; Hejl, A.; Grubbs, R. H.; Schrodi, Y. *Organometallics* **2004**, *23*, 5399-5401. (c) Benitez, D.; Goddard, W. A., III. *J. Am. Chem. Soc.* **2005**, *127*, 12218-12219. Poor initiation may account for the low activity found for related *cis*-Cl1221$_2$ catalysts. See: (d) Slugovc, C.; Perner, B.; Stelzer, F.; Mereiter, K. *Organometallics* **2004**, 122*23*, 13622-13626. (e) Ben-Asuly, A.; Tzur, E.; Diesendruck, C.E.; Sigalov, M.; Goldberg, I.; Lemcoff, N.G. *Organometallics* **2008**, 122*27*, 12811-12813. Ref. 3a demonstrates that the metathesis activity of cis-catecholate catalysts can be very high, once initiation is effected.

(6) Monfette, S.; Fogg, D.E. *Chem. Rev.* **2009**, *253*, ASAP article.

(7) Fogg, D.E.; Amoroso, D.; Drouin, S.D.; Snelgrove, J.; Conrad, J.; Zamanian, F. *J. Mol. Catal. A* **2002**, *190*, 177-184.

(8) Fürstner, A.; Ackermann, L.; Gabor, B.; Goddard, R.; Lehmann, C.W.; Mynott, R.; Stelzer, F.; Thiel, O.R. *Chem. Eur. J.* **2001**, *7*, 3236-3253.

(9) Selected examples include **2a** and derivatives containing styrenyl ethers, esters or sulfoxide. See (a) Huang, J.; Stevens, E.D.; Nolan, S.P.; Petersen, J.L. *J. Am. Chem. Soc.* **1999**, *121*, 2674-2678. (b) Garber, S.B.; Kingsbury, J.S.; Gray, B.L.; Hoveyda, A.H. *J. Am. Chem. Soc.* **2000**, *122*, 8168-8179. (c) Fürstner, A.; Thiel, O.R.; Lehmann, C.W. *Organometallics* **2002**, *21*, 331-335. (d) Szadkowska, A.; Makal, A.; Wozniak, K.; Kadyrov, R.; Grela, K. *Organometallics* **2009**, *28*, 2693-2700. .

(10) Sanford, M.S.; Love, J.A.; Grubbs, R.H. *Organometallics* **2001**, *20*, 5314-5318.

(11) Conrad, J.C.; Camm, K.D.; Fogg, D.E. *Inorg. Chim. Acta* **2006**, *359*, 1967-1973.

(12) Weskamp, T.; Schattenmann, W.C.; Spiegler, M.; Herrmann, W.A. *Angew. Chem., Int. Ed.* **1998**, *37*, 2490-2493.

(13) Chianese, A.R.; Li, X.; Janzen, M.C.; Faller, J.W.; Crabtree, R.H. *Organometallics* **2003**, *22*, 1663-1667.

(14) Doyle, M.J.; Lappert, M.F. *J. Chem. Soc., Chem. Commun.* **1974**, 679.

(15) Huang, J.; Stevens, E.D.; Nolan, S.P.; Petersen, J.L. *J. Am. Chem. Soc.* **1999**, *121*, 2674-2678.

(16) Gallagher, M.M.; Rooney, A.D.; Rooney, J.J. *J. Organomet. Chem.* **2008**, *693*, 1252-1260.

(17) Leuthaeusser, S.; Schmidts, V.; Thiele, C.M.; Plenio, H. *Chem. Eur. J.* **2008**, *14*, 5465-5481.

(18) Dible, B.R.; Sigman, M.S. *Inorg. Chem.* **2006**, *45*, 8430-8441.

(19) Ritleng, V.; Barth, C.; Brenner, E.; Milosevic, S.; Chetcuti, M.J. *Organometallics* **2008**, *27*, 4223-4228.

(20) Lee, J.P.; Ke, Z.; Ramirez, M.A.; Gunnoe, T.B.; Cundari, T.R.; Boyle, P.D.; Petersen, J.L. *Organometallics* **2009**, *28*, 1758-1775.

(21) Claridge, T.D.W., *High-Resolution NMR Techniques in Organic Chemistry*; Pergamon Press: Oxford, 1999; Vol. 19, p 319-320.

(22) Viviente, E.M.; Pregosin, P.S.; Schott, D., NMR spectroscopy and homogeneous catalysis. In *Mechanisms in Homogeneous Catalysis*, Heaton, B., Ed. Wiley-VCH: Weinheim, 2005; pp 1-80.

(23) Pregosin, P.S.; Rueegger, H., Nuclear magnetic resonance spectroscopy. In *Comprehensive Coordination Chemistry II*, Lever, A. B. P., Ed. Elsevier: Oxford, 2004; Vol. 2, pp 1-35.

(24) Derome, A.E., *Modern NMR Techniques for Chemistry Research*; Pergamon Press: Oxford, 1987; Vol. 6, p 240.

(25) Becke, A.D. *J. Chem. Phys.* **1993**, *98*, 5648-5652.

(26) Lee, C.; Yang, W.; Parr, R.G. *Phys. Rev. B* **1988**, *37*, 785-789.

(27) Godbout, N.; Salahub, D.R.; Andzelm, J.; Wimmer, E. *Can. J. Chem.* **1992**, *70*, 560-571.

(28) Colacino, E.; Martinez, J.; Lamaty, F. *Coord. Chem. Rev.* **2007**, *251*, 726-764.

(29) Burtscher, D.; Lexer, C.; Mereiter, K.; Winde, R.; Karch, R.; Slugovc, C. *J. Polym. Sci. A* **2008**, *46*, 4630-4635.

(30) Sinha, P.K.; Falvello, L.R.; Peng, S.M.; Bhattacharya, S. *Polyhedron* **2000**, *19*, 1673-1680.

(31) Darensbourg, D.J.; Fontal, B.; Chojnacki, S.S.; Klausmeyer, K.K.; Reibenspies, J.H. *Inorg. Chem.* **1994**, *33*, 3526-3532.

(32) Werner, H.; Braun, T.; Daniel, T.; Gevert, O.; Schulz, M. *J. Organomet. Chem.* **1997**, *541*, 127-141.

(33) Fries, G.; Ilg, K.; Pfeiffer, M.; Stalke, D.; Werner, H. *Eur. J. Inorg. Chem.* **2000**, 2597-2601.

(34) Catala, R.M.; Cruz-Garritz, D.; Hills, A.; Hughes, D.L.; Richards, R.L.; Sosa, P.; Torrens, H. *J. Chem. Soc., Chem. Commun.* **1987**, 261-262.

(35) Ulman, M.; Grubbs, R.H. *J. Org. Chem.* **1999**, *64*, 7202-7207.

(36) Hong, S.H.; Wenzel, A.G.; Salguero, T.T.; Day, M.W.; Grubbs, R.H. *J. Am. Chem. Soc.* **2007**, *129*, 7961-7968.

4. Ligand Effects in the Cycloaddition Step of Olefin Metathesis: Quantification by DFT Analysis

4.1 Introduction

DFT methods have been extensively used to investigate the mechanism by which Grubbs-class catalysts promote olefin metathesis. A major focus has been on evaluating the influence of phosphine and NHC ligands on the energy profiles for reaction, the effects of cis vs. trans ligand geometries on initiation, and the energy of dissociative and associative pathways.[1-8] Of particular interest are emerging perspectives on the origin of the well-known reactivity differences between the first- and second-generation Grubbs catalysts. Experimental studies by the Kennepohl group reveal that the Ru center is more electron-deficient in the NHC complexes, behaviour attributed to the poorer charge-donor capabilities of the carbene ligand, vs. phosphine.[9] This suggestion is supported by a recent charge decomposition analysis of the precatalysts and the 14-electron active species by the group of Carbo and Poblet.[10] As pointed out in the Kennepohl report, the greater Lewis acidity of the metal center would account for the low lability of the PCy_3 ligand in the second-generation catalysts, and hence their characteristically lower initiation efficiency.

Surprisingly, however, the electronic structure of the key Chauvin metallacyclobutane intermediate in the Grubbs systems has not been examined in the same detail.[11] As well, little attention has been paid to the influence of the anionic ligands on the energetics of reaction,[12-14] despite the importance of this question outlined in prior Chapters, and in contrast with the detailed understanding achieved in the Schrock group 6 systems.[15] To address these points, this Chapter undertakes the first quantitative study of metal-ligand electronic interactions in the transition state for olefin metathesis, with the intention of clarifying the independent and interdependent roles of the neutral and anionic ligands (denoted by L and X labels, respectively), and their influence on the energy profile for cycloaddition. Catalyst initiation has received much attention in many of the prior reports, and is thus not revisited here. In focusing on the active species generated upon loss of the "placeholder" ligand that stabilizes the various precatalysts, the present study complements the prior work while gaining in generality. Chapter 1 noted the convergence of a wide range of Ru-NHC metathesis precatalyts on $RuCl_2(NHC)(=CH_2)$ as the common active species, following one cycle of diene CM or RCM.

References page 78

Here we examine metal-ligand interactions in the Ru-catalyzed cross-metathesis of ethylene, using the fragment orbital (FO) approach advanced by Fukui,[16] Hoffmann,[17] and others[18,19] for analysis of bond order and charge and energy decomposition.[20,21] The first-generation Grubbs catalyst **1** is modelled by **7**, the second- and third-generation catalysts **2** and **3** (**a**: L = IMes; **b**: L = H_2IMes) by **8** and **9**, depending on the nature of L, and the aryloxide catalyst **5** by **10** (Figure 1). In catalysts **7-9**, which differ only in the nature of the L-donor ligand, differences in electronic structure necessarily arise from the Ru-L bonding interaction. While this affects the overall energy profile, the identity of L – somewhat unexpectedly – has minimal effect on the metal-olefin interaction. In contrast, replacement of a chloride ligand by pentabromoaryloxide drastically affects the electronic structure, the metal-olefin interaction, and the free energy profile for cycloaddition.

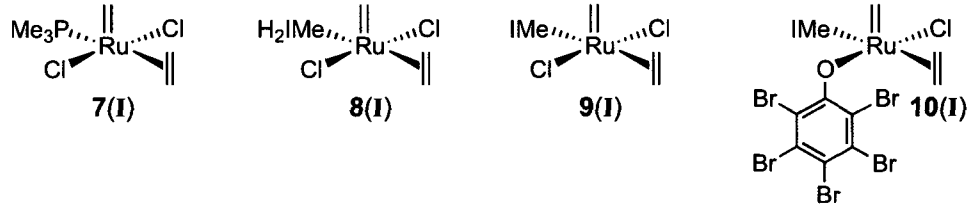

Figure 1. Model systems studied. The Ru···Br interaction present in perbromoaryloxide catalyst **5** (see Chapter 3) is lost following replacement of pyridine by ethylene.

4.2 Free Energy Profiles for Cycloaddition of Ethylene to 7-10

Scheme 1 depicts the species involved in cross-metathesis of ethylene via a five-coordinate Ru-methylidene species (which represents the resting state for the important PCy_3-bound precatalysts **1** and **2**). Following initiation by ligand loss, the key stages involve binding of ethylene to generate intermediate **I**, cycloaddition via transition state **II** to give ruthenacyclobutane **III**, and degenerate exchange. To establish a starting point for the FO analysis, minimum-energy structures were determined by computing the Gibbs free energies for **I-III**, relative to the sum of energies for the pyridine-bound [Ru]=CH_2 precatalysts and free ethylene. Isomers in which the methylidene group is situated in the basal plane are not considered, given the high apical site preference of this ligand. Solely trans-anionic structures are examined, in accordance with reported studies of **1** and **2**, and in keeping with the favoured geometry now established[22] for **5** (see previous Chapter). Consistent with prior computational findings[1,5] and Piers' NMR study of $RuCl_2(H_2IMes)(\kappa^2\text{-}CH_2CH_2CH_2)$,[23] intermediate **III** is found

References page 78

to have a trigonal bipyramidal geometry, with the L-ligand and metallacyclobutane moieties sharing the trigonal plane.

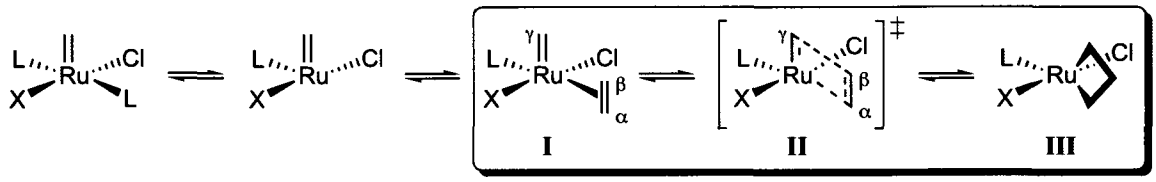

Scheme 1. Degenerate cross-metathesis of ethylene by catalysts **7**-**10**. Structures directly relevant to cycloaddition shown in box; carbon labels in **I** apply to frozen geometry.

The calculated free energy profiles for the first- and second-generation model systems **7**-**9** (Figure 2a) show the striking differences expected from the experimental data, as well as from prior theoretical investigations on related truncated[7,8] and non-truncated[1,4,5] systems. They thus serve to validate our experimental approach. The similar energies of intermediate **I** for the phosphine and NHC models indicate that the binding energy for coordination of ethylene is insensitive to the nature of L. The energies of **7(I)**-**9(I)** drop by ca. 4 kcal mol^{-1} once solvation in CH_2Cl_2 (a common metathesis solvent) is taken into account, but remain essentially identical for all three species, and the overall trends are unaffected. (Solvation in toluene, another common solvent for metathesis, is expected to yield energies intermediate between the gas-phase and CH_2Cl_2 values, based on solvent polarities).

For **7**, the energy of transition state **II** is fairly large (ca. +13.4 kcal mol^{-1}), and cycloaddition to give **7(III)** from **7(I)** is endergonic, consistent with metallacyclobutane formation as the rate-determining step.[5] In comparison, the NHC models **8** and **9** undergo only slight increases in energy on proceeding to transition state **II** (0.0 to 1.7 kcal mol^{-1}), and formation of the metallacyclobutane intermediate **III** is highly exergonic. Replacing a chloride ligand in **9** with a pentabromoaryloxide ligand to give **10** raises the overall energy of the system, and yields a flatter energy profile (Figure 2b). The consequently fast propagation of **10**, a counterbalance to its slow initiation, accounts for its high productivity,[24,25] which compares well with that of the exceptionally fast-initiating[26,27] system **3**. The electronic origin of these differences between the first- and second-generation systems, and between the chloride and aryloxide catalysts, is examined in detail in the following Sections.

The similarity between the free energy profiles found and those previously reported for the Grubbs systems was noted above. Possible limitations arising from truncation of the IMes

References page 78

ligand in **5** were examined by evaluating the free energy profile for the non-truncated system $Ru(=CH_2)Cl(OC_6Br_5)(IMes)(py)$, in comparison with the energy profile for **10**. The overall trends are conserved (Figure 3), though the energy of the non-truncated system is consistently lower in both the gas phase and solution. The energy differences reach a maximum of ca. 4 kcal mol^{-1} in the metallacyclobutane intermediate **III**, and are negligibly small for **I** and transition state **II**. The latter is particularly important, as it indicates that truncation has little effect on the key metal-olefin or metal-ligand interactions in the transition state for cyclization: this is verified by the electronic properties of **II** (Appendix C). In examining the electronic properties of the different catalyst systems and their impact on the energy profile, we thus confined ourselves to the truncated models.

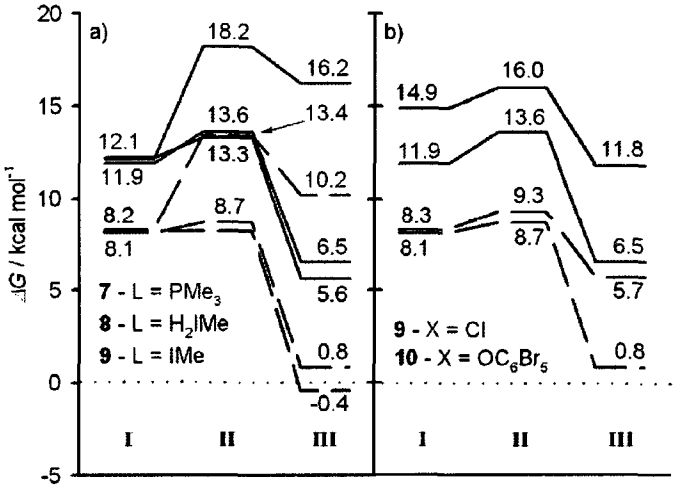

Figure 2. Gibbs free energy profiles for cycloaddition, normalized to the sum of the free energies for the py-bound precatalysts and ethylene. a) Effect of varying the L-donor in the Grubbs catalysts. b) Effect of replacing one chloride ligand with pentabromoaryloxide. Solid lines indicate gas-phase values; dashed lines, values in CH_2Cl_2.

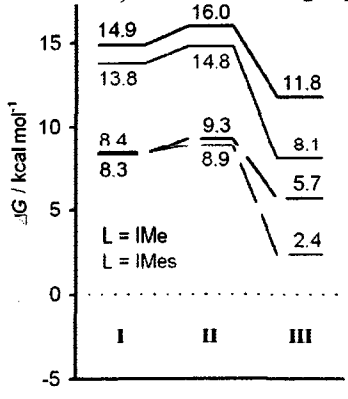

Figure 3. Effect of L-ligand truncation in **10**: Gibbs free energy profile for cycloaddition, normalized as in Fig. 2. Solid lines: gas-phase values; dashed lines: values in CH_2Cl_2.

4.3 Analysis of Electronic Interactions

4.3.1 Computational Methods: Evaluation of Charge, Population, and Strength of Interactions

To assess the donor abilities of the neutral (phosphine, NHC) and anionic (chloride, pentabromoaryloxide) ligands, we evaluated the individual atom or ligand charges, as well as the changes in charge and fragment orbital populations that occur on binding of the metal and ligand fragments. Fragment orbital populations were evaluated using extended charge decomposition analysis (ECDA).[28,29] The amount and distribution of electron density (in atomic units, a.u.) was evaluated by natural population analysis (NPA) and ECDA. Quantitative assessment of the metal-ligand interactions was undertaken by energy decomposition analysis (EDA) of the overall electronic bond energy ΔE_e. Since its development by Morokuma[20] and by Ziegler,[21] EDA has been used to evaluate the electronic interactions in many different types of chemical bonds between atoms across the periodic table,[30-34] including in a study of donor-acceptor interactions within the Grubbs catalysts.[10]

The key components of the electronic bond energy ΔE_e are given in Eqn 1. Here the electronic fragment preparation energy (ΔE_{prep}) corresponds to the energy required to promote the fragments from their equilibrium geometry and electronic ground state to the geometry and electronic state that they possess in the optimized molecular structure. The instantaneous interaction energy (ΔE_{int}), which represents the energy difference between the optimized molecule, and the fragments with frozen geometries in the complex, is in turn regarded as the sum of orbital and steric interaction energies (Eqn 2):

$$\Delta E_e = \Delta E_{prep} + \Delta E_{int} \quad (1)$$

$$\Delta E_{int} = \Delta E_{steric} + \Delta E_{orb} \quad (2)$$

The orbital term ΔE_{orb} accounts for charge transfer and polarization effects: that is, the stabilization arising from covalent interactions and changes in electrostatic energy upon interaction of the fragments, calculated when the orbitals relax to their optimal form. Covalent contributions to E_{orb} are qualitatively inferred from the metal-donor atom bond orders. The steric term (Eqn 3) is made up of (i) ΔE_{elstat}, the electrostatic contribution to the bonding interaction between the unperturbed charges of fragments A and B (calculated with the frozen electron density distribution in the fragments within a complex AB), and (ii) the Pauli term ΔE_{Pauli}, which represents the four-electron destabilizing interactions between occupied orbitals: that is, the inability of two electrons of the same spin to occupy the same region in space.

$$\Delta E_{steric} = \Delta E_{Pauli} + \Delta E_{elstat} \qquad (3)$$

4.3.2. Methylidene Rotation and ΔE_{prep}

Of keen interest is the influence of the ancillary ligands on the energy associated with methylidene rotation, which we identify as a key contributor to ΔE_{prep} in the transition from **I** to **II**. Straub has proposed[8] that the comparatively low reactivity of the first-generation Grubbs catalyst originates in stabilization of the "unproductive conformation" of the 14-electron intermediate, in which the relevant [Ru]=CH_2 and olefin π-symmetry orbitals are orthogonal (see **7(I)**, Figure 4). Consistent with this suggestion, we find that the productive conformer, in which these orbitals are appropriately aligned for cycloaddition, is higher in energy in the phosphine system (**7(I')**: 5.6 kcal mol^{-1}), whereas the corresponding rotamers **9(I)** and **9(I')** are energetically very similar (Table 1, Entry 1).[8] The energy cost of methylidene rotation in **7** arises from deformation of the metal fragment, rather than the ethylene fragment, as indicated by comparison of their respective ΔE_{prep} energies (Entries 2, 3).

The higher energy of the productive conformation **7(I')** is due largely to loss of the π-donor interaction between the chloride ligands and the [Ru]=CH_2 fragment, following rotation of the latter by 90°. The importance of the Ru-Cl interaction in stabilizing **7(I)** (Entries 5-7) is evident from its very negative ΔE_{int} value, relative to all other Ru-ligand fragment interactions (Entry 7, vs. 4-6). In the non-productive conformation, the symmetry of the Ru 4d LUFO+1 orbital with respect to the p orbitals on phosphorus enables π-donation from Cl (calculated as 0.23*e*-),[35] contributing to the negative ΔE_{orb} value (Entry 8). Figure 4 shows the orbitals and the change in population associated with Ru-Cl donation. While population of the LUFO and LUFO+2 populations is affected to a minor extent by Ru=CH_2 rotation, the significantly greater contribution of the methylidene carbon to the LUFO+1 orbital renders it very sensitive to the change in orientation. Rotation sharply reduces the extent to which it can overlap with the chloride p-orbital, curtailing donation from the latter. This accounts for the dramatically lower ΔE_{orb} value in **7(I')** (a drop of 28.2 kcal mol^{-1}; Entry 8), and the 0.18*e*- decrease in *q*Cl (Entry 10). (It will be noted, however, that the [Ru]-Cl fragment interaction energy remains very high, and the decrease in the total Ru-Cl bond order is therefore relatively small: see Entries 7, 11). Increased donation from the olefin and phosphine ligands to the Ru fragment (Entries 5, 6)

References page 78

partially compensates for the reduced charge donation from chloride, but the net effect is an increase in the energy of the productive species leading to **7(II)**.

Given the similarity in the energy profiles for H_2IMe system **8** and its unsaturated IMe analogue **9**, analysis of the Ru-Cl interactions in the NHC system focused on the latter. Model system **9** also stands in for **10**, which exhibits very similar qCl values,[36] as well as a strikingly similar energy profile in step **I** vs. **II** (Figure 2). Taken together, these indicate that π-donation from chloride to Ru is conserved. Rotation of the methylidene ligand from the non-productive to the productive conformation (i.e. **9(I) to 9(I')**) incurs loss of the stabilizing π-donation from Cl to Ru, just as in **7**, as indicated by the 17.3 kcal mol^{-1} drop in ΔE_{orb} (Ru-Cl) and the 0.06 a.u. increase in qCl. (Entries 8, 10). However, this is almost completely compensated for by the enhanced electrostatic attraction between chloride and Ru (Entry 9); a function of the more electropositive nature of the metal center in the second-generation systems, and enhanced charge donation from IMe and ethylene to Ru (see next section).

Table 1. Impact of Ru-Cl interactions on the energy difference between **I** and **II**, assessed via a charge and bonding analysis of fragment interactions.

Entry	Electronic properties	fragment(s)	**7(I)**	**7(II)**	**9(I)**	**9(II)**
1	ΔE [a]		0.0	5.6	0.0	1.6
2	ΔE_{prep}	$[RuCl_2(L)(=CH_2)]$	3.2	16.2	4.2	10.7
3	ΔE_{prep}	$[C_2H_4]$	0.6	1.5	0.6	1.2
5	ΔE_{in}	$[RuCl_2(L)(=CH_2)]$–$[C_2H_4]$	-10.6	-18.9	-10.5	-16.0
4	ΔE_{int}	$[RuCl_2(L)(C_2H_4)]$–$[=CH_2]$	-107.8	-108.1	-108.6	-108.6
6	ΔE_{int}	$[RuCl_2(C_2H_4)(=CH_2)]$–[L]	-50.9	-56.3	-59.7	-64.9
7	ΔE_{int}	$[Ru(L)(C_2H_4)(=CH_2)]$–$[Cl_2]$	-250.0	-235.8	-237.8	-230.0
8	ΔE_{orb}	$[Ru(L)(C_2H_4)(=CH_2)]$–$[Cl_2]$	-73.8	-59.7	-85.0	-67.7
9	ΔE_{steric}	$[Ru(L)(C_2H_4)(=CH_2)]$–$[Cl_2]$	-176.3	-176.2	-152.9	-162.3
10	qCl		-0.53	-0.62	-0.55	-0.61
11	B(Ru-Cl)		0.90	0.88	0.98	0.98

[a] Electronic energy relative to **I**. All energies in units of kcal mol^{-1}; q in a.u. Model systems **8** and **10** show properties similar to **8**.

References page 78

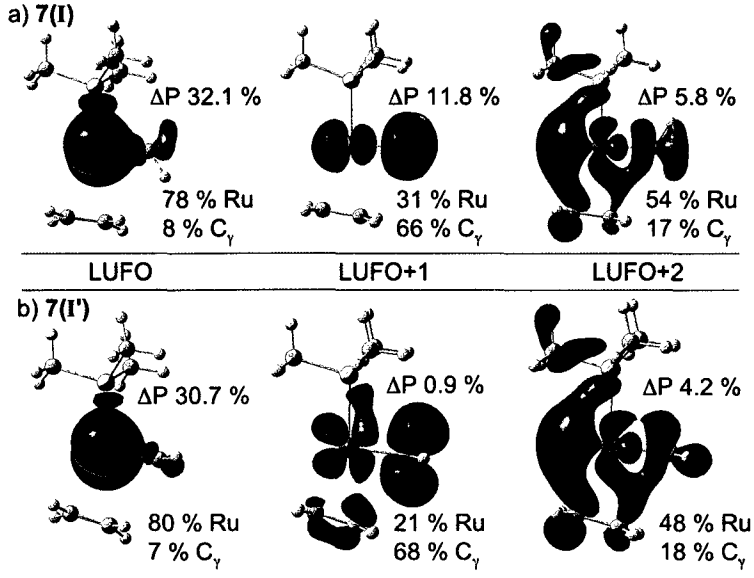

Figure 4. Fragment orbitals of RuL(=CH_2)(C_2H_4) in **7(I)** and **7(II)** responsible for binding with the two chloride ligands (σ: LUFO; π: LUFO+1; δ: LUFO+2), showing contribution of Ru and C_γ (methylidene carbon), and the change in population (ΔP) of the fragment orbitals that results from turning on the Ru-Cl_2 interactions. Isosurface contour value for orbitals is 0.04 a.u.

4.3.3. Electronic Properties in Transition State **II**

4.3.3.1. Electronic Properties of the [Ru]=CH_2–Ethylene Interaction

Notwithstanding the unexpected importance of stabilization associated with charge transfer form the chloride ligands, the most significant interaction in the transition state for cycloaddition is expected to be that between the [Ru]=CH_2 and ethylene fragments. Irrespective of any changes to the ligands present, whether neutral or anionic, the metal-ethylene interaction is dominated by a single orbital interaction, shown for **9** as a representative example (see Figure 5). This consists of σ-donation from the the highest occupied fragment orbital of C_2H_4 (HOFO; a π-orbital) to the lowest unoccupied fragment orbital of [Ru]=CH_2 (LUFO; a π*-orbital), albeit moderated by back-donation from the [Ru]=CH_2 HOFO to the C_2H_4 LUFO. ECDA reveals a slightly polarized interaction, with stronger σ-donation than π* back-donation (see Table 2, Entries 6-9), resulting in a small positive charge on the ethylene fragment. In comparison, the carbon atoms undergo minimal change in charge from **I** to **II**, irrespective of L/X ligand identities (see Appendix C, Table C4).

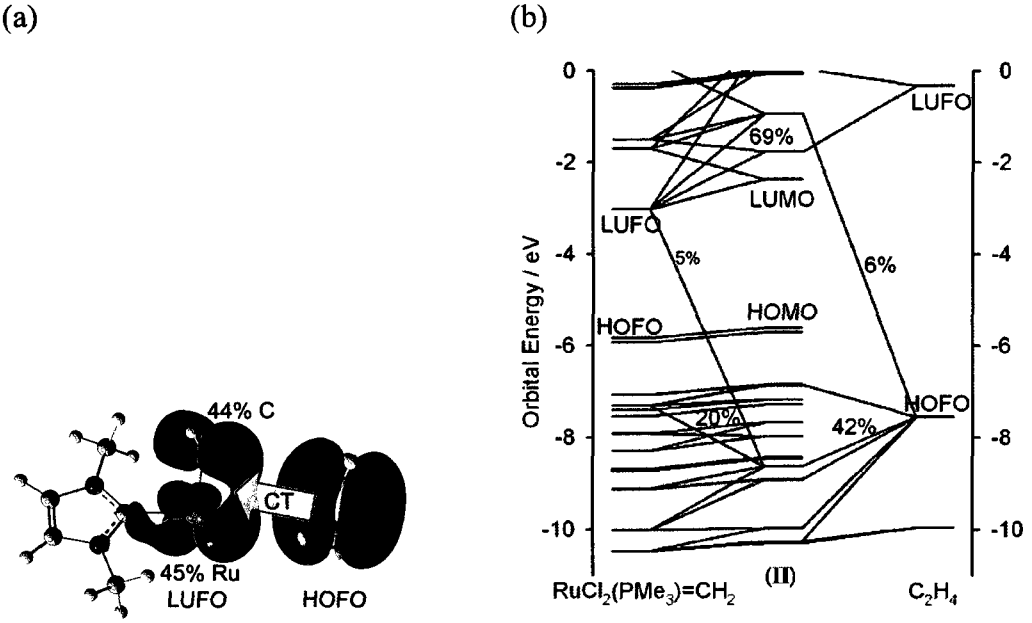

Figure 5. (a) Principal orbital interactions involved in [Ru]-C_2H_4 bonding in **9(II)**, showing the Ru and C_γ character in the Ru=CH_2 LUFO. (b) EDA-derived fragment orbital interaction diagram for **9(II)**, showing changes in orbital populations associated with turning on the interaction between the ethylene and Ru=CH_2 fragments. Changes of <5% omitted.

Table 2 summarizes the relative electronic energies (ΔE_e) of the transition states in **7-10**, and their components. Important contributors include ΔE_{prep}, as noted above (that is, the energy required to deform the equilibrium structures of the [Ru]=CH_2 and C_2H_4 fragments to their geometric and electronic state in **II**; Entries 2, 3); the interaction energies ΔE_{int} (Entry 4), the covalent (Mayer) bond orders B (Entry 5), and the population changes in the fragment orbitals (Entries 6-9). Within the Grubbs-class dichloride complexes, the phosphine intermediate **7(II)** is highest in energy, owing largely to the high [Ru]=CH_2 fragment preparation energy associated with loss of the stabilizing Cl→Ru π-donation, as discussed in the previous section. This is offset to some extent by the more negative interaction energy between [RuXCl(L)(=CH_2)] (F1) and [C_2H_4] (F2), a reflection of the stronger σ-donation from ethylene to the lower-energy [Ru]=CH_2 LUFO (see next). Despite the difference in interaction energies, however, the Ru-C_2H_4 covalent interaction is unaffected: that is, the fragment bond orders are essentially identical in **7(II)-9(II)**, irrespective of the nature of L (Entry 5).

Changing the X-donor ligand has a much more dramatic effect. The larger preparation energy for the ethylene fragment in **10(II)** (Entry 3, Table 2) signals a greater degree of

deformation of the olefin: that is, it indicates a later transition state for **10**, vs its chloride analogue **9**. Strong donation from ethylene to the metal fragment is reflected in the very negative ΔE_{int} value (nearly double that in **9(II)**; Entry 4) and the significantly higher [Ru]-C_2H_4 bond order (Entry 5). The orbital population changes are consistent with this picture. Thus, Entries 6-9 reveal increased σ-donation from the ethylene HOFO to the [Ru]=CH_2 LUFO, and back-donation from the [Ru]=CH_2 HOFO to the ethylene LUFO (Figure 5a).

Table 2. Interaction between the [RuXCl(L)(=CH_2)] (F1) and [C_2H_4] (F2) fragments in **7(II)-10(II)** and their contributions to the electronic energy of the transition state.[a]

Entry	Properties	7(II)	8(II)	9(II)	10(II)
1	ΔE_e	19.9	15.9	15.0	14.9
2	ΔE_{prep} (F1)	16.2	11.8	10.7	13.3
3	ΔE_{prep} (F2)	1.5	1.3	1.2	10.2
4	ΔE_{int} (F1–F2)	-18.9	-16.0	-16.0	-29.8
5	B(F1-F2)	0.76	0.78	0.78	1.38
6	ΔP ($F2_O$)	22.2	21.2	20.8	38.1
7	ΔP ($F1_U$)	20.6	19.6	19.4	34.3
8	ΔP ($F1_O$)	3.2	4.2	4.2	14.7
9	ΔP ($F2_U$)	1.1	2.8	2.6	12.3

[a] ΔE_e = relative electronic energies of the transition states in **7-10**. B(F1-F2) = bond order between fragments. The component two- and three-center Ru-C and C-C bond orders are given in Appendix C. ΔP = % change in population of occupied (O) and unoccupied (U) fragment orbitals once the F1-F2 interaction is turned on, based on Mulliken population analysis of the calculated electron density distribution. ΔP ($F2_O$) and ΔP ($F1_U$) reveal σ-donation, ΔP ($F1_O$) and ΔP ($F2_U$), π* back-donation.

As the capacity of the metal to receive electron density from ethylene is governed in large part by the energy of the RuXCl(L)(=CH_2) LUFO, we assessed these energies for **7(II)-10(II)**. Shown in Table 3 are the LUFO energies, the population changes that result from turning on the metal-ethylene fragment interactions, and the contribution of the Ru and the methylidene carbon to the orbital compositions. The improved π-acceptor capabilities of the metal fragment in **10(II)** can be seen to arise from its lower LUFO energy (0.57 eV lower than in **9**; Table 3, Entry 1). The strength of the interaction is manifested in the very large population change in Entry 2 (see also

the high Ru-ethylene bond order for **10(II)** in Table 2 above. The stabilizing influence of the pentabromophenoxide ligand on the LUFO energy in the [Ru]=CH_2 fragment is thus responsible for strengthening the metal-olefin interaction, and yielding a later transition state. A similar, if less dramatic effect is seen within the dichloride series, in which the lower LUFO energy for phosphine system **7(II)**, relative to the NHC systems **8(II)** or **9(II)** (Entry 1), likewise enables a stronger metal-ethylene fragment interaction.

Table 3. LUFO energies governing extent of charge donation from ethylene. Energy, population change, and composition of the RuXCl(L)(=CH_2) LUFO in **7(II)-10(II)**.

Entry		**7(II)**	**8(II)**	**9(II)**	**10(II)**
1	ΔE_e (eV)	-3.47	-3.01	-3.03	-3.60
2	ΔP (%)[a]	15.0	11.8	11.5	28.6
3	Ru (%)[b]	46.2	42.8	44.9	46.4
4	C_γ (%)[b,c]	40.2	45.1	44.2	40.4

[a]ΔP = change in LUFO population once fragment interaction with ethylene is turned on. [b]Atomic contribution to the LUFO, as assessed by Mulliken population analysis (MPA). [c]C_γ = methylidene carbon.

4.3.3.2. Influence of the Phosphine and NHC Ligands on the Transition State for Cycloaddition

The early view of NHC ligands as "pure" σ-donors is now recognized as a considerable oversimplification.[37] Recent theoretical studies emphasize the contribution of electrostatic, as well as covalent, forces in determining the strength of M-NHC (and M-PR_3) bonds, and highlight the potential for M→NHC π-backbonding.[32,37-39] Within the Grubbs systems, emerging views suggest that the H_2IMes ligands – long regarded as stronger donors than phosphines – are in fact poorer covalent charge donors, which nevertheless form stronger M-L bonds, owing to the compensating effect of π-back-donation, and reduced electrostatic repulsion. Kennepohl's recent X-ray absorption spectroscopy study of $RuCl_2$(L)(PCy_3)(=CHPh) systems was a key experimental finding in this regard, unexpectedly revealing an more electron-deficient metal center in the H_2IMes complex, vs. its PCy_3 analogue.[9] Consistent with the experimental data is the higher Mulliken charge on Ru calculated for the second-generation precatalyst[9,10] and for its 14-electron active species.[10] EDA analysis supports the view that the H_2IMes ligand is a poorer σ charge-donor, and better π-acceptor, than PCy_3.[10]

References page 78

It is unclear how these properties may be modulated during the cycloaddition step (and how they are influenced by the electronic properties of the anionic ligands: see following section). We therefore examined the influence of the neutral ligands on the transition state energetics, by evaluating the covalent and electrostatic components of the electronic interactions between the metal and ligand fragments in **II**. The charges on Ru and the donor atom of the neutral ligands, and the charge on the ligands as a whole (Table 4, Entries 1-3), are compared with the Ru-L donor atom bond orders (Entry 4: a measure of covalent charge transfer), and the interaction energies between the metal and L-donor fragments (Entries 5-7).

As with the precatalysts, the L-donor ligands in **7-10** bear a positive charge, which tends to concentrate in the donor atom directly bonded to the metal (Entries 2, 3). Notable is the particularly high positive charge on phosphorus in **7(II)**, relative to that on the NHC donor carbons in **8(II)** or **9(II)**, a reflection of the strong Ru-P covalent bonding (Entries 2, 4). This P→Ru charge donation is not significantly offset by back-donation ($0.66e^-$ σ-donation, $0.04e^-$ back-donation).[40] It thus results in a high Ru-P electrostatic repulsion, manifested in the positive ΔE_{steric} values in Entries 6 and 7, which indicate that the [Ru]=CH_2 fragment and the L-donor ligands are mutually repelled prior to invoking the stabilizing orbital interactions. The net result is significant weakening of the Ru-L interaction for L = PR_3, vs. L = NHC (Entry 5), and a more electron-deficient metal in the Ru-NHC complexes (Entry 1), consistent with the experimental data,[9] as well as the revised views of the Ru-L bonding interactions described above.

Saturated NHC ligands are often viewed as stronger donors than their unsaturated counterparts.[37,41-43] The Ru-C_{NHC} covalent interaction is indeed slightly stronger in **8**, as indicated by the slightly lower positive charge on Ru, and its higher ΔE_{orb} value, vs. **9** (Table 4, Entries 4, 1, 6). This is offset, however, by the increased electrostatic repulsion between the metal centre and C_{H2IMe}, on which a larger positive charge is present (Entries 7 and 2), and the Ru-C_{NHC} bond order is only slightly higher for **8(II)**. The metal-olefin fragment interaction energies are identical for **8(II)** and **9(II)** (Table 2, Entry 4), while those for the metal-L fragment interaction (Table 4, Entry 5) show minimal difference. The absence of any significant effect on the energy profiles of saturation of the NHC backbone is thus unsurprising.

An unexpected feature of the Ru-L bonding in aryloxide **10** is the weaker interaction between the IMe and RuClX(=CH_2)(C_2H_4) fragments, as compared to **9**. Weaker covalent charge donation in **10(II)**, indicated by the lower *q*NHC and higher *q*Ru values, diminishes the Ru-C_{NHC}

References page 78

bond order and fragment interaction energy (Entries 1-3 and 4-5, respectively). The increased electrophilicity of the metal center contributes to the strong σ-donation from ethylene noted above. Retention of a high positive charge on Ru indicates that the σ-interaction is considerably reinforced by back-donation (see also Table 2), leading to the late transition state noted above.

Table 4. Analysis of the Ru-L charge and bonding interactions in transition state **II**.[a]

Entry		**7(II)**	**8(II)**	**9(II)**	**10(II)**
1	qRu	+0.52	+0.64	+0.66	+0.72
2	qL (donor atom)	+1.13	+0.39	+0.28	+0.26
3	qL^b	+0.52	+0.43	+0.42	+0.16
4	B(Ru–L) (donor atom)	0.92	0.85	0.80	0.74
5	ΔE_{int} [RuXCl(C_2H_4)=CH_2]–[L]	-56.3	-63.8	-64.9	-61.4
6	ΔE_{orb}	-69.4	-79.9	-77.0	-70.6
7	ΔE_{steric}	+13.1	+16.1	+12.1	+9.2

[a]Energies in units of kcal mol^{-1}; q in a.u. [b]L = entire ligand.

4.3.3.3. Influence of the Anionic Ligands on the Transition State for Cycloaddition

While replacing a chloride ligand in **9** by pentabromoaryloxide to give **10** has little effect on the activation barrier to cycloaddition (i.e. the energy difference between **I** and **II**; Figure 2b), the net process (i.e. **10(III)** from **10(I)**) is less exergonic by 2.3 kcal mol^{-1}. The higher energy of **10(III)** that causes this flattening of the overall energy profile suggests destabilization of the Ru(IV) intermediate by the more weakly donating pentabromophenoxide ligand. The weaker Lewis basicity of the aryloxide ligand, relative to chloride, is confirmed by the higher positive charge on Ru and the higher negative charge on the anionic donor atom in **10(II)** vs. **9(II)** (Table 4, Entry 1; Table 5, Entries 1-2). It is further supported by the much lower Ru-X covalent bond order in **10(II)** (Table 5, Entry 3). The stronger electrostatic attraction arising from the higher charges on Ru and the X-donor atom in the aryloxide complex is offset by some dispersion of negative charge density over the aryloxide ligand, which results in a less negative ΔE_{steric} interaction energy despite the near-identical ΔE_{orb} values (Entries 2, 5, 6). The net result is a weaker Ru-X donor interaction in **10(II)** (Entry 4). Thus, neither the NHC ligand nor the aryloxide ligand in **10(II)** is able to quench the comparatively high charge on Ru. This

contributes to the stronger orbital interaction E_{int} with ethylene (Table 2, Entry 4): it also accounts for the low initiation efficiency observed for **5**,[24] although this point is not a specific focus of the present analysis.

Table 5. Analysis of the Ru-L and Ru-X charge and bonding interactions in transition state **II**.[a]

Entry		**9(II)**	**10(II)**
1	qX (donor atom)	-0.61	-0.71
2	qX (fragment)	-0.61	-0.67
3	B(Ru–X) (donor atom)	0.98	0.45[b]
4	ΔE_{int} [RuCl(L)(C_2H_4)=CH_2]–[X]	-141.2	-116.8
5	ΔE_{orb} [RuCl(L)(C_2H_4)=CH_2]–[X]	-60.1	-60.4
6	ΔE_{steric} [RuCl(L)(C_2H_4)=CH_2]–[X]	-81.1	-56.4

[a]Energies in units of kcal mol^{-1}; q in a.u. In **10**, X signifies the OC_6Br_5 ligand. The electronic effect of changing the X ligand is assessed by comparison of **9** and **10** only. Ru-X charge transfer limited to X→Ru donation (σ, π). [b]B = 1.03 for the interaction between Ru and the remaining Cl ligand in **10**.

4.4. Conclusions

Changes in the neutral donor ligands exert a profound effect on the activity of the Grubbs-class metathesis catalysts. It is now well established that the activity of the second-generation Grubbs catalysts – dramatically higher than the first-generation catalyst, despite the much reduced lability of the PCy_3 ligand – lies in their lower barrier to metallacyclobutane formation. The foregoing serves to clarify the electronic origin of the effect. The NHC ligand is better able to stabilize the productive conformation of the catalyst: that is, the conformation in which the Ru=CH_2 and ethylene orbitals are appropriately aligned for cycloaddition. In all systems studied, p-donation from the chloride ligands into an acceptor Ru=CH_2 orbital strongly stabilizes the non-productive conformation, by ca. 25 kcal mol^{-1}. In **7**, loss of this stabilizing interaction in the productive conformation contributes to the sharp rise in the energy of the transition state. In **9**, in contrast, significant compensating stabilization comes from the increased Ru-Cl electrostatic attraction, a function of the higher positive charge on the metal in the second-generation complex. The weaker charge donation from the NHC ligand is thus a key factor in the higher reactivity of the Ru-NHC catalysts.

References page 78

This conclusion accords with Poblet's EDCA analysis of the initiation step: both reinforce the Kennepohl suggestion that the barrier to initiation in the second-generation catalysts lies in inhibition of ligand loss by the higher positive charge on the metal. Despite the stronger covalent donor ability of the phosphine ligand, relative to NHC, indicated by the high charge on the former, localization of this positive charge on the phosphorus donor atom has the somewhat paradoxical effect of weakening the Ru-PR_3 bond via Ru-P electrostatic repulsion. Loss of phosphine is thus lower in energy for the first-generation complexes.

Unexpectedly, however, a fragment orbital analysis indicates that the neutral donor ligands have very little effect on the Ru-olefin interaction in the transition state for cycloaddition. Thus, the bond orders between the metal and ethylene fragments in transition state **II** are essentially unaffected by replacing a phosphine with an NHC ligand. The effect of replacing a chloride ligand with pentabromophenoxide, which renders the metal more electrophilic, is considerably more dramatic. The poor charge donation capabilities of the NHC ligand leave it unable to compensate. The higher positive charge on Ru, and the lower energy of the LUFO on the $RuCl(OC_6Br_5)(L)(=CH_2)$ fragment, greatly strengthen ethylene binding, resulting in a late transition state. The considerable flattening of the energy profile for cycloaddition accounts for the very high reactivity of the Ru-aryloxide catalysts once initiation has commenced.

The foregoing analysis of metal-ligand bonding in the reaction coordinate for cycloaddition enables a fuller appreciation of the factors responsible for the differences in reactivity of the Grubbs catalysts **1** and **2**, and aryloxide catalyst **5**, and suggests possible improvement in reaction scope and catalyst design. Thus, the lower LUFO energy in **5** suggests a propensity for reaction with electron-rich olefins or alkynes. General reactivity could potentially be heightened by use of more strongly donating anionic ligands to stabilize states **I-III**, with the added advantage of increasing initiation efficiency.

4.5. References

(1) Cavallo, L. *J. Am. Chem. Soc.* **2002**, *124*, 8965-8973.

(2) Benitez, D.; Goddard, W.A., III. *J. Am. Chem. Soc.* **2005**, *127*, 12218-12219.

(3) Garcia-Fandino, R.; Castedo, L.; Granja, J.R.; Cardenas, D.J. *Dalton Trans.* **2007**, 292.

(4) Tsipis, A.C.; Orpen, A.G.; Harvey, J.N. *Dalton Trans.* **2005**, 2849-2858.

(5) Adlhart, C.; Chen, P. *J. Am. Chem. Soc.* **2004**, *126*, 3496-3510.

(6) Webster, C.E. *J. Am. Chem. Soc.* **2007**, *129*, 7490-7491.

(7) Vyboishchikov, S.E.; Buhl, M.; Thiel, W. *Chem. Eur. J.* **2002**, *8*, 3962-3975.

(8) Straub, B.F. *Angew. Chem., Int. Ed.* **2005**, *44*, 5974 - 5978.

(9) Getty, K.; Delgado-Jaime, M.U.; Kennepohl, P. *J. Am. Chem. Soc.* **2007**, *129*, 15774-15776.

(10) Antonova, N.S.; Carbo, J.J.; Poblet, J.M. *Organometallics* **2009**, *28*, 4283-4287.

(11) Extended Huckel calculations undertaken in early work on Group 4, 6, and 8 metal systems by Eisenstein, Hoffmann, and Rossi identified several key structural and electronic features of the cycloaddition step, including several that have been experimentally validated in recent years. These include the importance of the olefin-alkylidene conformation, the possibility of agostic stabilization of the metallacyclobutane intermediate, and the importance of π bonding at d6 metals in contributing a driving force for metathesis. See: Eisenstein, O.; Hoffmann, R.; Rossi, A. R. *J. Am. Chem. Soc.* **1981**, *103*, 5582-5584. More recently, Suresh and Koga examined the molecular orbital interactions in the metallacycle intermediate for the Grubbs I model system (L = PH_3). See: Suresh, C.H.; Koga, N. *Organometallics* **2004**, *23*, 76-80.

(12) Monfette, S.; Camm, K.D.; Gorelsky, S.I.; Fogg, D.E. *Organometallics* **2009**, *28*, 944-946.

(13) Krause, J.O.; Nuyken, O.; Buchmeiser, M.R. *Chem. Eur. J.* **2004**, *10*, 2029-2035.

(14) Buchowicz, W.; Ingold, F.; Mol, J.C.; Lutz, M.; Spek, A.L. *Chem. Eur. J.* **2001**, *7*, 2842.

(15) Schrock, R.R. *Angew. Chem., Int. Ed.* **2006**, *45*, 3748-3759.

(16) Fukui, K. *Les Prix Nobel* **1982**, 149-166.

(17) Hoffmann, R., *Solids and Surfaces: A Chemist's View of Bonding in Extended Structures*; Wiley-VCH: Weinheim, Fed. Rep. Ger., 1989.

(18) Gorelsky, S.I.; Lever, A.B.P. *J. Organomet. Chem.* **2001**, *635*, 187-196.

References page 78

(19) Rusanova, J.; Rusanov, E.; Gorelsky, S.I.; Christendat, D.; Popescu, R.; Farah, A.A.; Beaulac, R.; Reber, C.; Lever, A.B.P. *Inorg. Chem.* **2006**, *45*, 6246-6262.

(20) Kitaura, K.; Morokuma, K. *Int. J. Quantum Chem.* **1976**, *10*, 325-340.

(21) Ziegler, T.; Rauk, A. *Theor. Chim. Acta* **1977**, *46*, 1-10.

(22) Kotyk, M.W.; Gorelsky, S.I.; Conrad, J.C.; Carra, C.; Fogg, D.E. *Organometallics* **2009**, 5424–5431.

(23) Romero, P.E.; Piers, W.E. *J. Am. Chem. Soc.* **2005**, *127*, 5032-5033.

(24) Conrad, J.C.; Camm, K.D.; Fogg, D.E. *Inorg. Chim. Acta* **2006**, *359*, 1967-1973.

(25) Conrad, J.C.; Parnas, H.H.; Snelgrove, J.L.; Fogg, D.E. *J. Am. Chem. Soc.* **2005**, *127*, 11882-11883.

(26) Choi, T.-L.; Grubbs, R.H. *Angew. Chem., Int. Ed.* **2003**, *42*, 1743-1746.

(27) Love, J.A.; Morgan, J.P.; Trnka, T.M.; Grubbs, R.H. *Angew. Chem., Int. Ed.* **2002**, *41*, 4035-4037.

(28) Gorelsky, S.I.; Solomon, E.I. *Theor. Chem. Account* **2008**, *119*, 57–65.

(29) Gorelsky, S.I.; Ghosh, S.; Solomon, E.I. *J. Am. Chem. Soc.* **2006**, *128*, 278-290.

(30) Frenking, G.; Wichmann, K.; Froehlich, N.; Grobe, J.; Golla, W.; Van, D.L.; Krebs, B.; Laege, M. *Organometallics* **2002**, *21*, 2921-2930.

(31) Frenking, G.; Wichmann, K.; Frohlich, N.; Loschen, C.; Lein, M.; Frunzke, J.; Rayon, V.M. *Coord. Chem. Rev.* **2003**, *238-239*, 55-82.

(32) Nemcsok, D.; Wichmann, K.; Frenking, G. *Organometallics* **2004**, *23*, 3640-3646.

(33) Lein, M.; Frenking, G. *Theory Appl. Comput. Chem.* **2005**, 291-372.

(34) Tonner, R.; Heydenrych, G.; Frenking, G. *Chem. Asian J.* **2007**, *2*, 1555-1567.

(35) The extent of π-donation from the Cl ligands is calculated from the change in population of the LUFO+1; this figure is double the per-Cl change in population shown in Fig. 4.

(36) The values of qCl in **10(I)** and **10(II)**, for comparison, are -0.60 a.u. and -0.64, respectively.

(37) Jacobsen, H.; Correa, A.; Poater, A.; Costabile, C.; Cavallo, L. *Coord. Chem. Rev.* **2009**, *253*, 687-703.

(38) Boehme, C.; Frenking, G. *Organometallics* **1998**, *17*, 5801-5809.

(39) Tafipolsky, M.; Scherer, W.; Öfele, K.; Artus, G.; Pedersen, B.; Herrmann, W.A.; McGrady, G.S. *J. Am. Chem. Soc.2002, 124, 5865* **2002**, *124*, 5865–5880.

(40) The extent of P→Ru charge donation and Ru→P back-donation is assessed from the changes in orbital population as for the chloride ligands; see above.

(41) Scholl, M.; Ding, S.; Lee, C.W.; Grubbs, R.H. *Org. Lett.* **1999**, *1*, 953-956.

(42) Hillier, A.C.; Sommer, W.J.; Yong, B.S.; Petersen, J.L.; Cavallo, L.; Nolan, S.P. *Organometallics* **2003**, *22*, 4322-4326.

(43) Denk, K.; Sirsch, P.; Herrmann, W.A. *J. Organomet. Chem.* **2002**, *649*, 219-224.

Expanded reproduction of molecular orbitals and energy diagram of Figure 5

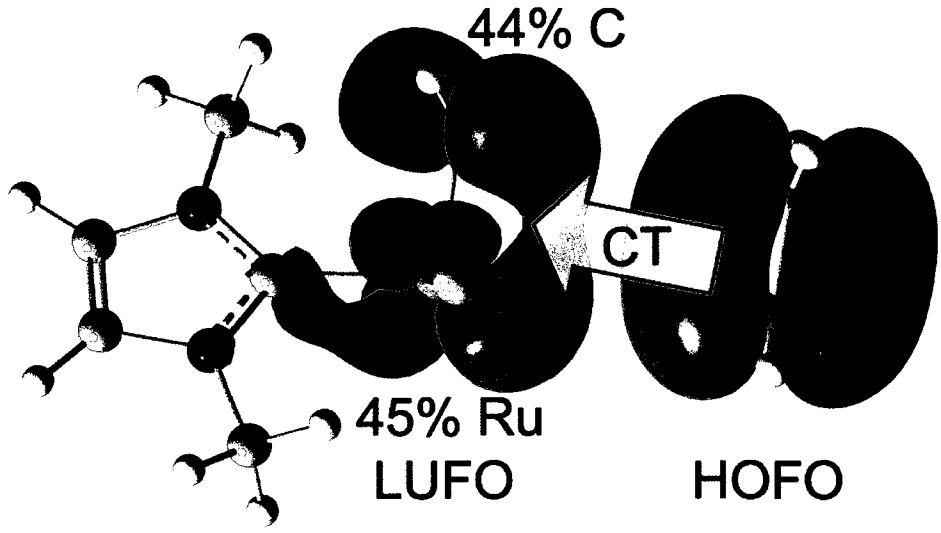

5 Improved Routes to NHC Ligands and Ru-NHC Metathesis Catalysts

5.1 Introduction

Wanzlick first investigated the behaviour of NHCs in 1962,[1,2] but it was not until nearly 30 years later that Arduengo reported the first isolated stable NHC in 1991.[3] In the same year, Arduengo claimed the first modular NHC salt synthesis in the patent literature.[4] Since then, NHCs have become established ligands in catalysis, often improving catalyst reactivity and stability over analogous catalysts containing phosphine ligands.[5-10] The NHC ligand class has developed rapidly, despite the first modular synthetic procedure only being reported in the open literature in 1999,[11] a surprising eight years after the isolation of the first free carbene.[3] The explosion in the use of these neutral two-electron donor ligands has been due to the stability of their complexes (in some cases under air and oxidative conditions),[12] their capacity to form relatively strong bonds to metal centres,[7,13,14] their unique electronic properties (for which see previous Chapter), as well as their highly tunable steric properties. In particular, the use of N-aryl NHCs in ruthenium-catalyzed olefin metathesis has enhanced activity and selectivity.[5,15]

Despite the enormous research interest in these Ru-NHC complexes, however, the reported synthetic routes remained poorly optimized until quite recently. This is true for both the routes to the NHCs themselves, and, in the ruthenium-catalyzed metathesis literature, the methods used to install these ligands on the Ru precursor. Drawbacks in the reported NHC syntheses include the reliance on high reaction temperatures,[11,16] extended reaction times,[11,16] toxic reagents,[11] expensive and high-waste reagents,[17] and hazardous methods for generation of the free carbenes.[18-20] Likewise, reported syntheses of the Ru-NHC complexes typically utilize unnecessarily high reaction temperatures,[21] solvents which render the reaction heterogeneous,[22,23] and use of precipitating solvents that trigger formation of undesired by-products.[5,22,24] Only recently have reliable synthetic methods to the NHC salts been published[25,26] or patented.* These methods were followed in the work described below. While the reagents and reaction temperatures are identical, changes in the solvent used for reaction or workup were found in some cases to improve purification and isolation of the NHC salts. We sought to

* Note added in revisions: see Nolan, S.P. "Synthesis of 1,3 disubstituted imidazolium salts", US Patent 7,109,348, 2006.

develop facile, reliable and (where possible) aerobic procedures for preparing multigram quantities of NHC salts with varying steric bulk and backbone substitution (Figure 1). We also sought to develop optimal methodologies for installation of these ligands onto [Ru]=CHR precursors, with the goal of obtaining the desired Ru-NHC complexes free of by-products.

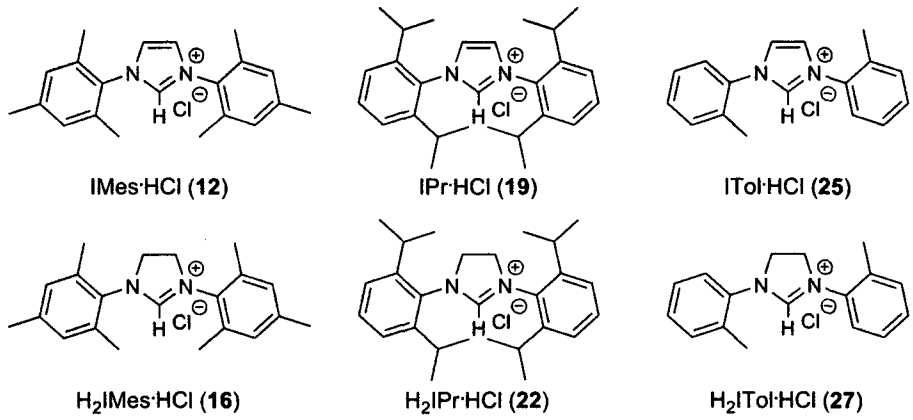

Figure 1. Structures of targeted NHC•HCl salts. Compounds **12**,[11,*] **16**,[11] **19**,[11,*] **22**,[11] and **27**[17] are all known compounds: **27** is unreported.

5.2 Improved Syntheses of NHC ligands

The standard procedures for synthesis of the NHC ligands summarized in Scheme 1 carry the following advantages. They require relatively few steps (2–4 reactions), a number of them can be carried out in air, they are scalable to multigram quantities, and most importantly to the synthetic chemist, they require minimal purification between steps (e.g. no column chromatography). In each case, the desired substituted aniline is first condensed with glyoxal to form the corresponding *N,N'*-disubstituted ethylenediimine (**11**: $R_1 = R_2 = R_3 = Me$; prepared by Sebastien Monfette of this research group; **18**: $R_1 = R_2 = {}^{i}Pr$, $R_3 = H$) according to reported methods (step a), Scheme 1).[11,25,26] These procedures are improved by use of methanol solvent in place of *n*-propanol or ethanol, which causes the diimine product to precipitate, facilitating isolation and drying.* This condensation can be easily performed on 500 g scale, as demonstrated in work carried out by Sebastien Monfette of this research group, to yield a common precursor to ligands containing saturated or unsaturated NHC rings. As the extent of substitution on the aniline ring decreases, however[27] (e.g. compound **24**: $R_1 = Me$, $R_2 = R_3 = H$),

* See: Nolan, S.P. "Synthesis of 1,3 disubstituted imidazolium salts", US Patent 7,109,348, 2006.

References page 91

the solubility of the ethylenediimine product in methanol increases substantially, and higher yields are then obtained by carrying out the reaction in neat aniline.

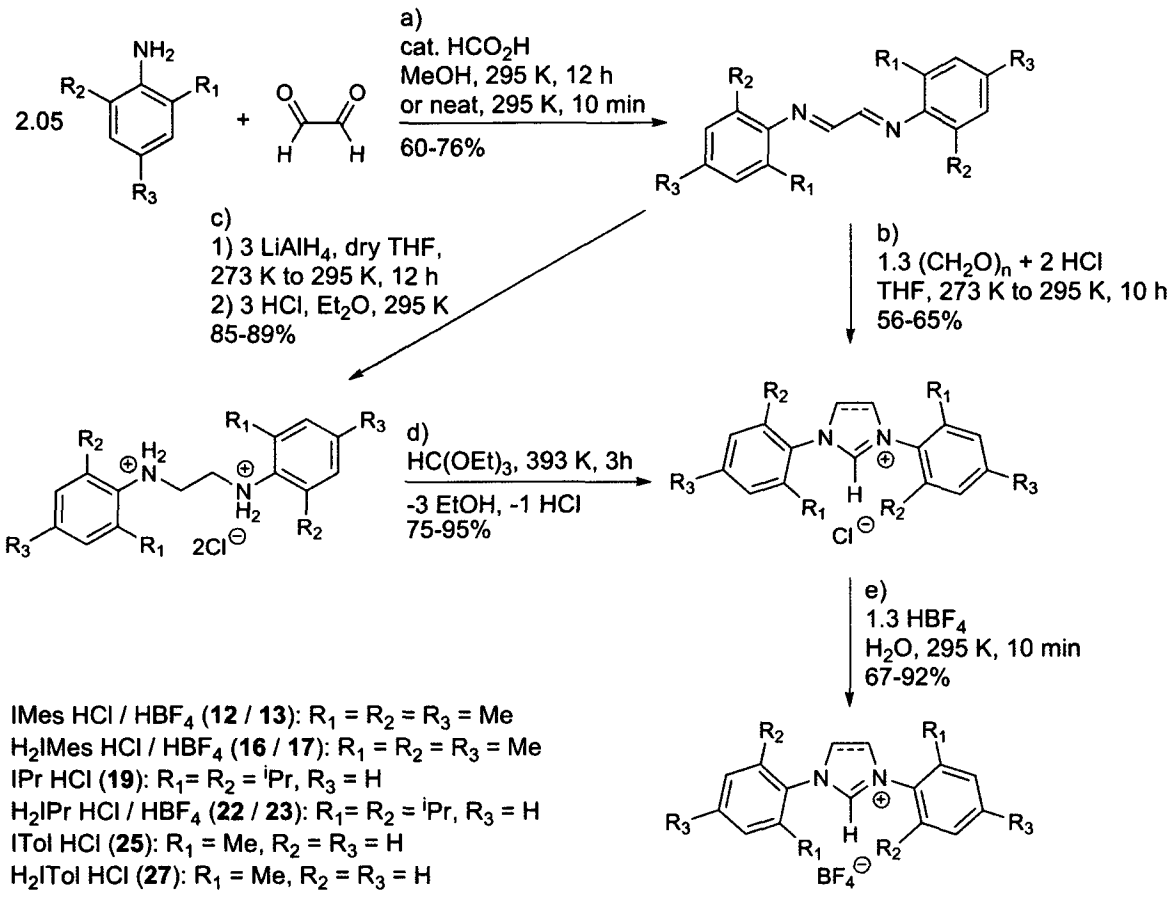

Scheme 1. Literature routes to unsaturated (steps a-b-e) and saturated (steps a-c-d-e) NHC salts, and attempted synthesis of new ITol analogue. a) Diimine synthesis.[11,16,25,26] b) Cyclization of diimine with paraformaldehyde.[16,25,26] c) Reduction of diimine.[11,17,25,26] d) Cyclization of diamine with triethylorthoformate.[11,17,25,26] e) Conversion of chloride to BF_4 salt. *Note:* Yields in Step b) are reportedly higher at a shorter reaction time of 2.5 h on use of ethyl acetate as solvent.*

Direct cyclization of the ethylenediimine product with paraformaldehyde and HCl can be carried out on up to 100 g scale in THF.established methods.[16,25,26,*] This results in precipitation of the unsaturated NHC•HCl salt (step b, Scheme 1: **12**, **19**). The convenience of the one-step cyclization compensates for its modest yields (56-65%). These methods were found to be of limited utility, however, in gaining access to the previously unreported ITol•HCl salt (**25**). Salt

* See: Nolan, S.P. "Synthesis of 1,3 disubstituted imidazolium salts", US Patent 7,109,348, 2006.

25 was isolated in only 9% yield, highlighting the sometimes drastic effects of minor changes in substitution. Optimization of this synthesis was not pursued.

Alternative established methods[11,17,25,26] cyclize the *N,N'*-disubstituted ethylenediimine to the saturated NHC•HCl salt in a two-step sequence, beginning with $LiAlH_4$ reduction to the diamine. Isolation and purification in high yield is accomplished by precipitating and filtering the dihydrochloride salt from diethyl ether (Et_2O; step c), compounds **15**, **21**, and **26**). Reduction is typically performed on 10-20 g scale to cope with the highly exothermic nature of the $LiAlH_4$ reduction, and the typically slow filtration of the quenched aluminum salts. ($LiAlH_4$ is also added in ca. 0.5 g portions in order to limit the reaction exotherm). Cyclization of the isolated diamine salt[11,17,25,26] is achieved by heating in triethylorthoformate (step d), compounds **16**, **22**, and **27**), the product is again isolated by filtration. Cyclization of the saturated ring is typically performed on a 5-10 g scale in a distillation apparatus: the distilled EtOH and excess triethylorthoformate are collected in separate fractions, the latter being reused in subsequent syntheses.

Both unsaturated and saturated NHC•HCl salts can be quickly and easily converted to the NHC•HBF_4 salts on ca. 10 g scale by dissolving the HCl salt in water, filtering off any undissolved material, and adding HBF_4 (step e), compounds **13**, **17**, and **23**). The NHC•HBF_4 salts instantly precipitate, and are isolated by filtration. Use of the NHC•HBF_4 salts, rather than the parent hydrochlorides, is advantageous in the subsequent deprotection with NaH or KO^{t}Bu (vide infra). The tetrafluoroborate salts of the alkali metals are readily separated from the free carbene by filtration (at least in the case of IMes), in contrast with their hydrochlorides, which form a gummy residue that clogs the filter, even on use of Celite to aid filtration. For some NHCs, however (e.g. IPr, H_2ITol), separation from the chloride salts is less problematic.

The reactions of Scheme 1 afford the NHC salts at 1-4% of commercial costs (Table 1)

Table 1. Cost per gram of commercially available NHC salts.[a]

	Scheme 1	Aldrich
IMes•HCl (**12**)	\$2.55[b]	\$78.50
H_2IMes•HCl (**16**)	\$2.15[b]	\$69.00
H_2IMes•HBF_4 (**17**)	\$2.95[b]	\$82.90
IPr•HCl (**19**)	\$2.15	\$171.25
H_2IPr•HCl (**22**)	\$2.94	\$69.20
H_2IPr•HBF_4 (**23**)	\$2.95	\$82.90

[a]Calculated from reagent costs (Aldrich; Jun 2009) and reaction yields. [b]The yield of **11** was taken to be that of **18**.

The Grubbs[17] and Danopoulos[28] groups have demonstrated that when the saturated NHC is the desired target, the appropriate aniline can be condensed with oxalyl chloride and triethylamine in diethyl ether to yield the product oxalamide, which precipitates out of solution. The resulting slurry is filtered and washed with methanol to remove the triethylamine hydrochloride, affording the isolated oxalamide in excellent yields (step a), Scheme 2, compounds **28** and **29**). Again highlighting the surprisingly large effects of seemingly minor changes in substitution, the 2-methylphenyl oxalamide (**28**) is considerably more difficult to reduce than the 2-methoxyphenyl oxalamide (**29**). This difference results in significantly lower isolated yields of the diamine dihydrochloride salt (**26**: 63%; **30**: 92%, step b). As before, the isolated diamine salt is cyclized by heating in triethylorthoformate (step c), compounds **27** and **31**) and the saturated NHC•HCl salt is isolated in excellent yields by filtration.

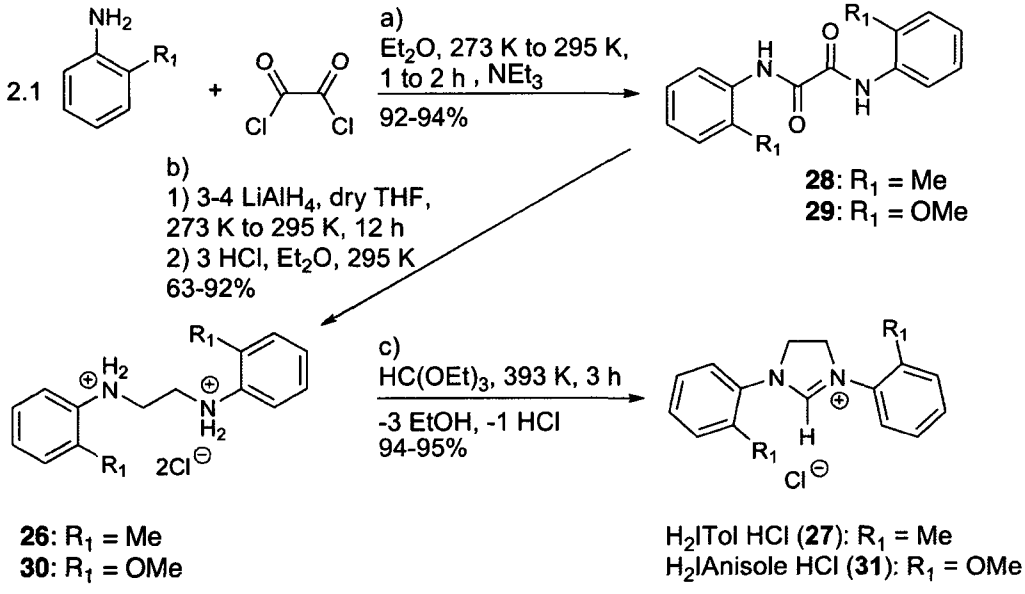

Scheme 2. Alternative literature route to saturated NHC salts **27** and **31**.[17,28]

The H_2IAnisole•HCl salt (**31**) was successfully demethylated with BBr_3 in good yield (Scheme 3) to generate the H_2IPhenol•HCl salt (**32**). When fully deprotonated by treatment with 3 equivalents of base, **32** should yield a tridentate bis-aryloxide NHC ligand.[29] This ligand design is intended to enforce a trans-anionic geometry.[29,30] It could potentially provide a platform for systematically tuning inductive effects without perturbing steric parameters, as previously demonstrated with the cis-anionic *o*-catechol platform **4a**.[31]

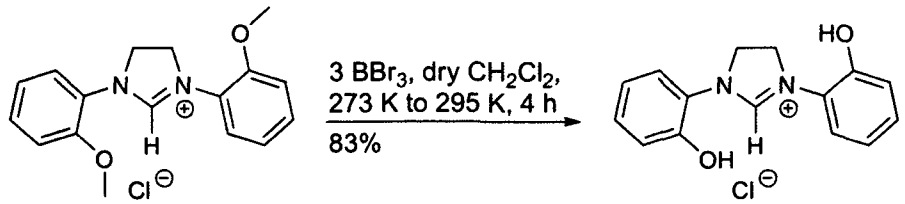

H_2IAnisole HCl (**31**) H_2IPhenol HCl (**32**)

Scheme 3. Synthesis of H_2IPhenol•HCl (**32**).

Scheme 4 depicts the general literature methods[3,11] used to generate the free carbenes by deprotonation of their precursor salts. These involve addition of an appropriate base to to a slurry of the NHC salt. Bases such as KO^{t}Bu, potassium hexamethyldisilazane (KHMDS), or NaH (the latter used as 0.9 equivalents with 0.1 equivalents of KO^{t}Bu) all work well, though it is notable that use of NaH without KO^{t}Bu did not deprotonate the IMes, H_2IMes or IPr salts. Most free carbenes were generated in situ by deprotonation, and were immediately added to a solution of **1**. However, the unsaturated,[32] sterically encumbered IMes and IPr were readily isolated as the free carbenes in good yields, and could be stored as solids at -35 °C for ca. two weeks without evidence of decomposition. Unsurprisingly, the sterically less protected carbene H_2ITol was found to dimerize rapidly. Thus, 30 min after the addition of base, a yellow solid precipitated out of the THF solution,[33] which underwent no reaction on addition to **1** (Section 2.3.10). Short deprotonation times and multiple additions of carbene to the Ru precursor were required to achieve high yields of the targeted Ru-H_2ITol complex **37**.

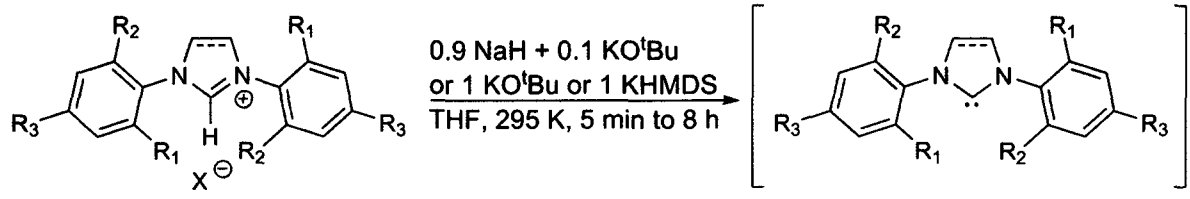

Scheme 4. General literature methods for deprotection of NHC salts.[3,11]

5.3 Synthesis of [Ru]-NHC Metathesis Catalysts

The reported methods[5,6,34] were used to prepare the [Ru]-NHC metathesis catalysts. Thus, the Grubbs catalyst **1** was dissolved in benzene and treated with the desired NHC (whether free or generated in situ) in THF (Scheme 5). Temperatures employed were the minimum required, and ranged from ambient to a maximum of 60 °C. Where the free carbene was generated in situ, salts were removed by filtering the crude reaction mixture through Celite. The solvent was

stripped off and excess PCy_3 was removed by dissolving the crude reaction mixture in hexanes, cooling (to -77°C in acetone-dry ice, or to -94 °Cin acetone-liquid N_2) and filtering. Both **1** and PCy_3 are soluble in hexanes at low temperature, but the solubility of the Ru-NHC complexes drastically decreases upon cooling to -77 °C.

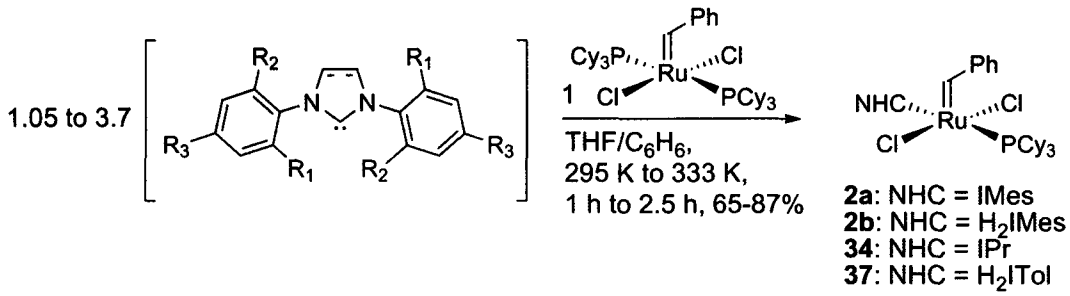

Scheme 5. Incorporation of the NHC ligand into the first generation Grubbs catalyst **1**.[5,6,34] Compounds **2a**,[6,34] **2b**,[5] **34**,[16] and **37**[17] are all known compounds.

Installation of the NHC ligand on the Ru benzylidene complexes differed dramatically, depending on the steric and electronic properties of the former. For example, IMes reacted quickly at ambient temperature with **1**, whereas gentle heating (60 °C) was required with H_2IMes. The bulky IPr ligand was likewise slow to react at ambient temperature, and gentle heating (45 °C) was required. In the case of H_2ITol, the free carbene dimerized rapidly, requiring multiple additions of the ligand **27**. Thus, nearly four equivalents of the free carbene were necessary to reach 90% conversion to **37**, as shown in Figure 2. As a compensating advantage, however, the insolubility of the H_2ITol dimer facilitated its removal by filtration, along with the inorganic salts. Synthesis of the Ru complexes of H_2IPr, H_2IAnisole, and H_2IPhenol (of which the latter two remain unknown) was not pursued given time constraints.

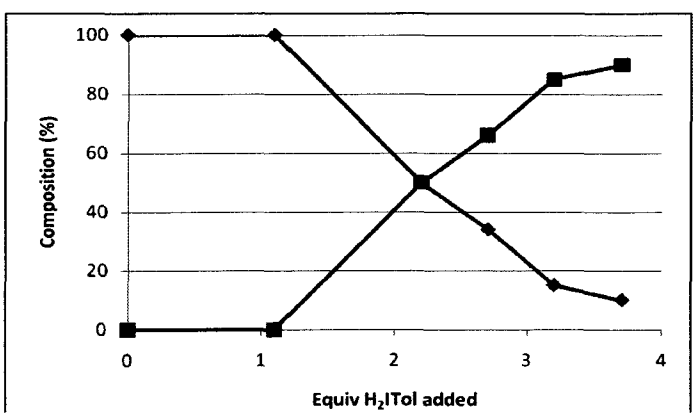

Figure 2. Conversion of **1** (blue) to **37** (red) according to the method of Scheme 5. Conditions: room temperature, THF-benzene; conversions determined by $^{31}P\{^1H\}$ NMR analysis).

References page 91

The established methods[35-38] enable transformation of the second-generation catalysts to their faster-initiating third-generation analogues in good to excellent yields by addition of either pyridine or 3-bromopyridine (py or py*, respectively; Scheme 6). The pyridine catalysts were isolated by precipitation with hexanes or pentane followed by filtration. Interestingly, exchange of the pyridine ligands was observed on the NMR timescale by EXSY. This exchange was sufficiently slow to permit observation of their independent NOESY correlations, and hence assignment as cis (py_c) or trans (py_t), relative to the benzylidene ligand.

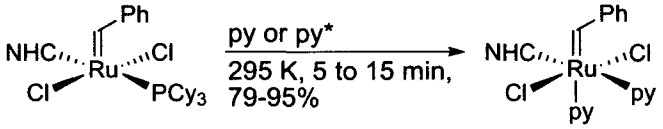

NHC = IMes: **3a**: py = py, **33a**: py = py*
NHC = H_2IMes: **3b**: py = py, **33b**: py = py*
NHC = IPr: **35**: py = py, **36**: py = py*
NHC = H_2ITol: **38**: py = py

Scheme 6. General synthesis of third-generation Grubbs metathesis catalysts (py = pyridine; py* = 3-bromopyridine). Catalysts **3a**,[36] **3b**,[35] **33a**,[37] and **33b**[38] are known compounds.

5.4 Conclusions

The procedures above describe short, aerobic routes to multigram quantities of a variety of NHC salts with excellent cost-efficiency. Changes in the nature of the NHC backbone and substituents was found to dramatically affect the stability of the free carbene and the ease of access to the Ru-NHC complexes.

5.5 References

(1) Wanzlick, H.W. *Angew. Chem., Int. Ed. Engl.* **1962**, *1*, 129-134.

(2) Wanzlick, H.W.; Schoenherr, H.J. *Angew. Chem., Int. Ed. Engl.* **1968**, *7*, 141-142.

(3) Arduengo, A.J.; Harlow, R.L.; Kline, M. *J. Am. Chem. Soc.* **1991**, *113*, 361-363.

(4) Arduengo, A.J., III *Preparation of 1,3-Disubstituted Imidazolium Salts.* U.S. Patent No. 5077414, 1991.

(5) Scholl, M.; Ding, S.; Lee, C.W.; Grubbs, R.H. *Org. Lett.* **1999**, *1*, 953-956.

(6) Scholl, M.; Trnka, T.M.; Morgan, J.P.; Grubbs, R.H. *Tetrahedron Lett.* **1999**, *40*, 2247-2250.

(7) Herrmann, W.A. *Angew. Chem., Int. Ed.* **2002**, *41*, 1290-1309.

(8) Kantchev, E.A.B.; O'Brien, C.J.; Organ, M.G. *Angew. Chem., Int. Ed.* **2007**, *46*, 2768-2813.

References page 91

(9) Despagnet-Ayoub, E.; Ritter, T. *Top. Organomet. Chem.* **2007**, *21*, 193-218.

(10) Organ, M.G.; Chass, G.A.; Fang, D.-C.; Hopkinson, A.C.; Valente, C. *Synthesis* **2008**, 2776-2797.

(11) Arduengo, A.J.; Krafczyk, R.; Schmutzler, R.; Craig, H.A.; Goerlich, J.R.; Marshall, W.J.; Unverzagt, M. *Tetrahedron* **1999**, *55*, 14523-14534.

(12) Rogers, M.M.; Stahl, S.S. *Top. Organomet. Chem.* **2007**, *21*, 21-46.

(13) Crudden, C.M.; Allen, D.P. *Coord. Chem. Rev.* **2004**, *248*, 2247-2273.

(14) Jacobsen, H.; Correa, A.; Poater, A.; Costabile, C.; Cavallo, L. *Coord. Chem. Rev.* **2009**, *253*, 687-703.

(15) Funk, T.W.; Berlin, J.M.; Grubbs, R.H. *J. Am. Chem. Soc.* **2006**, *128*, 1840-1846.

(16) Jafarpour, L.; Stevens, E.D.; Nolan, S.P. *J. Organomet. Chem.* **2000**, *606*, 49-54.

(17) Stewart, I.C.; Ung, T.; Pletnev, A.A.; Berlin, J.M.; Grubbs, R.H.; Schrodi, Y. *Org. Lett.* **2007**, *9*, 1589-1592.

(18) Kuhn, N.; Kratz, T. *Synthesis* **1993**, 561-562.

(19) Herrmann, W.A.; Elison, M.; Fischer, J.; Koecher, C.; Artus, G.R.J. *Chem. Eur. J.* **1996**, *2*, 772-780.

(20) Herrmann, W.A.; Koecher, C.; Goossen, L.J.; Artus, G.R.J. *Chem. Eur. J.* **1996**, *2*, 1627.

(21) Jafarpour, L.; Nolan, S.P. *Organometallics* **2000**, *19*, 2055-2057.

(22) Jafarpour, L.; Hillier, A.C.; Nolan, S.P. *Organometallics* **2002**, *21*, 442-444.

(23) The Ru-benzylidene complexes have been shown to react with methanol to form hydride by-products; the presence of base further amplifies this decomposition pathway. See: Dinger, M.B.; Mol, J.C. *Organometallics* **2003**, **20***22*, 1089-1095; Dinger, M.B.; Mol, J.C. *Eur. J. Inorg. Chem.* **2003**, 2827-2833; Trnka, T.M.; Morgan, J.P.; Sanford, M.S.; Wilhelm, T.E.; Scholl, M.; Choi, T.-L.; Ding, S.; Day, M.W.; Grubbs, R.H. *J. Am. Chem. Soc.* **2003**, **2***125*, 2546-2558.

(24) Fürstner, A.; Ackermann, L.; Gabor, B.; Goddard, R.; Lehmann, C.W.; Mynott, R.; Stelzer, F.; Thiel, O.R. *Chem. Eur. J.* **2001**, *7*, 3236-3253.

(25) Leuthaeusser, S.; Schwarz, D.; Plenio, H. *Chem. Eur. J.* **2007**, *13*, 7195-7203.

(26) Leuthaeusser, S.; Schmidts, V.; Thiele, C.M.; Plenio, H. *Chem. Eur. J.* **2008**, *14*, 5465.

(27) Metal-NHC complexes in which the *N*-aryl substituents are not substituted at the ortho positions are particularly susceptible to decomposition by C-H activation. See, for example: Hong, S.H.; Chlenov, A.; Day, M.W.; Grubbs, R.H. *Angew. Chem., Int. Ed.* **2007**, **20***46*, 5148-

5151; Mathew, J.; Koga, N.; Suresh, C.H. *Organometallics* **2008**, **20***27*, 4666-4670; Chung, C.K.; Grubbs, R.H. *Org. Lett.* **2008**, **20***10*, 2693-2696.

(28) Stylianides, N.; Danopoulos, A.A.; Pugh, D.; Hancock, F.; Zanotti-Gerosa, A. *Organometallics* **2007**, *26*, 5627-5635.

(29) Bellemin-Laponnaz, S.; Welter, R.; Brelot, L.; Dagorne, S. *J. Organomet. Chem.* **2009**, *694*, 604-606.

(30) Yagyu, T.; Oya, S.; Maeda, M.; Jitsukawa, K. *Chem. Lett.* **2006**, *35*, 154-155.

(31) Monfette, S.; Camm, K.D.; Gorelsky, S.I.; Fogg, D.E. *Organometallics* **2009**, *28*, 944-946.

(32) Unsaturated NHCs have a reduced tendency to dimerize compared to their saturated counterparts, however, owing to their lower singlet-triplet gap. See: Poater, A.; Ragone, F.; Giudice, S.; Costabile, C.; Dorta, R.; Nolan, S.P.; Cavallo, L. *Organometallics* **2008**, **20***27*, 2679-2681.

(33) Poater, A.; Ragone, F.; Giudice, S.; Costabile, C.; Dorta, R.; Nolan, S.P.; Cavallo, L. *Organometallics* **2008**, *27*, 2679-2681.

(34) Huang, J.; Stevens, E.D.; Nolan, S.P.; Petersen, J.L. *J. Am. Chem. Soc.* **1999**, *121*, 2674.

(35) Sanford, M.S.; Love, J.A.; Grubbs, R.H. *Organometallics* **2001**, *20*, 5314-5318.

(36) Conrad, J.C.; Parnas, H.H.; Snelgrove, J.L.; Fogg, D.E. *J. Am. Chem. Soc.* **2005**, *127*, 11882-11883.

(37) Conrad, J.C.; Amoroso, D.; Czechura, P.; Yap, G.P.A.; Fogg, D.E. *Organometallics* **2003**, *22*, 3634-3636.

(38) Love, J.A.; Morgan, J.P.; Trnka, T.M.; Grubbs, R.H. *Angew. Chem., Int. Ed.* **2002**, *41*, 4035-4037.

6 Conclusions and Future Directions

The work described in this thesis was driven by the need to understand the origin of the unique reactivity profile of the Ru-pentabromophenoxide metathesis precatalyst **5**. The aryloxide precatalysts **4a** and **5** show a high kinetic selectivity for cyclization vs. oligomerization in the RCM of large ring, and the latter is particularly efficient in enyne metathesis, even in the absence of an ethylene atmosphere. The first step in determining the origin of this selectivity was to determine the geometrical structure of **5**. Could the selectivity be due to a cis-anionic catalyst geometry?

On the basis of DFT calculations, electronic absorption spectra, 2D NMR analysis, and X-ray crystallographic analysis of chlorination product **6**, the ground-state structure of the perbromoaryloxide catalyst **5** is identified as containing trans-anionic ligands. The additional ligation of an ortho-Br atom results in a six-coordinate complex containing a κ^2-*O,Br*-chelated aryloxide ligand. Catalysts of known trans- or cis-anionic geometry (the third-generation Grubbs catalyst **3a** and the *o*-catecholate catalyst **4a**, respectively), provided a basis for comparison. Of interest, the symmetry deduced from coupling relationships within the C_1-symmetric complexes **4a** and **5** indicate that rotation about the Ru-C_{NHC} bond is more favourable than N-C_{Mes} rotation. Evidence for the trans-anionic structure for **3a** and **5** includes the absence of a NOESY NMR correlation between the IMes and pyridine signals (a feature observed in cis-anionic **4a**), and the greater stability calculated by DFT methods for *trans*-**5a**, relative to its cis isomers. As well, TD-DFT analysis predicts electronic absorption maxima consisting of a Ru 4d-CHPh π^* orbital transition for both *trans*-**3a** and *trans*-**5a** species. Both the energy and the intensity of these bands match well with those experimentally observed for **3a** and **5**. These features of the principal visible absorption band are closely conserved for **3a** and **5**, and may thus constitute a spectroscopic signature for the trans-anionic geometry, a feature that has previously been very difficult to ascertain. The trans-anionic structure of **5** accounts, in part, for its higher activity relative to **4**. It also rules out the possibility that the important kinetic selectivity of the trans- and cis-anionic catalysts **5a** and **4a** is due to a trans-anionic structure.

A fragment orbital analysis of the transition state for cycloaddition indicates that the neutral donor ligands have little effect on the Ru-olefin interaction. PMe_3 is found to be a stronger covalent donor than H_2IMe or IMe, as indicated by the high charge on the ligand. Because much of this positive charge is localized on the phosphorus donor atom, however, this

has the somewhat paradoxical effect of weakening the [Ru]-PR_3 bond, owing to Ru-P electrostatic repulsion. A stronger [Ru]-IMe bond is found in **9**, in which poorer charge donation from the ligand reduces the extent of electrostatic repulsion. The neutral donor ligands have been shown to exert a profound effect on the activity of the Grubbs-class metathesis catalysts. We show that this is in part due to their relative ability to stabilize the productive conformation of the catalyst: that is, the conformation in which the π-symmetry [Ru]=CH_2 and ethylene orbitals are appropriately aligned for cycloaddition. The stabilizing π-donation from the chloride ligands into the [Ru]=CH_2 LUFO+1 orbital (ca. 25 kcal mol^{-1} in both **7(I)** and **9(I)**) inhibits rotation from the non-productive into the productive conformation. This stabilizing interaction is lost in the productive conformation. In the phosphine system, this contributes to the sharp rise in the energy of the transition state **7(II)**, relative to **7(I)**. In the IMe system **9**, in contrast, significant stabilization comes from the increased Ru-Cl electrostatic attraction, a function of the higher positive charge on the metal in the second-generation complex. The weaker charge donation from the NHC ligand is thus a key factor in the higher reactivity of the latter catalysts.

It is now well established that the profound differences in reactivity between the first- and second-generation Grubbs catalysts arise from two major sources: first, the lower lability of the PCy_3 ligand in the second-generation catalysts, and secondly, the higher barrier to metallacyclobutane formation for the first-generation systems. The foregoing serves to elucidate the origin of the barrier in the latter case. As well, it suggests an origin for the barrier to initiation in the second-generation catalysts: the more positive charge on the metal inhibits ligand loss.

The nature of the anionic ligand has a dramatic effect on the orbital interactions between the metal and ethylene fragments in the transition state. Replacing a chloride ligand with pentabromophenoxide makes Ru more electrophilic. The [Ru]-NHC interaction is unable to compensate for this, and while the Ru-O electrostatic attraction affords some stabilization, the higher positive charge on Ru and its lower LUFO energy greatly increase the [Ru]-ethylene interaction. The much flatter transition state for cyclization helps to explain the voracity of this catalyst in the propagation step.

The lower LUFO energy of the Ru pentabromophenoxide fragment suggests this catalyst may be more suited to electron-rich olefin or alkyne (enyne) substrates. More strongly donating anionic ligands could increase initiation efficiency, as well as heightening reactivity with electron-poor olefins. This description of metal-ligand bonding in the cycloaddition transition

state accounts for the observed differences in initiation, reactivity and Ru-ligand bonding interactions in **1**, **2** and **5**. However, the origin of the important selectivity for cyclization vs. oligomerization of the aryloxide catalysts **5a** and **4a** remains unknown, deconvoluting the steric and electronic effect remains a challenge.

Improved procedures have been developed for the synthesis of NHC salts in relatively large scale, over fewer steps, under aerobic conditions. This will aid in exploration of the optimum steric and electronic properties of these important ligands with excellent cost efficiency. Generation and installation of the free carbene under mild conditions was optimized in the preparation of second-generation Grubbs catalysts. Changes in the NHC backbone and substituents were found to drastically affect the stability of the free carbene and the ease of access to the Ru-NHC complexes.

The ability to independently modify the sterics and electronics of the NHC ligand provides an opportunity to probe the origin of the kinetic bias of the aryloxide catalysts toward ring-closing, vs. oligomerization. Specifically, increases or decreases in the steric bulk of the NHC ligand (H_2ITol, IPr) would suggest whether the steric bulk around the metal center affects this selectivity. As well, the lower free energy barrier established for Ru-C_{NHC} rotation relative to N-C_{Mes} rotation provides insight into asymmetric metathesis by Ru complexes containing chiral NHCs. The commonly employed chiral NHCs in metathesis contain "geared" backbones which transfer chirality to the unsymmetrical N-aryl rings by defining their orientation. Racemization of these chiral NHCs is inhibited by the high free energy barrier to N-C_{Ar} rotation. However, the corresponding chiral NHC catalysts show low enantioinduction, suggesting poor definition of the chiral pocket. Bulkier chiral N-substituents may improve definition of this pocket while not requiring a "geared" NHC backbone.

Finally, identification of **5** as a six-coordinate complex opens up new possibilities in tandem catalysis, especially since this catalyst shows unusually high activity in enyne metathesis. A tandem enyne-cyclopropanation strategy could be envisioned with the addition of a trigger to terminate metathesis and turn on cyclopropanation. The trigger could simply be the straightforward addition of a non-labile NHC (such as free IMes) to replace the labile pyridine ligand, ensuring coordinative saturation necessary for outer sphere cyclopropanation. Indeed, this tandem catalysis strategy is currently being investigated by Justin Lummiss of this research group.

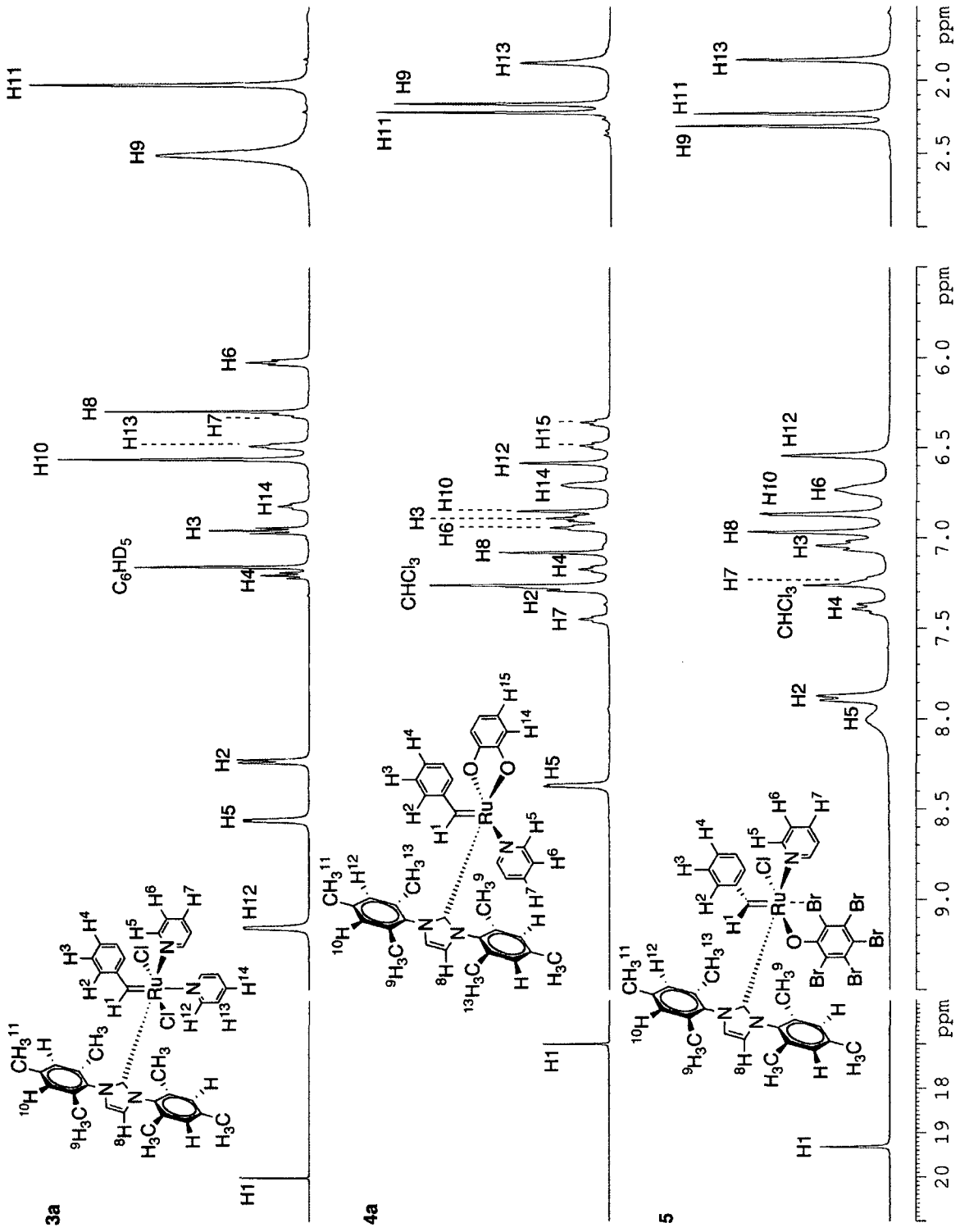

Figure A1. ^{1}H spectra of Ru(=CHPh)Cl_2(IMes)$(py)_2$, **3a** (C_6D_6, 500 MHz, 298 K); Ru(=CHPh)(*o*-cat)(IMes)(py), **4a** ($CDCl_3$, 500 MHz, 298 K); Ru(=CHPh)Cl(κ^2-*O,Br*-OC_6Br_5)(IMes)(py), **5** ($CDCl_3$, 300 MHz, 298 K). Spectra of **5** at 500 MHz show greater signal broadening for H^5, in particular: see Figure 13.

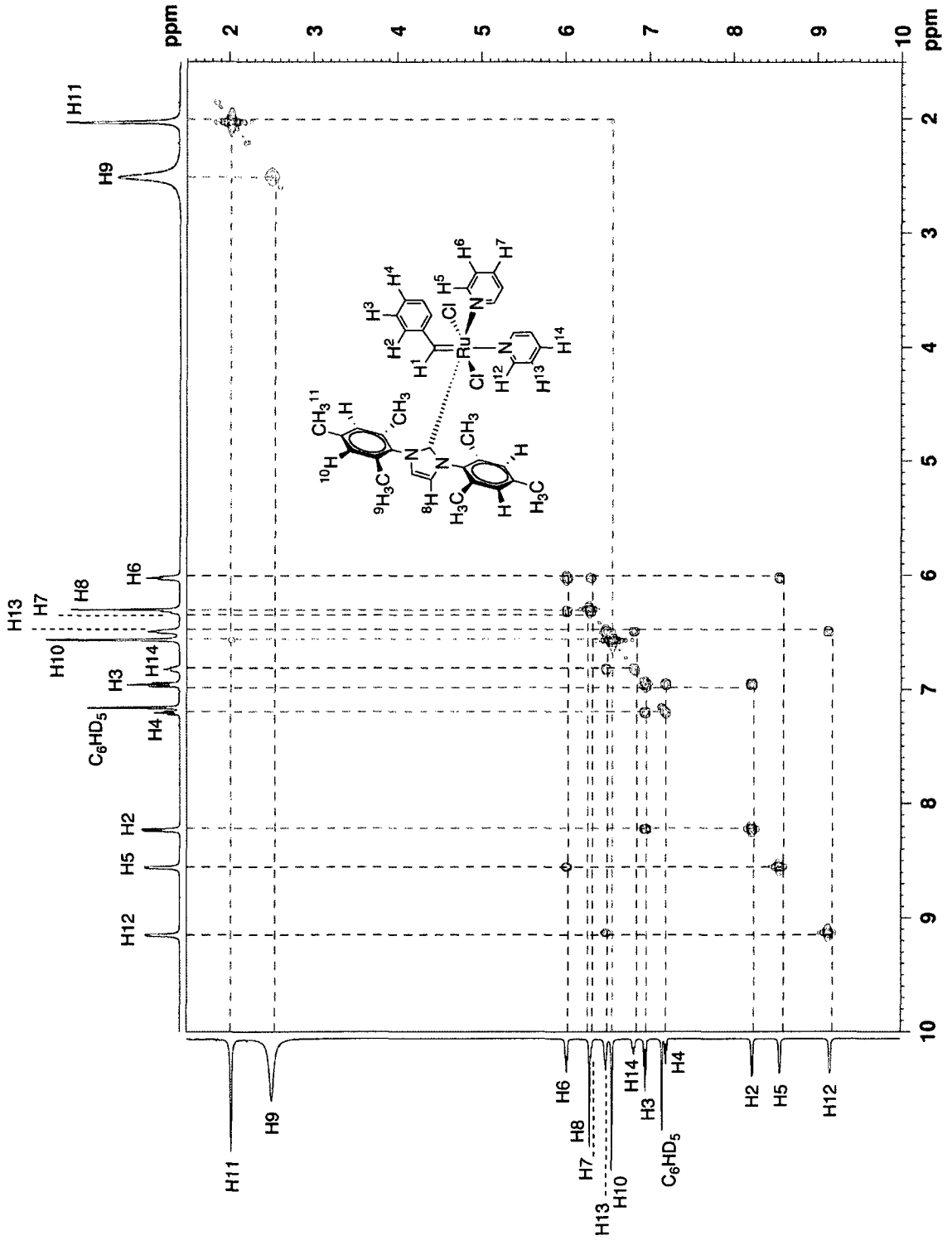

Figure A2. ^{1}H-^{1}H COSY spectrum of Ru(=CHPh)Cl_2(IMes)$(py)_2$, **3a** (C_6D_6, 500 MHz, 298 K). Expansion highlighting aromatic and aliphatic correlations.

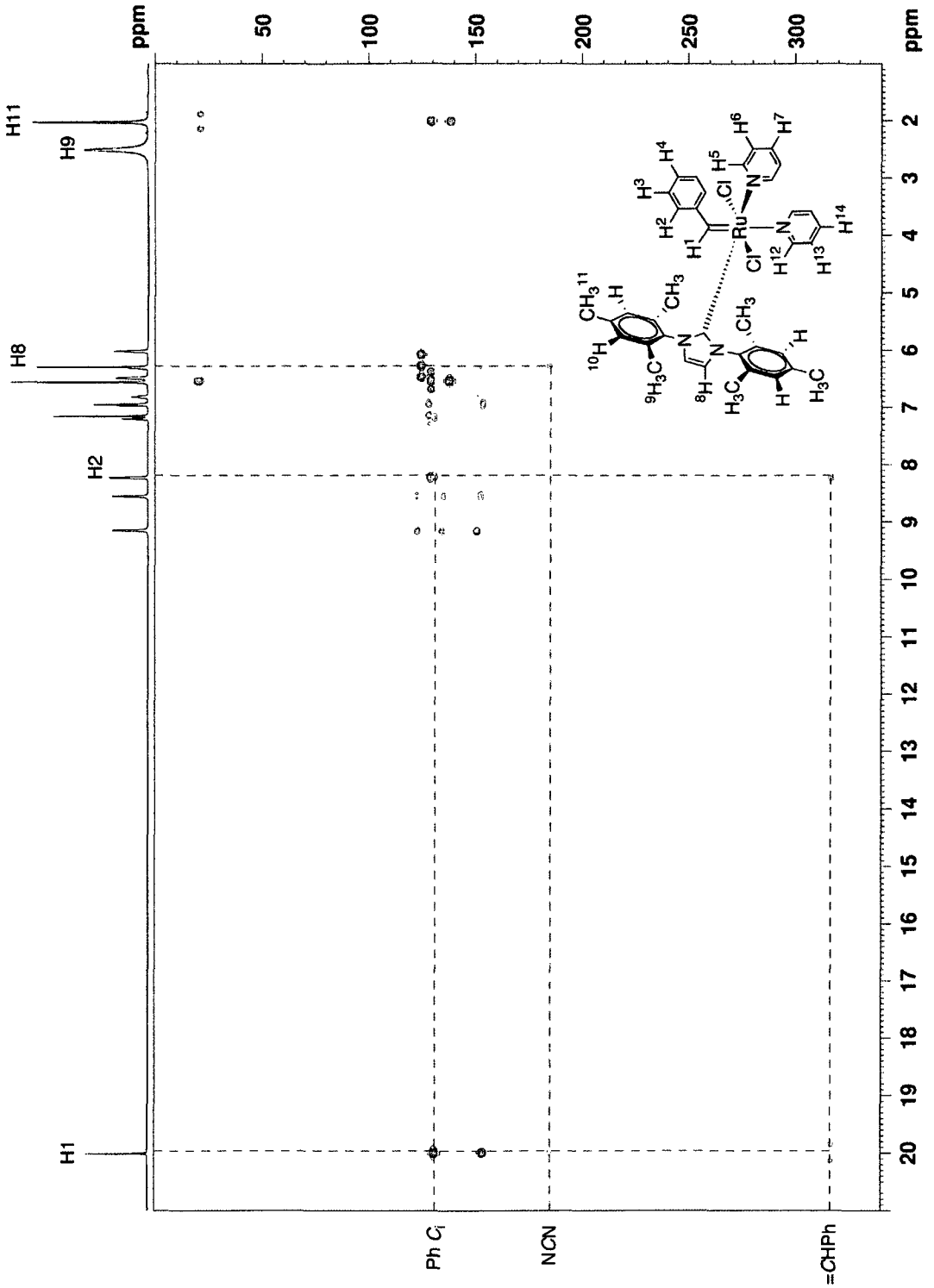

Figure A3. ^{1}H-^{13}C HMBC spectrum of $Ru(=CHPh)Cl_2(IMes)(py)_2$, **3a** ($C_6D_6$, 500 MHz, 298 K).

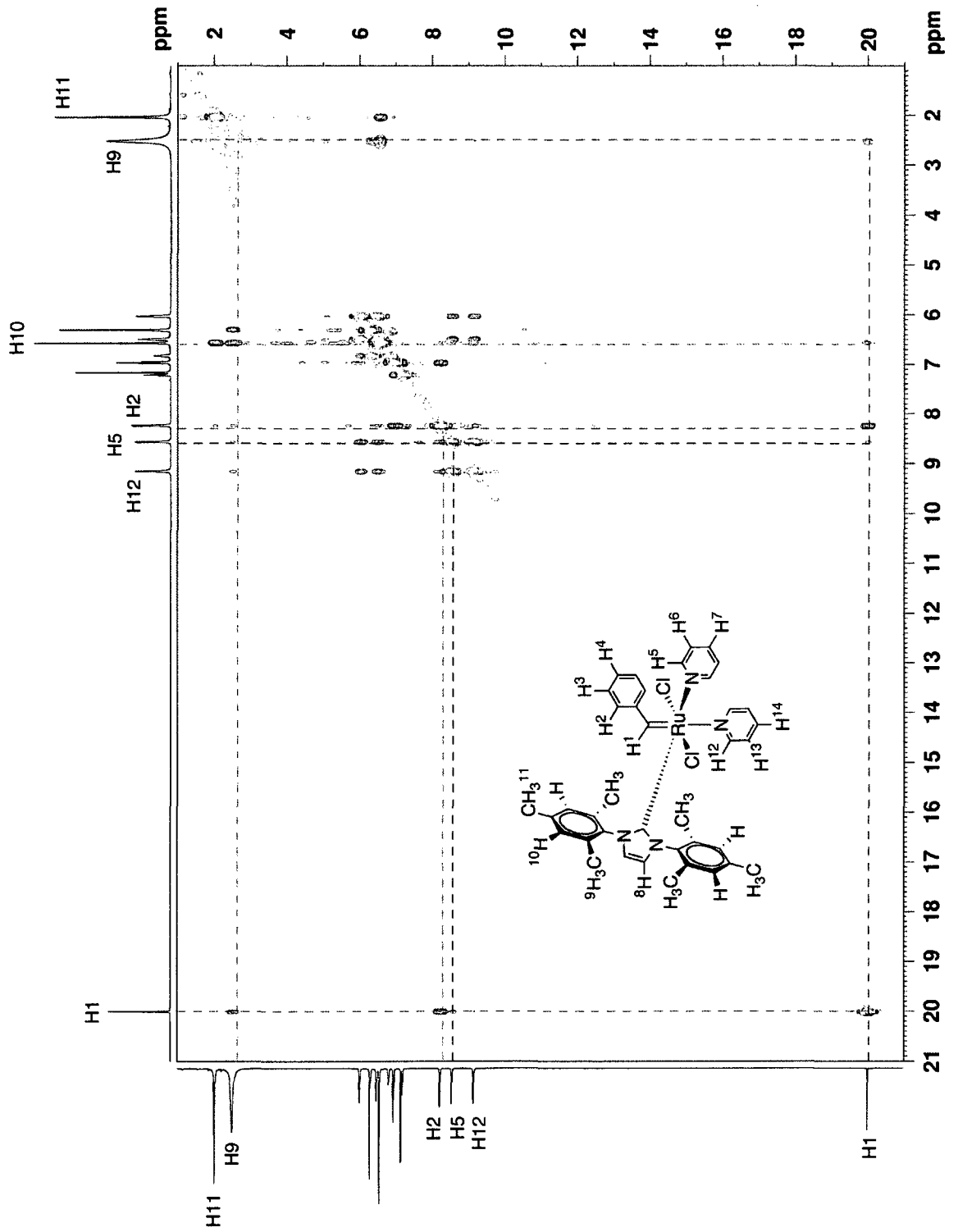

Figure A4. NOESY / EXSY spectrum of Ru(=CHPh)Cl_2(IMes)$(py)_2$, **3a** (C_6D_6, 500 MHz, 298 K, 900 ms mixing time), highlighting benzylidene correlations. Contours in red indicate negative (EXSY) correlations; in black, positive (NOE) correlations.

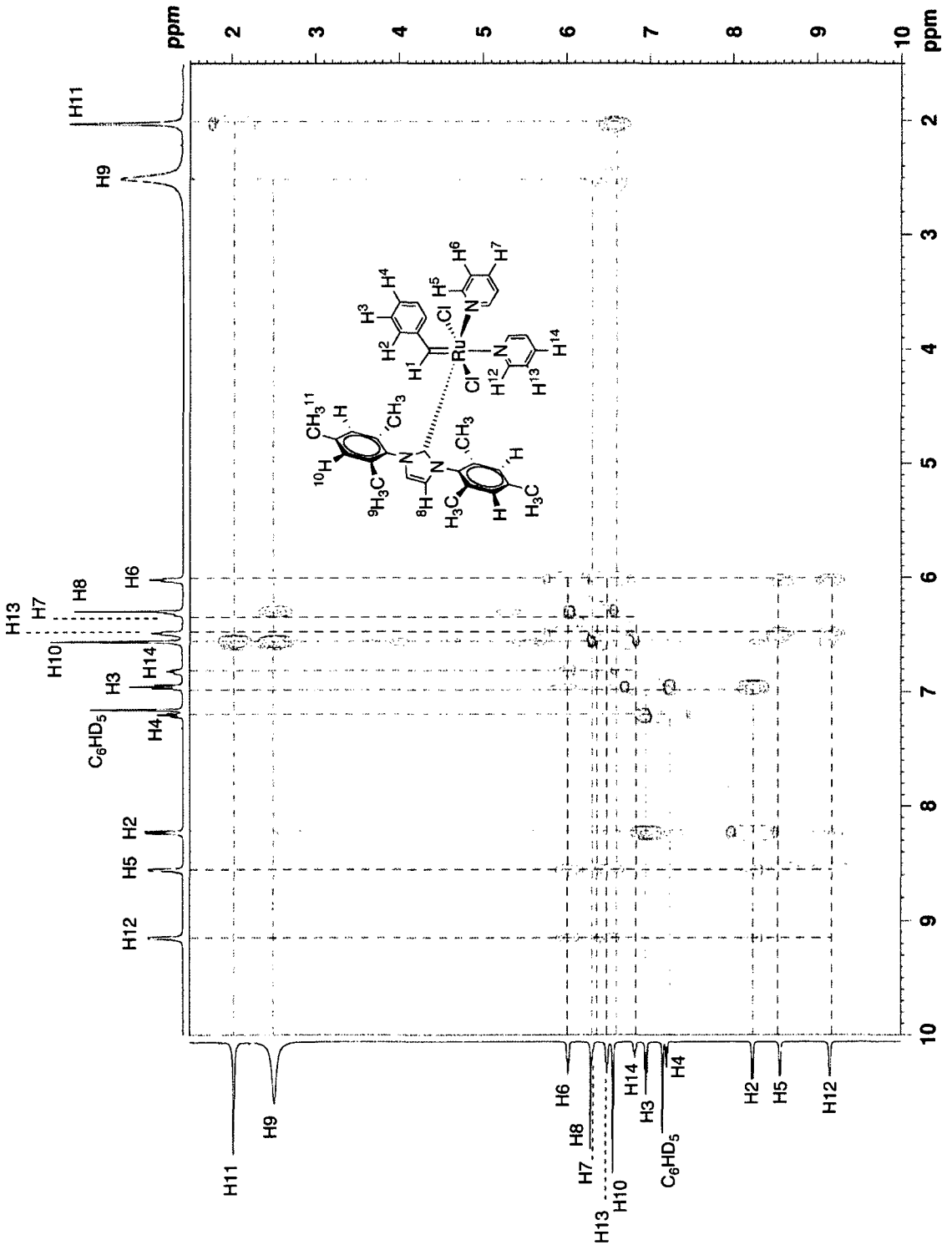

Figure A5. NOESY / EXSY spectrum of Ru(=CHPh)Cl_2(IMes)$(py)_2$, **3a** (C_6D_6, 500 MHz, 298 K, 900 ms mixing time). Expansion highlighting aromatic and aliphatic correlations. Contours in red indicate negative (EXSY) correlations; in black, positive (NOE) correlations.

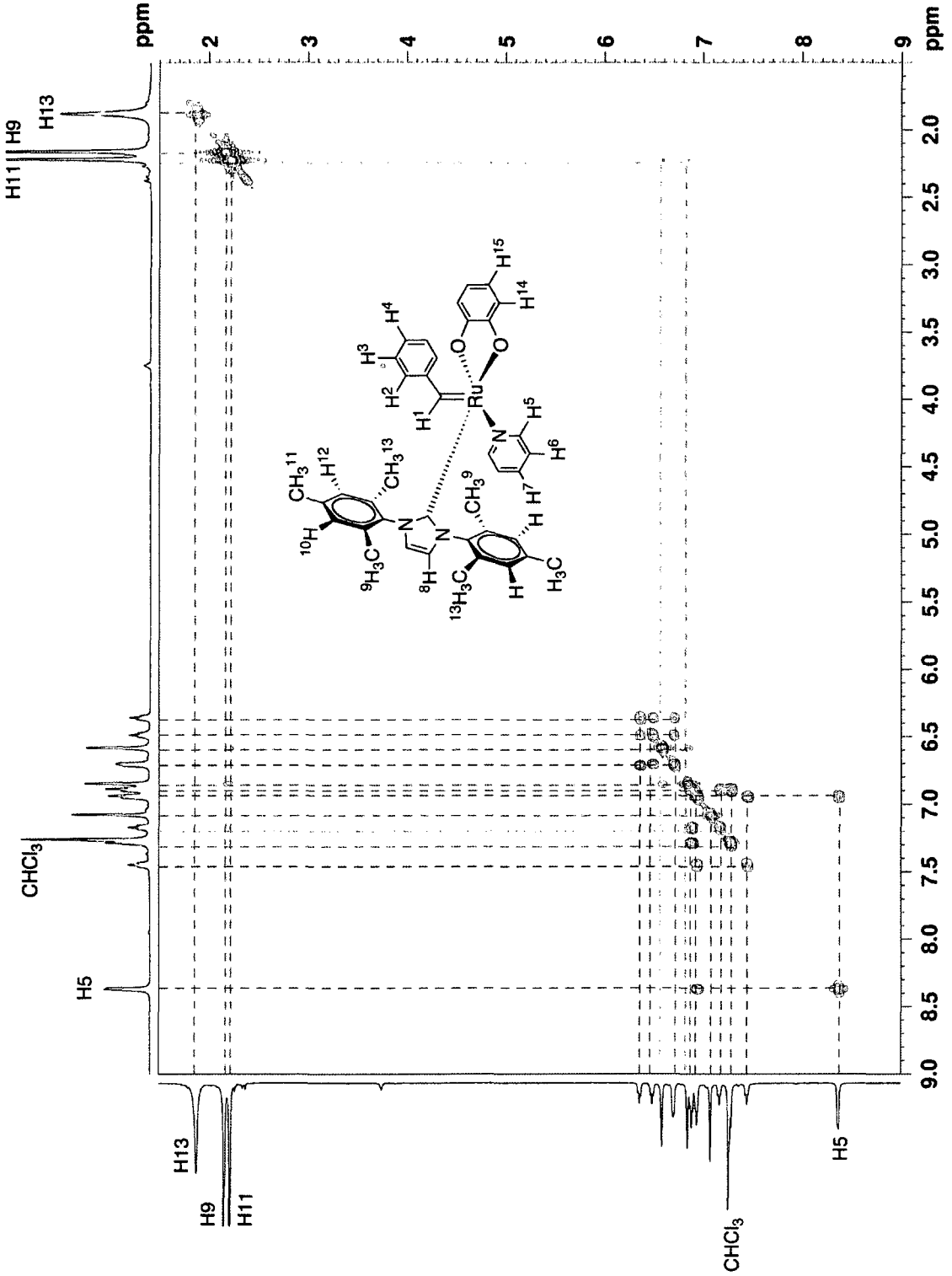

Figure A6. ^{1}H-^{1}H COSY spectrum of Ru(=CHPh)(*o*-cat)(IMes)(py), **4a** ($CDCl_3$, 500 MHz, 298 K). Expansion highlighting aromatic and aliphatic correlations.

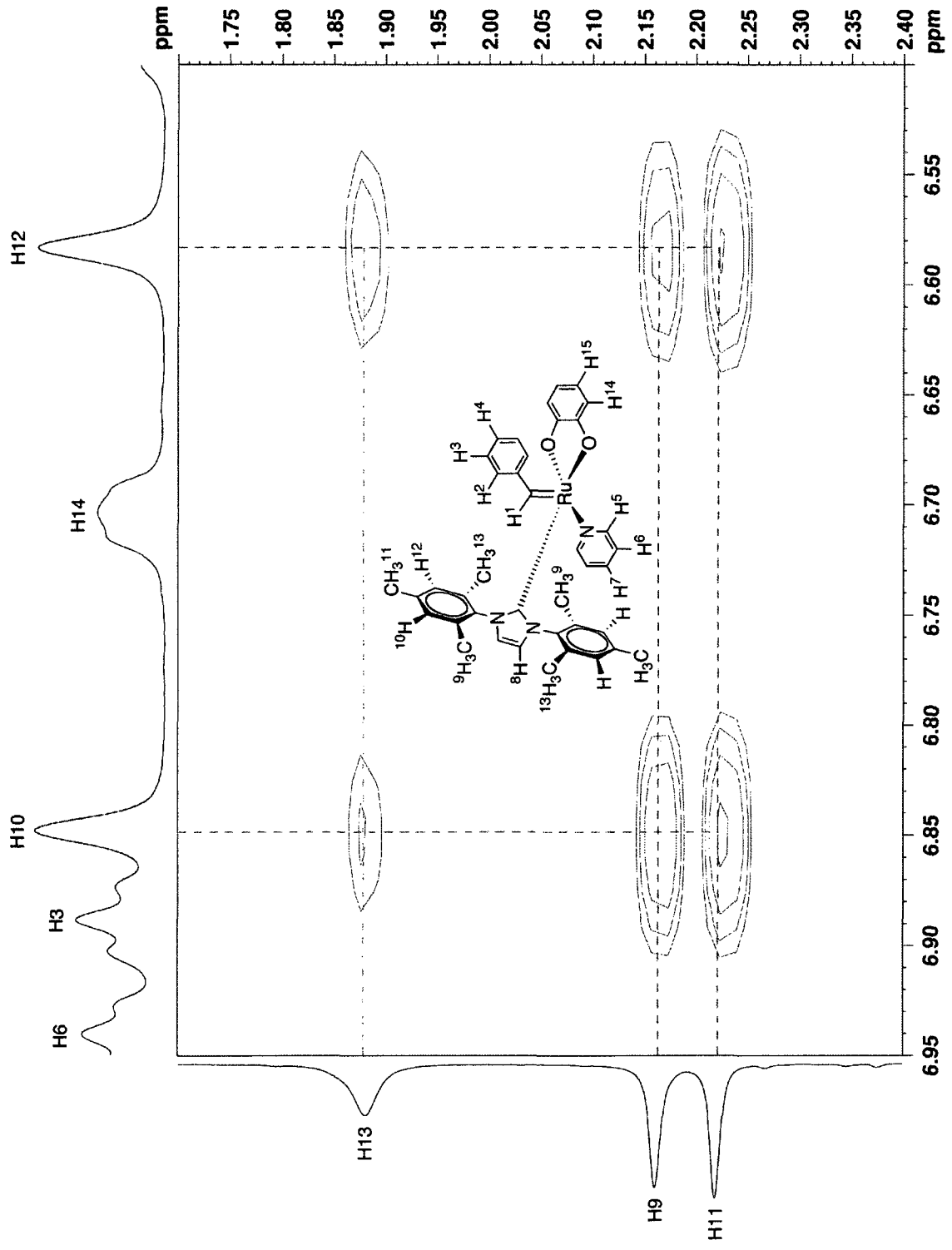

Figure A7. ^{1}H-^{1}H COSY spectrum of Ru(=CHPh)(*o*-cat)(IMes)(py), **4a** ($CDCl_3$, 500 MHz, 298 K). Expansion highlighting aromatic-aliphatic correlations.

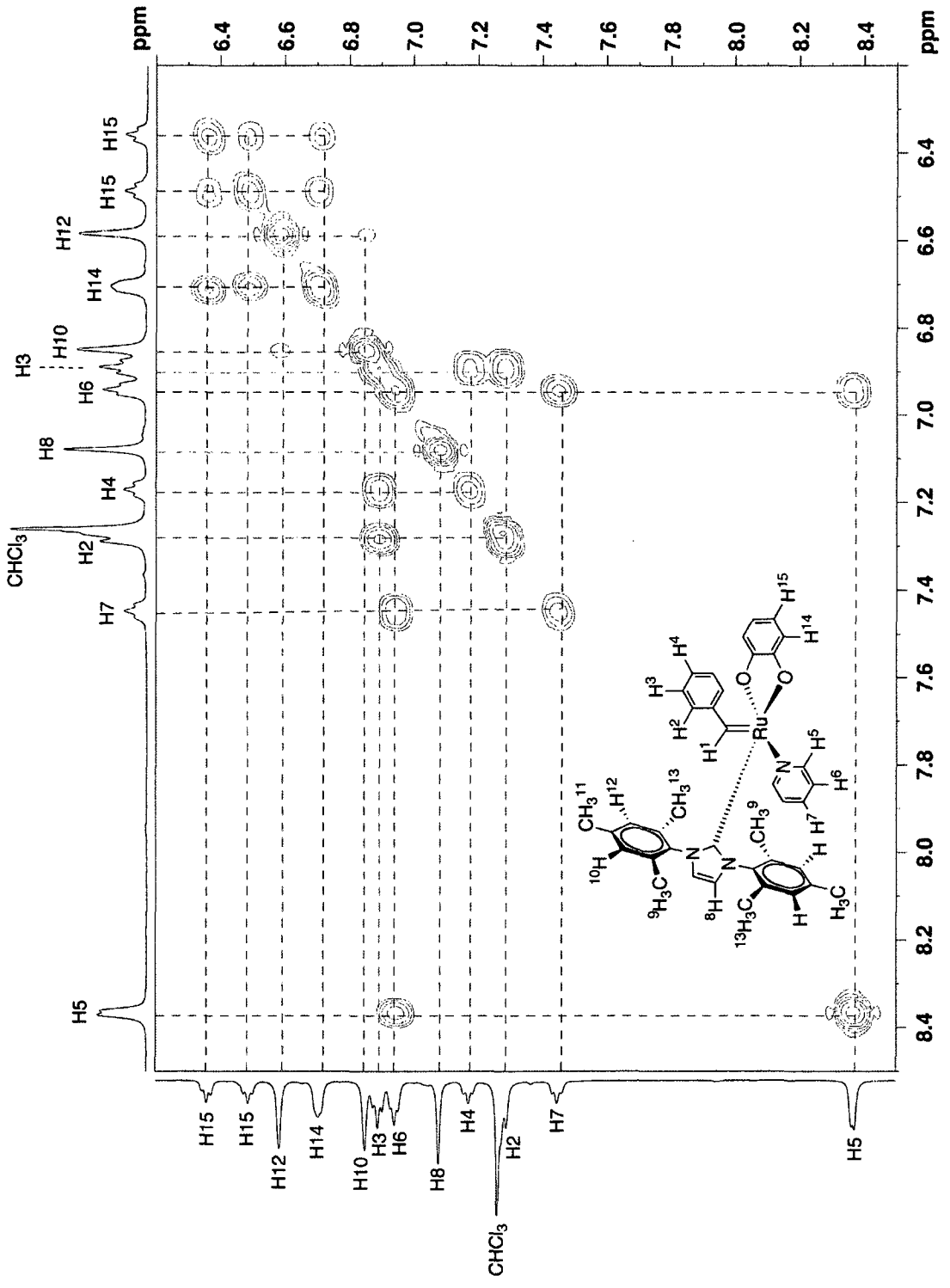

Figure A8. ^{1}H-^{1}H COSY spectrum of Ru(=CHPh)(*o*-cat)(IMes)(py), **4a** ($CDCl_3$, 500 MHz, 298 K). Expansion highlighting aromatic correlations.

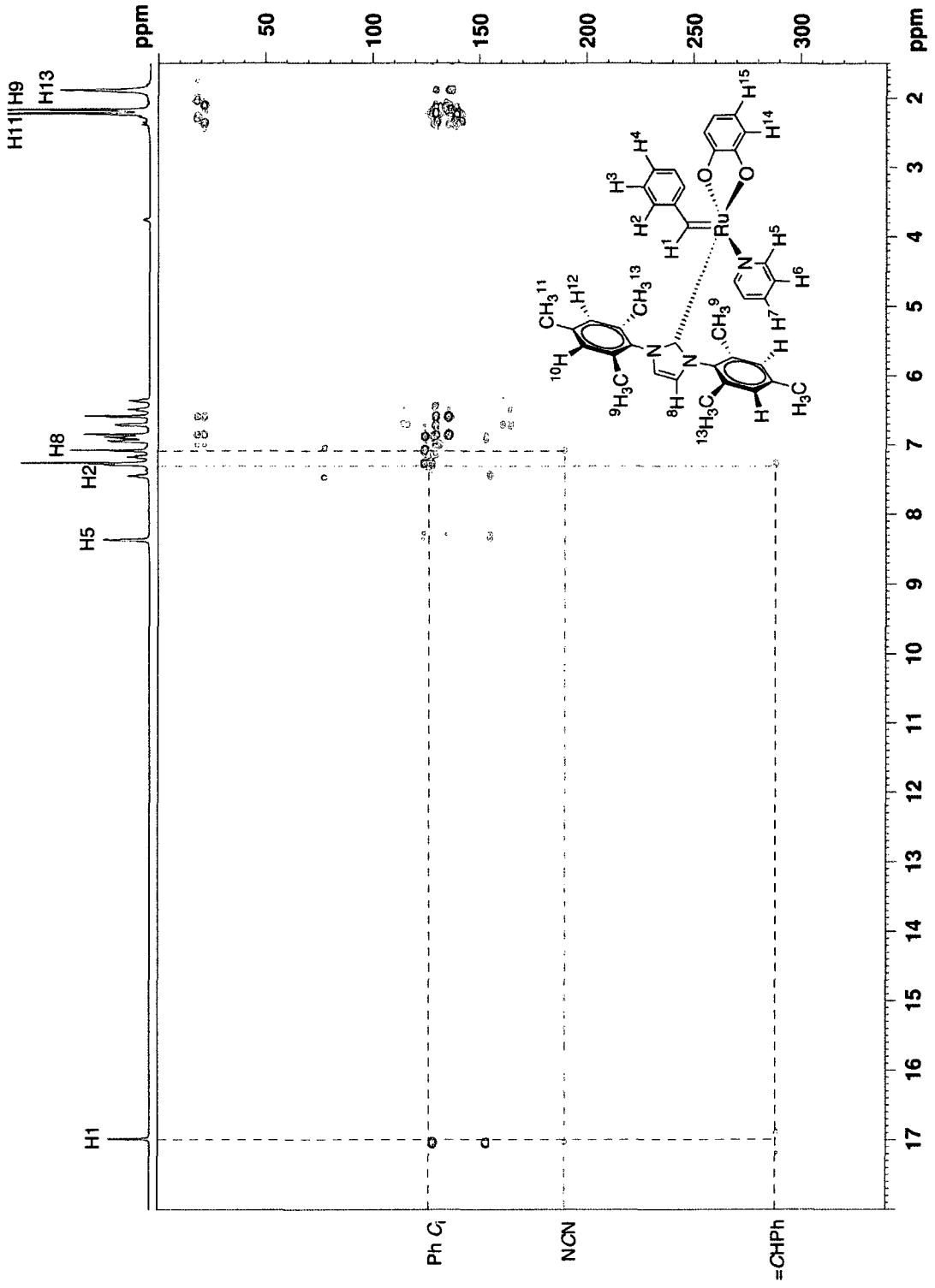

Figure A9. ^{1}H-^{13}H HMBC spectrum of Ru(=CHPh)(*o*-cat)(IMes)(py), **4a** ($CDCl_3$, 500 MHz, 298 K).

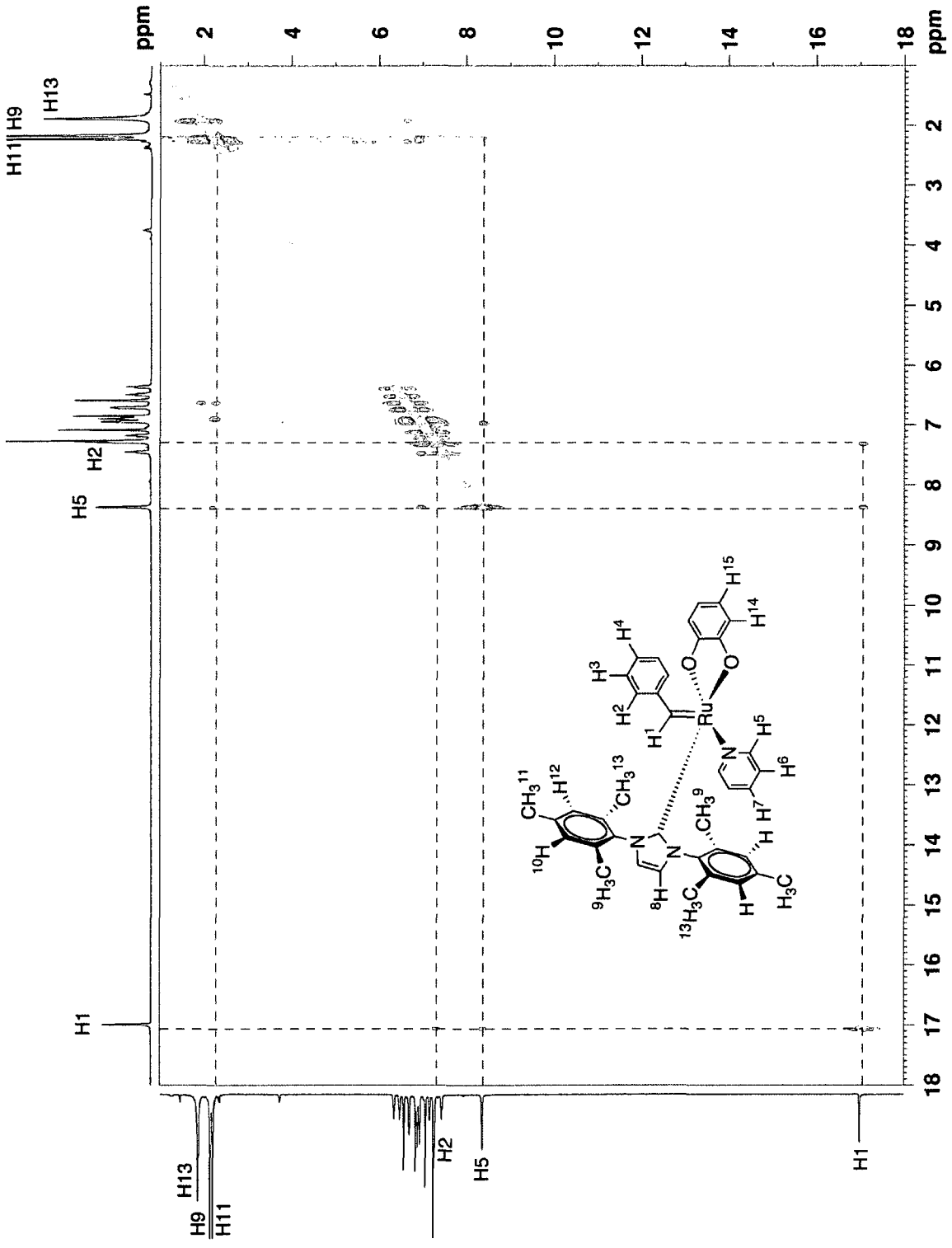

Figure A10. NOESY spectrum of Ru(=CHPh)(*o*-cat)(IMes)(py), **4a** ($CDCl_3$, 500 MHz, 298 K, 800 ms mixing time), highlighting benzylidene correlations.

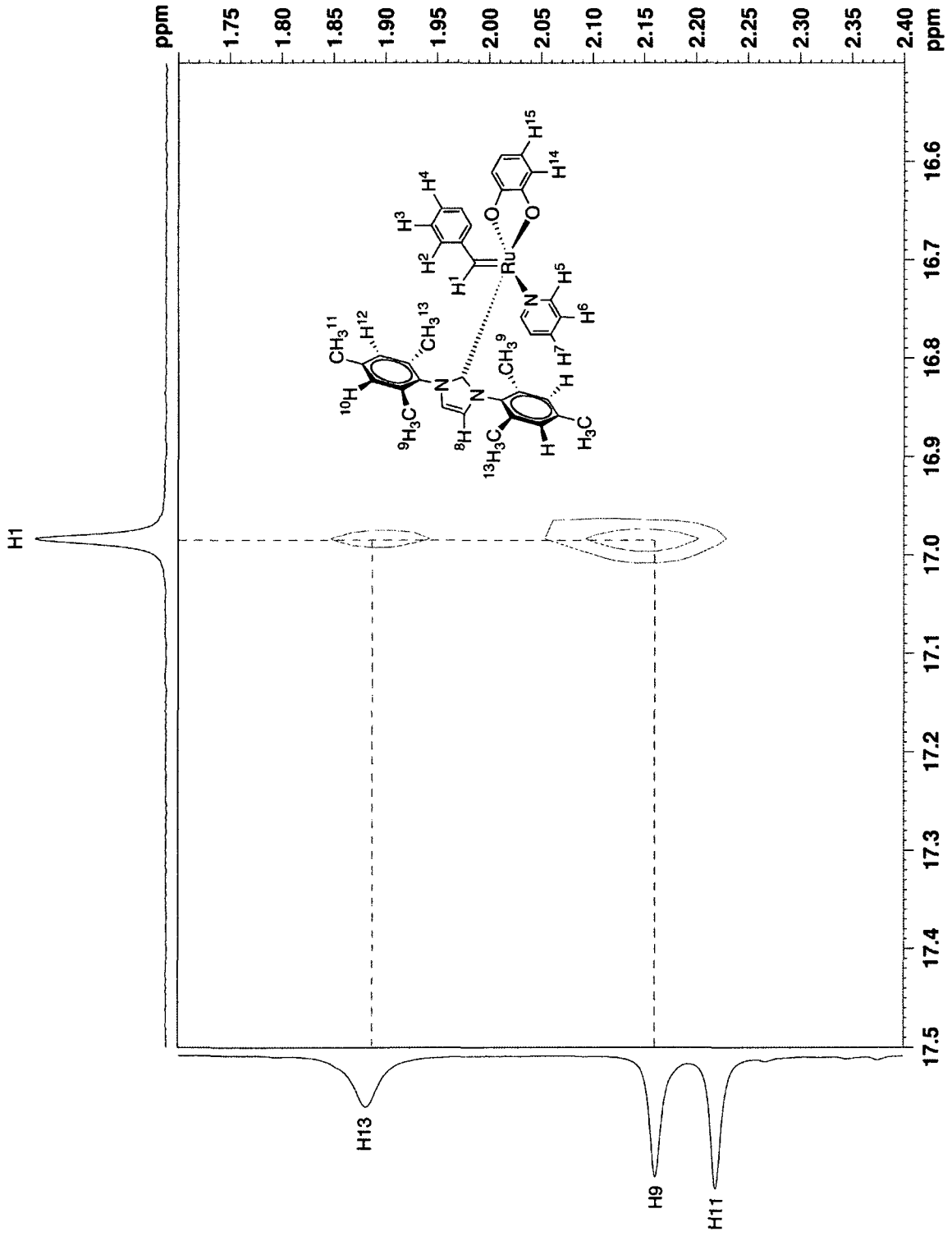

Figure A11. NOESY spectrum of Ru(=CHPh)(*o*-cat)(IMes)(py), **4a** ($CDCl_3$, 500 MHz, 298 K, 800 ms mixing time). Expansion highlighting benzylidene-aliphatic correlations.

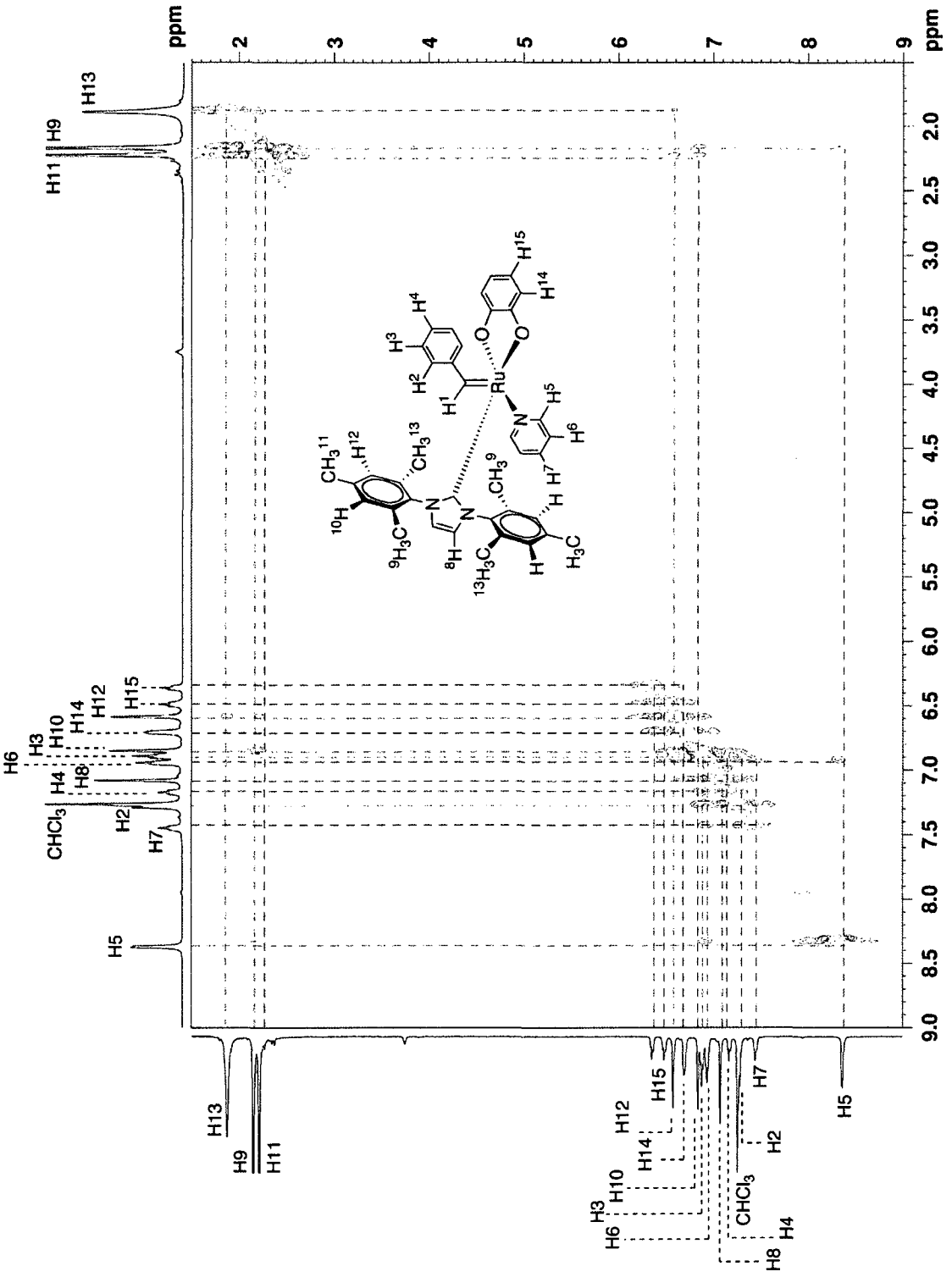

Figure A12. NOESY spectrum of Ru(=CHPh)(*o*-cat)(IMes)(py), **4a** ($CDCl_3$, 500 MHz, 298 K, 800 ms mixing time). Expansion highlighting aromatic and aliphatic correlations.

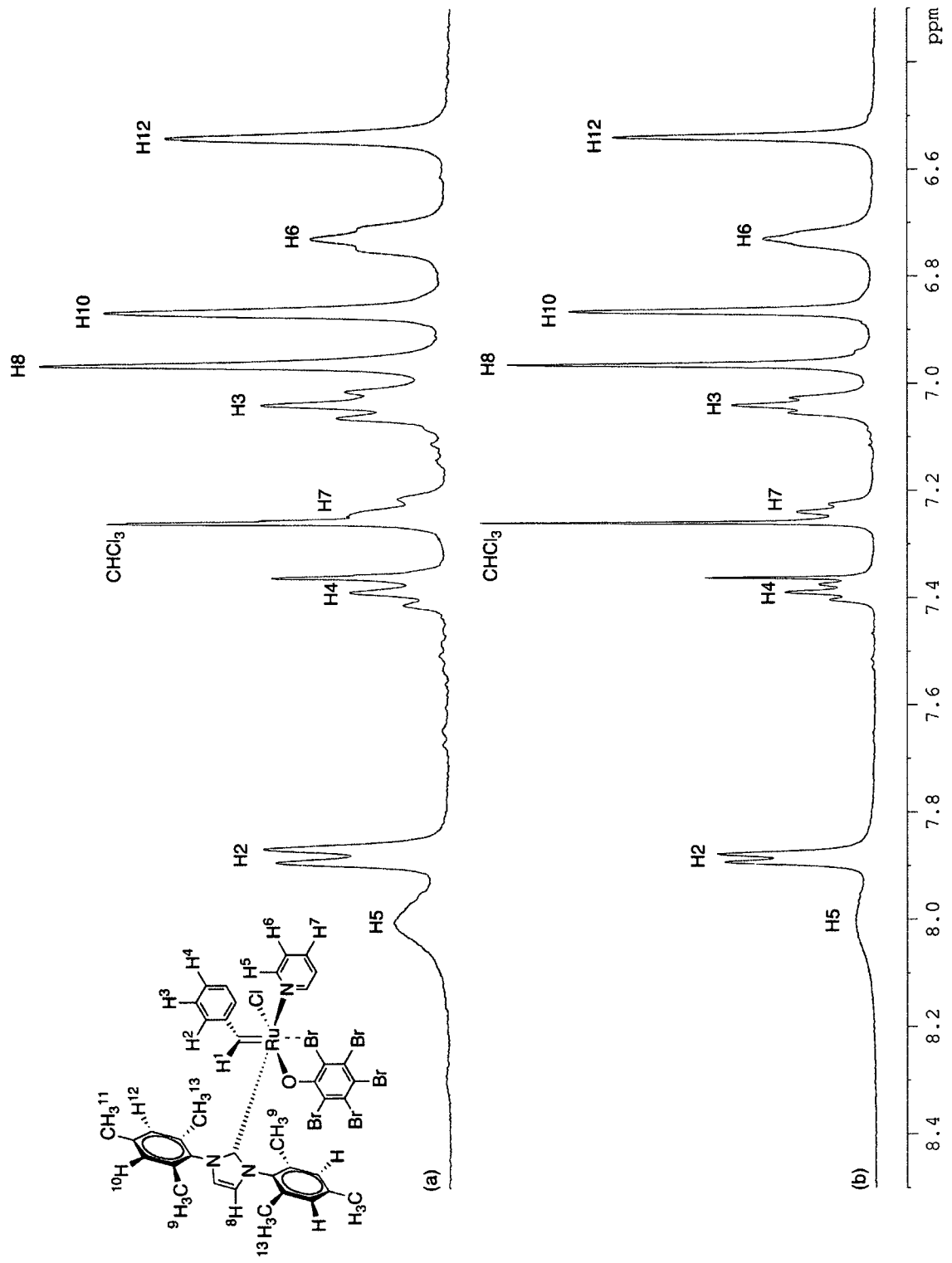

Figure A13. ^{1}H spectra ($CDCl_3$, 298 K) of Ru(=CHPh)Cl(κ^2-*O,Br*-OC_6Br_5)(IMes)(py), **5** at (a) 300 and (b) 500 MHz. Expansion highlighting aromatic peaks.

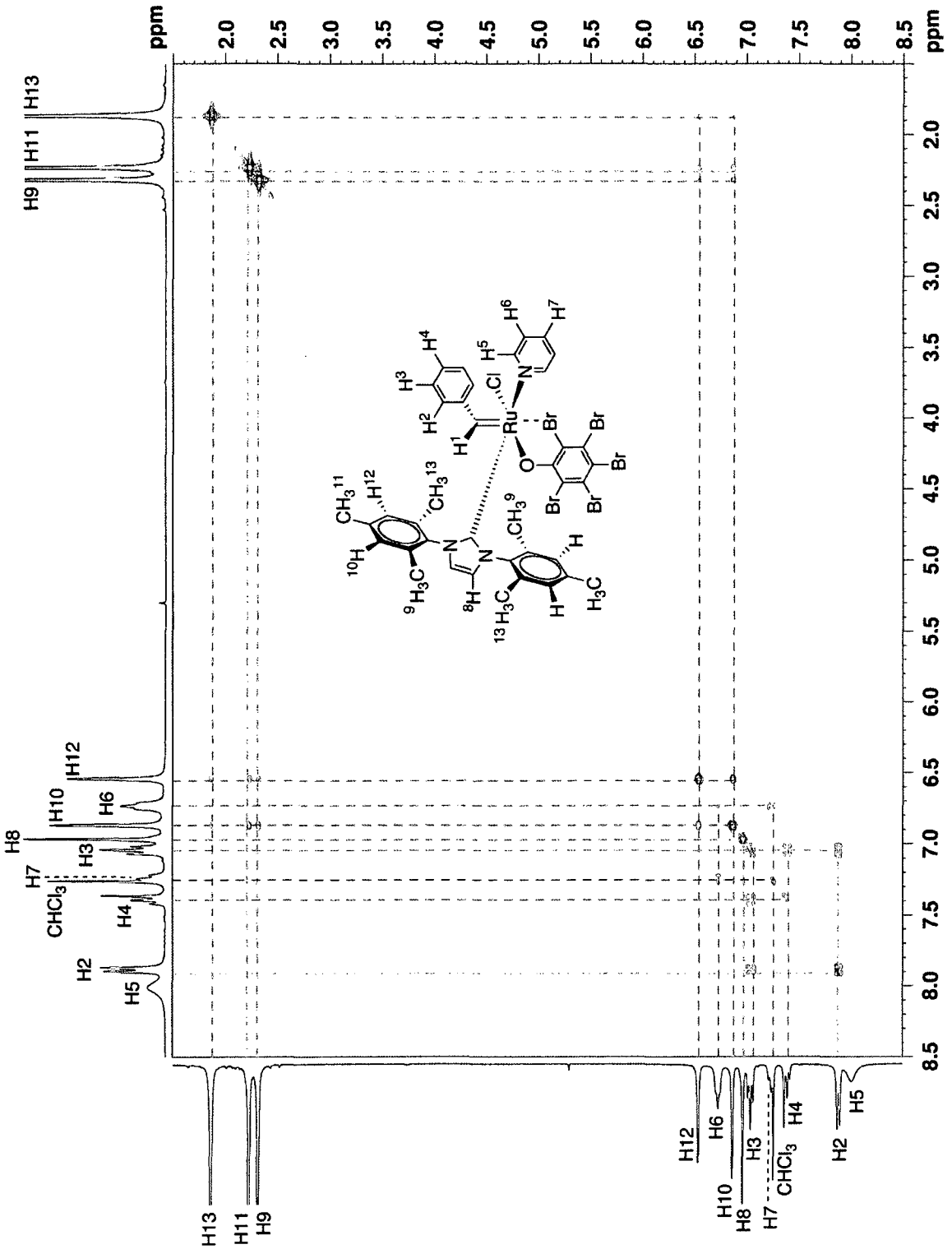

Figure A14. ^{1}H-^{1}H COSY spectrum of Ru(=CHPh)Cl(κ^2-*O,Br*-OC_6Br_5)(IMes)(py), **5** ($CDCl_3$, 300 MHz, 298 K). Expansion highlighting aromatic and aliphatic correlations.

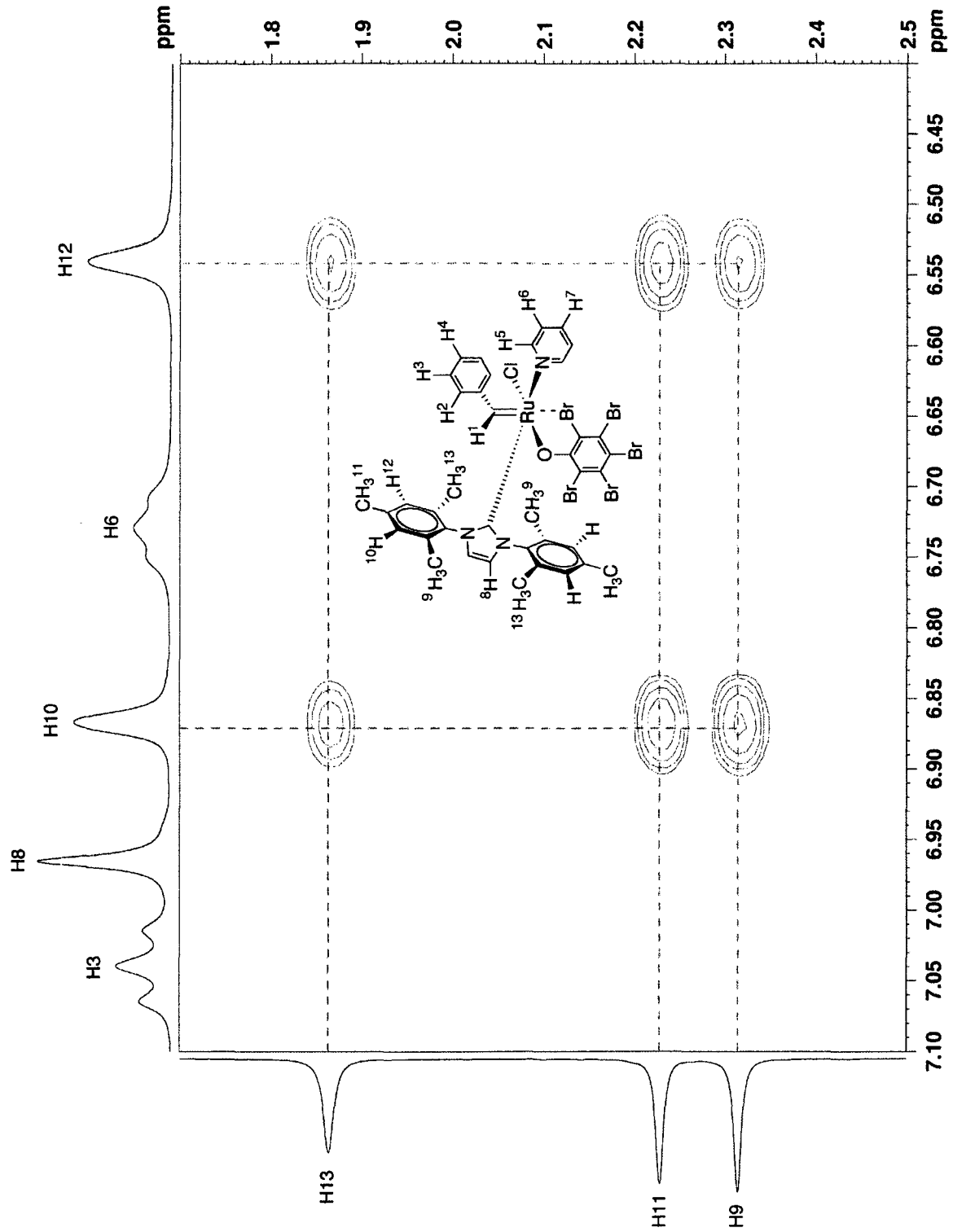

Figure A15. ^{1}H-^{1}H COSY spectrum of Ru(=CHPh)Cl(κ^2-*O,Br*-OC_6Br_5)(IMes)(py), **5** ($CDCl_3$, 300 MHz, 298 K). Expansion highlighting aromatic-aliphatic correlations.

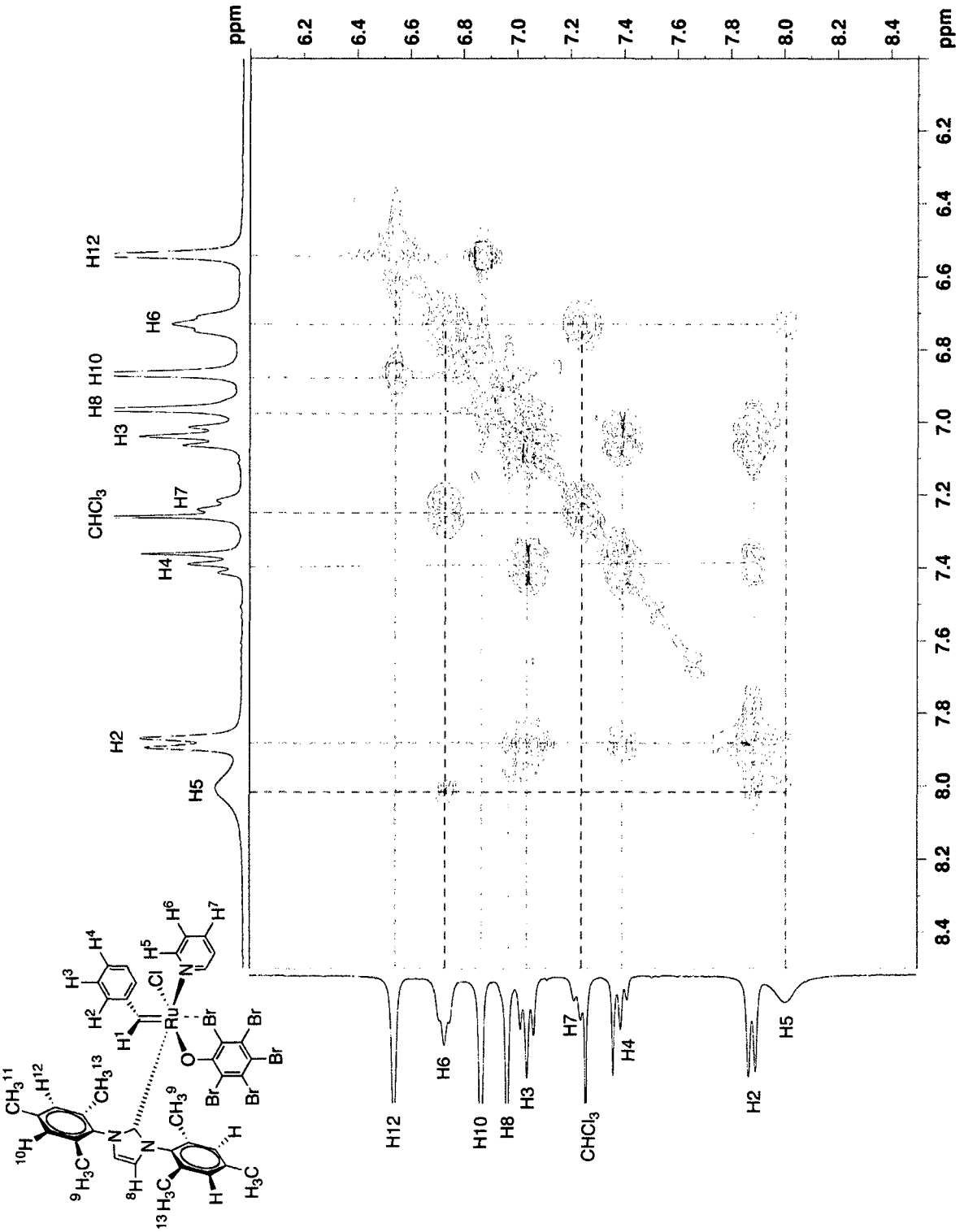

Figure A16. ^{1}H-^{1}H COSY spectrum of Ru(=CHPh)Cl(κ^2-*O,Br*-OC_6Br_5)(IMes)(py), **5** ($CDCl_3$, 300 MHz, 298 K). Expansion highlighting aromatic correlations.

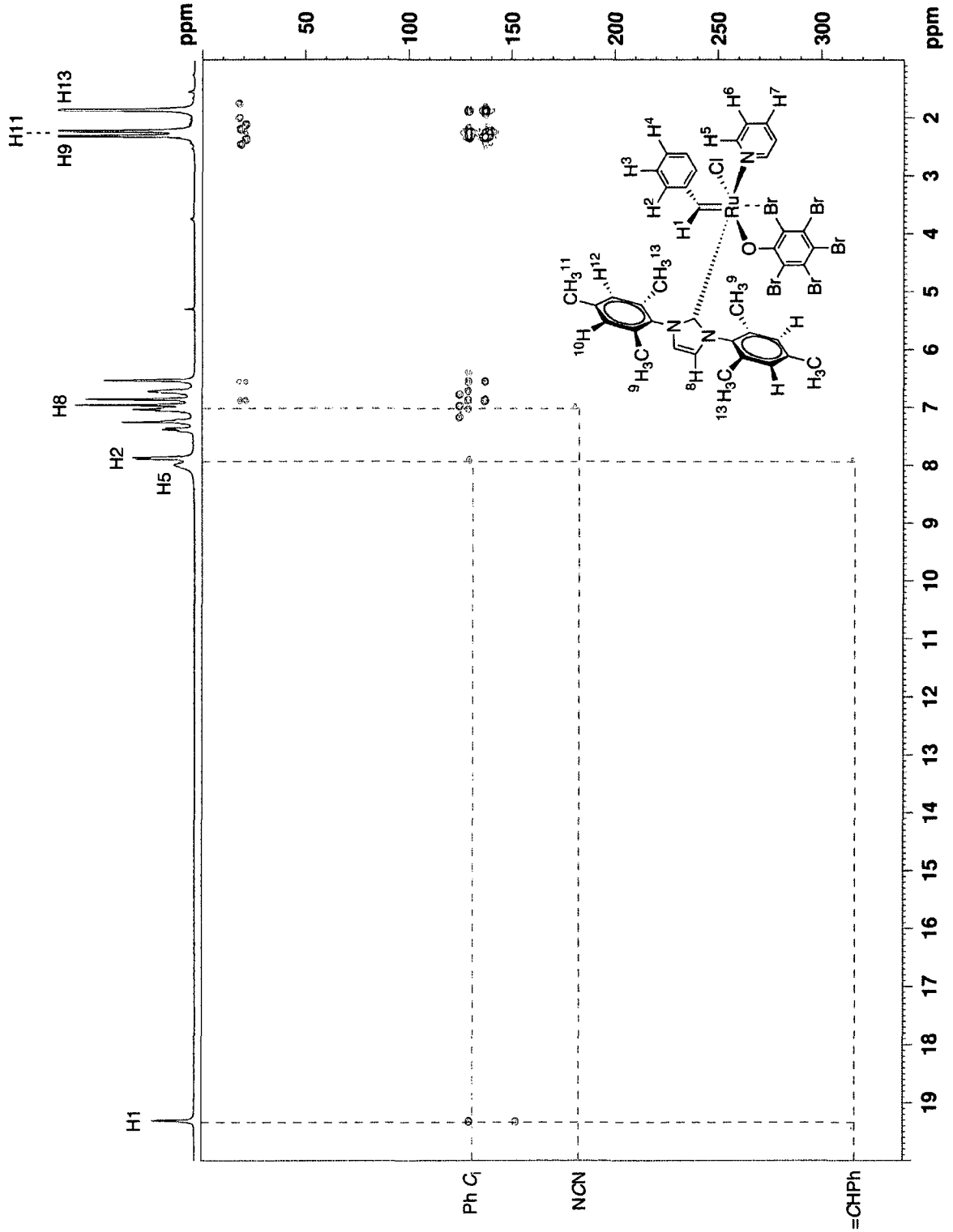

Figure A17. ^{1}H-^{13}H HMBC spectrum of Ru(=CHPh)Cl(κ^2-*O,Br*-OC_6Br_5)(IMes)(py), **5** ($CDCl_3$, 500 MHz, 298 K).

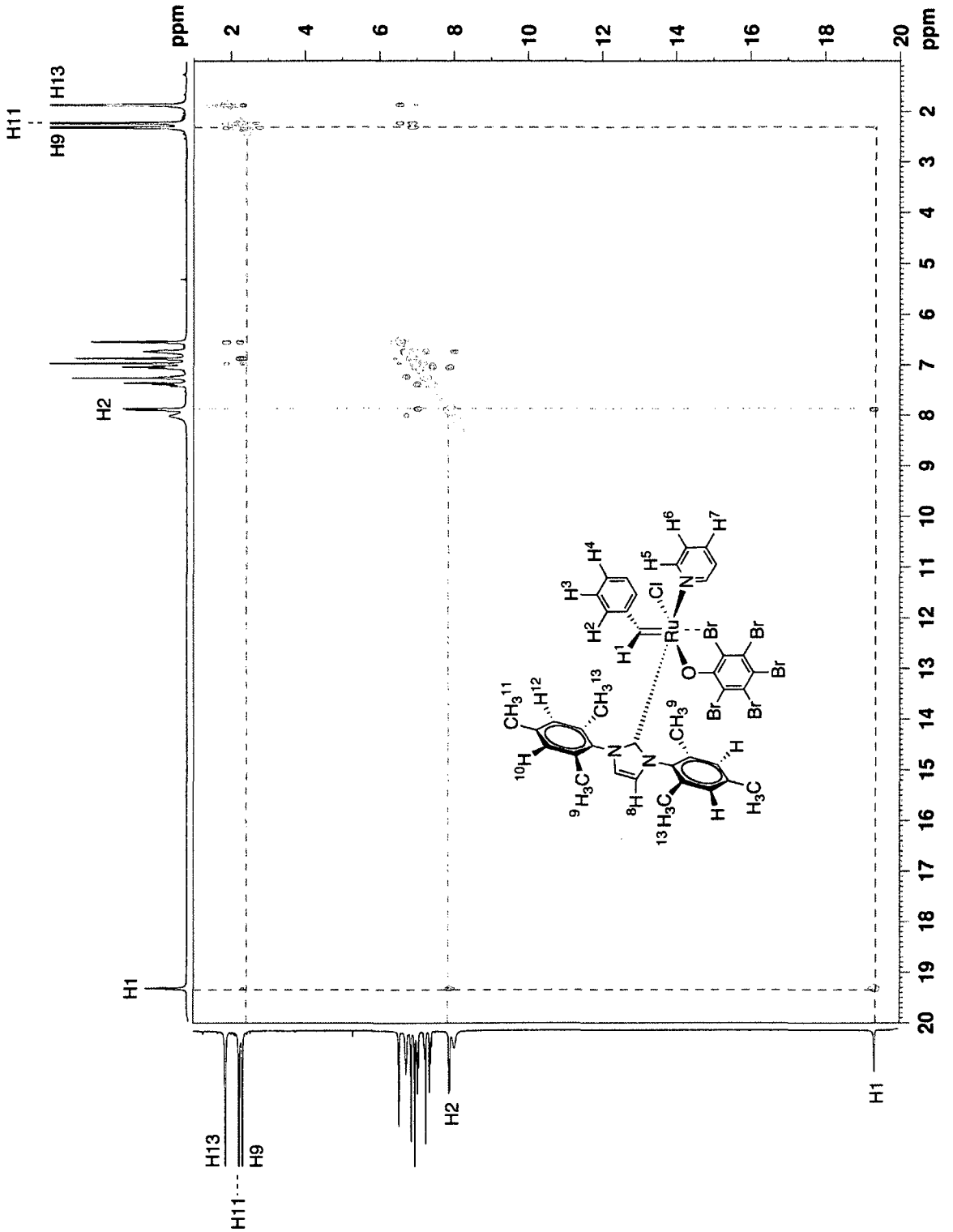

Figure A18. NOESY spectrum of Ru(=CHPh)Cl(κ^2-*O,Br*-OC_6Br_5)(IMes)(py), **5** ($CDCl_3$, 300 MHz, 298 K, 900 ms mixing time), highlighting benzylidene correlations.

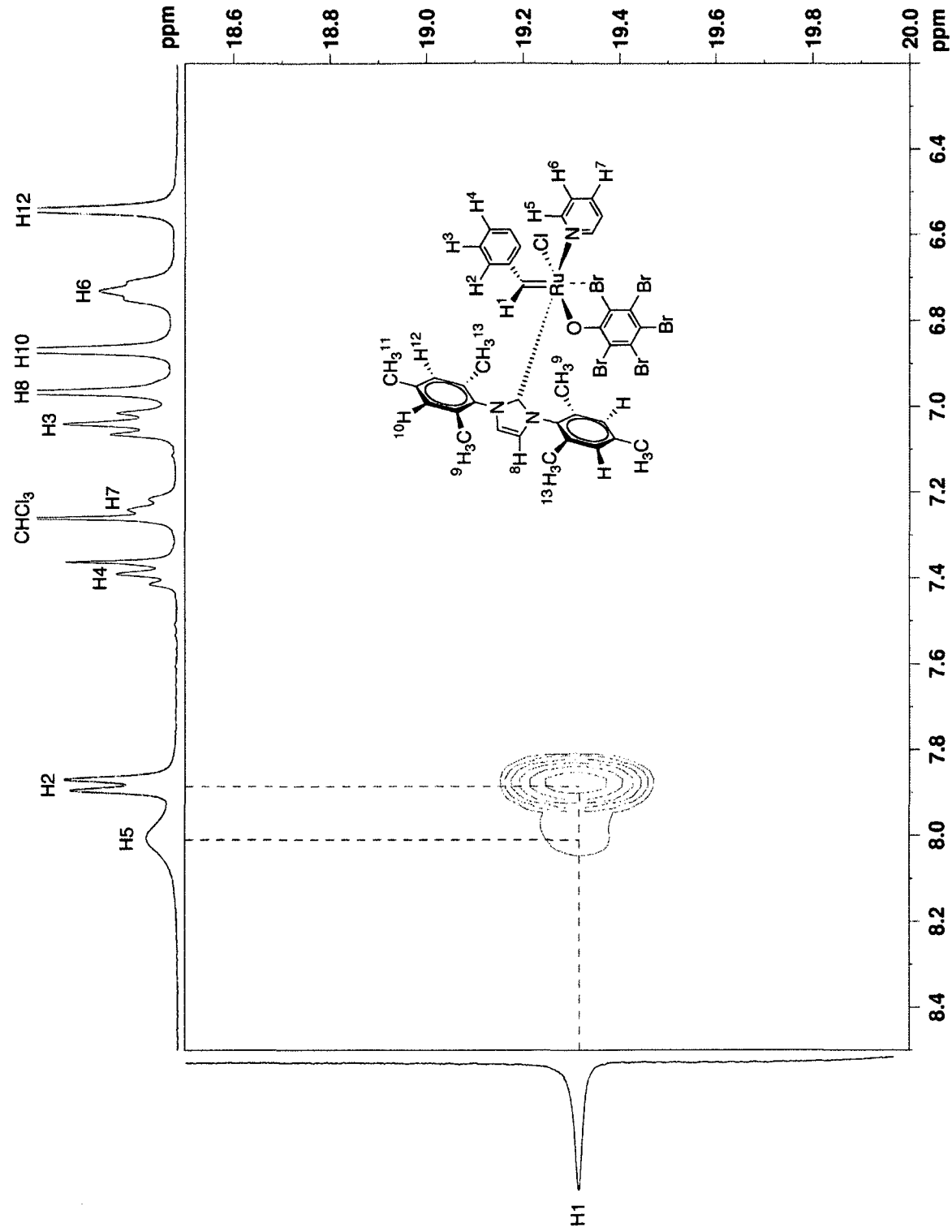

Figure A19. NOESY spectrum of Ru(=CHPh)Cl(κ^2-*O,Br*-OC_6Br_5)(IMes)(py), **5** ($CDCl_3$, 300 MHz, 298 K, 900 ms mixing time). Expansion highlighting benzylidene-aromatic correlations.

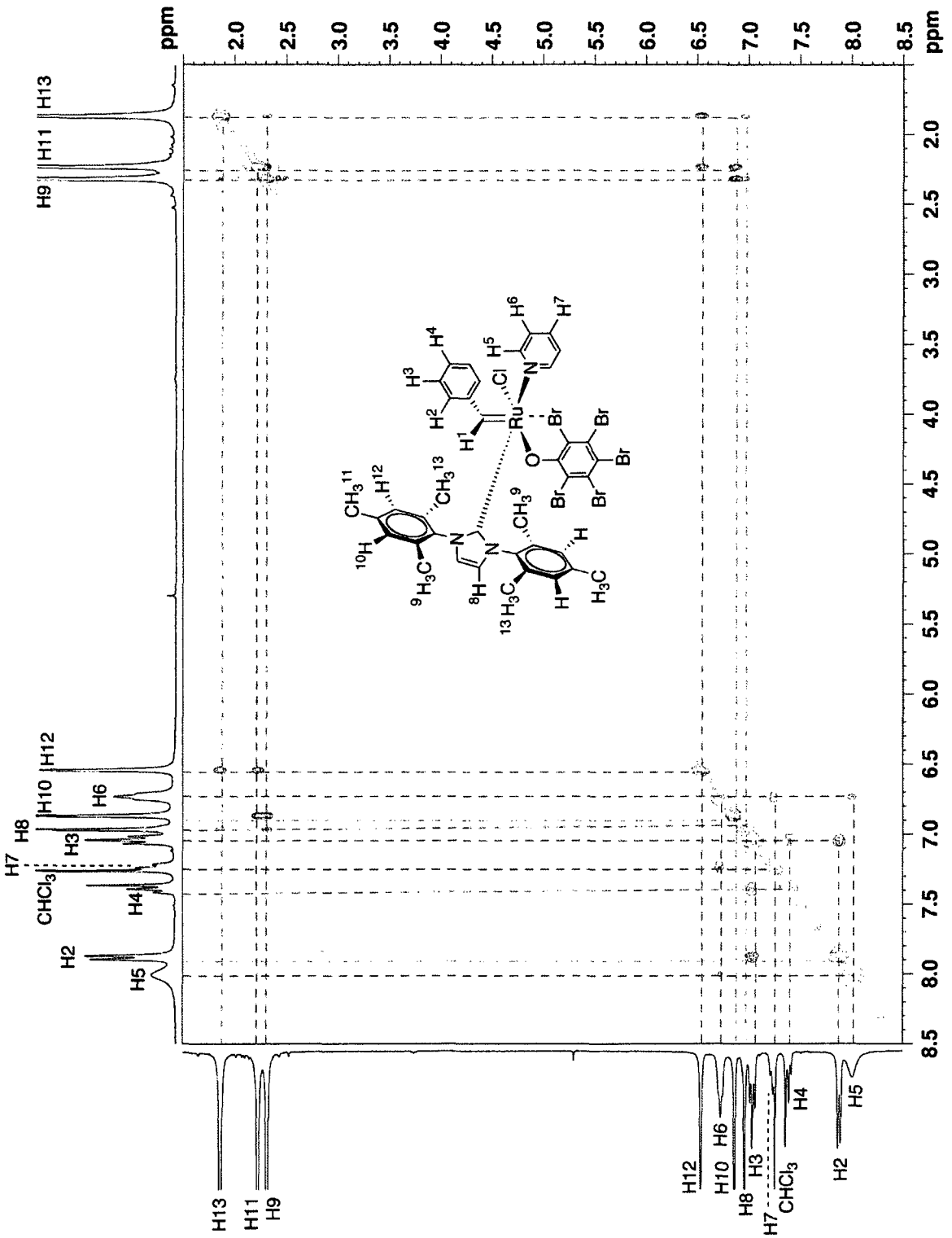

Figure A20. NOESY spectrum of Ru(=CHPh)Cl(κ^2-*O,Br*-OC_6Br_5)(IMes)(py), **5** ($CDCl_3$, 300 MHz, 298 K, 900 ms mixing time). Expansion highlighting aromatic and aliphatic correlations.

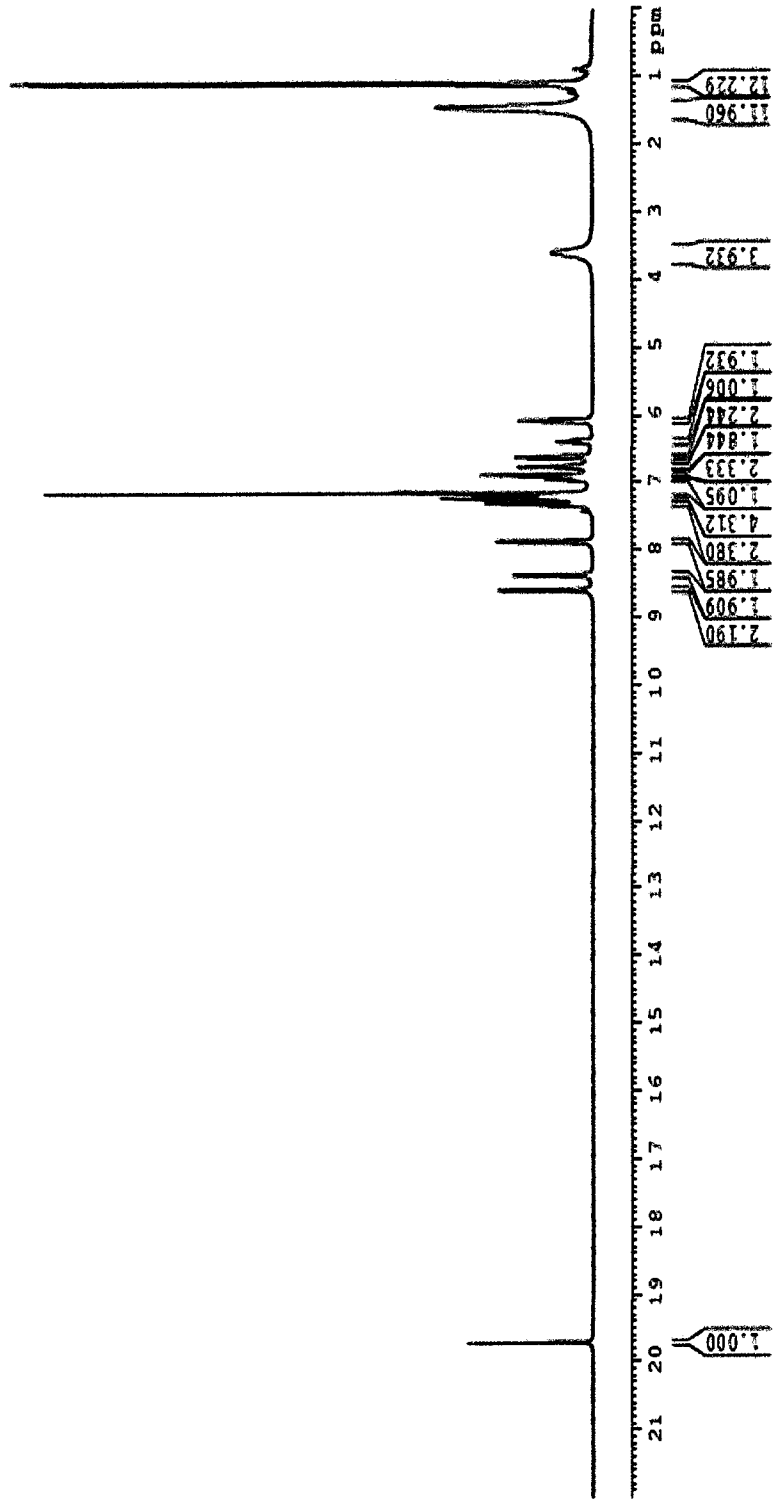

Figure A21. ^{1}H spectra of $Ru(=CHPh)Cl_2(IPr)(py)_2$, **35** (C_6D_6, 500 MHz, 298 K).

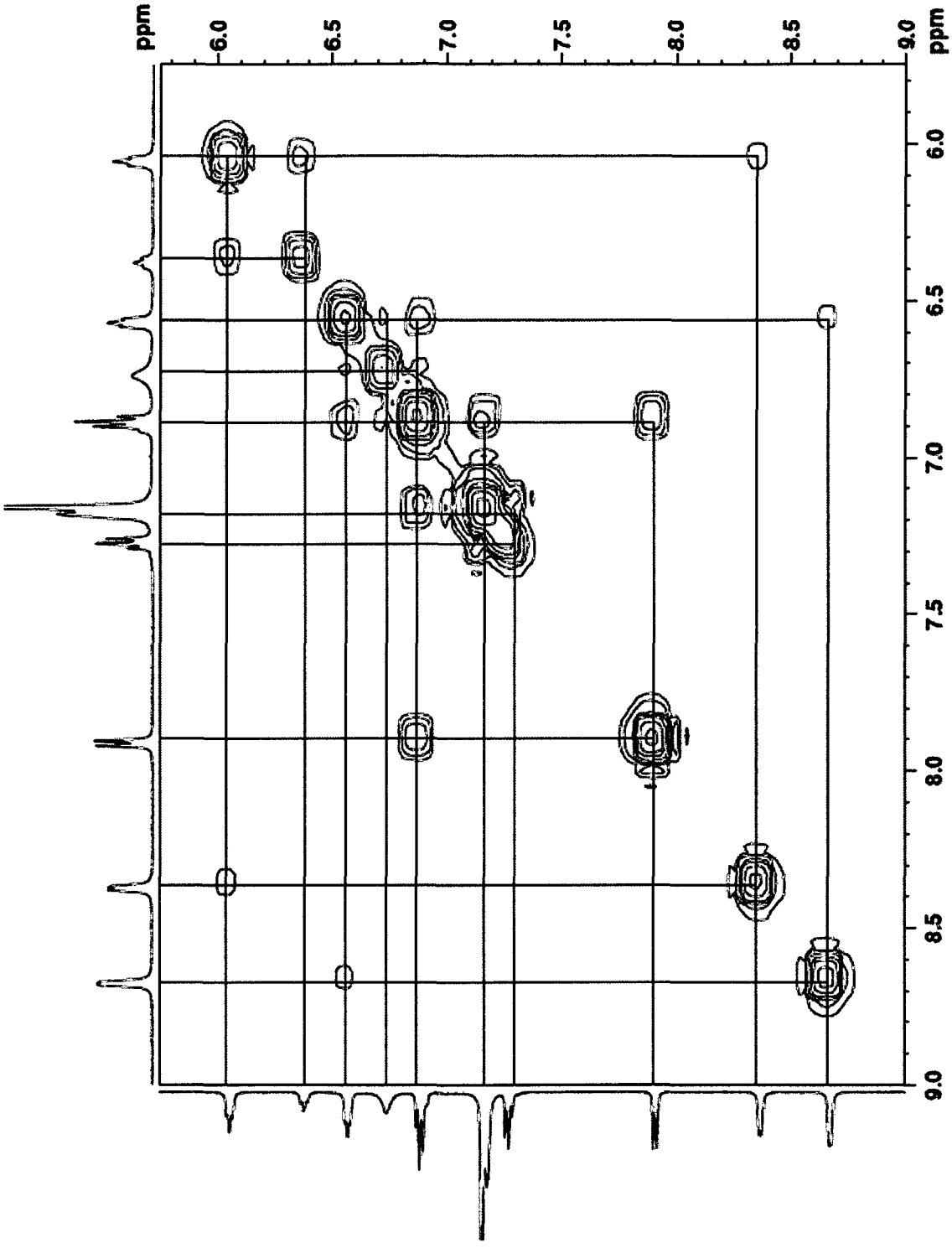

Figure A22. ^{1}H-^{1}H COSY spectrum of Ru(=CHPh)Cl_2(IPr)$(py)_2$, **35** (C_6D_6, 500 MHz, 298 K). Expansion highlighting aromatic-aromatic correlations.

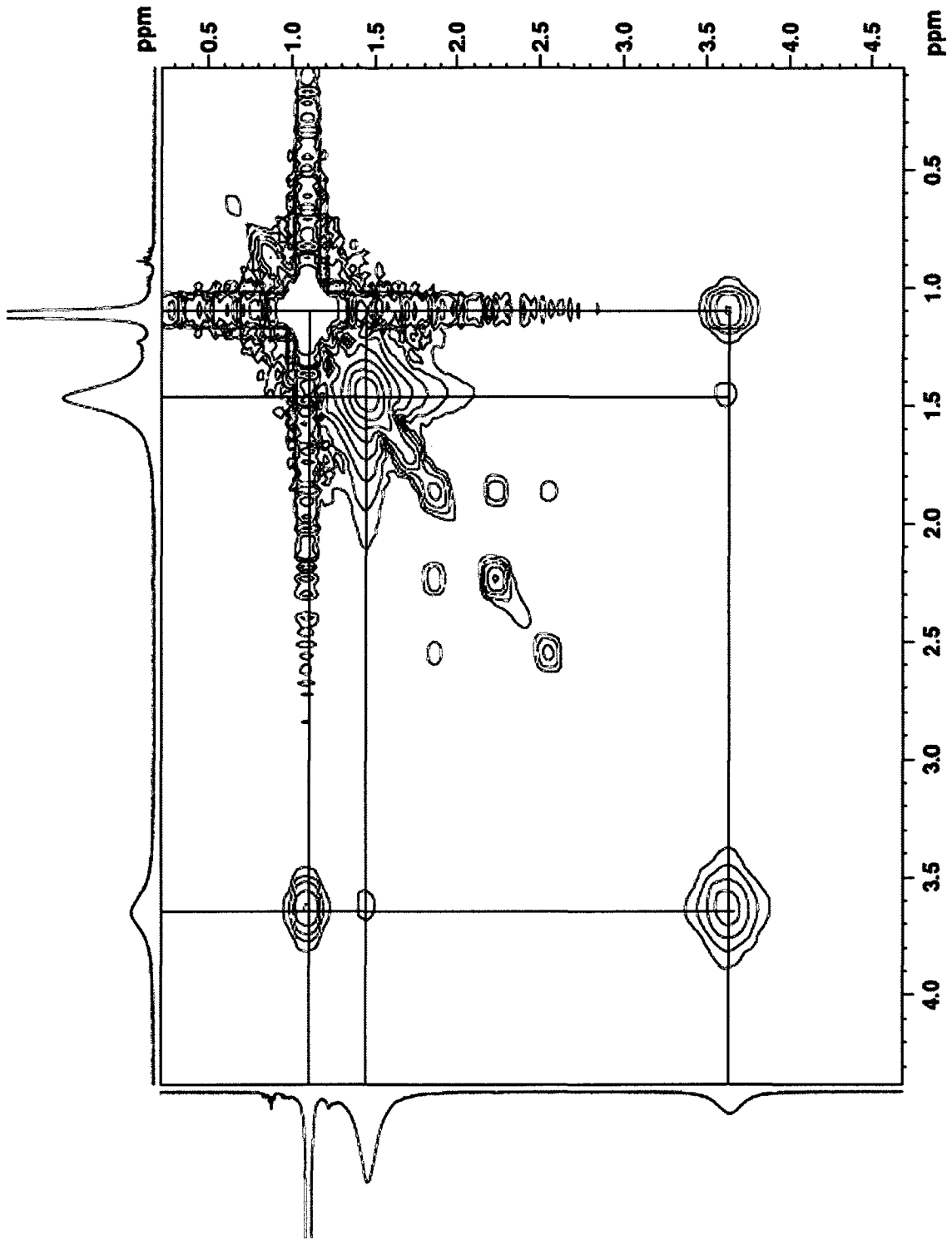

Figure A23. ^{1}H-^{1}H COSY spectrum of $Ru(=CHPh)Cl_2(IPr)(py)_2$, **35** (C_6D_6, 500 MHz, 298 K). Expansion highlighting aliphatic-aliphatic correlations.

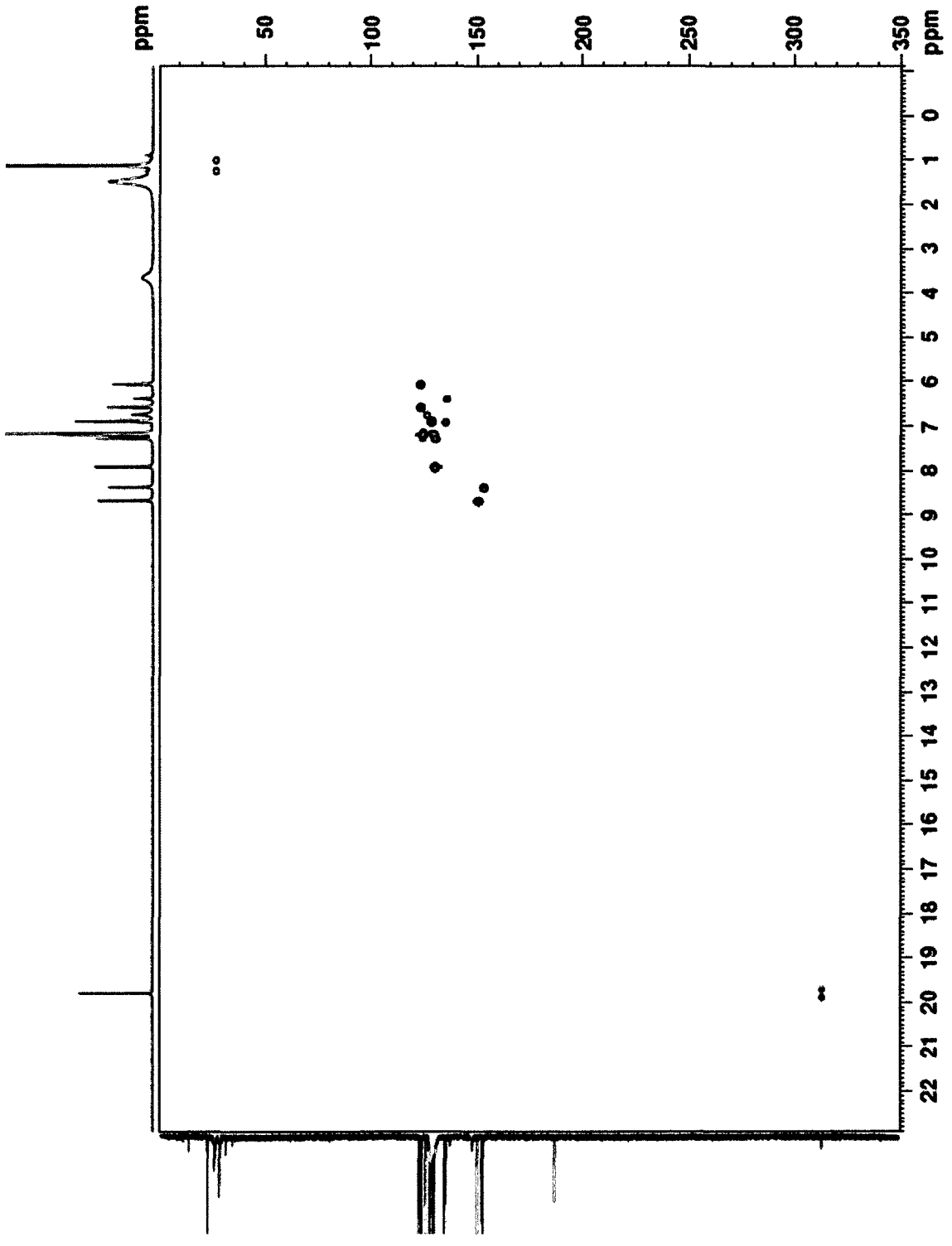

Figure A24. ^{1}H-^{13}C HMQC spectrum of $Ru(=CHPh)Cl_2(IPr)(py)_2$, **35** (C_6D_6, 500 MHz, 298 K).

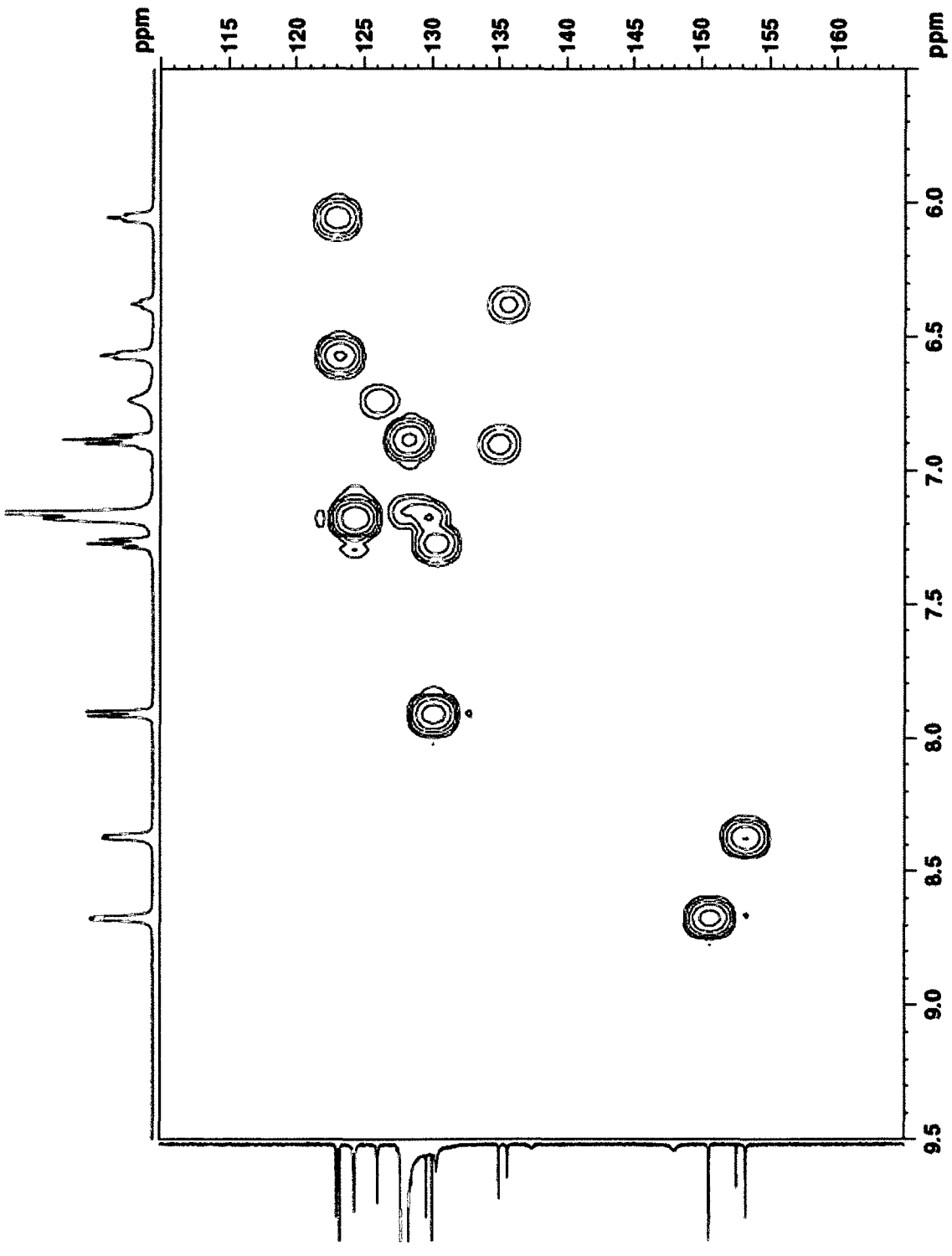

Figure A25. ^{1}H-^{13}C HMQC spectrum of Ru(=CHPh)Cl_2(IPr)$(py)_2$, **35** (C_6D_6, 500 MHz, 298 K). Expansion highlighting aromatic correlations.

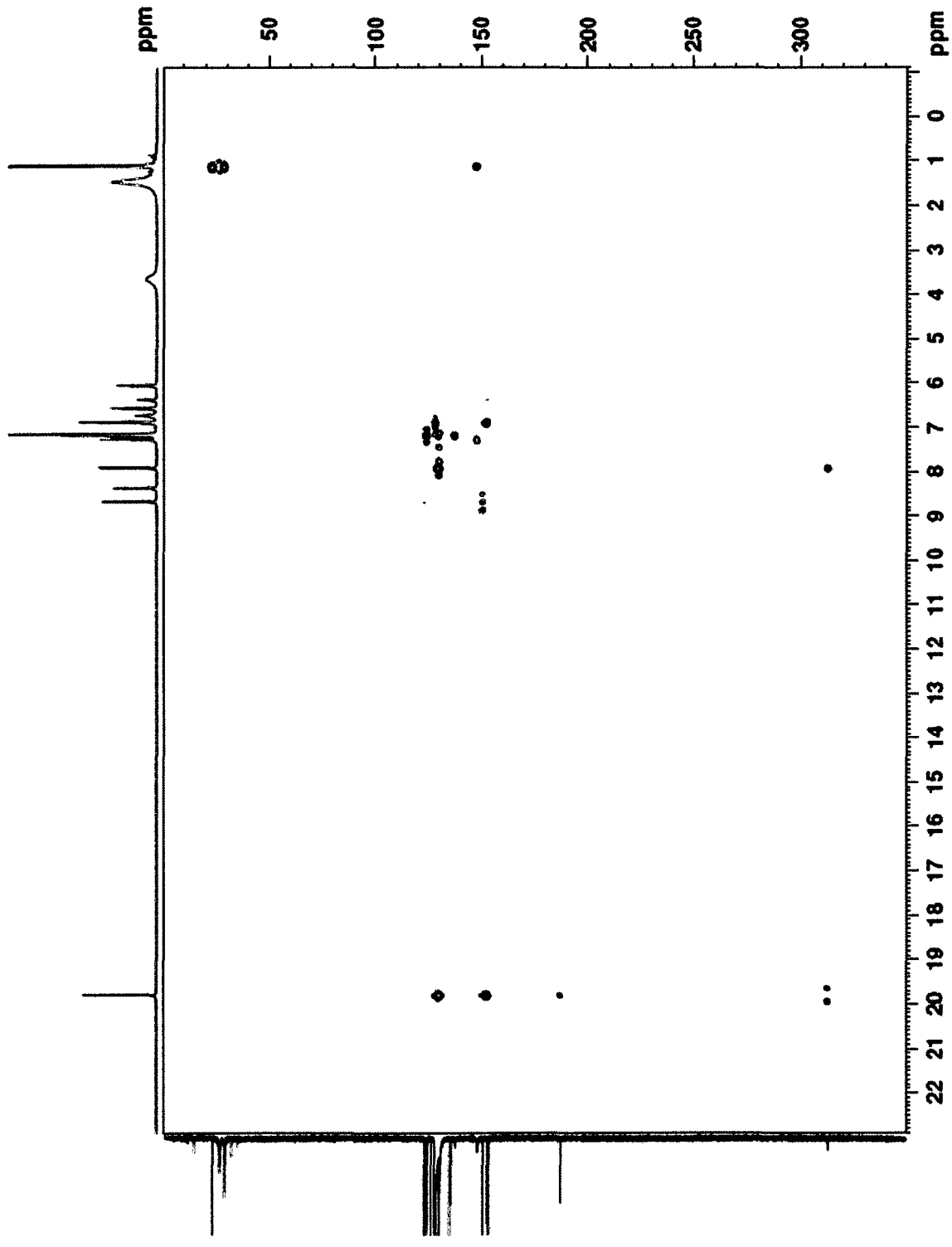

Figure A26. ^{1}H-^{13}C HMBC spectrum of $Ru(=CHPh)Cl_2(IPr)(py)_2$, **35** (C_6D_6, 500 MHz, 298 K).

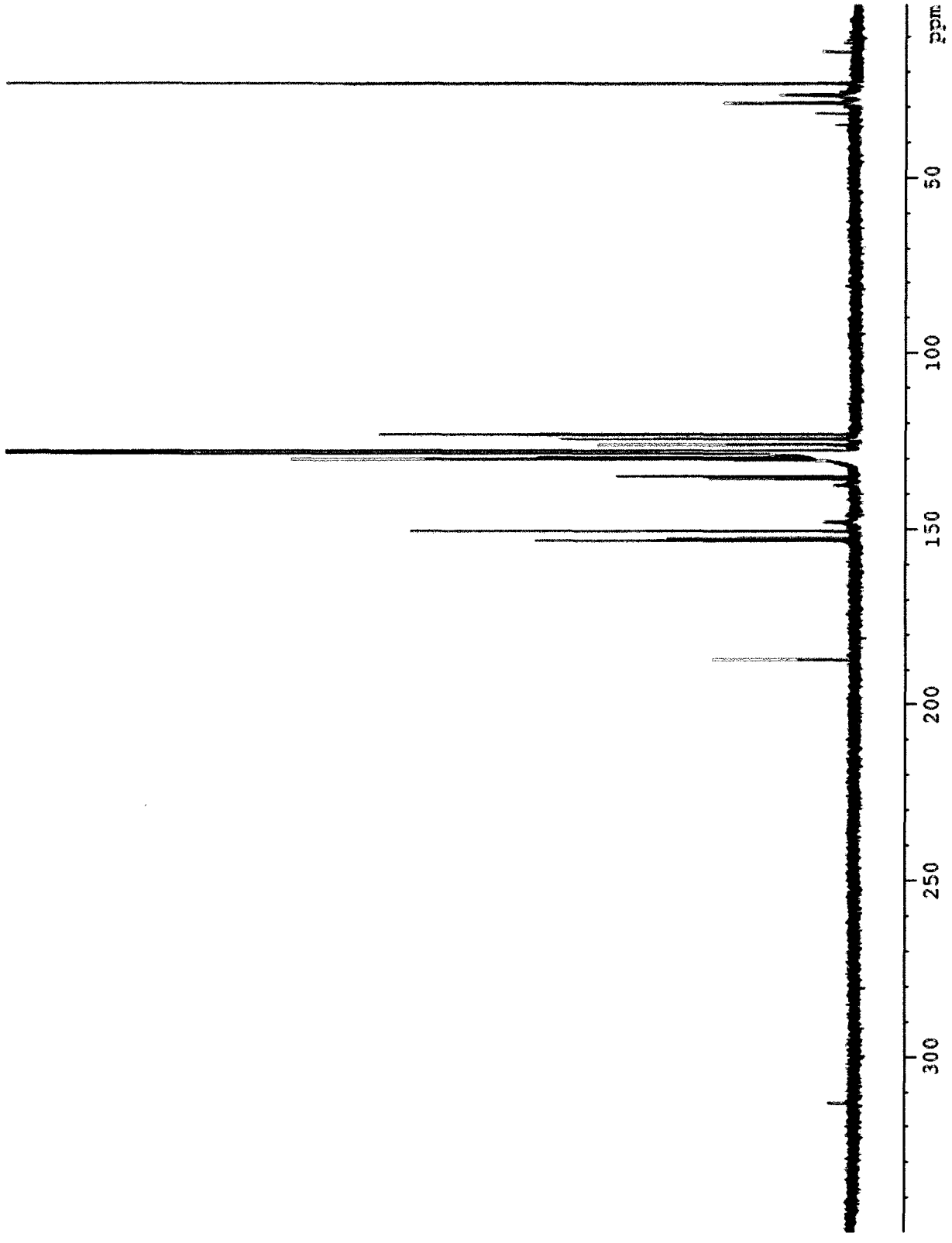

Figure A27. $^{13}C\{^{1}H\}$ spectrum of $Ru(=CHPh)Cl_2(IPr)(py)_2$, **35** (C_6D_6, 500 MHz, 298 K).

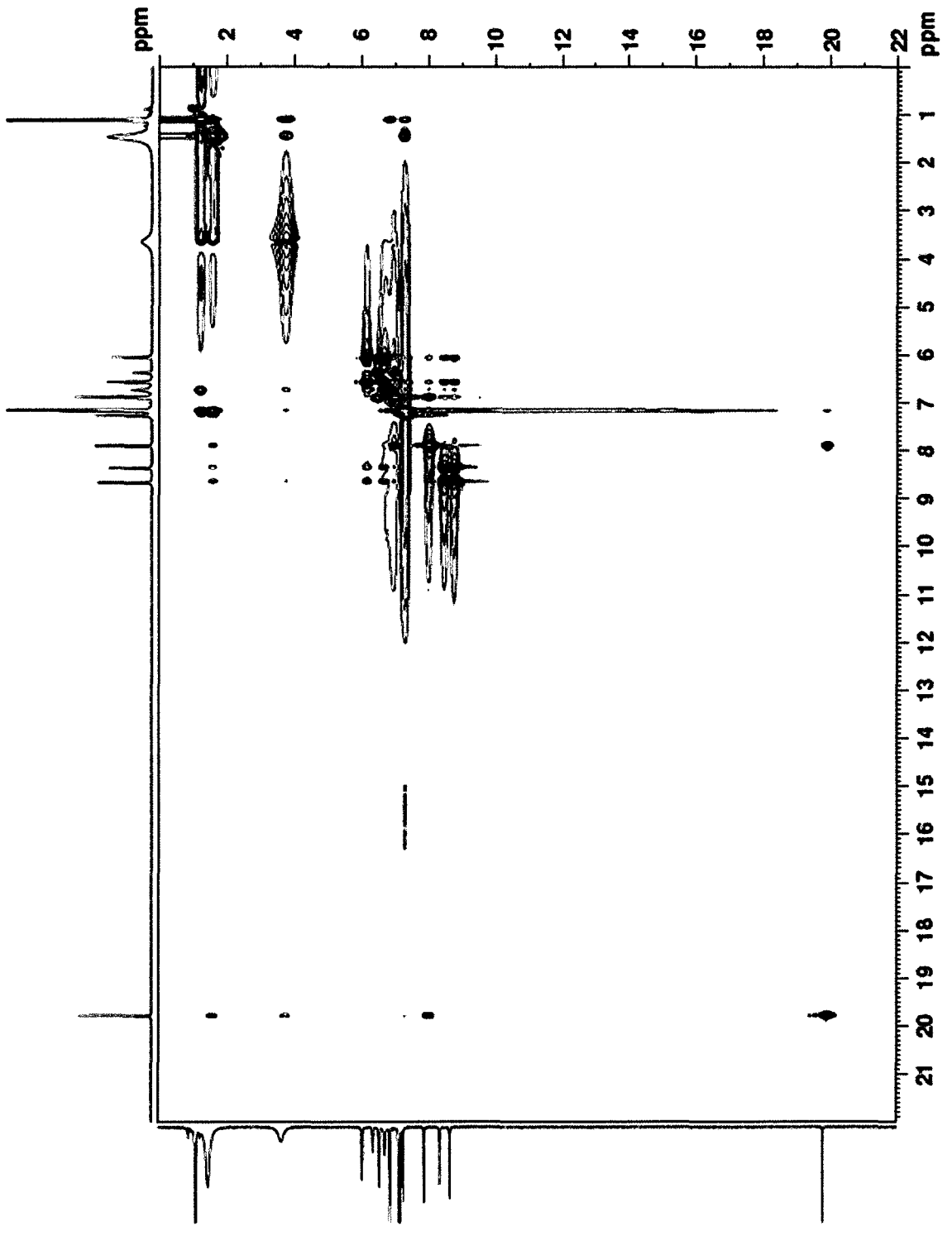

Figure A28. NOESY / EXSY spectrum of Ru(=CHPh)Cl_2(IPr)$(py)_2$, **35** (C_6D_6, 500 MHz, 298 K, 1000 ms mixing time). Contours in red indicate negative (EXSY) correlations; in black, positive (NOE) correlations.

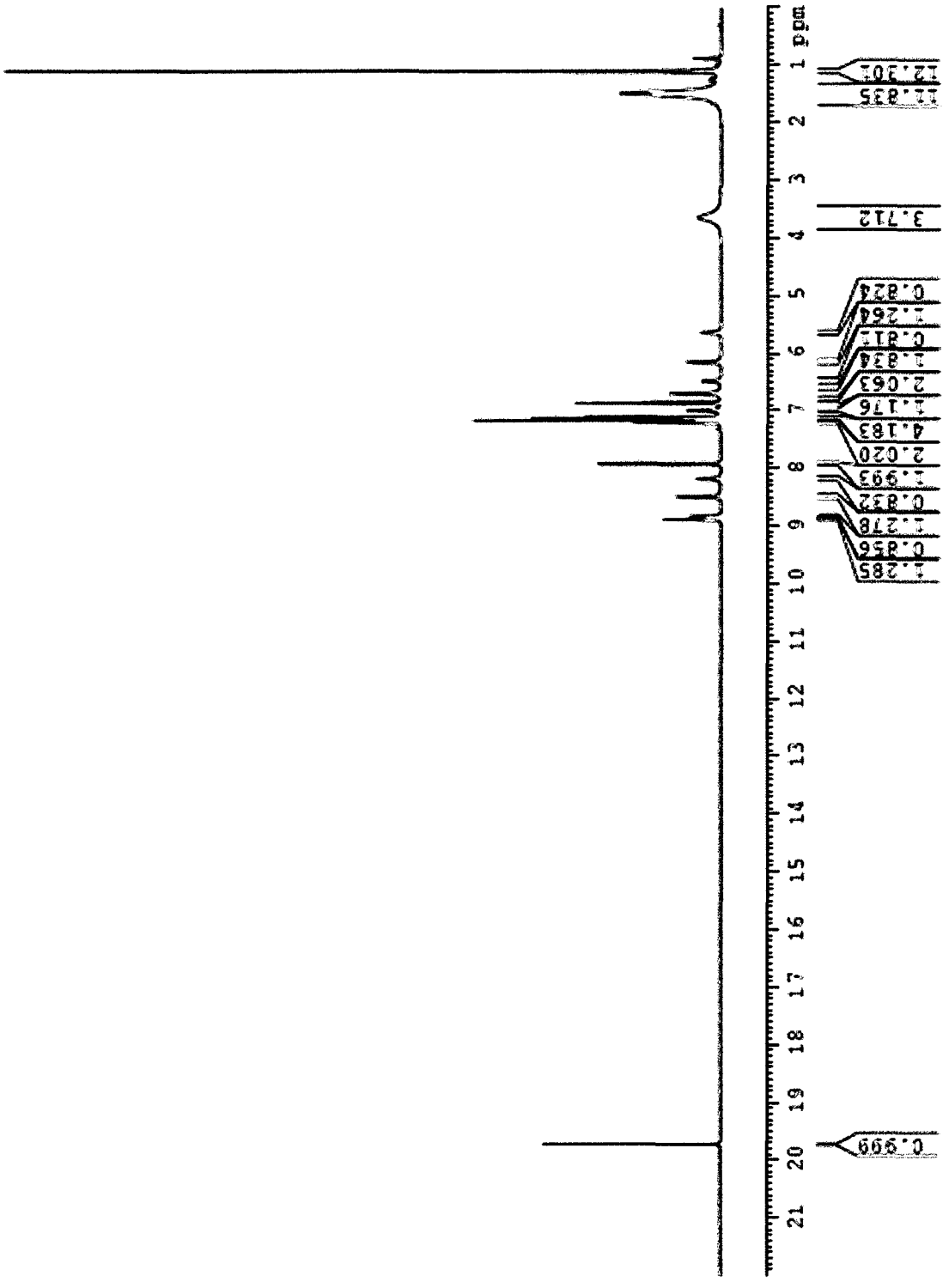

Figure A29. ^{1}H spectra of $Ru(=CHPh)Cl_2(IPr)(py^*)_2$, **36** ($C_6D_6$, 500 MHz, 298 K).

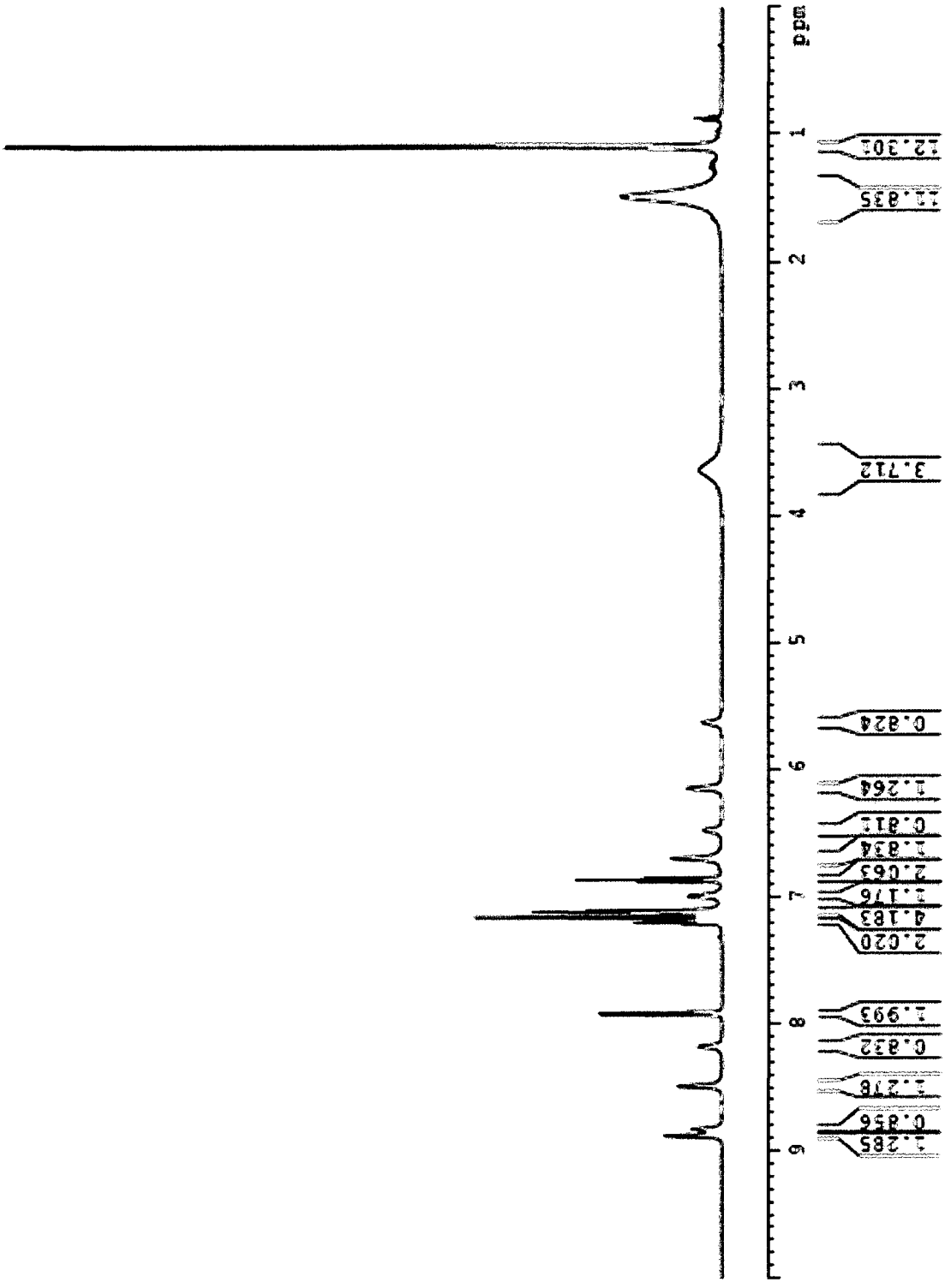

Figure A30. ^{1}H spectra of $Ru(=CHPh)Cl_2(IPr)(py^*)_2$, **36** ($C_6D_6$, 500 MHz, 298 K). Expansion highlighting aromatic and aliphatic peaks.

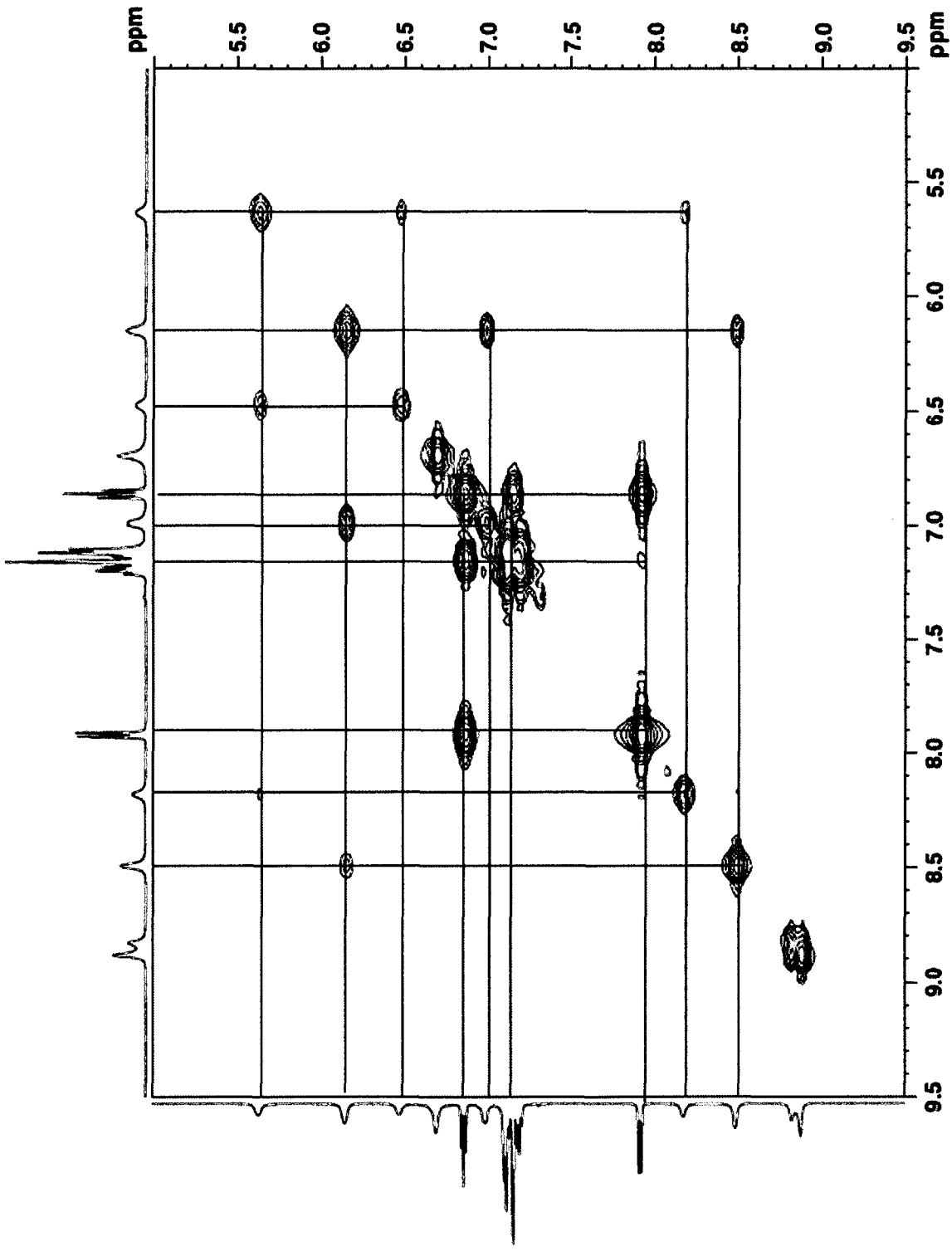

Figure A31. ^{1}H-^{1}H COSY spectrum of Ru(=CHPh)Cl_2(IPr)(py*)$_2$, **36** (C_6D_6, 500 MHz, 298 K). Expansion highlighting aromatic-aromatic correlations.

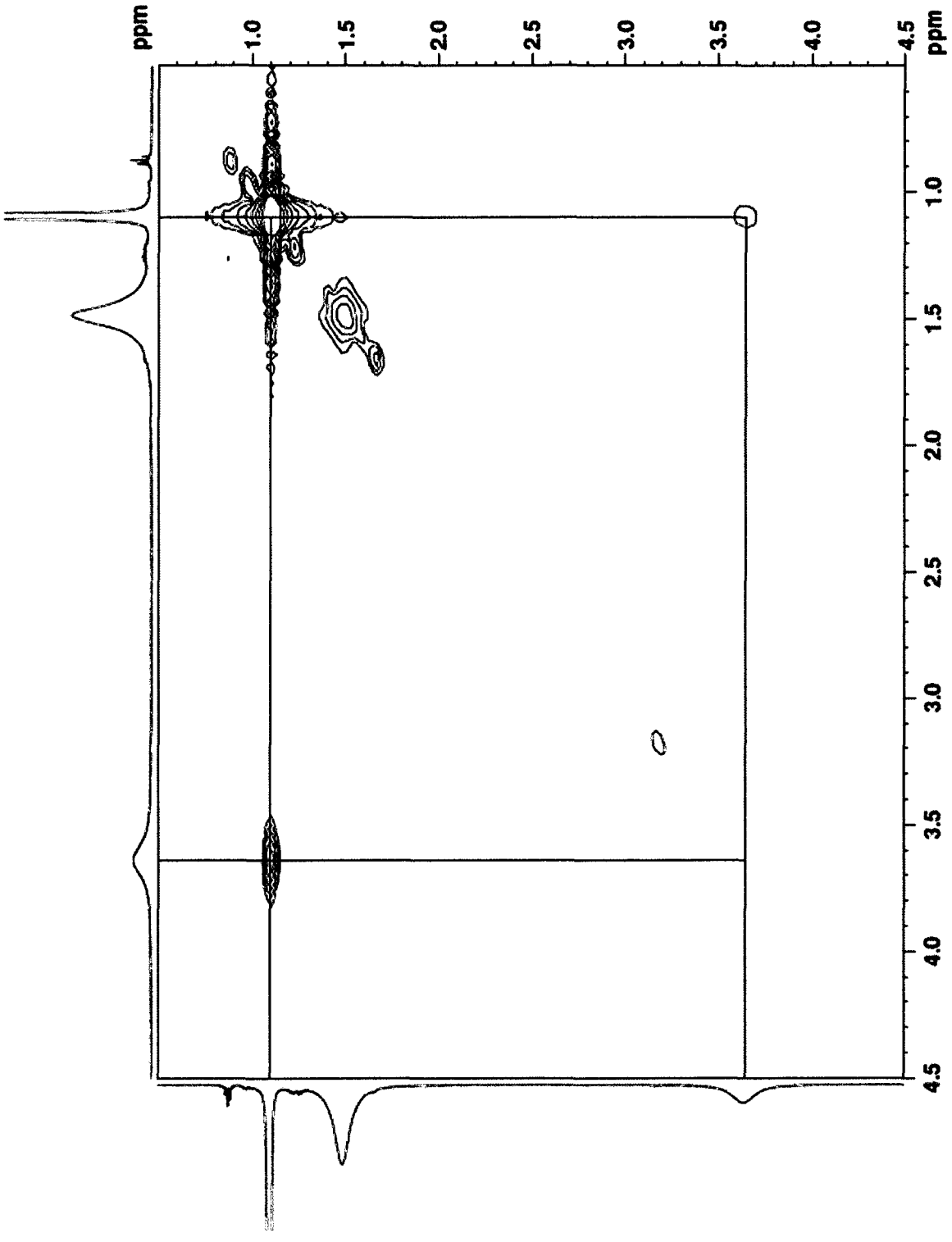

Figure A32. ^{1}H-^{1}H COSY spectrum of Ru(=CHPh)Cl_2(IPr)(py*)$_2$, **36** (C_6D_6, 500 MHz, 298 K). Expansion highlighting aliphatic-aliphatic correlations.

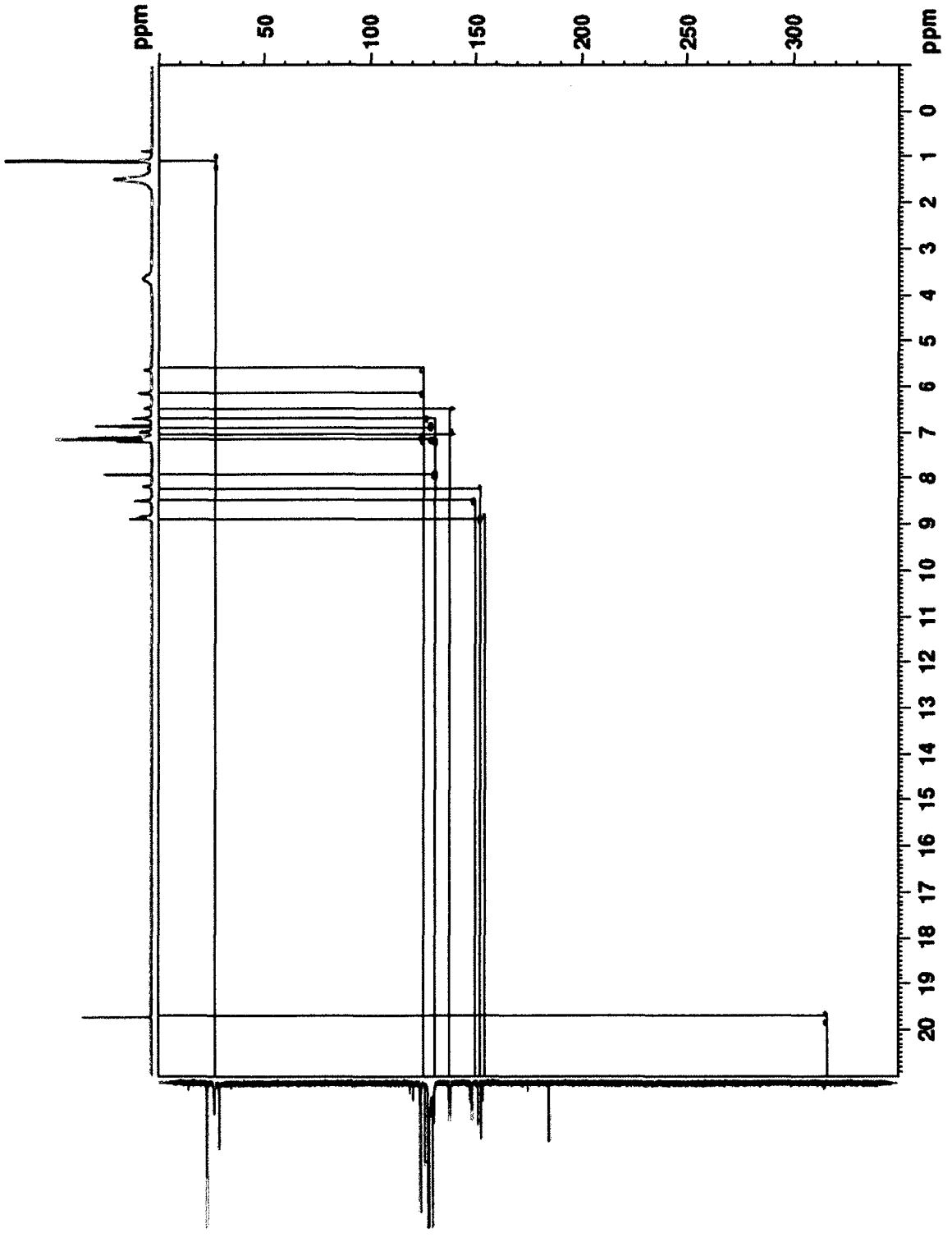

Figure A33. ^{1}H-^{13}C HMQC spectrum of $Ru(=CHPh)Cl_2(IPr)(py^*)_2$, **36** ($C_6D_6$, 500 MHz, 298 K).

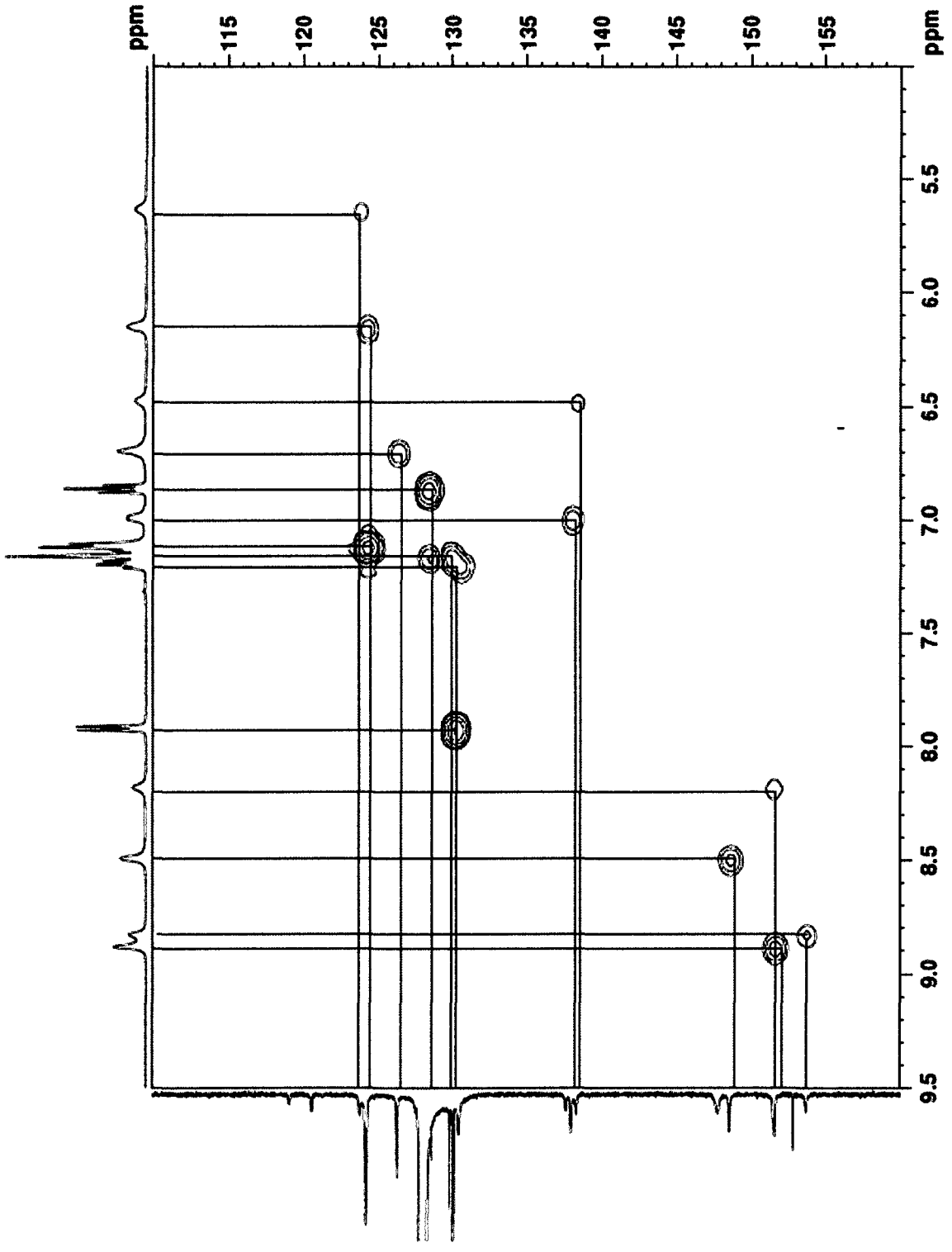

Figure A34. ^{1}H-^{13}C HMQC spectrum of Ru(=CHPh)Cl_2(IPr)(py*)$_2$, **36** (C_6D_6, 500 MHz, 298 K). Expansion highlighting aromatic correlations.

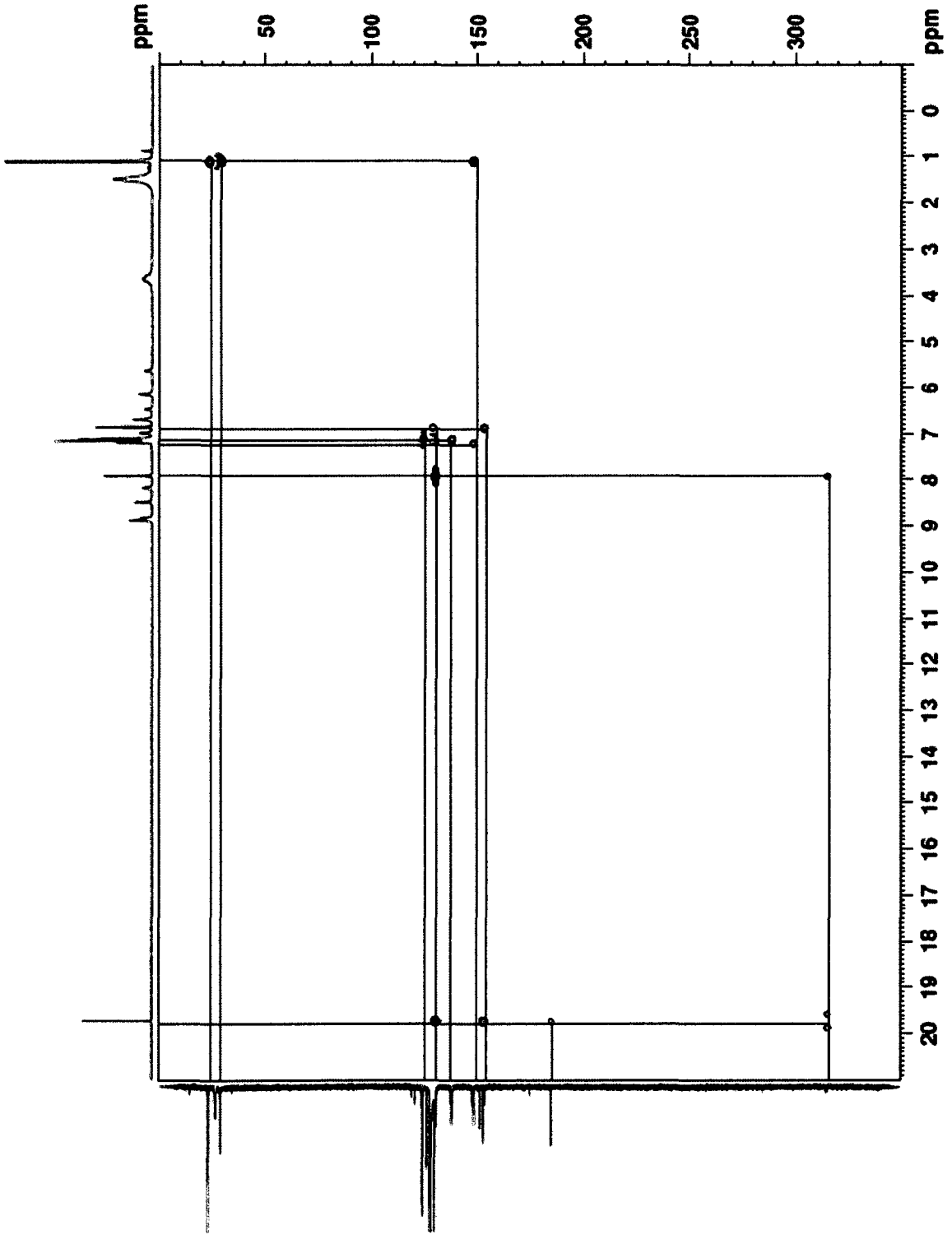

Figure A35. ^{1}H-^{13}C HMBC spectrum of $Ru(=CHPh)Cl_2(IPr)(py^*)_2$, **36** ($C_6D_6$, 500 MHz, 298 K).

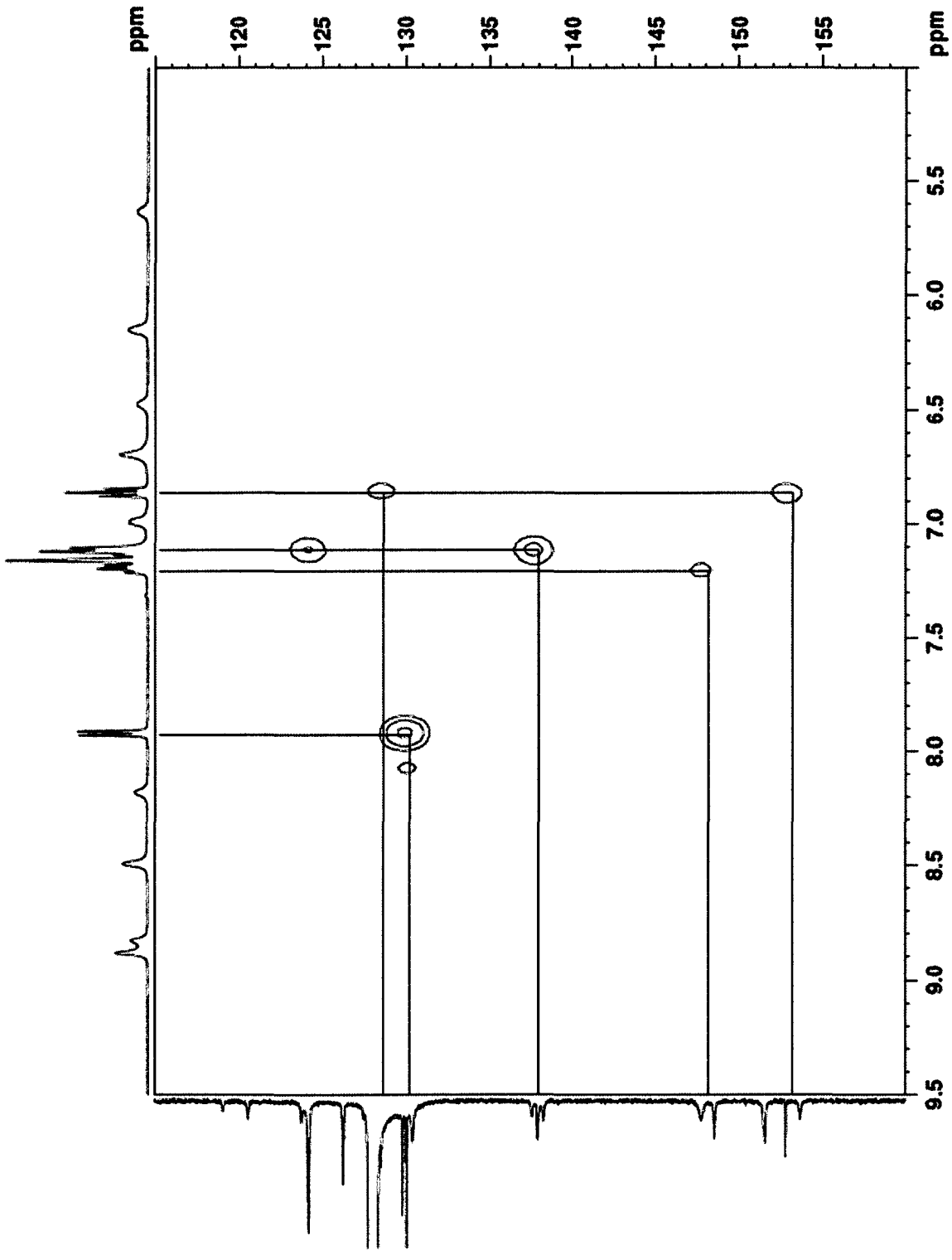

Figure A36. ^{1}H-^{13}C HMBC spectrum of Ru(=CHPh)Cl_2(IPr)(py*)$_2$, **36** (C_6D_6, 500 MHz, 298 K). Expansion highlighting aromatic correlations.

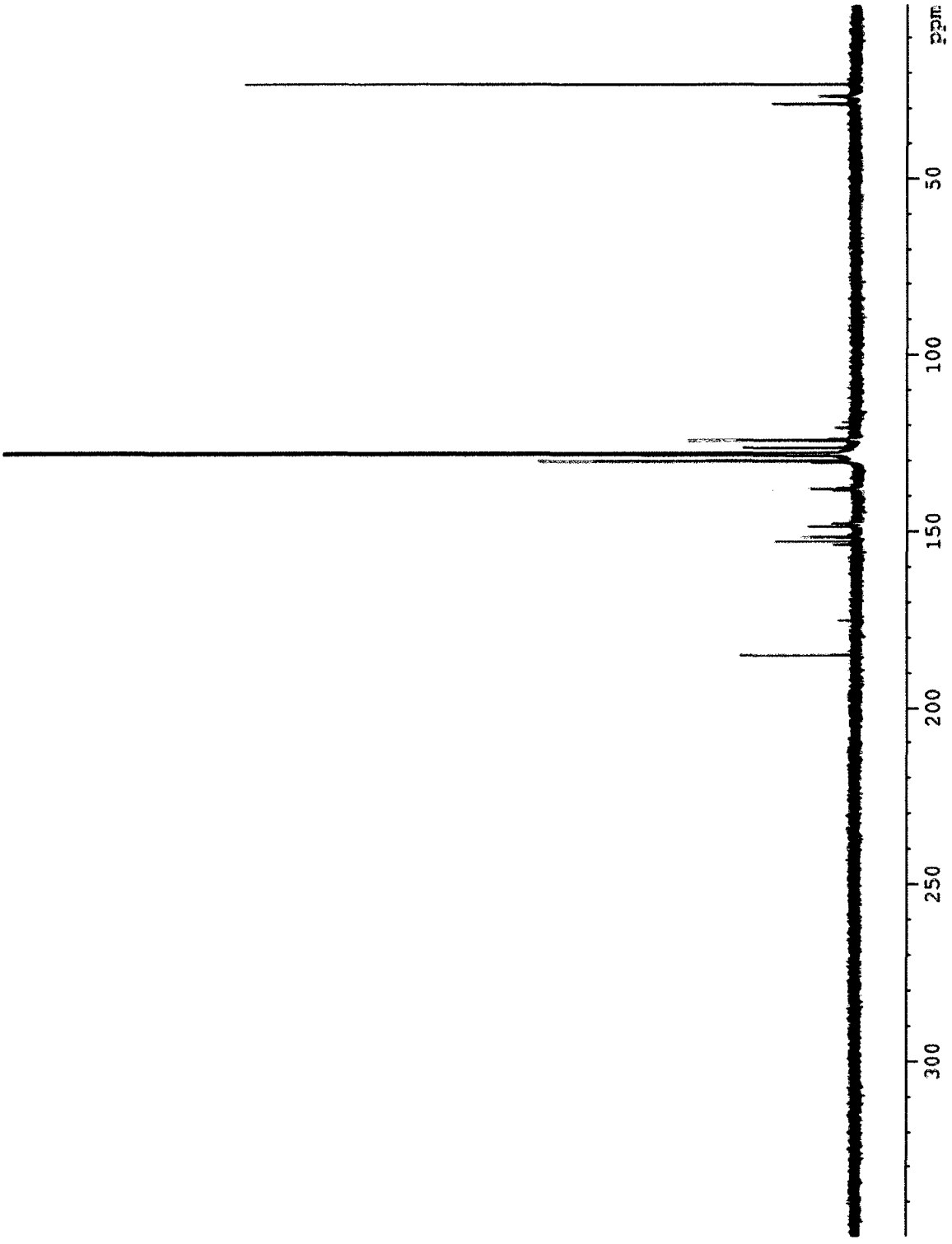

Figure A37. $^{13}C\{^{1}H\}$ spectrum of $Ru(=CHPh)Cl_2(IPr)(py^*)_2$, **36** ($C_6D_6$, 500 MHz, 298 K).

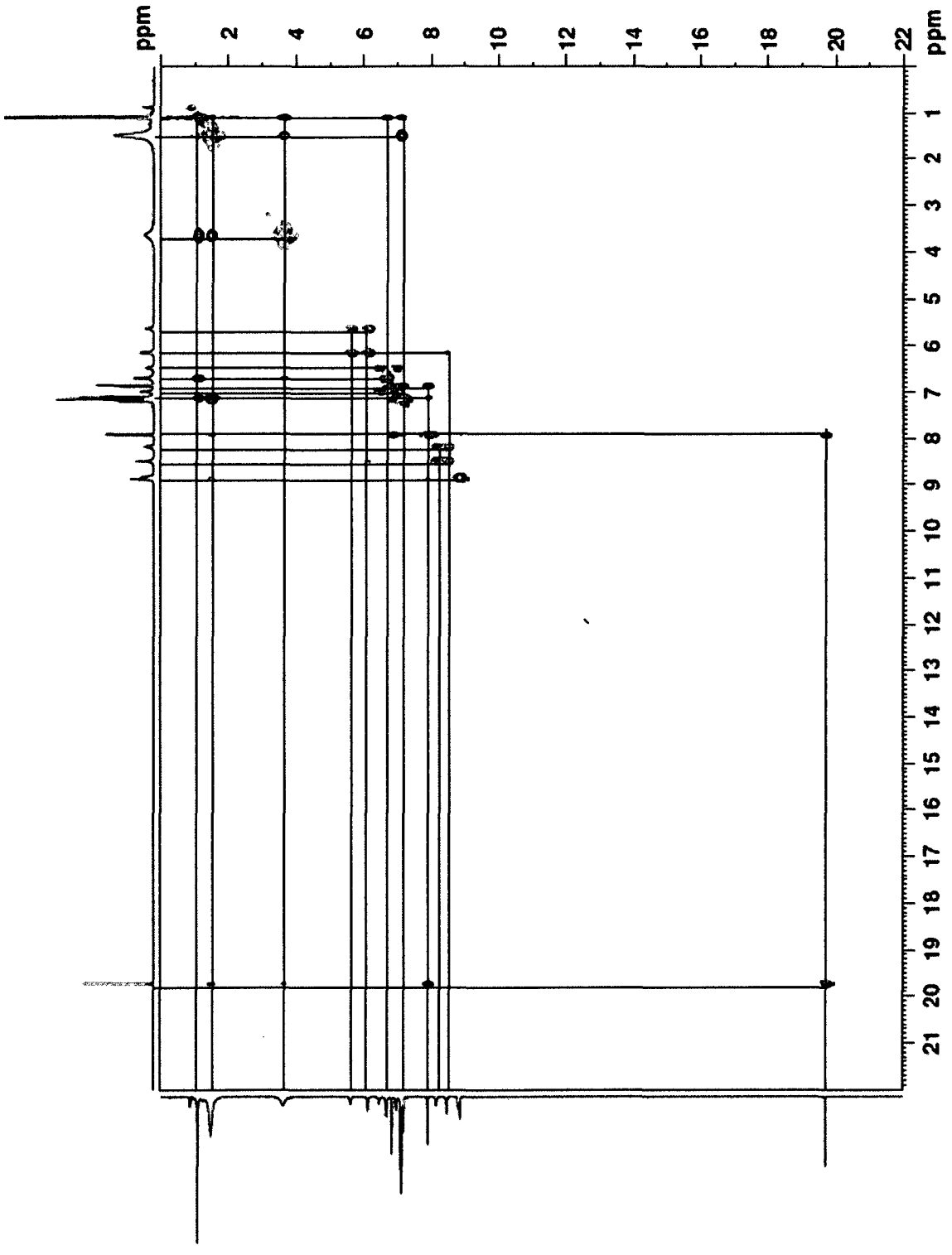

Figure A38. NOESY / EXSY spectrum of Ru(=CHPh)Cl_2(IPr)(py*)$_2$, **36** (C_6D_6, 500 MHz, 298 K, 1000 ms mixing time). Contours in red indicate negative (EXSY) correlations; in black, positive (NOE) correlations.

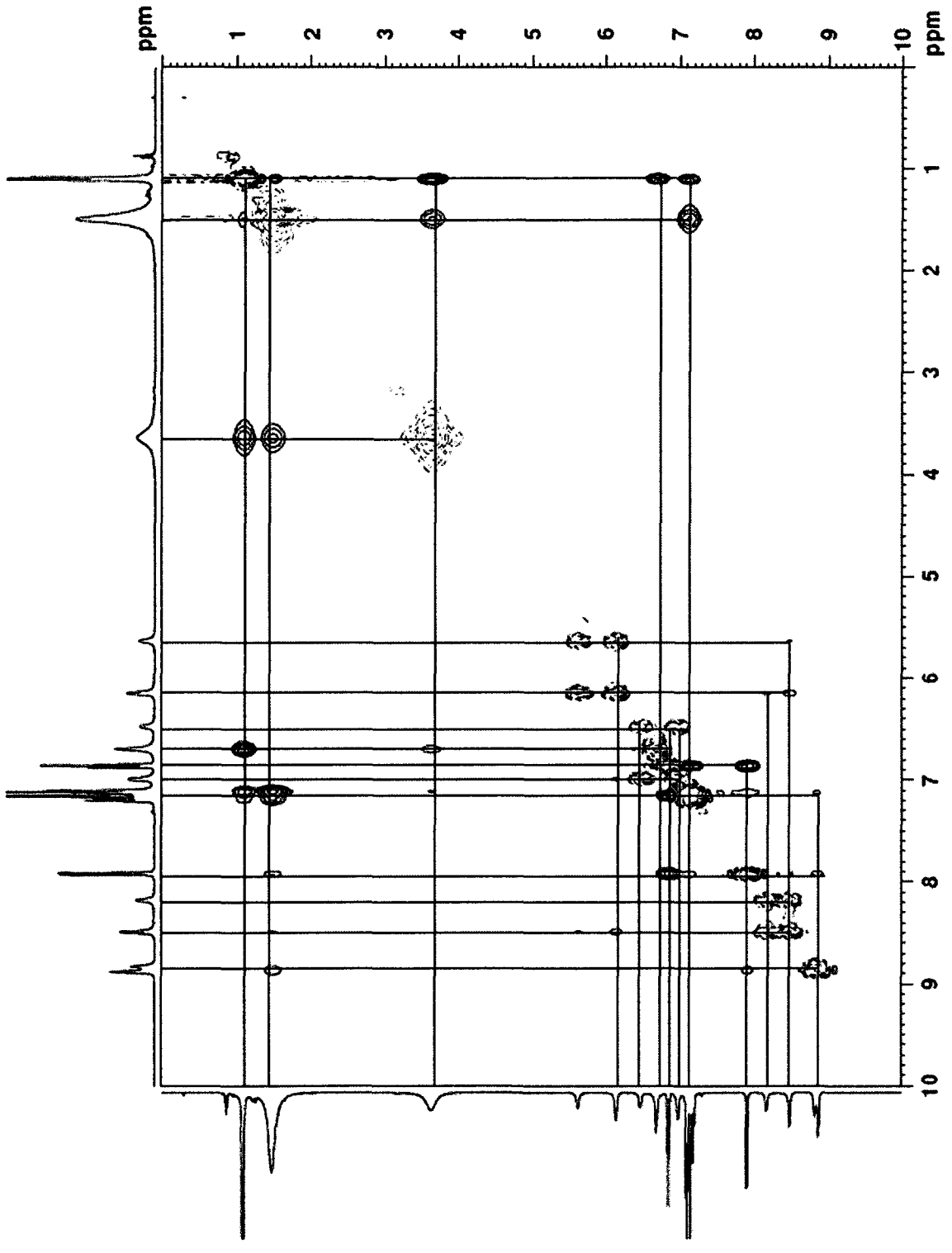

Figure A39. NOESY / EXSY spectrum of Ru(=CHPh)Cl_2(IPr)(py*)$_2$, **36** (C_6D_6, 500 MHz, 298 K, 1000 ms mixing time). Expansion highlighting aromatic and aliphatic correlations. Contours in red indicate negative (EXSY) correlations; in black, positive (NOE) correlations.

Table B1. Crystal data details and structure refinement for $RuCl_2(\kappa^2\text{-}O,Br\text{-}OC_6Br_5)(IMes)(py)$, **6**.

Crystallographer	Dr. Bob McDonald	
Identification code	OTT0802	
Formula	$C_{33}H_{30}Br_5Cl_5N_3ORu$	
Formula weight	1162.47	
Crystal dimensions	0.42 × 0.24 × 0.09 (mm)	
Crystal system	monoclinic	
Space group	$P2_1/c$ (No. 14)	
Unit cell parameters[a]	a = 22.170(8) Å	α = 90.00°
	b = 9.634(3) Å	β = 113.043(5)°
	c = 19.597(7) Å	γ = 90.00°
Volume	3852(2) Å^3	
Z	4	
Density (calculated)	2.005 (g cm^{-3})	
Absorption coefficient	5.974 (mm^{-1})	
Temperature	173 K	
Scan type	ω scans (0.3°) (25 s exposures)	
Data collection 2θ limit	51.62°	
Total data collected	27508 ($-27 \le h \le 27$, $-11 \le k \le 11$, $-23 \le l \le 24$)	
Independent reflections	7399 (R_{int} = 0.1077)	
Number of observed reflections (*NO*)	5242 [$F_o^2 \ge 2\sigma(F_o^2)$]	
Structure solution method	Patterson search/structure expansion (*DIRDIF–99*[b])	
Refinement method	Full-matrix least-squares on F^2 (*SHELXL–97*[c])	
Absorption correction method	Multi-scan (*SADABS*)	
Range of transmission factors	0.6095–0.1881	
Data/restraints/parameters	7399 [$F_o^2 \ge -3\sigma(F_o^2)$] / 0 / 439	
Goodness-of-fit (S)[d]	1.001 [$F_o^2 \ge -3\sigma(F_o^2)$]	
Final R indices[e]	R_1 [$F_o^2 \ge 2\sigma(F_o^2)$]	0.0462
	wR_2 [$F_o^2 \ge -3\sigma(F_o^2)$]	0.1302
Largest difference peak and hole	1.829 and –1.419 e Å^{-3}	

[a]Obtained from least-squares refinement of 9272 reflections with $4.52° < 2\theta < 50.70°$.

[b]Beurskens, P. T.; Beurskens, G.; de Gelder, R.; Garcia-Granda, S.; Israel, R.; Gould, R. O.; Smits, J. M. M. (1999). The *DIRDIF-99* program system. Crystallography Laboratory, University of Nijmegen, The Netherlands.

[c]Sheldrick, G. M. *Acta Crystallogr.* **2008**, *A64*, 112–122.

[d]$S = [\Sigma w(F_o^2 - F_c^2)^2/(n-p)]^{1/2}$ (n = number of data; p = number of parameters varied; $w = [\sigma^2(F_o^2) + (0.0714P)^2]^{-1}$ where $P = [\text{Max}(F_o^2, 0) + 2F_c^2]/3$).

[e]$R_1 = \Sigma||F_o| - |F_c||/\Sigma|F_o|$; $wR_2 = [\Sigma w(F_o^2 - F_c^2)^2/\Sigma w(F_o^4)]^{1/2}$.

Table B2. Bond distances (Å) in $RuCl_2(\kappa^2\text{-}O,Br\text{-}OC_6Br_5)(IMes)(py)$, **6**.

Atom1	Atom2	Distance	Atom1	Atom2	Distance
Ru	Br1	2.5064(10)	C7	C8	1.398(9)
Ru	Cl1	2.3409(16)	C8	C9	1.395(8)
Ru	Cl2	2.3597(16)	C11	C12	1.396(8)
Ru	O	2.021(4)	C11	C16	1.405(8)
Ru	N3	2.080(5)	C12	C13	1.383(9)
Ru	C1	2.116(6)	C12	C17	1.493(9)
Br1	C5	1.901(6)	C13	C14	1.375(10)
Br2	C6	1.871(6)	C14	C15	1.379(10)
Br3	C7	1.882(6)	C14	C18	1.501(10)
Br4	C8	1.884(6)	C15	C16	1.413(10)
Br5	C9	1.882(6)	C16	C19	1.492(9)
O	C4	1.310(7)	C21	C22	1.400(8)
N1	C1	1.374(8)	C21	C26	1.405(9)
N1	C2	1.367(7)	C22	C23	1.396(9)
N1	C11	1.438(8)	C22	C27	1.491(9)
N2	C1	1.389(7)	C23	C24	1.390(10)
N2	C3	1.377(8)	C24	C25	1.390(10)
N2	C21	1.427(8)	C24	C28	1.502(10)
N3	C31	1.343(8)	C25	C26	1.373(10)
N3	C35	1.340(8)	C26	C29	1.497(9)
C2	C3	1.320(9)	C31	C32	1.383(9)
C4	C5	1.396(9)	C32	C33	1.370(10)
C4	C9	1.414(8)	C33	C34	1.379(9)
C5	C6	1.392(8)	C34	C35	1.379(9)
C6	C7	1.383(8)			

Table B3. Bond angles (°) in $RuCl_2(\kappa^2\text{-}O,Br\text{-}OC_6Br_5)(IMes)(py)$, **6**.

Atom1	Atom2	Atom3	Angle	Atom1	Atom2	Atom3	Angle
Br1	Ru	Cl1	88.32(5)	C5	C6	C7	119.7(6)
Br1	Ru	Cl2	86.76(5)	Br3	C7	C6	120.3(5)
Br1	Ru	O	82.59(12)	Br3	C7	C8	121.0(4)
Br1	Ru	N3	162.72(13)	C6	C7	C8	118.6(5)
Br1	Ru	C1	98.54(17)	Br4	C8	C7	120.1(4)
Cl1	Ru	Cl2	174.65(6)	Br4	C8	C9	118.9(5)
Cl1	Ru	O	90.25(12)	C7	C8	C9	121.0(5)
Cl1	Ru	N3	91.64(13)	Br5	C9	C4	116.2(5)
Cl1	Ru	C1	89.96(15)	Br5	C9	C8	122.3(5)
Cl2	Ru	O	91.21(12)	C4	C9	C8	121.4(6)
Cl2	Ru	N3	93.68(13)	N1	C11	C12	118.1(5)

Cl2	Ru	C1	88.67(15)	N1	C11	C16	118.7(5)
O	Ru	N3	80.13(17)	C12	C11	C16	123.0(6)
O	Ru	C1	178.9(2)	C11	C12	C13	117.5(6)
N3	Ru	C1	98.7(2)	C11	C12	C17	121.0(6)
Ru	Br1	C5	94.03(18)	C13	C12	C17	121.5(6)
Ru	O	C4	124.1(4)	C12	C13	C14	122.1(6)
C1	N1	C2	112.3(5)	C13	C14	C15	118.9(7)
C1	N1	C11	128.6(5)	C13	C14	C18	121.0(7)
C2	N1	C11	119.0(5)	C15	C14	C18	120.1(7)
C1	N2	C3	110.8(5)	C14	C15	C16	122.4(6)
C1	N2	C21	129.9(5)	C11	C16	C15	115.5(6)
C3	N2	C21	119.1(5)	C11	C16	C19	122.4(6)
Ru	N3	C31	116.6(4)	C15	C16	C19	122.1(6)
Ru	N3	C35	123.5(4)	N2	C21	C22	120.5(5)
C31	N3	C35	118.3(5)	N2	C21	C26	117.3(5)
Ru	C1	N1	127.6(4)	C22	C21	C26	121.8(6)
Ru	C1	N2	130.5(4)	C21	C22	C23	117.7(6)
N1	C1	N2	101.9(5)	C21	C22	C27	121.4(6)
N1	C2	C3	107.1(6)	C23	C22	C27	120.9(6)
N2	C3	C2	107.9(6)	C22	C23	C24	121.6(6)
O	C4	C5	123.3(5)	C23	C24	C25	118.4(7)
O	C4	C9	121.2(6)	C23	C24	C28	120.1(7)
C5	C4	C9	115.5(5)	C25	C24	C28	121.4(7)
Br1	C5	C4	115.9(4)	C24	C25	C26	122.6(7)
Br1	C5	C6	120.4(5)	C21	C26	C25	117.7(6)
C4	C5	C6	123.6(6)	C21	C26	C29	121.1(6)
Br2	C6	C5	118.5(4)	C25	C26	C29	121.2(6)
Br2	C6	C7	121.8(5)	N3	C31	C32	121.2(6)
C31	C32	C33	120.2(6)	C33	C34	C35	119.4(6)
C32	C33	C34	118.2(6)	N3	C35	C34	122.4(6)

Table C1. Interaction between the [RuXCl(L)(=CH_2)] (F1) and [C_2H_4] (F2) fragments in **10(II)** and their contributions to the electronic energy of the transition state.[a]

	ΔE_e	ΔE_{prep} (F1)	ΔE_{prep} (F2)	ΔE_{int} (F1–F2)	B (F1-F2)	ΔP ($F2_O$)	ΔP ($F1_U$)	ΔP ($F1_O$)	ΔP ($F2_U$)
IMe	14.9	13.3	10.2	-29.8	1.38	38.1	34.3	14.7	12.3
IMes	15.0	26.8	8.7	-29.4	1.24	32.0	30.0	11.4	7.3

[a] ΔE_e: relative electronic energies. B(F1-F2): bond order between fragments. ΔP: population change (%) of occupied (O) and unoccupied (U) fragment orbitals once the F1-F2 interaction is turned on, based on Mulliken population analysis of calculated electron density distributions. ΔP for $F2_O$, $F1_U$ reveal σ-donation; $F1_O$, $F2_U$, π* back-donation.

Table C2. LUFO energies governing extent of charge donation from ethylene. Energy, population change, and composition of the RuXCl(L)(=CH_2) LUFO in **10(II)**.

	ΔE_e (eV)	ΔP (%)[a]	Ru (%)[b]	C_γ (%)[b,c]	Cl, O (%)[b]
IMe	-3.60	28.6	46.4	40.4	2.4, 1.3
IMes	-3.58	24.8	51.9	36.8	3.3, 0.4

[a]ΔP = change in LUFO population once fragment interaction with ethylene is turned on. [b]Atomic contribution to the LUFO, as assessed by Mulliken population analysis (MPA). [c]C_γ = methylidene carbon.

Table C3. Analysis of the Ru-L charge and bonding interactions in transition state **10(II)**.[a]

	*q*Ru	*q*L (donor atom)	*q*L[b]	B (Ru–L) (donor atom)	ΔE_{int} [RuXCl(C_2H_4) (=CH_2)]–[L]	ΔE_{orb}	ΔE_{steric}
IMe	+0.72	+0.26	+0.16	0.74	-61.4	-70.6	+9.2
IMes	+0.81	+0.27	-0.02	0.80	-66.0	-71.0	+5.0

[a]Energies in units of kcal mol^{-1}; *q* in a.u. [b]L = entire ligand.

Table C4. Analysis of charge interactions in **I** and **II**.

Entry	Charge (a.u.)	**1b(I)**	**1b(II)**	**2b(I)**	**2b(II)**	**3b(I)**	**3b(II)**	**4b(I)**	**4b(II)**
1	q Ru	+0.51	+0.52	+0.63	+0.64	+0.64	+0.66	+0.67	+0.72
2	q Cl	-0.53	-0.62	-0.55	-0.61	-0.55	-0.61	-0.60	-0.60
3	q Cl/O	-0.53	-0.62	-0.55	-0.61	-0.55	-0.61	-0.70	-0.71
4	q C_α	-0.40	-0.45	-0.40	-0.44	-0.40	-0.44	-0.44	-0.44
5	q C_β	-0.41	-0.33	-0.40	-0.35	-0.41	-0.35	-0.34	-0.38
6	q C_γ	-0.29	-0.21	-0.26	-0.22	-0.26	-0.22	-0.22	-0.27
7	q C_2H_4	+0.06	+0.12	+0.05	+0.09	+0.05	+0.09	+0.10	+0.08

Table C5. Ru-C and C-C 2- and 3-center Mayer bond orders in (**II**).

Entry		**7(II)**	**8(II)**	**9(II)**	**10(II)**
1	B (Ru-C_α)	0.39	0.37	0.38	0.66
2	B (Ru-C_β)	0.26	0.30	0.30	0.29
3	B (Ru-C_γ)	1.75	1.84	1.83	1.38
4	B ($C_\alpha C_\beta$)	1.46	1.50	1.50	1.13
5	B ($C_\beta C_\gamma$)	0.10	0.08	0.06	0.41
6	B (Ru-$C_\alpha C_\beta$)	0.13	0.12	0.12	0.05
7	B (Ru-$C_\alpha C_\gamma$)	0.00	0.00	0.00	0.00
8	B (Ru-$C_\beta C_\gamma$)	0.04	0.04	0.03	0.13

Table D1. Coordinates of *trans*-**3a** (Å).

atom	*x*	*y*	*z*	atom	*x*	*y*	*z*
Ru	0.321828	0.534785	0.201164	H	5.196931	-0.720421	-2.524121
Cl	0.420226	0.288339	2.651064	C	6.871697	-0.015440	-0.481544
Cl	0.661879	0.841890	-2.200113	H	5.520784	-0.822783	1.754853
C	0.393190	-1.551704	-0.012303	C	3.133075	-1.957812	2.311756
N	-0.566496	-2.532555	-0.038740	H	3.285735	-1.460059	-3.636980
C	0.001961	-3.799582	-0.175495	H	2.709740	-2.943744	-2.866675
C	1.342419	-3.622279	-0.240441	H	1.735578	-1.463530	-2.793818
N	1.572450	-2.252849	-0.141038	H	7.495806	-0.286641	0.375436
H	2.151091	-4.329897	-0.347142	H	7.395062	-0.319701	-1.393440
H	-0.603446	-4.692816	-0.214704	H	6.796136	1.079015	-0.498145
C	-4.024784	-2.453470	1.335254	H	2.272711	-1.361921	2.628354
C	-4.786782	-2.191563	0.189953	H	2.816079	-3.006923	2.291402
C	-4.119296	-2.031457	-1.032195	H	3.915422	-1.859051	3.069284
C	-2.726112	-2.125310	-1.134324	C	-1.530346	0.723930	0.299871
C	-1.998407	-2.375612	0.044311	H	-2.020908	0.085747	1.041451
C	-2.626619	-2.555164	1.289110	C	-4.736791	2.573983	-0.324399
H	-4.526001	-2.582444	2.292748	C	-3.792902	1.678586	0.175915
C	-6.295941	-2.101090	0.258480	C	-2.457592	1.676353	-0.301633
H	-4.696060	-1.824733	-1.931943	C	-2.109140	2.603711	-1.312327
C	-2.037386	-1.955550	-2.468530	C	-3.058570	3.491235	-1.816267
C	-1.831765	-2.822677	2.546937	C	-4.371016	3.484434	-1.324494
H	-6.764681	-2.977486	-0.205220	H	-5.754135	2.564392	0.059846
H	-6.648790	-2.046169	1.292398	H	-4.077823	0.966750	0.947175
H	-6.665839	-1.217865	-0.273346	H	-1.099436	2.596816	-1.705627
H	-1.401950	-2.817258	-2.702368	H	-2.777040	4.193383	-2.597526
H	-2.773565	-1.853317	-3.270249	H	-5.104874	4.183660	-1.719272
H	-1.393096	-1.070324	-2.480654	N	0.746397	2.701017	0.506879
H	-2.498839	-2.932717	3.406168	C	1.663954	3.329044	-0.258078
H	-1.240083	-3.741212	2.462777	C	0.196066	3.390360	1.528991
H	-1.132447	-2.005787	2.757178	C	2.060855	4.647082	-0.032117
C	2.907016	-1.696349	-0.220246	H	2.067824	2.749540	-1.081871
C	3.469143	-1.463867	-1.491883	C	0.527328	4.714333	1.810774
C	4.758864	-0.921388	-1.548224	H	-0.513624	2.845465	2.140550
C	5.499805	-0.646650	-0.391661	C	1.480532	5.359033	1.019409
C	4.939399	-0.976802	0.847762	H	2.808048	5.097956	-0.678802
C	3.652347	-1.521155	0.962397	H	0.045173	5.219553	2.642551
C	2.754718	-1.851991	-2.765640	H	1.764319	6.389782	1.217936

Table D2. Coordinates of *cis*-**3a** (Å).

atom	*x*	*y*	*z*	atom	*x*	*y*	*z*
Ru	0.280738	0.921359	-0.133815	C	6.804188	0.589092	-0.670818
Cl	-0.062625	1.245417	-2.508230	H	5.435798	-0.713302	1.311702
C	0.370434	-1.151786	-0.526216	C	3.065525	-1.990693	1.546876

N	-0.560691	-2.159659	-0.648841	H	3.391544	-0.330907	-4.163802
C	0.025358	-3.343131	-1.099691	H	2.461140	-1.737554	-3.628471
C	1.346336	-3.093161	-1.260595	H	1.819896	-0.113191	-3.369918
N	1.547640	-1.762251	-0.906395	H	7.404766	0.180643	0.147614
H	2.156581	-3.726523	-1.590162	H	7.364226	0.457895	-1.601911
H	-0.554955	-4.239382	-1.261361	H	6.703999	1.668109	-0.501001
C	-3.685215	-2.592400	1.335624	H	2.010480	-1.785074	1.732581
C	-4.672065	-2.203730	0.423018	H	3.163393	-3.073852	1.401368
C	-4.269096	-1.806841	-0.859215	H	3.627592	-1.726325	2.446051
C	-2.923328	-1.770771	-1.242986	C	-1.503405	0.986756	0.415922
C	-1.958151	-2.132162	-0.282501	H	-1.817987	0.321294	1.232814
C	-2.323310	-2.580697	0.999409	C	-4.956023	2.449913	0.262535
H	-3.976686	-2.925112	2.330425	C	-3.867352	1.644722	0.587277
C	-6.139006	-2.233322	0.791955	C	-2.590608	1.865130	0.008489
H	-5.023837	-1.511703	-1.585676	C	-2.443167	2.942832	-0.898324
C	-2.538239	-1.377846	-2.647269	C	-3.536127	3.749478	-1.214403
C	-1.304197	-3.099494	1.991397	C	-4.791719	3.507166	-0.643728
H	-6.668090	-3.018777	0.239338	H	-5.927333	2.263914	0.715303
H	-6.282605	-2.424369	1.859331	H	-3.993821	0.826518	1.293081
H	-6.627945	-1.283706	0.549039	H	-1.470839	3.142787	-1.330038
H	-1.967416	-2.174880	-3.138149	H	-3.406588	4.577331	-1.907225
H	-3.430184	-1.183371	-3.248575	H	-5.637417	4.143281	-0.896265
H	-1.908246	-0.483176	-2.660379	N	0.982323	0.757764	1.947317
H	-1.693475	-3.046551	3.012407	C	2.161844	1.343540	2.253832
H	-1.065308	-4.151068	1.789510	C	0.301384	0.177718	2.956743
H	-0.362345	-2.548859	1.952586	C	2.687905	1.358379	3.545733
C	2.867396	-1.170197	-0.862118	H	2.679302	1.831028	1.436850
C	3.439477	-0.644910	-2.038179	C	0.750782	0.157629	4.275185
C	4.722275	-0.088055	-1.944358	H	-0.645379	-0.281106	2.698969
C	5.444178	-0.068350	-0.745140	C	1.973111	0.760154	4.583240
C	4.871616	-0.672075	0.381521	H	3.639882	1.850440	3.721998
C	3.593786	-1.243992	0.342427	H	0.143786	-0.320361	5.038684
C	2.737947	-0.708263	-3.373079	H	2.352942	0.765428	5.601824
H	5.168054	0.339258	-2.840362	Cl	0.934656	3.264975	0.037627

Table D3. Coordinates of *trans*-**5a** (Å).

atom	*x*	*y*	*z*	atom	*x*	*y*	*z*
Ru	1.429437	0.568930	0.671835	C	-2.052168	3.551267	-1.955725
Cl	2.746985	2.168437	1.977619	C	-2.147952	4.684727	-1.136679
C	-1.958510	-1.829270	-0.906145	C	-0.988657	5.145828	-0.502723
C	-1.267023	-0.723213	-0.310077	C	0.247353	4.498248	-0.646974
C	-2.099517	0.198676	0.393686	C	-0.768959	1.662274	-3.041758
C	-3.486896	0.044005	0.488563	H	-2.940452	3.187873	-2.469241
C	-4.127254	-1.050432	-0.117762	C	-3.478000	5.374966	-0.932767
C	-3.341963	-1.988803	-0.819283	H	-1.040060	6.037027	0.119942

O	0.017540	-0.621098	-0.449458	C	1.486394	5.054367	0.016272
Br	-0.854054	-3.088139	-1.831249	H	-1.759141	1.407848	-3.427995
Br	-4.178548	-3.493717	-1.651689	H	-0.115886	1.857075	-3.901081
Br	-6.022995	-1.264092	0.007331	H	-0.369284	0.786876	-2.522872
Br	-4.519269	1.336829	1.452328	H	-3.351985	6.371532	-0.499701
Br	-1.230265	1.709149	1.200473	H	-4.023129	5.481288	-1.876579
C	2.095134	1.576686	-1.079990	H	-4.114232	4.794440	-0.253838
N	3.247790	1.358313	-1.806576	H	1.965338	4.316033	0.665942
C	3.410000	2.309323	-2.811846	H	2.231523	5.361670	-0.727253
C	2.350569	3.144578	-2.734521	H	1.236907	5.932534	0.617957
N	1.555789	2.691120	-1.684961	C	2.596981	-0.883983	0.445584
H	2.077011	4.008700	-3.321252	H	2.363542	-1.471411	-0.450009
H	4.257234	2.289664	-3.480909	C	4.840978	-3.588871	1.776533
C	6.341272	-0.583660	-1.067021	C	5.353367	-3.000797	2.940155
C	6.124946	-1.757802	-1.800092	C	4.972085	-1.698176	3.291912
C	4.928126	-1.883117	-2.517050	C	4.076057	-0.985741	2.497262
C	3.950769	-0.879250	-2.505596	C	3.547897	-1.561152	1.317156
C	4.194058	0.269246	-1.728672	C	3.956358	-2.873361	0.970996
C	5.397853	0.449648	-1.021667	H	5.131698	-4.600258	1.502050
H	7.271681	-0.464748	-0.514814	H	6.045592	-3.554851	3.570359
C	7.154982	-2.864878	-1.800499	H	5.374300	-1.241232	4.193073
H	4.750762	-2.779510	-3.108538	H	3.783103	0.024571	2.762836
C	2.676715	-1.037833	-3.304621	H	3.565555	-3.326949	0.063416
C	5.683030	1.718177	-0.254190	N	0.737075	-0.431592	2.576898
H	6.982846	-3.575031	-2.614595	C	0.270306	-1.696310	2.534295
H	8.169763	-2.467300	-1.906405	C	0.744421	0.197922	3.768557
H	7.122565	-3.424516	-0.857699	C	-0.202272	-2.368612	3.660112
H	2.553437	-0.224889	-4.028921	H	0.276512	-2.173273	1.559813
H	2.683941	-1.980002	-3.858850	C	0.292558	-0.404150	4.942726
H	1.789143	-1.031034	-2.663069	H	1.137194	1.209642	3.764551
H	6.637569	1.640819	0.273036	C	-0.192470	-1.712347	4.892533
H	5.741729	2.583558	-0.925293	H	-0.569665	-3.385685	3.560320
H	4.898674	1.931607	0.477599	H	0.323210	0.154018	5.873985
C	0.286481	3.339644	-1.440034	H	-0.554827	-2.207572	5.790042
C	-0.845628	2.865177	-2.128969				

Table D4. Coordinates of *cis*-**5b** (Å).

atom	*x*	*y*	*z*	atom	*x*	*y*	*z*
Ru	1.269978	0.252699	0.347119	C	0.117707	4.919064	-1.777248
Cl	0.213165	0.314509	-1.829063	C	-0.294492	5.572235	-0.608338
C	-2.372832	-1.583064	0.746764	C	0.366581	5.263893	0.583954
C	-1.814652	-0.275774	0.774259	C	1.395662	4.311942	0.641263
C	-2.671109	0.778355	0.350137	C	1.574545	3.332647	-3.078354
C	-3.955617	0.537367	-0.145180	H	-0.369874	5.158413	-2.720004
C	-4.454212	-0.777462	-0.218297	C	-1.432450	6.566579	-0.638282

C	-3.656078	-1.836830	0.250586	H	0.083222	5.778826	1.500068
O	-0.617797	-0.047776	1.253910	C	2.079772	4.057256	1.963254
Br	-1.292971	-2.975204	1.491207	H	0.969596	3.711371	-3.905948
Br	-4.325902	-3.628520	0.216690	H	2.624329	3.552989	-3.303937
Br	-6.195136	-1.118072	-0.931836	H	1.455095	2.246950	-3.041687
Br	-5.040395	2.002152	-0.726945	H	-1.398524	7.243886	0.220236
Br	-1.975060	2.544015	0.531696	H	-1.412830	7.170839	-1.550861
C	2.888241	1.355865	-0.399102	H	-2.397467	6.046296	-0.611748
N	4.172337	0.998955	-0.763782	H	1.616384	3.216693	2.488547
C	4.925292	2.117089	-1.127742	H	3.142242	3.830474	1.841313
C	4.118428	3.194292	-1.001037	H	1.995744	4.934192	2.611272
N	2.878302	2.729125	-0.566792	C	2.173667	-1.392973	0.328038
H	4.295599	4.243299	-1.186423	H	2.926227	-1.497688	1.122394
H	5.951992	2.028950	-1.450349	C	2.675064	-5.018540	-0.497529
C	6.222910	-2.101767	-0.349260	C	1.786396	-5.219940	-1.561042
C	5.961062	-2.780388	-1.542608	C	1.007667	-4.152418	-2.027864
C	5.091418	-2.182701	-2.465076	C	1.105402	-2.892522	-1.441443
C	4.472233	-0.954688	-2.216918	C	2.003590	-2.663343	-0.373026
C	4.726365	-0.321953	-0.980007	C	2.782835	-3.756667	0.084361
C	5.625766	-0.867902	-0.048133	H	3.274814	-5.844254	-0.121326
H	6.917111	-2.533663	0.369591	H	1.692665	-6.203981	-2.015061
C	6.591674	-4.121621	-1.839843	H	0.306540	-4.309571	-2.843910
H	4.891143	-2.684639	-3.409647	H	0.487402	-2.075799	-1.795039
C	3.577401	-0.331158	-3.259539	H	3.473892	-3.605888	0.910589
C	5.971777	-0.190564	1.259559	N	1.931458	0.375822	2.457957
H	7.047238	-4.136168	-2.835857	C	3.066200	0.974037	2.875088
H	7.366151	-4.374243	-1.109925	C	1.174680	-0.242717	3.393922
H	5.836940	-4.916563	-1.817357	C	3.478122	0.995909	4.206353
H	3.912365	0.679461	-3.520341	H	3.659302	1.457092	2.109621
H	3.579873	-0.931214	-4.173086	C	1.517987	-0.268234	4.745716
H	2.544123	-0.247939	-2.908573	H	0.267184	-0.707161	3.025155
H	6.983205	-0.463038	1.574919	C	2.688765	0.362549	5.168711
H	5.923771	0.899151	1.193845	H	4.401141	1.503544	4.471688
H	5.287976	-0.501895	2.057259	H	0.865059	-0.780494	5.446244
C	1.748079	3.644364	-0.543502	H	2.979474	0.359954	6.216265
C	1.138987	3.964496	-1.777347				

Table D5. Coordinates of **7(II)** (Å).

atom	*x*	*y*	*z*	atom	*x*	*y*	*z*
Ru	-0.557676	-0.000639	-0.009915	C	2.321019	-0.070850	1.808138
Cl	-0.555412	-2.434308	0.155447	H	1.917211	-0.980916	2.251687
Cl	-0.611606	2.429896	0.163752	H	3.409207	-0.078512	1.894288
C	-0.772007	-0.000926	-1.832295	H	1.924591	0.793680	2.340833
H	-0.848264	0.933631	-2.394592	C	2.657246	1.504477	-0.625497
H	-0.863408	-0.935774	-2.391795	H	3.725834	1.467842	-0.406599

C	-2.695654	-0.039957	1.040391	H	2.510932	1.548018	-1.704906
H	-2.623910	0.878959	1.609556	H	2.203812	2.391210	-0.186087
C	-3.072258	-0.006335	-0.261801	C	2.665303	-1.403259	-0.761648
H	-3.285293	0.933943	-0.753287	H	3.733299	-1.383462	-0.537641
H	-3.292977	-0.920087	-0.798224	H	2.214569	-2.328285	-0.406057
H	-2.626890	-0.984951	1.564695	H	2.521994	-1.345009	-1.840927
P	1.808966	0.014263	0.037680				

Table D6. Coordinates of **8(II)** (Å).

atom	*x*	*y*	*z*	atom	*x*	*y*	*z*
Ru	0.802327	-0.037423	-0.041068	C	-1.277163	1.818182	1.681824
Cl	0.711691	2.169667	-1.103395	C	-1.946364	-1.929036	-1.457696
Cl	0.882805	-2.007800	1.367888	H	-2.544798	-2.751328	-1.054601
C	1.036752	-0.867693	-1.657784	H	-0.901465	-2.216477	-1.399065
H	1.581657	-1.811875	-1.739014	H	-2.228797	-1.769029	-2.501651
H	0.669500	-0.426224	-2.587587	H	-0.308396	1.468954	2.037755
C	2.944946	0.590902	0.851331	H	-1.905772	1.994100	2.556326
H	2.855765	0.114748	1.820337	H	-1.129935	2.748802	1.130567
C	3.333855	-0.128083	-0.226480	C	-3.544101	-0.420262	-0.248214
H	3.533295	-1.188348	-0.142496	H	-4.188053	-0.252941	-1.112361
H	3.569823	0.359716	-1.163206	H	-3.950454	-1.256267	0.331388
H	2.874470	1.670067	0.795032	C	-3.345535	0.835276	0.604128
N	-2.168882	-0.734754	-0.669554	H	-3.606234	1.749253	0.060022
C	-1.258179	-0.032273	0.023095	H	-3.907682	0.812923	1.538504
N	-1.900688	0.798574	0.858050				

Table D7. Coordinates of **9(II)** (Å).

atom	*x*	*y*	*z*	atom	*x*	*y*	*z*
Ru	-0.764088	-0.031409	0.021099	H	1.394161	1.796732	-2.427421
Cl	-0.959559	2.240651	0.923039	H	1.121473	-2.569069	0.732769
Cl	-0.641777	-2.092149	-1.258091	H	1.551453	-1.794648	2.285259
C	1.313702	0.072792	0.028509	H	2.791573	-2.634408	1.336539
N	2.214912	-0.802168	0.547999	C	-0.963548	-0.765759	1.687479
C	3.508882	-0.404657	0.263189	H	-1.454907	-1.731500	1.829329
C	3.418171	0.730332	-0.462731	H	-0.618318	-0.249509	2.586609
N	2.070811	1.014532	-0.594051	C	-2.906858	0.292060	-1.020101
C	1.891573	-2.025538	1.275099	H	-2.780238	-0.329610	-1.897311
C	1.564511	2.123632	-1.400141	C	-3.288888	-0.249600	0.158619
H	4.180091	1.355223	-0.892831	H	-3.457218	-1.315011	0.249369
H	4.366602	-0.958757	0.599559	H	-3.550828	0.377939	1.000119
H	2.304100	2.922472	-1.396091	H	-2.874139	1.368580	-1.139801
H	0.643471	2.492951	-0.955741				

Table D8. Coordinates of **10(II)** (Å).

atom	*x*	*y*	*z*	atom	*x*	*y*	*z*
Ru	2.810152	0.460870	-0.609118	C	2.040748	2.077887	2.391260
Cl	5.097998	-0.274531	-1.042858	C	3.949217	-2.383703	1.348987
C	-1.502997	1.395622	-0.117362	H	3.717699	-1.893379	4.046996
C	-0.311613	0.627245	-0.294083	H	2.626915	0.573772	4.636915
C	-0.510903	-0.776658	-0.347092	H	4.797404	-2.773099	1.910334
C	-1.764451	-1.370798	-0.217780	H	4.288464	-2.112218	0.353764
C	-2.903042	-0.582083	-0.030948	H	3.166273	-3.141427	1.302242
C	-2.756335	0.814611	0.013553	H	1.447628	2.170344	1.486892
O	0.824387	1.229536	-0.391903	H	2.855131	2.804442	2.381225
Br	-1.259079	3.290465	-0.075462	H	1.408693	2.262509	3.258325
Br	-4.292661	1.921604	0.256946	C	3.432328	2.227187	-0.716284
Br	-4.622846	-1.387660	0.163169	H	4.482897	2.488856	-0.835908
Br	-1.923944	-3.274627	-0.296250	H	2.731724	3.054892	-0.593268
Br	1.049610	-1.874471	-0.638987	C	2.433082	0.278901	-2.781691
C	2.954054	-0.066789	1.442422	H	1.368514	0.147088	-2.916835
N	2.575124	0.721039	2.485060	C	2.948940	1.580731	-2.688074
C	2.842741	0.104899	3.693606	H	2.259259	2.409310	-2.785784
C	3.382298	-1.098595	3.404975	H	3.976876	1.740512	-2.986067
N	3.451785	-1.188030	2.027114	H	3.084241	-0.516890	-3.117565

1) M. W. Kotyk, S. I. Gorelsky, J. C. Conrad, C. Carra, D. E. Fogg*, "Geometric and Electronic Structure of a C_1-Symmetric Ru-Aryloxide Metathesis Catalyst: An Experimental and Computational Study", *Organometallics*, **2009**, *28,* 5424-5431.

2) M. W. Kotyk, S. I. Gorelsky*, D. E. Fogg* "Ligands Effects in the Cycloaddition Step of Olefin Metathesis: Quantification by DFT Analysis." Manuscript in preparation.